

---

**Development of quantitative lipidomic  
strategies in neurological diseases for  
discovery and monitoring of tissue and  
blood markers -  
Application to kainic acid mouse model  
of epilepsy**

---

Dissertation

zur Erlangung des Grades

„Doktor der Naturwissenschaften“

am Fachbereich Biologie der



JOHANNES GUTENBERG  
UNIVERSITÄT MAINZ

**Raissa Lerner**

geb. am 24.09.1985 in Bad Schwalbach

Mainz, November 2017

*To my parents*

## TABLE OF CONTENT

<b>1</b>	<b>SUMMARY / ZUSAMMENFASSUNG.....</b>	<b>1</b>
1.1	Summary.....	1
1.2	Zusammenfassung.....	3
<b>2</b>	<b>INTRODUCTION.....</b>	<b>6</b>
2.1	Lipids.....	6
2.1.1	Phospholipids.....	11
2.1.2	Endocannabinoids.....	16
2.1.3	Clinical relevance.....	20
2.2	Mass spectrometry of lipids.....	24
2.2.1	Phospholipid analysis.....	31
2.2.2	Endocannabinoid analysis.....	34
2.2.3	MS imaging.....	35
2.3	Aim of the study.....	38
<b>3</b>	<b>MATERIALS AND METHODS.....</b>	<b>39</b>
3.1	Reagents and chemicals.....	39
3.2	Calibration- and internal lipid standards.....	39
3.3	Research equipment.....	40
3.4	Mass spectrometric tools.....	41
3.5	Data processing and statistical analysis.....	41
<b>4</b>	<b>LIPIDOMIC PROFILING VIA MASS SPECTROMETRY.....</b>	<b>42</b>
4.1	Introduction.....	42
4.2	Materials and methods.....	43
4.2.1	LC/MRM method development.....	43

4.2.2	Development of lipid extraction protocol .....	48
4.2.3	LC/MRM qualitative and quantitative profiling .....	51
4.3	Results.....	55
4.3.1	LC/MRM method development .....	55
4.3.2	Development of lipid extraction protocol .....	62
4.3.3	LC/MRM qualitative and quantitative profiling .....	66
4.4	Discussion .....	69
<b>5</b>	<b>DUAL EXTRACTION METHOD FOR LIPIDOMIC AND TRANSCRIPTOMIC PROFILING.....</b>	<b>71</b>
5.1	Introduction .....	71
5.2	Materials and methods .....	71
5.2.1	RNA and lipid co-extraction .....	71
5.2.2	Lipidomic profiling .....	72
5.2.3	Transcriptomic profiling .....	73
5.3	Results.....	74
5.4	Discussion .....	78
<b>6</b>	<b>APPLICATION TO ACUTE EPILEPTIC SEIZURE MODEL .....</b>	<b>79</b>
6.1	Introduction.....	79
6.2	Material and methods .....	80
6.2.1	Induction of acute excitotoxic seizures.....	80
6.2.2	Preparation of six brain regions and periphery from KA-induced / control mice and extraction for lipidomic profiling .....	80
6.2.3	Punching of brain regions from KA-induced / control mice and simultaneous lipidomic and transcriptomic profiling .....	81
6.2.4	Brain sectioning from KA-induced / control mice and MS imaging.....	82
6.3	Results.....	83
6.3.1	Lipid signal profiling in six brain regions and periphery from KA-induced epileptic seizure mice ...	83

6.3.2 Lipidomic and transcriptomic profiling in brain punches from KA-induced epileptic seizure mice..	89
6.3.3 MS imaging on brain sections from KA-induced epileptic seizure mice.....	93
6.4 Discussion.....	95
6.4.1 Lipid signal profiling in six brain regions and periphery from KA-induced epileptic seizure mice...	95
6.4.2 Lipidomic and transcriptomic profiling in brain punches from KA-induced epileptic seizure mice and PLs in MS imaging .....	99
<b>7 CONCLUSIONS AND PERSPECTIVES.....</b>	<b>106</b>
<b>8 REFERENCES.....</b>	<b>109</b>
<b>9 APPENDIX.....</b>	<b>132</b>
9.1 Abbreviations .....	132
9.2 List of figures.....	135
9.3 List of tables .....	136
9.4 Curriculum vitae .....	137



## 1 SUMMARY / ZUSAMMENFASSUNG

### 1.1 Summary

Lipids are small hydrophobic or amphipathic biomolecules, which are soluble in organic solvents and originate by carbanion based condensations of ketoacyl thioesters or by carbocation-based condensations of isoprene units. They depict a large structural heterogeneity and are divided into eight main categories according to shared structural features, further subdivided into several subclasses. Since additional variability of lipid structures arises from their different chain length, double bonds location and number, chirality and various possible modifications, up to 200,000 or more distinct lipid structures may exist. Accordingly, this huge structural heterogeneity reflects the diversity of lipid function. Neutral lipids represent the main energy storage and are therefore crucial for energy homeostasis. The amphipathic nature of phospholipids enables the formation of membranes, which are essential for cellular architecture and subcellular compartmentalization. The more hydrophilic lipids serve important function in cell recognition and cell-cell interaction. As main membrane components, lipids are able to control the biophysical properties of the membrane, and thus are directly involved in important events such as synaptic transmission. Moreover, lipids serve as precursors for signaling molecules as well as direct signaling molecules such as endocannabinoids and intracellular second messengers such as phosphatidylinositol phosphate.

Considering this broad spectrum of lipid functions, it becomes obvious that lipid related disturbances are implicated in several disorders. Consequently, a growing number of studies have evidenced the involvement of lipids in the development and progression of various diseases, such as epilepsy. This neurological disease, affecting about 1% of the human population, is characterized by recurrent seizures. A mouse model which mimics mainly seizures observed in temporal lobe epilepsy, a category of epilepsy which mainly occurs in the limbic system, can be obtained by injection of kainic acid, a ligand for a specific group of ionotropic glutamate receptors. A growing number of studies reveal alterations in lipid levels using such epileptic seizure models and thus evidence the implication of lipid signals and their potential role as biomarkers or therapeutic targets. In order to provide a tool for future lipid analysis under pathological conditions in clinical and research samples, we developed a method for lipidomic profiling and applied it in a first proof of concept study to a mouse model of epileptic seizures induced by systemic kainic acid injection.

Mass spectrometry allows concurrent qualitative and quantitative profiling of multiple lipids without previous molecule identification and antibodies, thereby rendering the highest amount of structural data in short analysis time and at lower costs compared to other techniques. Moreover, mass spectrometry combined with liquid chromatography provides highest sensitivity for molecule

quantification, thus allowing analysis of lowest sample amounts, which is often inevitable when investigating biological systems. Hence, mass spectrometry represents an adequate tool for comprehensive lipidomic research, most suitable for biological and clinical investigations and accordingly the technique of choice in this study.

The protocol developed for lipidomic profiling was proved to be suitable for simultaneous analysis of phospholipids, endocannabinoids and endocannabinoid-related compounds from microgram amounts of tissue, e.g. brain punches, and revealed new insights in lipid plasticity associated with epileptic seizures.

Since thorough elucidation of lipid pathways requires additional knowledge about other molecules involved, such as enzymes and receptors, in a second objective of this study, we developed a protocol for combined lipidomic and transcriptomic profiling. Therefore, we optimized the protocol for lipid extraction in order to allow simultaneous mRNA extraction and subsequent analysis. We demonstrated the established method as an excellent, versatile tool for combined lipidomic and transcriptomic profiling from microgram tissue amounts, and therefore benefiting analysis time and costs, as well as data reliability by circumventing pitfalls deriving from different animal batches and tissue heterogeneity.

Applied to brain punches of the epileptic seizure mouse models, we gained new information about lipid-related processes within epilepsy at higher spatial resolution where distinct, less expected pathways of lipid metabolism are affected at acute epilepsy phase. Moreover, our data strongly support the need for subregional specificity when investigating neurological diseases, as for instance the dorsal and the ventral hippocampus showed contrary lipid changes, hence differentially regulated lipid metabolism, which might be masked when analyzing the whole hippocampus at once. This result was further underlined by mass spectrometry imaging experiments, applied in a third objective to the epileptic seizure mouse models, aiming at increased spatial resolution to target lipids across cell layers and populations. An additional outcome of these experiments revealed alterations in phospholipid adduct ions associated with epileptic seizures, pointing toward ion conversion in membrane lipids with acute epilepsy, which constitutes further potential target for disease treatment.

In conclusion, the methods established in this thesis, represent valuable tools to increase our understanding about disturbances in lipid pathways associated with diseases, leverage new mechanistic knowledge on the diseases, enhance the predictability of diseases and thus allow reliable diagnosis and design of new therapeutic schemes for patients.



## **1.2 Zusammenfassung**

Lipide sind kleine hydrophobe oder amphipathische Biomoleküle, welche sich in organischen Lösungsmitteln lösen, nicht aber in Wasser, und durch Carbanion basierte Kondensation von Ketoacyl Thioestern oder Carbokation basierte Kondensation von Isopreneinheiten gebildet werden. Sie umfassen eine große strukturelle Heterogenität und werden abhängig von gemeinsamen strukturellen Eigenschaften in acht Hauptkategorien eingeteilt. Da zusätzliche Variabilität in Lipid-Strukturen durch ihre Kettenlänge, Anzahl und Lage der Doppelbindungen, Chiralität sowie diverse mögliche Modifikationen entsteht, gehen Schätzungen über die Anzahl von unterschiedlichen Lipid-Strukturen von bis zu 200000 aus, oder sogar darüber hinaus. Diese extreme strukturelle Heterogenität der möglichen Lipid-Strukturen spiegelt dementsprechend die Diversität der Lipid-Funktionen wider. Neutrale Lipide repräsentieren den Hauptenergiespeicher und sind somit wesentlich für die Energiehomöostase. Die amphipathische Natur von Phospholipiden ermöglicht die Bildung von biologischen Membranen, welche essentiell für die Zellarchitektur sowie die subzelluläre Kompartimentierung sind. Die stärker hydrophilen Lipide dienen wichtigen Funktionen in der Zell-Erkennung und Zell-Zell Interaktion. Als Hauptmembranbestandteile sind Lipide in der Lage die biophysikalischen Eigenschaften von Membranen zu kontrollieren und dadurch direkt an wichtigen Funktionen wie der synaptischen Übertragung beteiligt. Darüber hinaus dienen Lipide nicht nur als Vorläufer für Signalmoleküle, sondern auch direkt selbst als Signalmoleküle wie zum Beispiel die Endocannabinoide oder die intrazellulären sekundären Botenstoffe wie Phosphoinositol Phosphat.

In Anbetracht dieses breiten Spektrums an verschiedenen Lipidfunktionen ist es naheliegend, dass mit Lipiden zusammenhängende Störungen bei vielen Krankheiten beobachtet werden können. Dementsprechend bestätigt eine steigende Anzahl von Studien die Involvierung von Lipiden in Entwicklung und Verlauf diverser Krankheiten wie z.B. Epilepsie. Diese neurologische Krankheit, welche ungefähr 1% der Weltbevölkerung betrifft, ist durch wiederkehrende Krampfanfälle charakterisiert.

Durch Injektion von Kainat kann ein Mausmodell induziert werden, welches größtenteils Anfälle nachahmt, die man in der Schläfenlappenepilepsie vorfindet, eine Epilepsievariante die vornehmlich auf das limbische System beschränkt ist. Immer mehr Studien enthüllen Veränderungen in Lipid Konzentrationen in solchen Epilepsie-Mausmodellen und bestätigen damit die mögliche Einbeziehung von Lipid Signalen und damit verbunden deren mögliche Rolle als Biomarker oder therapeutische Pharmaka. Um die Möglichkeit bereitzustellen, zukünftig Lipide unter pathologischen Bedingungen in klinischen oder Forschungs-Proben analysieren zu können, haben wir eine Methode zur Untersuchung von Lipidprofilen entwickelt und sie in einem ersten Testlauf an dem beschriebenen Mausmodell für Schläfenlappenepilepsie angewandt.

Massenspektrometrie ermöglicht gleichzeitig die qualitative und quantitative Analyse zahlreicher Lipide ohne die Notwendigkeit für deren vorangehende Identifizierung oder den Gebrauch von zusätzlichen Antikörpern und erzielt darüber hinaus die größte Menge an strukturellen Daten in kürzester Analysezeit zu vergleichsweise niedrigen Kosten. Zusätzlich bietet die mögliche Kombination mit Flüssigkeitschromatographie sehr hohe Sensitivität bei der Quantifizierung von Molekülen und erlaubt damit die Analyse von sehr geringen Probenmengen, ein Umstand der bei der Erforschung von biologischen Systemen oft unvermeidlich ist. Demnach repräsentiert die Massenspektrometrie ein adäquates Instrument zur umfangreichen Untersuchung von Lipidprofilen, optimal geeignet für biologische und klinische Forschung und ist somit die Technik unserer Wahl in dieser Studie. Wir konnten zeigen, dass das von uns entwickelte Protokoll zur Lipidanalyse für die gleichzeitige Messung und anschließende Quantifizierung von Phospholipiden, Endocannabinoiden und mit Endocannabinoiden in Verbindung stehenden Lipiden geeignet ist. Dabei ist es ausreichend sensitiv für die Untersuchung von Proben im Mikrogrammbereich, wie z.B. Gehirnausstanzungen und seine Anwendung hat bereits dazu geführt, neue Einblicke in die mit epileptischen Anfällen verbundene Lipidplastizität zu erlangen.

Da die umfassende Untersuchung von Lipidsignalwegen und Funktionen auch der zusätzlichen Analyse von weiteren involvierten Molekülen wie Enzymen oder Rezeptoren bedarf, befasste sich eine zweite Zielvorgabe dieser Studie mit der Entwicklung eines Protokolls zur simultanen Analyse von Lipiden und RNA. Um dies zu erreichen, optimierten wir das zuvor entwickelte Protokoll für die Lipidanalyse dahingehend, es mit RNA-Extraktion und deren anschließender Messung zu kombinieren. Hierbei konnten wir zeigen, dass die von uns entwickelte Methode ein exzellentes Instrument für die kombinierte Analyse von Lipiden und RNA ist, folglich Zeit sparend und Kosten senkend, und darüber hinaus sensitiv genug für Probenmengen im Mikrogramm Bereich. Überdies fördert die Anwendung der hier entwickelten Methode die Reliabilität der Daten, indem Fehlinterpretationen entstehend durch Gewebheterogenität oder den Gebrauch verschiedener Mausversuchsgruppen zur jeweiligen Analyse von Lipiden und RNA vermieden werden.

Angewandt an dem beschriebenen Mausmodell für epileptische Anfälle, konnten wir durch Analyse von Gehirnausstanzungen im Milli- bis Mikrogramm Bereich mit entsprechend höherer räumlicher Auflösung neue Informationen über lipidabhängige Prozesse gewinnen und damit verbunden auf mRNA Ebene die Beeinflussung weniger erforschter Lipid- Stoffwechselwege identifizieren. Ferner belegen unsere Daten eindeutig die Notwendigkeit für subregionale Spezifizierung bei der Untersuchung von neurologischen Krankheiten. Dies zeigt sich in Anbetracht der gemessenen gegensätzlichen Lipidveränderungen im ventralen und dorsalen Hippocampus, welche sich durch Analyse des Hippocampus im Ganzen gegenseitig aufheben könnten und damit unbemerkt bleiben würden. Dieses Ergebnis wurde zusätzlich durch die

Experimente zur bildgebenden Massenspektrometrie unterstützt, welche als weitere Zielvorgabe dieser Studie an dem beschriebenen Mausmodell für epileptische Anfälle angewandt wurde, für eine obendrein erhöhte räumliche Auflösung, um Lipide durch Zellschichten und Populationen hinweg zu erfassen. Ein zusätzliches Resultat dieser Experimente wies auf mit epileptischen Anfällen verbundene Veränderungen in den Addukten der Phospholipide hin, ein Zeichen für mögliche Ionenkonvertierung in den Membranlipiden und damit ein potentieller Ansatzpunkt für die Behandlung der Krankheit.

Zusammenfassend repräsentieren die von uns etablierten Methoden wertvolle Hilfsmittel zur Erweiterung unseres Verständnisses über mit Krankheiten verbundene Störungen im Lipidhaushalt, ermöglichen neues mechanistisches Wissen über Krankheiten, erhöhen damit die Vorhersehbarkeit dieser und helfen so bessere Diagnosen zu stellen und passende therapeutische Behandlungen für Patienten zu kreieren.

## 2 INTRODUCTION

### 2.1 Lipids

Lipids are one of the four basic categories of molecules, which are essential for building life. No precise definition of the term “lipid” exists, but it is classically defined as any of a group of organic compounds, which are soluble in organic solvents, but insoluble in water. The modern study of lipid biochemistry and physiology has its origin in the 17<sup>th</sup> and 18<sup>th</sup> centuries (McNamara *et al.*, 2006). Robert Boyle, an Anglo-Irish philosopher and chemist, noted already in 1665 the milky appearance of blood in animals after eating and Otto Tachenius, a German doctor and pharmacist, described in his work *Hippocrates Chimicus* (1673) that an acid compound is hidden in fats. Progress in lipid analysis was made in 1769 by Poulletier de la Salle who isolated a lipid (cholesterol) from gallstones, while Antoine Francois de Fourcroy introduced in 1783 a method based on alcohol to extract lipids from brain (McNamara *et al.*, 2006). Breakthrough advancement in lipid research was done by the chemist Michel-Eugen Chevreul in the 19<sup>th</sup> century. Among other things, he described for the first time several fatty acids (FAs) and showed that fats are composed of FAs and glycerol. However, the extreme advances in technology over the time enabled the identification of thousands of lipid structures. Based on this knowledge and well defined chemical and biochemical principles, the international Lipid Classification and Nomenclature Committee on the initiative of the LIPID MAPS Consortium suggested in 2005 a lipid classification system (Tab. 2.1), with the concept of two fundamental “building blocks”: ketoacyl groups and isoprene groups (Fahy *et al.*, 2005). This concept led to a more precise definition of the term lipid, as a small hydrophobic or amphipathic molecule, that may originate entirely or in part by carbanion- based condensations of ketoacyl thioesters and/or by carbocation-based condensations of isoprene units (Fahy *et al.*, 2005). This comprehensive classification system, that comprise eukaryotic and prokaryotic sources, divides lipids into eight main categories: fatty acyls, glycerolipids, glycerophospholipids, sphingolipids, saccharolipids and polyketides (“ketoacyl building block”); and sterol lipids and prenol lipids (“isoprene building block”) (Fig. 2.1) (Fahy *et al.*, 2005, 2009). As depicted in (Tab. 2.1), every category is further divided into classes, which all have their own subclasses or even more subdivisions. On the basis of this classification system, the LIPID MAPS Nature Lipidomic Gateway website provides a database for lipid structures (LMSD) (LIPID MAPS Nature Lipidomics Gateway, <http://www.lipidmaps.org>).

**Table 2.1 LIPID MAPS Classification system:** Lipid classification based on the classification system developed by the International Lipid Classification and Nomenclature Committee on the initiative of the LIPID MAPS Consortium (Fahy et al. 2005) (LIPID MAPS Nature Lipidomics Gateway, <http://www.lipidmaps.org>). This comprehensive classification system divides lipids into eight main categories: fatty acyls, glycerolipids, glycerophospholipids, sphingolipids, saccharolipids and polyketides (“ketoacyl building block”); and sterol lipids and prenol lipids (“isoprene building block”).

<b>Sterol Lipids [ST]</b>	<b>Fatty Acyls [FA]</b>
Sterols <a href="#">[ST01]</a>	Fatty Acids and Conjugates <a href="#">[FA01]</a>
Steroids <a href="#">[ST02]</a>	Octadecanoids <a href="#">[FA02]</a>
Secosteroids <a href="#">[ST03]</a>	Eicosanoids <a href="#">[FA03]</a>
Bile acids and derivatives <a href="#">[ST04]</a>	Docosanoids <a href="#">[FA04]</a>
Steroid conjugates <a href="#">[ST05]</a>	Fatty alcohols <a href="#">[FA05]</a>
Other Sterol lipids <a href="#">[ST00]</a>	Fatty aldehydes <a href="#">[FA06]</a>
	Fatty esters <a href="#">[FA07]</a>
	Fatty amides <a href="#">[FA08]</a>
	Fatty nitriles <a href="#">[FA09]</a>
	Fatty ethers <a href="#">[FA10]</a>
	Hydrocarbons <a href="#">[FA11]</a>
	Oxygenated hydrocarbons <a href="#">[FA12]</a>
	Fatty acyl glycosides <a href="#">[FA13]</a>
	Other Fatty Acyls <a href="#">[FA00]</a>
<b>Prenol Lipids [PR]</b>	<b>Glycerolipids [GL]</b>
Isoprenoids <a href="#">[PR01]</a>	Monoradylglycerols <a href="#">[GL01]</a>
Quinones and hydroquinones <a href="#">[PR02]</a>	Diradylglycerols <a href="#">[GL02]</a>
Polyprenols <a href="#">[PR03]</a>	Triradylglycerols <a href="#">[GL03]</a>
Hopanoids <a href="#">[PR04]</a>	Glycosylmonoradylglycerols <a href="#">[GL04]</a>
Other Prenol lipids <a href="#">[PR00]</a>	Glycosyldiradylglycerols <a href="#">[GL05]</a>
	Other Glycerolipids <a href="#">[GL00]</a>
<b>Polyketides [PK]</b>	<b>Glycerophospholipids [GP]</b>
Linear polyketides <a href="#">[PK01]</a>	Glycerophosphocholines <a href="#">[GP01]</a>
Halogenated acetogenins <a href="#">[PK02]</a>	Glycerophosphoethanolamines <a href="#">[GP02]</a>
Annonaceae acetogenins <a href="#">[PK03]</a>	Glycerophosphoserines <a href="#">[GP03]</a>
Macrolides and lactone polyketides <a href="#">[PK04]</a>	Glycerophosphoglycerols <a href="#">[GP04]</a>
Ansamycins and related polyketides <a href="#">[PK05]</a>	Glycerophosphoglycerophosphates <a href="#">[GP05]</a>
Polyenes <a href="#">[PK06]</a>	Glycerophosphoinositols <a href="#">[GP06]</a>
Linear tetracyclines <a href="#">[PK07]</a>	Glycerophosphoinositol monophosphates <a href="#">[GP07]</a>
Angucyclines <a href="#">[PK08]</a>	Glycerophosphoinositol bisphosphates <a href="#">[GP08]</a>
Polyether antibiotics <a href="#">[PK09]</a>	Glycerophosphoinositol trisphosphates <a href="#">[GP09]</a>
Aflatoxins and related substances <a href="#">[PK10]</a>	Glycerophosphates <a href="#">[GP10]</a>
Cytochalasins <a href="#">[PK11]</a>	Glyceropyrophosphates <a href="#">[GP11]</a>
Flavonoids <a href="#">[PK12]</a>	Glycerophosphoglycerophosphoglycerols <a href="#">[GP12]</a>
Aromatic polyketides <a href="#">[PK13]</a>	CDP-Glycerols <a href="#">[GP13]</a>
Non-ribosomal peptide/polyketide hybrids <a href="#">[PK14]</a>	Glycosylglycerophospholipids <a href="#">[GP14]</a>
Other Polyketides <a href="#">[PK00]</a>	Glycerophosphoinositolglycans <a href="#">[GP15]</a>
	Glycerophosphonocholines <a href="#">[GP16]</a>
	Glycerophosphonoethanolamines <a href="#">[GP17]</a>
	Di-glycerol tetraether phospholipids <a href="#">[GP18]</a>
	Glycerol-nonitol tetraether phospholipids <a href="#">[GP19]</a>
	Oxidized glycerophospholipids <a href="#">[GP20]</a>
	Other Glycerophospholipids <a href="#">[GP00]</a>
<b>Saccharolipids [SL]</b>	<b>Sphingolipids [SP]</b>
Acylaminosugars <a href="#">[SL01]</a>	Sphingoid bases <a href="#">[SP01]</a>
Acylaminosugar glycans <a href="#">[SL02]</a>	Ceramides <a href="#">[SP02]</a>
Acyltrehaloses <a href="#">[SL03]</a>	Phosphosphingolipids <a href="#">[SP03]</a>
Acyltrehalose glycans <a href="#">[SL04]</a>	Phosphonosphingolipids <a href="#">[SP04]</a>
Other acyl sugars <a href="#">[SL05]</a>	Neutral glycosphingolipids <a href="#">[SP05]</a>
Other Saccharolipids <a href="#">[SL00]</a>	Acidic glycosphingolipids <a href="#">[SP06]</a>
	Basic glycosphingolipids <a href="#">[SP07]</a>
	Amphoteric glycosphingolipids <a href="#">[SP08]</a>
	Arsenosphingolipids <a href="#">[SP09]</a>
	Other Sphingolipids <a href="#">[SP00]</a>

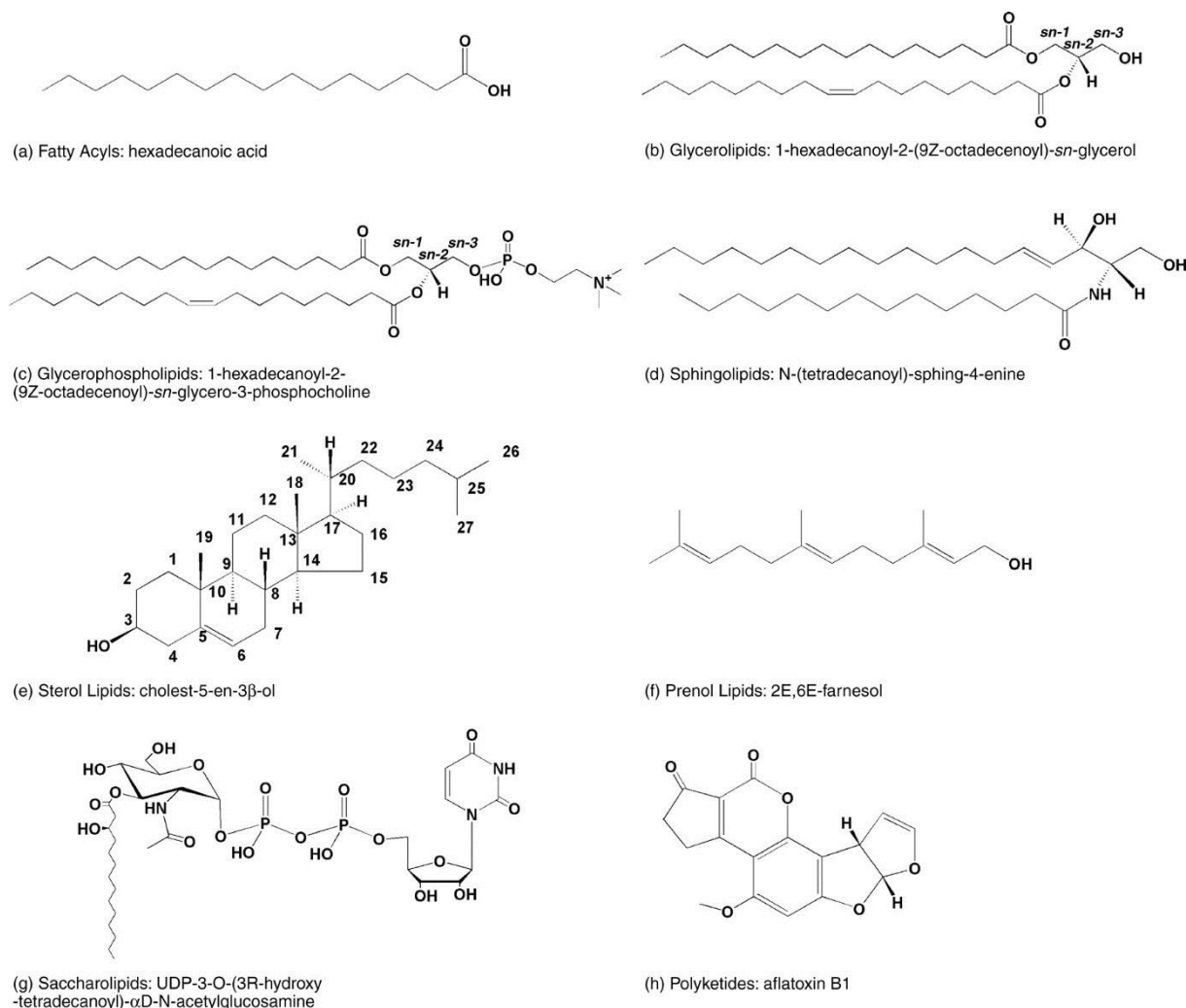


**Figure 2.1 Exemplary structures of lipid categories:** Representative structures from each of the 8 LIPID MAPS lipid categories (from Fahy *et al.*, 2005).

Different sources such as LIPID MAPS Consortium's core laboratories, LIPIDAT, Cyberlipids, book chapters etc. were used to establish LMSD, which so far contains already over 30000 lipid structures (Fahy *et al.*, 2011). Solid estimations of the number of structurally diverse lipids occurring in nature do not exist. However, considering their variable chain length, precise double bond location, chirality or biochemical transformations due to reductive, oxidative or substitutional processes or other modifications, as much as 200,000 or more distinct structures might exist (Yetukuri *et al.*, 2008; Brown and Marnett, 2011; Fahy *et al.*, 2011).

This remarkable structural diversity is for instance associated with the evolution of higher cognitive abilities in primates (Li *et al.*, 2017) and consequently reflects the diversity in lipid function. One crucial function of lipids is their role as energy storage. Especially neutral lipids such as triglycerides and cholesterol esters are used as caloric reserve, due to their relatively reduced state. They are stored during time of energy excess in lipid droplets, as an energy

reservoir in case of starvation and are therefore, important for energy homeostasis. Furthermore, lipid droplets are the source for other molecules important for cell signaling and membrane biogenesis (Welte, 2015; Gluchowski *et al.*, 2017). Serving as primary constituents of membranes is another major function of lipids. The amphipathic nature of phospholipids (PLs), in particular, allows spontaneous membrane formation by self-assembling in a hydrophilic environment. Thereby, lipids are able to control biophysical parameters of the membrane, such as fluidity, thickness and curvature, important for membrane fusion, cell division etc. (van Meer, Dennis R. Voelker, *et al.*, 2008; Lauwers *et al.*, 2016). Thus, lipids are essential for the cell architecture and, moreover the subcellular compartmentalization that allows the co-existence of organelles with distinct functions and improved biochemical efficiency by separation of chemical reactions. Furthermore, there are specialized lipids like phosphatidylinositol phosphates (PtdInsPs) that influence membrane trafficking by binding to proteins crucial for synaptic transmission or ion channels as for instance the Kir2 potassium channel, thereby triggering its conformational change which leads to the opening of the channel pore (Lauwers *et al.*, 2016). Finally, lipids serve as intracellular second messengers as well as direct ligands for receptors. Signaling lipids such as endocannabinoids (eCBs), eicosanoids (eiCs), phosphoinositides, sphingolipids, lysophosphatidic acids and poly unsaturated FAs (PUFAs), in particular arachidonic acid (AA), play important roles in cellular function (Wymann and Schneider, 2008; Brown and Marnett, 2011; Xiang *et al.*, 2013). Several receptors are involved in mediating lipid signals, as for instance G protein coupled receptors like prostanoid receptors and leukotriene receptors, or nuclear receptors as peroxisome proliferator-activated receptors (PPARs). A more recently discovered way for lipids to influence signaling is through production of electrophiles via spontaneous PUFA autoxidation, which then couple to intracellular nucleophiles, thereby manipulating DNA replication and cell toxicity (Brown and Marnett, 2011). Another possible regulation through lipids is via modification of proteins. Several vitamins also belong to the group of lipids (vitamin A, D, E, K) and have multiple essential functions. For instance retinal, a group A vitamin, combines with opsin to build rhodopsin, a light absorbing protein, necessary for vision (Palczewski *et al.*, 2000). Of course enzymes involved in lipid metabolism are also a relevant manipulation site for lipid function. The plasma membrane, even if it is not able to build autonomously its structural constituents, contains several proteins for synthesizing and degrading lipids, that are involved in signaling cascades (Di Paolo and De Camilli, 2006).

The main site for the lipid biosynthesis is the endoplasmic reticulum (ER). Especially cholesterol, triacylglycerols and various PLs are produced in the ER. Another organelle, which is important for sorting lipids as well as their synthesis, in particular of sphingolipids, is the Golgi apparatus. The primary destination of lipids, synthesized in the Golgi apparatus, is the plasma membrane (van Meer, Dennis R. Voelker, *et al.*, 2008). Since mitochondria are of bacterial origin they produce also bacterial lipids, such as cardiolipins and are the main synthesis source for PE (van Meer,

## INTRODUCTION

---

Dennis R. Voelker, *et al.*, 2008). Lipid transport can be achieved via different mechanism. Some lipids are able to laterally diffuse through membrane continuities, but most of the lipid transport is conducted via the vesicular transport through budding and fusion of membrane vesicles. Transport via lipid-transfer proteins is also described and can for instance be used for organelles such as peroxisomes and mitochondria, which are not connected to the vesicular transport system (van Meer, Dennis R. Voelker, *et al.*, 2008; Lev, 2010).

To date a lot is known about lipids and their metabolism and function. Yet, we are still only scratching the surface. Progress in research strongly relies on available technologies. Inventions, such as the ultracentrifuge in the early 20<sup>th</sup> century, used for proper lipid separation, or nuclear magnetic resonance (NMR) greatly improved lipid research (Wenk, 2010). In particular mass spectrometry (MS) heavily bolsters modern lipid research. New methodologies such as vibrational microscopy (Neef and Schultz, 2009), click chemistry (Yu *et al.*, 2014) and mass spectrometry imaging (Murphy *et al.*, 2009) enable investigation of spatial lipid patterns (Wenk, 2010; Lauwers *et al.*, 2016). Emerging internet platforms such as LIPID MAPS (Fahy *et al.*, 2011) that collects and stores information gathered by all these technologies represent valuable tools for lipid assignment, identification, information-driven lipid analysis and data processing. For instance, lipid structural formulas and mass spectrometric lipid data on sequencing and profiling are accessible on this website. In the present study we retrieved from this platform information for the targeted molecules (Fig. 2.2).



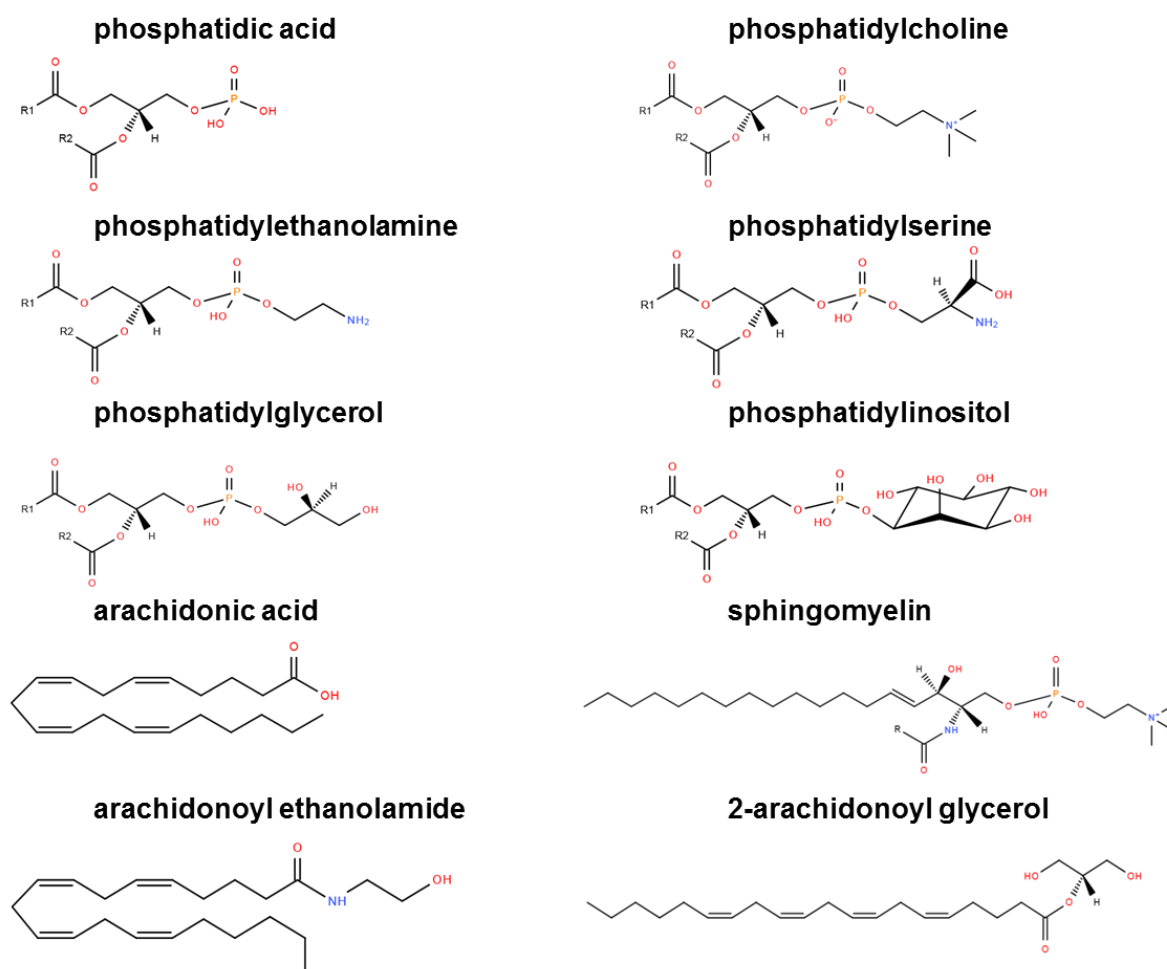


**Figure 2.2 Exemplary structures of targeted lipids:** Representative structures for the headgroups of the targeted PLs species as well as ERCs (The lipid structures were taken from LIPID MAPS structure database (LMSD), available on <http://www.lipidmaps.org>).

### 2.1.1 Phospholipids

The earliest document published in English language containing the word “phospholipids” dates back to 1884 by J.L. William Thudichum. This reads: “Phospholipids are the centre of life, and chemical soul of all bioplasm whatever, that of plants as well as animals... Amongst these properties [of phospholipids] none are more deserving of further inquiry than those which may be described as their power of colloidation. Without this power no brain as an organ would be possible, as indeed the existence of all bioplasm is dependent on the colloid state”. Indeed, the prominent characteristic of PLs is their amphipathic nature, owning a hydrophobic and a hydrophilic moiety. Due to this, PLs are able to self-associate forming a bilayer, driven by the energetically favorable state in which the hydrophobic ends self-assemble in the core away from water and the hydrophilic ends interact with the aqueous environment. This fundamental feature of PLs allows the spontaneous generation of biological membranes, “the margin between life and death” (van Meer, Dennis R Voelker, *et al.*, 2008; Lauwers *et al.*, 2016). The PLs targeted in this

## INTRODUCTION

---

study belong to the glycerophospholipids and sphingolipids, both lipid categories from the “ketoacyl building block” (Fahy *et al.*, 2011) (Tab. 2.2).

**Table 2.2 LIPID MAPS Classification system - PLs:** Classification of PLs based on the classification system developed by the International Lipid Classification and Nomenclature Committee on the initiative of the LIPID MAPS Consortium (LIPID MAPS Nature Lipidomics Gateway, <http://www.lipidmaps.org>). Blue marks the targeted PL classes.

### Glycerophospholipids [GP]

Glycerophosphocholines [GP01]	Phosphatidylcholines (PC)
Glycerophosphoethanolamines [GP02]	Lysophosphatidylcholines (LPC)
Glycerophosphoserines [GP03]	Phosphatidylethanolamines (PE)
Glycerophosphoglycerols [GP04]	Phosphatidylserines (PS)
Glycerophosphoglycerophosphates [GP05]	Phosphatidylglycerols (PG)
Glycerophosphoinositols [GP06]	Phosphatidylinositols (PI)
Glycerophosphoinositol monophosphates [GP07]	
Glycerophosphoinositol bisphosphates [GP08]	
Glycerophosphoinositol trisphosphates [GP09]	
Glycerophosphates [GP10]	Phosphatidic acids (PA)
Glyceropyrophosphates [GP11]	Lysophosphatidic acids (LPA)
Glycerophosphoglycerophosphoglycerols [GP12]	
CDP-Glycerols [GP13]	
Glycosylglycerophospholipids [GP14]	
Glycerophosphoinositolglycans [GP15]	
Glycerophosphoncholines [GP16]	
Glycerophosphonoethanolamines [GP17]	
Di-glycerol tetraether phospholipids [GP18]	
Glycerol-nonitol tetraether phospholipids [GP19]	
Oxidized glycerophospholipids [GP20]	
Other Glycerophospholipids [GP00]	

### Sphingolipids [SP]

Sphingoid bases [SP01]	
Ceramides [SP02]	
Phosphosphingolipids [SP03]	Sphingomyelins (SM)
Phosphosphingolipids [SP04]	
Neutral glycosphingolipids [SP05]	
Acidic glycosphingolipids [SP06]	
Basic glycosphingolipids [SP07]	
Amphoteric glycosphingolipids [SP08]	
Arenosphingolipids [SP09]	
Other Sphingolipids [SP00]	

Glycerophospholipids are the major structural constituents of membranes. Among them, phosphatidic acids (PA), phosphatidylcholines (PC), phosphatidylethanolamines (PE), phosphatidylglycerols (PG), phosphatidylinositols (PI) and phosphatidylserines (PS) are the main PL classes. They consist of a hydrophobic tail with DAG as backbone esterified at the sn-1 and/or sn-2 position with FAs and a polar head group linked through a phosphate residue at the sn-3 position (Fig. 2.2). Sphingolipids represent another class of structural constituents with ceramide

as hydrophobic backbone and sphingomyelin (SM) as one of the most prominent examples, which possess likewise PC choline as headgroup (Fig. 2.2) (Fahy *et al.*, 2011; Pati *et al.*, 2016a). PLs can be distinguished by their hydrophilic headgroup and their hydrophobic tail and consequently differ in shape, size and charge. Given this molecular architecture and its diversity, PLs can modulate the biochemical properties of the membrane. Their fatty acyl chains for instance, are key factors for the determination of membrane fluidity. Unsaturated FAs from PLs have mostly a *cis* geometry of their double bonds, disrupting the linearity of the hydrophobic tail. This leads to distortions in the membrane bilayer, thereby increasing its fluidity (Hazel and Eugene Williams, 1990; Brown and Marnett, 2011). Moreover, the thickness of the membrane is dependent of the length and saturation level of the FAs and is even more increased relative to the amount of inserted cholesterol. Cholesterol is the major unpolar membrane constituent in mammalian cells, belonging to the class of sterols and known to straighten flexible FAs (Ledesma *et al.*, 2012; Lauwers *et al.*, 2016). The shape of PLs not only depends on the type and amount of bound FAs but also on the area their headgroup is occupying (Fig. 2.2). PC for instance, which constitutes over 50 % of PLs in the majority of eukaryotic membranes, possess two FA chains and a relatively big headgroup and thus has a cylindrical geometry. This geometry predicts a planar structure of the lipid bilayer. Other lipids with a smaller headgroup but two FAs, such as PA, PE or DAG have a cone shape. In turn, lysophosphatidylcholine (LPC), exhibits a big headgroup and only one FA chain and is thus shaped as inverted cone (Lauwers *et al.*, 2016). Insertion of cone shaped lipids in the membrane destabilizes the bilayer and thereby promotes curvature, which can even lead to spontaneous membrane fusion. Thus, cone shaped lipids are sometimes referred to as "fusiogenic" lipids and are also important for synaptic transmission, the communication between neurons and the basis for cognitive- and motor-function of the brain. A central event for synaptic transmission is the release of neurotransmitters stored in the synaptic vesicles upon action potential-induced  $\text{Ca}^{2+}$ -influx. This so called exocytosis of the neurotransmitters, occurs at the active zone of the presynaptic terminal that face the clustered neurotransmitter receptors on the postsynaptic density of another neuron (Südhof and Malenka, 2008). To render exocytosis, the energetically favorable interactions between PL headgroups and water must be overcome, so that the *cis*-leaflets (the inner leaflet of the plasma membrane and the outer leaflet of the vesicle membrane) of plasma membrane and synaptic vesicle come close enough together to fuse. This process can be supported by the insertion of cone-shaped PLs in the *cis* leaflet and inverse cone-shaped PLs in the *trans* leaflet of plasma membranes (Lauwers *et al.*, 2016). For instance, insertion of cone shaped PEs in a PC bilayer can induce curvature, whereas an increased amount of SM in a membrane bilayer reduces fusion efficiency in a model vesicle system (Haque *et al.*, 2001). Consistently, a study using phospholipases and electron microscopy revealed a heterogeneous PL composition in the leaflets of erythrocytes, with PC and SM accumulated in the outer leaflet, and PE and PS in the inner cytosolic leaflet (Verkleij *et al.*, 1973). A recently introduced lipid exchange study using cyclodextrins confirmed this

## INTRODUCTION

---

heterogeneous PL distribution between the leaflets of membranes in living mammalian cells (Li *et al.*, 2016). Since most of the lipid synthesis occurs at the cytoplasmic leaflet of the ER, flippases and scramblases catalyze the movement of lipids, which otherwise cannot easily flip from one leaflet to the other one (Downward, 2001; Pomorski and Menon, 2006), providing thereby an additional mechanism for regulation of the membrane activity. For instance, exposure of PS to the cell surface leaflet is known to be a receptor-mediated signal for phagocytosis (Leary *et al.*, 2000).

The distinct membrane lipid composition of the various organelles may also reflect their distinct functions. The mitochondria membrane is enriched in PE and changes in the PE/PC ratio, which is also a specific determinant for different human brain regions (Söderberg *et al.*, 1990), affects the mitochondria driven energy production via oxidative phosphorylation (van der Veen *et al.*, 2017). The ER membrane shows low concentrations of sterols and sphingolipids. Since sphingolipids consist mainly of saturated or trans-unsaturated FAs and by that are able to build narrower cylinders than PCs, they also pack tighter. The resulting relatively loose packing of ER membranes supports its function in the synthesis, insertion and transport of proteins and lipids. In contrast, the plasma membrane displays higher levels of sphingolipids and sterols and the resulting higher density allows more resistance against mechanical stress (Slotte and Ramstedt, 2007; van Meer, Dennis R. Voelker, *et al.*, 2008). Additional to the distinct lipid distribution of organelle membranes or between the two leaflets of a membrane bilayer, also lateral heterogeneity in membranes lipid composition is described. The active zone of synapses is enriched in PUFA-containing PLs. PUFAs fill more space in the hydrophobic core of the membrane and have a higher conformational flexibility, being thus able to circumvent energetically inefficient lipid packing and support membrane bending facilitating the synaptic vesicle fusion process (Antonny *et al.*, 2015).

Of particular importance is the lateral asymmetric lipid distribution for the function of integrated proteins. Such transmembrane proteins are another essential component of biological membranes. They span the bilayer and are essential for a plethora of functions including synaptic transmission. By controlling the membrane bilayer parameters, lipids are able to influence the function and fate of the integrated proteins. In the classical membrane fluid mosaic model, the lipid bilayer serves solely as two-dimensional solvent for proteins, which are able to freely move (Singer and Nicolson, 1972). Meanwhile, this reductionist concept has changed. Various lipid-lipid and lipid-protein interactions have been described that form functional lipid domains. Preferential association between cholesterol and sphingolipids for instance can lead to formation of relatively ordered and tighter packed (s.a.) sub micrometer (10-200 nm) membrane domains that display functional platforms and can recruit specific lipids and proteins (Simons and Ikonen, 1997). Such compartmentalized plasma membrane domains were termed "lipid rafts". Since lipid rafts elude

direct detection via microscopy, their existence and relevance is still under debate. However, recent findings enabled by advanced research techniques support the presence and function of such domains (Sezgin *et al.*, 2017). Several proteins, such as palmitoylated transmembrane proteins, glycosylphosphatidylinositol (GPI) anchored proteins and G-protein coupled receptor (GPCR) effector proteins are known to interact with lipid rafts (Simons and Toomre, 2000). Consistently, studies revealed that SMs can directly bind to and by that recruit specific proteins (Yamaji *et al.*, 1998; Contreras *et al.*, 2012). Moreover, it was described that clustering of neurotransmitter receptors and components of receptor-activated signaling cascades occur in lipid rafts (Allen *et al.*, 2007). Sphingolipids have been shown to be involved in clustering and stability of AMPA neuroreceptors in hippocampal neurons to ensure their proper function (Hering *et al.*, 2003). Additionally, the lateral mobility of proteins can be modulated by lipid domains of distinct viscosities and accelerated by increased membrane fluidity. Thus, the amount of the glutamate neuroreceptors NMDA and AMPA at the active zone of postsynapses is also influenced by such lateral diffusion within the plasma membrane from extrasynaptic areas (Choquet and Triller, 2003; Heine *et al.*, 2008; Bard and Groc, 2011). The presynaptic active zone is optimized for efficient neurotransmitter release and a highly skilled membrane remodeling machinery. 1 millisecond is enough for a synaptic vesicle to fuse with the plasma membrane upon an arriving action potential and this vesicle fusion can be maintained at a frequency of 100 Hz or higher (Lauwers *et al.*, 2016). Despite the enrichment of PUFA-containing PLs in the active zone, it contains the core machinery of exocytosis encompassing Q-SNAREs, Syntaxin 1 and SNAP25, as well as additional proteins, which function in membrane remodeling (Südhof, 2012). Negatively charged PSs are for instance shown to bind to the positively charged domain of the synaptic vesicle R-SNARE and the calcium sensor synaptotagmin-1, thereby regulating the efficiency of exocytosis (Williams *et al.*, 2009; Caccin *et al.*, 2015). Activity of proteins per se can also be dependent on the biophysical properties of membranes. Increased membrane thickness allows not only the integration of bigger transmembrane proteins, but together with membrane fluidity enables higher conformational plasticity of proteins and can therefore, be permissive for proper protein activation, as it is described for the photoreceptor rhodopsin (Wheeler *et al.*, 1975). Generally, the biophysical parameter of the membrane can be influenced by the activity of lipid kinases, phosphates and hydrolases, thus offering additional regulatory mechanism (Sengupta *et al.*, 2007). Hydrolysis of membrane PLs is performed by enzymes collectively known as phospholipases encompassing PLA<sub>1</sub>, PLA<sub>2</sub>, PLC, PLD and their isoforms, respectively. Since several lipases show calcium sensitivity, localized calcium influx at the active zone may lead to specified production of fusiogenic lipids, such as PA, hence supporting synaptic transmission (Ledesma *et al.*, 2012).

Beside the plentitude of functions exerted by PLs as the main membrane components, they also serve as signaling molecules, involved in a plentitude of cellular processes, such as the case of

## INTRODUCTION

---

lysophosphatidylcholine (LPC) and lysophosphatidic acid (LPA) via platelet-activating factor receptors, GPCRs or PPARs, as well as reservoir for downstream lipid signals, e.g. eCBs (Huang *et al.*, 1999; J Choi and Chun, 2013; Xiang *et al.*, 2013; Ong *et al.*, 2015; Lerner *et al.*, 2016).

### 2.1.2 Endocannabinoids

The endocannabinoid system (ECS) represents an excellent example for lipid signaling. It encompasses two G-Protein coupled cannabinoid receptors (CB1 and CB2 receptor), the lipophilic eCBs acting as their endogenous ligands, and the synthesizing and degrading enzymes of these ligands. Its name derives from the plant *cannabis sativa* whose main psychoactive compound,  $\Delta^9$ -tetrahydrocannabinol (THC) was first isolated and described in 1964 (Gaoni and Mechoulam, 1964) and found to act through a receptor finally cloned and termed CB1 receptor in 1990 (Matsuda *et al.*, 1990). The first identified eCB was arachidonoyl ethanolamide (AEA), in 1992 (Devane *et al.*, 1992), termed anandamide coined from the Sanskrit word “Ananda” meaning bliss. Three years later, in 1995, 2-arachidonoylglycerol (2-AG) was the second endogenous ligand found to be acting on CB receptors (Mechoulam *et al.*, 1995). While 2-AG represents a full agonist of both CB1 and CB2 and was found to be highly concentrated in the brain, AEA is only a partial agonist for both receptors and of lower concentration (Gonsiorek *et al.*, 2000; Lerner *et al.*, 2016).

Beside these two major eCBs, additional compounds including 2-arachidonoyl glyceryl ether (noladin ether), O-arachidonoyl ethanolamine (virodhamine) and N-arachidonoyl dopamine (NADA) were identified as eCBs (Porter *et al.*, 2002; Redmond *et al.*, 2016). eCB-like structures, that are, N-palmitoyl ethanolamide (PEA) and N-oleoyl ethanolamide (OEA), have also been shown to accompany the eCBs in tissues, possibly as competitors to eCBs for catabolic enzymes, a feature called ‘entourage’ effect (Lambert and Di Marzo, 1999). eCBs belong to the fatty acyls and glycerolipids, likewise PLs, lipid categories originating from the “ketoacyl building block” (Fahy *et al.*, 2011) (Tab. 2.3).

**Table 2.3 LIPID MAPS classification system – eCBs and ERCs:** Classification of eCBs and ERCs based on the classification system developed by the International Lipid Classification and Nomenclature Committee on the initiative of the LIPID MAPS Consortium (LIPID MAPS Nature Lipidomics Gateway, <http://www.lipidmaps.org>). Matching colors define eCBs and ERCs and their specific lipid classes, respectively.

<b>Fatty Acyls [FA]</b>	
<b>Fatty Acids and Conjugates [FA01]</b>	<b>Arachidonic acid (AA)</b>
Octadecanoids [FA02]	
Eicosanoids [FA03]	
Docosanoids [FA04]	
Fatty alcohols [FA05]	
Fatty aldehydes [FA06]	
Fatty esters [FA07]	
Fatty amides [FA08]	Anandamide (AEA)
Fatty nitriles [FA09]	N-oleoyl ethanolamine (OEA)
Fatty ethers [FA10]	N-palmitoyl ethanolamine (PEA)
Hydrocarbons [FA11]	N-arachidonoyl dopamine (NADA)
Oxygenated hydrocarbons [FA12]	
Fatty acyl glycosides [FA13]	
<b>Other Fatty Acyls [FA00]</b>	<b>Virodhamine (O-AEA)</b>
<b>Glycerolipids [GL]</b>	
<b>Monoradylglycerols [GL01]</b>	<b>2-Arachidonoylglycerol (2-AG)</b>
Diradylglycerols [GL02]	<b>2-Arachidonoyl glycerol ether (2-AGe)</b>
Triradylglycerols [GL03]	
Glycosylmonoradylglycerols [GL04]	
Glycosyldiradylglycerols [GL05]	
Other Glycerolipids [GL00]	

eCBs are bioactive lipids generated *de novo* or on-demand from membrane PL precursors through neuronal stimulation via increased intracellular calcium ion levels and, in turn, serve themselves as precursors to other bioactive molecules such as eiCs (Fig. 2.3) (Marsicano, Stelt, *et al.*, 2003; Rouzer and Marnett, 2011).

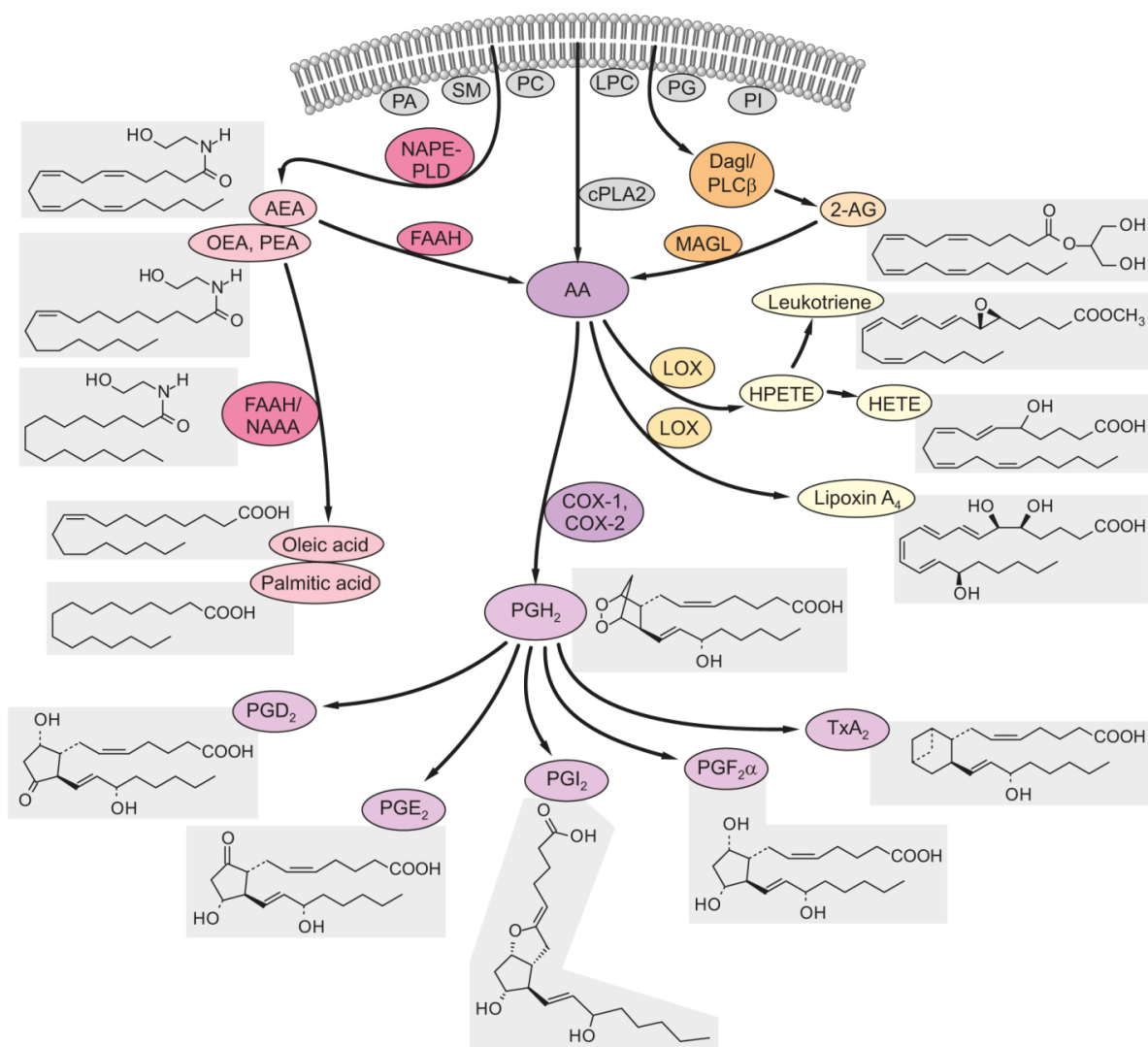


**Figure 2.3 Interplay of lipid signaling:** Schematic representation of the interplay between PLs, eCBs, NAEs and eiCs. Membrane PLs serve as precursors for OEA and PEA as well as for the eCBs, AEA and 2-AG. The resulting AA is enzymatically metabolized to various eiCs through LOX or COX dependent oxidation (from Lerner et al., 2016).

Both 2-AG and AEA are derivatives of AA (Fig. 2.2). AA, OEA and PEA are further referred to in this work as eCBs related compounds (ERCs). Synthesis of 2-AG is catalyzed by two sn-1-specific diacylglycerol lipases (DAGL- $\alpha$  and DAGL- $\beta$ ) from 1,2-diacylglycerols (DAG), which can be generated from phosphorylated PI species through the phospholipase C  $\beta$  (PLC $\beta$ ). DAGL- $\alpha$  exerts a primary role in the brain, whereas DAGL- $\beta$  acts mainly in peripheral tissues (Bisogno *et al.*, 2003). The enzymatic transfer through the serine hydrolase PLA2G4E of AA from the sn-1 position of membrane PLs to the primary amine of PE generates N-arachidonoyl phosphatidylethanolamine (NArPE), which serves as precursor for AEA (Ogura *et al.*, 2016). The direct hydrolysis of NArPE to AEA is carried out by N-acyl phosphatidylethanolamine-selective phospholipase D (NAPE-PLD). However, also distinct mechanisms are proposed by which NArPE is converted to AEA. For instance, PLA<sub>2</sub>-driven O-deacylation of NArPE and subsequent



hydrolysis of the phosphodiester bond via a lyso-PLD enzyme, sequential deacylation by lyso(NAPE)-lipase hydrolase 4 (ABHD4) and subsequent glycerophosphodiesterase 1 (GDE1)-induced cleavage of the phosphodiester bond, as well as conversion to phospho-AEA through a phospholipase C (PLC)-like enzyme followed by tyrosine phosphatase (PTPN22) or inositol phosphatase (SHIP) catalyzed dephosphorylation (Blankman and Cravatt, 2013)

A plethora of effects is mediated via eCBs signaling (Piomelli, 2003; Castillo *et al.*, 2012). While CB1 is the most abundant G-protein coupled receptor in the brain, CB2 is primarily located in the periphery and involved in the immune system (Marsicano and Lutz, 1999; Malfitano *et al.*, 2014). A special characteristic of the ECS is the retrograde signaling of its ligands to perform synaptic regulation and thereby, ensuring a potential feedback mechanism for the information flow between neurons (Kano *et al.*, 2009). Therefore, the postsynaptically released eCBs travel through the synaptic cleft to the presynapse. The mechanism behind this movement of the highly hydrophobic eCBs through the extracellular space is not yet completely understood. Activation of the presynaptically localized CB1 receptor results in presynaptic inhibition of transmitter release, which can occur as depolarization induced suppression of inhibition (DSI) involving decreased  $\gamma$ -aminobutyric acid (GABA) release of interneurons or depolarization induced suppression of excitation (DSE), resulting in a decreased release of glutamate. Several mechanisms underline the inhibited transmitter release, including suppression of presynaptic voltage-gated calcium ion channels (Diana and Marty, 2004). Retrograde signaling implies the main eCB synthesis site to be postsynaptically located, as shown for DAGL (Katona and Freund, 2012). NAPE-PLD, in contrast, is found to be located in both the presynapse and postsynapse. Noteworthy, it was shown that AEA can also act anterogradely on postsynaptic transient receptor potential cation channel subfamily V member 1 (TRPV1) (Chávez *et al.*, 2010). Degradation to AA through different enzymes terminates the eCBs signaling. Fatty acid amide hydrolase (FAAH) catalyzes the hydrolysis of AEA, whereas 2-AG is predominantly hydrolyzed via monoacylglycerol lipase (MAGL) (Deutsch *et al.*, 2002; Nomura *et al.*, 2008). A minor part of 2-AG can also be degraded by the enzymes  $\alpha$ - $\beta$  hydrolase 6 (ABHD6) and  $\alpha$ - $\beta$  hydrolase 12 (ABHD12), which due to their distinct subcellular distributions in a compartment-selective manner, may control different 2-AG pools *in vivo* (Blankman *et al.*, 2007; Savinainen *et al.*, 2012). Furthermore, cyclooxygenase (COX), lipoxygenase (LOX) or cytochromes P450 induced oxygenation of eCBs or their metabolic product AA is known to generate prostaglandins, leukotrienes and related derivatives, which can induce inflammation (Nomura *et al.*, 2011; Rouzer and Marnett, 2011).

Altogether the data collected so far on the eCBs signaling and PLs function strongly support their necessity for body homeostasis and predict their involvement in diseases.

### 2.1.3 Clinical relevance

Investigations revealed that the application of the plant *cannabis sativa* as psychoactive or medicinal agent may date back to 3500 BC (Solymosi and Kofalvi, 2017) and cannabis extracts have been used as pharmacological treatment for epilepsy since centuries (Mechoulam and Lichtman, 2003). Hippocrates was known to exploit leaves of the willow tree to treat pain and fever already 400 BC. Their ingredient salicylic acid serves also as an important active metabolite of acetylsalicylic acid known as aspirin, which was synthesized for the first time in 1897 and is meanwhile one of the most commonly used pain killers worldwide. Further research in this field led to the development of novel, now frequently used, non-steroidal anti-inflammatory drugs (NSAIDs) (Norn *et al.*, 2009). Thus, the use of lipophilic components, or those that modulate lipid metabolism, for treatment of disease, has a longstanding practice. About 5 % of the genome exists only to ensure lipid diversity (van Meer, Dennis R. Voelker, *et al.*, 2008) and lipids represent 60 % of the human brain content (Chang *et al.*, 2009), which is a further indicator of the importance of proper lipid function for healthy development. Consequently and considering also all the physiological processes lipids are mandatory for as described above, it is not surprising that disturbance of the lipid metabolism can lead to the development of several diseases. Hence, a growing number of studies address the role of lipid function in disease. As main energy provider, it is very likely that lipids are involved in the metabolic syndrome as well as its accompanying symptoms, such as cellular stress and increase in production of reactive oxygen species (ROS), inflammation and insulin resistance (Wymann and Schneider, 2008; Lamari *et al.*, 2013). Metabolic syndrome is often caused by constant oversupply of energy rich nutrients, especially saturated FAs and sterols, accumulation of which can lead to cellular damage through stress on membranes. In particular, the ER membrane, which is also main source of ROS, is sensitive to this kind of stress (Wei *et al.*, 2006) and elevated levels of ROS in turn can induce insulin resistance (Houstis *et al.*, 2006). However increased plasma levels of free FAs are already sufficient to provoke insulin resistance (Boden *et al.*, 2005) and saturated FAs are known to induce COX2 mediated pro inflammatory response via Toll-like receptors (Lee *et al.*, 2001). Orlistat, a drug developed and used to treat obesity, displays an inhibitor of hormone-sensitive lipase, thereby reducing the levels of free FAs.

Impaired neuronal functions are often associated with lipid dysregulation (Ong *et al.*, 2015; Iannotti *et al.*, 2016). Glia cells, astrocytes and neurons belong to the cells that compose the brain. Their membranes are critical factors to maintain ion and chemical balance and to ensure their proper functioning. Hence lipids play a crucial role in brain development and synaptic plasticity (Chevalleyre *et al.*, 2006; Chang *et al.*, 2009; Ledesma *et al.*, 2012). Disturbances may lead to neurodegeneration (Farooqui *et al.*, 2004), as occurs during aging (McGahon *et al.*, 1998; Favrelère *et al.*, 2000; Bilkei-Gorzo, 2012; Ledesma *et al.*, 2012). Burger and Rouser showed for the first time possible changes of membrane lipid composition in human brain during aging

(Ledesma *et al.*, 2012). Increment of SM levels with aging was found in different rat brain regions (Giusto *et al.*, 1992) as well as in synaptosomes of mice (Yamamoto *et al.*, 2008) and may evidence possible adaptation of membranes to prevent neuronal cell loss, by recruiting survival receptors through lipid rafts (Paratcha and Ibáñez, 2002). For instance, activation of the neurotrophin receptor TrkB, which is also involved in neuronal survival, is known to be modulated by SM (Trovo *et al.*, 2011). Vice versa, a strong increase in SM levels may point towards reduced fusion efficiency and thus decreased synaptic transmission, because of the low curvature of SM-enriched membranes (Cheng and London, 2011). A reduction of PUFA levels was detected with aging, in particular of AA and docosahexaenoic acid (DHA) in the hippocampus of rats (McGahon *et al.*, 1998). This decrease can negatively influence synaptic transmission as described in 2.1.1. Consistently, a study revealed that the age-related impairment in LTP could be reversed by dietary restoration of DHA and AA levels in rat brain (McGahon *et al.*, 1999). The decrease in PUFA levels is associated with an increase in desaturase activity. Since enhanced amounts of PUFAs can render increase in pro inflammatory response and toxic products (s.a.), their age-associated reduction could be also a protective mechanism (Ledesma *et al.*, 2012). Of course, neurodegeneration is also a common factor in neurological disorders. Neurodegeneration in ischemia, neuronal trauma and Alzheimer disease (AD) may arise through cytosolic PLA<sub>2</sub> (cPLA<sub>2</sub>) and plasmalogen-selective PLA<sub>2</sub> (PLsEtn-PLA<sub>2</sub>) induced alterations in PL metabolism and the accompanying accumulation of lipid peroxides (Farooqui *et al.*, 2004). In line with this, the PE content of synaptosomal membranes was found to be reduced (Viani *et al.*, 1995) and free FAs markedly increase in the brain via PLA<sub>2</sub> activity in ischemic injury (Bazán, 1970). Alterations of PL levels were also shown for AD (Kosicek *et al.*, 2010; Zhu *et al.*, 2015). Levels of PE and PI were found to be decreased in neural membranes of AD patients in a brain regions specific manner (Prasad *et al.*, 1998) and cPLA<sub>2</sub> activity was likewise elevated in human AD brain (Stephenson *et al.*, 1996). Moreover, a study evidenced that such changes in PLs composition can occur before any clinical manifestation of the disease (Pettegrew *et al.*, 1995) hence disturbed PL metabolism can be involved in the genesis of disease and represents thus a possible target for their early diagnosis. It is also apparent that membrane thickness determines the cleavage site of the gamma-secretase substrate, whose abnormally folded fibrillary form is the primary component of amyloid plaques found in the brains of AD patients. Thicker membranes allow better alignment of the enzyme and its substrate, minimizing thereby hydrophobic mismatch and producing more of the less toxic A $\beta$ 40 peptide instead of the AD associated A $\beta$ 42/43 peptide (Winkler *et al.*, 2012). Mutations in the gene encoding the calcium-independent PLA<sub>2</sub> (iPLA<sub>2</sub>) generally underlie a phenotypic spectrum of neurodegenerative disease termed phospholipase-associated neurodegeneration (PLAN) (Karkheiran *et al.*, 2015). An increasing number of studies has also evidenced the implication of PLs in the neurological disorders Parkinson's disease (Wang *et al.*, 2014; Abbott *et al.*, 2015), Huntington's disease (Mehrotra *et al.*, 2015; Vodicka *et al.*, 2015) as well, as in neuropsychiatric disorders such as schizophrenia (SCZ) (McEvoy *et al.*, 2013; Mirendil

## INTRODUCTION

---

*et al.*, 2015) major depressive disorder (MDD) and bipolar disorder (BD) (Sethi *et al.*, 2015). Enhanced levels of PCs, PEs, LPCs and LPEs and decreased levels of free FAs were found in plasma of patients suffering from MDD (Liu *et al.*, 2015). Reduced concentrations of different PUFAs, especially AA, were also detected for SCZ patients (Skosnik and Yao, 2003). Another study showed significant changes in the levels of free FAs and PC in brain tissue of SCZ and BD patients (Schwarz *et al.*, 2008). Upregulation of brain AA metabolism in BD was indicated in post-mortem studies and chronically given mood stabilizers such as lithium, carbamazepine, olanzapine and valproate are effective for BD treatment by downregulating AA turnover (Rapoport *et al.*, 2009). Moreover, SCZ patients exhibit increased PL breakdown of PC and SM but enhanced concentrations of PS. The increased PL breakdown in SCZ may be associated with decreased myelination and oligodendrocyte dysfunction, as PC is also the choline donor to SM, one of the main myelin membrane components (Schmitt *et al.*, 2004). LPA signaling was also proposed to contribute to demyelination, causing neuropathic pain (Velasco *et al.*, 2017).

Finally, a plethora of studies is likewise evidencing the implication of eCB signaling in numerous physiological processes such as brain development (Harkany *et al.*, 2008), synaptic plasticity (Chevalleyre *et al.*, 2006), learning and memory (Marsicano and Lafenêtre, 2009), as well as emotion (Lutz, 2009). Furthermore, the therapeutic potential of eCBs in several pathophysiological states, including anxiety, stress and fear (Lutz *et al.*, 2015), pain (Lomazzo *et al.*, 2014), Parkinson (Kreitzer and Malenka, 2007), SCZ (Saito *et al.*, 2013) and AD (Karl *et al.*, 2012), but also in cardiovascular diseases (Cannon, 2005) and obesity (Vemuri *et al.*, 2008; Massa *et al.*, 2010), has been described.

Thus, the ECS represents a valuable target of pharmacotherapy (Pacher *et al.*, 2006). Yet, development of medical drugs requires high specificity to preclude unwanted effects. Rimonabant, a drug to treat obesity released by Sanofi Aventis, is a relevant example. As blocker of the CB1 receptor, it can decrease appetite and improve fat, glucose and cholesterol metabolism (Wierzbicki, 2006), but it also became clear that it can induce depressive symptoms and suicidal behavior (Moreira and Crippa, 2009). Since activity of lipids encompass so many physiological processes, it is essential to increase our understanding of the detailed role of lipid function for more targeted pharmaceutical treatment and reduction of such possible side effects.

### **Epilepsy**

Epilepsy is a common neurological disorder, which affects about 1% of the worldwide human population (Xu *et al.*, 2013). It is characterized by recurrent seizures, with a broad spectrum of manifestations. Multiple possible causes of epilepsy were identified so far, including genetic, physiological, metabolic factors, but about 60% of the epilepsy cases have unknown causes (Cully, 2014; Narain, 2014; Amini *et al.*, 2015). This reflects in the multiple types of epilepsy,

which were categorized according to the brain regions involved as follows a) partial epilepsy affects one brain part and is often the result of an accident; b) generalized epilepsy, which affects most or all of the brain and can lead to unconsciousness, falling and jerky convulsions; c) frontal lobe epilepsy is associated with motor function loss and can lead to alterations in personality, and d) temporal lobe epilepsy (TLE) which mainly occurs in the limbic system and is associated with memory loss and emotional dysfunctions.

Research in epilepsy lags far behind that of other neurological disorders such as Parkinson or AD. Despite its higher incidence in the human population, cultural and religious stigma substantially contribute to this aspect (Savage, 2014). Available therapeutic treatments mostly address the frequency, duration and extent of the seizures, but not their reoccurrence and/or epileptogenesis. Moreover, 30-40% of the patients exhibit drug resistance, especially those suffering from TLE. Although TLE responds well to surgery (80% success rate), post-surgery reoccurrence of seizures remains a concern (Eisenstein, 2014; Savage, 2014). In the last decade, the essential role of inflammation in the onset of epileptic disorder has been recognized, where by it is assumed that brain inflammation defines seizure threshold in specific, susceptible brain regions. In addition, a positive feedback loop between brain inflammation and peripheral immune responses was assumed to mainly cause epileptogenesis. Briefly, the recurrent seizures lead to up-regulation of pro-inflammatory mediators, such as AA-derived eiCs (Harizi *et al.*, 2008), and an activation of the immune response to further increase seizure susceptibility, promote neuronal excitability and induce the breakdown of the blood brain barrier (BBB) (Vezzani *et al.*, 2013; Xu *et al.*, 2013). On another hand, AA-derived eiCs serve under certain conditions also as anti-inflammatory mediators and are involved in immune responses or autoimmune disorders. Brain inflammation processes, especially caused by COX-2 signaling pathways, are associated with BBB damage and assumed to mainly contribute to epileptogenesis (Serrano *et al.*, 2011; Vezzani *et al.*, 2013). Pro-inflammatory signaling molecules exert also essential roles after brain injuries, which can initiate the onset of neurodegenerative dysfunctions. Hence neuroinflammatory conditions enhance the risk of neurological disorders, such as epilepsy (Farooqui *et al.*, 2000; Vercueil, 2006; Tassoni *et al.*, 2008; Kosicek and Hecimovic, 2013).

Several studies using different epileptic seizure models have revealed specific alterations of PL metabolism (Yegin *et al.*, 2002; Guan *et al.*, 2006; de Freitas *et al.*, 2010) and neuroprotective effects of the ECS, as well as of eCB-related molecules, such as OEA and PEA against excitotoxicity (Lutz, 2004; Monory *et al.*, 2006; Guggenhuber *et al.*, 2010; Bojnik *et al.*, 2012; Chiarlone *et al.*, 2014; Fezza *et al.*, 2014; Flemming, 2014; Mattace Raso *et al.*, 2014). Excitotoxicity is a process, which can be induced by excessive glutamate release, in particular during epileptic seizures, and can lead to neuronal death. Enhanced 2-AG levels for instance were shown to exert a counteracting role against excitotoxicity (Soltesz *et al.*, 2015). Since eCBs

are synthesized from membrane PLs and enzymatically degraded to AA, the precursor for eiCs synthesis, metabolism of PLs, eCBs and eiCs is interrelated (Fig. 2.3) (Smith, 1989; Vila *et al.*, 2007; Nomura *et al.*, 2011; Alhouayek and Muccioli, 2014). Thus inhibitors of PLA<sub>2</sub>, which mediates AA release from PLs, act at an early step in the biosynthesis of inflammatory mediators. The cPLA<sub>2</sub> inhibitors Quinacrine and arachidonyl trifluoromethyl ketone for instance have been reported to reduce neurodegeneration caused via kainic acid (KA)-induced excitotoxicity (Lu *et al.*, 2001; Ong *et al.*, 2003). However, these inhibitors are non-specific and an ideal PLA<sub>2</sub> inhibitor should be harmless and display regional specificity.

Altogether the involvement of lipids in the onset and developmental course of diseases provides further potential in the development of new agents for therapeutic interventions, and in the discovery of plasma biomarker discovery for early diagnosis and follow-up monitoring (Kegel-Gleason, 2013; Rosenthal and Kamboh, 2014; Holemans *et al.*, 2015). Accordingly, quantitative determination of the reference and altered concentrations of lipids in various biological tissues is imperative to dissect their function and site of action and discover new drug targets. This led us to establish methods within our lab for the identification and quantification of various lipid species from different tissues as perspective tool for the investigation of pathological conditions, and from biological fluids such as plasma for prospective biomarkers and predictor markers for epilepsy development and therapy monitoring. Since PL and eCB involvement in epilepsy is supported by several studies, we used KA-induced excitotoxicity, which models the acute phase in epileptiform seizures, as application system to proof the reliability of the here developed methods and to get further insights into the lipid plasticity associated with epileptic seizures. The established lipidomic approach is based on tailored lipid extraction in conjunction with quantitative liquid chromatography/ mass spectrometry (LC/MS).

### 2.2 Mass spectrometry of lipids

Lipidomics, initially defined by Han and Gross (Han, 2003), is a branch of metabolomics, and is along with proteomics, transcriptomics and genomics part of “omics” research field. Huge progress was made in the field of lipidomics over the last decades, but it still needs advancement to reach the same level of knowledge as genomics, transcriptomics and proteomics. In contrast to genes and proteins, which are mainly built up by a linear combination of 4 nucleic acids and 20 amino acids, respectively, lipids display a higher structural diversity, hence heterogeneity due to more diverse chemical bonds, functional groups, structural branching etc. which in turn renders a broader range of chemical and biophysical properties (s.a.). This structural complexity is a main reason why lipidomics has lagged behind the other “omic” approaches (Zhao *et al.*, 2014).

However, ongoing advances in mass spectrometry (MS) have greatly improved the ability of lipid detection, identification and quantification in complex biological systems, bringing lipidomics to the realm of the other “omic” strategies (Wenk, 2010; Yang and Han, 2016; Sethi and Brietzke, 2017a).

MS is an analytical technique, which enables the determination of ionized molecules by their mass to charge ( $m/z$ ) ratio, based on the concept that the ions can be manipulated using electric and magnetic fields. Several scientists were involved in the development of the mass spectrometer. In 1886 the basis was set by the German physicist Eugene Goldstein, who described for the first time the presence of positively charged anode rays, which traveled in straight lines in a perforated cathode (Goldstein, 1898). The German physicist Wilhelm Wien discovered, that these so called “Kanalstrahlen” (canal rays) were deflected in a magnetic field and invented based on that the “*Wien Filter*”, a device to separate the positive rays according to their  $m/z$  ratio (Wien 1898). Further work and refinement by reducing the pressure to create vacuum led in 1913 to the development of the mass spectrograph through the British physicist John Joseph Thomson (Dahl, 1997). Finally, in 1918 and 1919, the Canadian-American physicist Arthur Jeffery Dempster and the student of Thomson, Francis William Aston independently designed the first modern mass spectrometers (Dempster, 1918; Aston, 1919). A mass spectrometer consists of three fundamental parts, the ion source, the mass analyzer and the detector (Fig 2.4).

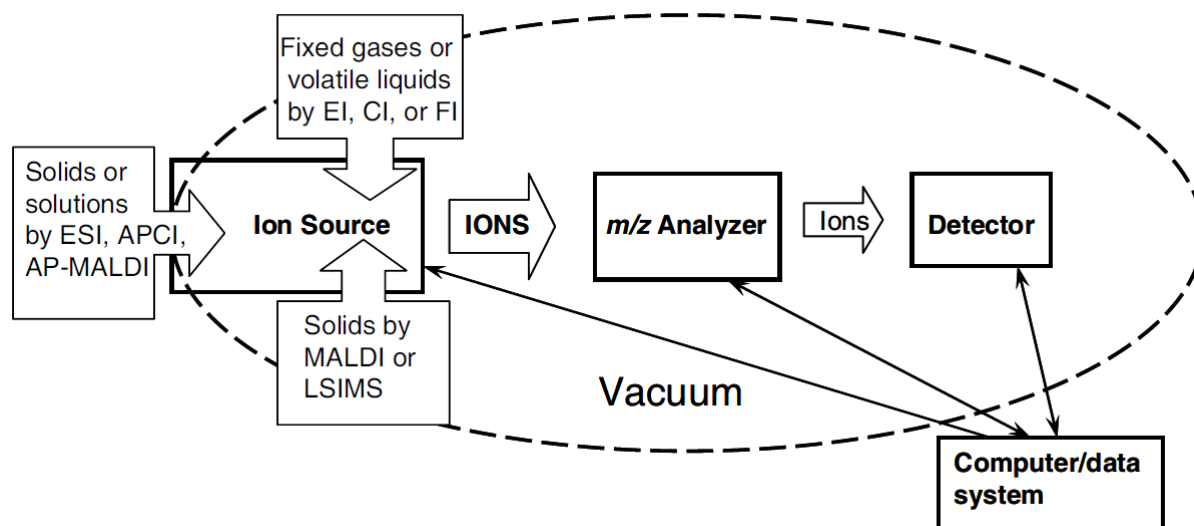


**Figure 2.4 Conceptual illustration of a mass spectrometer:** This conceptual illustration of the mass spectrometer shows its fundamental components, i.e., sample inlets; ion source;  $m/z$  analyzer; detector; vacuum system and the computer (from Watson and Sparkman, 2007).

The front end located ion source generates at first gas phase ions from the analytes. These ions are then separated by their specific  $m/z$  ratio in the mass analyzer. Here, an evacuated

## INTRODUCTION

---

environment is required to provide a collision free path for the ions to reach the detector, on one hand and not to get decomposed before detection, on the other hand. In order to obtain the mass spectrum, the detector monitors the ion current and transmits the arising signal to the data system, which plots the  $m/z$  values against their intensities (Watson and Sparkman, 2007).

Existence of ions in the gas-phase is mandatory for the following separation process and various types of ion sources emerged. Initially methods for the ionization process such as electron ionization (EI) first used by Dempster in his 1918 developed mass spectrometer, are more aggressive and led often to in-source fragmentations of the analyzed molecules (Dempster, 1918). With the development of chemical ionization (CI), a softer ionization method was introduced in 1966, since it is based on ion/molecule reactions instead of electron removal and therefore needs less energy (Munson and Field, 1966). However, both still very valuable methods require gas-phase molecules to create gas-phase ions (Watson and Sparkman, 2007). Measurement of nonvolatile and thermally labile molecules became possible with the invention of desorption/ionization (DI) techniques in 1969 (Beckey, 1969). The commonly used fast atom bombardment (FAB) for instance, which was developed in 1981, allows generation of gas-phase ions directly from the condensed phase, enabling thereby the protection of the analytes via a nonvolatile chemical environment, termed matrix (Barber *et al.*, 1981). Nanomole concentrations of the analyte were sufficient, using this method, to generate reliable mass spectra. Another very soft DI technique, developed 1985, was the matrix-assisted laser desorption/ionization (MALDI), requiring only picomoles or femtomoles of the analyte (Karas *et al.*, 1985). High sensitivity can be also achieved by spray ionization methods such as atmospheric pressure chemical ionization (APCI) developed in 1973 (Horning *et al.*, 1973) or electrospray ionization (ESI) first reported in 1984 (Yamashita and Fenn, 1984). The latter generates aerosol particles from a liquid solution through application of a high voltage. Unlike FAB and MALDI, these ion sources do not require vacuum conditions for ionisation, but atmospheric pressure. Improvements in technology enabled the generation of ion sources, which allow alternate on-line ESI and APCI scans, or ESI and MALDI (Gallagher *et al.*, 2003). While the ionization using APCI occurs in the gas phase, ionization via ESI occurs in the liquid phase. APCI is more suited than ESI for thermally stable compounds. ESI has a distinct advantage of which enabling the formation of multiply charged ions, thereby extending the mass range of the analyzed molecules. Due to the capability of ESI as well as MALDI to ionize thermally labile and non-volatile analytes and in combination with mass analyzers to render the ionization/detection at low femto- to atomolar range, MS evolved as a fundamental molecular analytical technique in biological science.

Following the ionization process the resulting ions are separated by the mass analyzer. Various systems emerged, such as time-of-flight (TOF), quadrupoles or Fourier transform ion cyclotron resonance (FTICR) separating ions according to the  $m/z$  values in space and/or time, differing in



their mass accuracy, resolution, sensitivity, dynamic range and ability for tandem MS approaches, thus all owning specific advantages and disadvantages, respectively. The first TOF mass spectrometer was built in 1948 by A. Cameron and D. Eggers (Cameron and Eggers, 1948). As the name implies, ions are separated in this mass spectrometer by the time they need to reach the detector. They are instantaneously accelerated by an electric field, so that ions with the same charge receive the same kinetic energy. When they traverse the integrated “field-free” tube, they have different velocities as a function of their  $m/z$  values, thus ions with higher  $m/z$  values are slower and need more time to reach the detector (Mamyrin, 2001). This operating principle of ion separation has the advantage of no upper  $m/z$  limit.

Resolving power is the difference in  $m/z$  values of ions that still can be separated from each other and can be calculated using the full width at half-maximum height (FWHM) method (Watson and Sparkman, 2007). In order to improve the resolving power, a reflectron can be used. This kind of ion mirror corrects for different energy distribution of ions, since ions with higher energy penetrate deeper into the mirror and compensate thereby their higher velocity and thus it promotes focusing of ions with the same  $m/z$  values. In this way resolving powers up to 20,000 FWHM can be reached (Mamyrin, 1994). In 1953 Wolfgang Paul and colleagues developed the first transmission quadrupole mass analyzer (Paul and Steinwedel, 1953), which found its way into the analytical laboratories in the mid-1960s. Due to the easier handling and cheaper manufacture of the quadrupole, its request quickly expanded and set the basis for the ubiquitous use of MS today. The quadrupole consist of four cylindrical, parallel electrodes with a voltage applied between. The resulting two-dimensional oscillating electric field pushes and pulls ions during their way along the  $z$  axis. Depending on the applied voltage only ions with specific  $m/z$  ratio have a stable trajectory through the quadrupole and are allowed to pass to the detector. Thus, by adapting the voltage one can filter the ions of interest according to their  $m/z$  ratio (Miller and Denton, 1986). A useful feature is the possibility to connect transmission quadrupoles in line as it is realized for the triple quadrupole, which was developed by J.D. Morrison (Morrison, 1991) leading to the triple quadrupole mass spectrometer (TQMS), which became for the first time commercial available in the late 1970s (Yost and Enke, 1978). This advanced arrangement offers the additional capability for tandem mass spectrometry (MS/MS) and the TQMS still represents the most common tandem-in-space mass spectrometer today. For this operation mode the first and third quadrupole are used as  $m/z$  analyzer, separated by another quadrupole that serves as a collision cell. The induced fragmentation of specific ions, occurring in the collision cell, can be used for additional validation of the analytes of interest (Hoffmann, 1996). Another invention Wolfgang Paul is credited for, is the quadrupole ion trap (QIT), which became for the first time in 1983 commercially available as component of a mass spectrometer (March, 1997). This type of ion trap uses dynamic electric fields, to trap ions of specific  $m/z$  values. One can differentiate the 3D QIT mass spectrometer, which uses a three-dimensional electric field for ion trapping in

## INTRODUCTION

---

concentric orbitals and the linear ion trap (LIT), which's structure is analogue to the transmission quadrupole, but instead of filtering specific ions, it is used to trap them, allowing subsequent ejection of ions with specific  $m/z$  values (March, 1997; Londry and Hager, 2003). Integration of the LIT as the third stage of a triple quadrupole instrument was also realized with the QTRAP (Hager and Yves Le Blanc, 2003). The orbitrap is the most recent addition in trapping devices used as  $m/z$  analyzer, developed by A. Makarov (Makarov, 2000). In contrast to the dynamic electric field applied by the quadrupole ion trap it makes use of a static electrostatic field. The improved technology of the orbitrap makes it in specific cases capable to high mass resolving powers even above 1,000,000 FWHM (Denisov *et al.*, 2012). Another high mass resolution instrument is the FTICR mass spectrometer, developed 1974 by Marshall and Comisarow (Comisarow and Marshall, 1974), based on the knowledge, that ions move in a magnetic field at a frequency according to their  $m/z$  ratio. Since frequency can very accurately be determined, it possess high potential for precise mass resolution, which can exceed 1,000,000 FWHM (Weisbrod *et al.*, 2008). Moreover, this system allows increment of sensitivity and resolution by prolonged measurement time. Both, orbitrap as well as FTICR can also be used for tandem-in time MS. Further potential for improved sensitivity and resolution can be achieved by combining different operating systems thus creating so called hybrid instruments. Such mass spectrometers are also capable for in-space MS/MS, as it is the case for the transmission quadrupole-TOF (Q-TOF) mass spectrometer or the TOF-TOF mass spectrometer (Watson and Sparkman, 2007). Another device used in hybrid instruments is the ion mobility spectrometry, which makes use of a flight tube similar to TOF mass spectrometers, called ion-mobility cell, where unlike TOF instruments the ions drift under the influence of an electric field, allowing additional ion separation due to their size or cross-sectional area. The Synapt is such a commercially available hybrid instrument, which integrates ion mobility spectrometry with MS (Craven, 2013).

Chromatography is another very valuable tool to improve analyte separation and is often used as a front end technique to mass spectrometers. Chromatography was developed and first described 1903 by Mikhail Tswett (Ettre and Sakodynskii, 1993). This separation technique makes use of the principle that distinct molecules partition differently between various solvents and surfaces. Accordingly, to induce the separation, a molecule mixture is dissolved in a mobile phase, which transports the molecules along another composed stationary phase. Molecules with a higher affinity for the surfaces of the stationary phase travel slower and thus need more time for passing through e.g. eluting. This time needed for elution is called the retention time (RT) and is specific for distinct analytes. Depending on the type of the mobile phase, one can differentiate gas chromatography (GC) from liquid chromatography (LC). Both methods can be carried out with the stationary phase placed within a column (Levinson, 2001). Improvement of LC led to the development of high performance liquid chromatography (HPLC) with significantly higher operational pressures applied. In order to implement on-line separation and detection of analytes

with MS, chromatography can be used as a direct inlet system for MS. On-line coupling of GC to MS was for the first time described in 1959 (Gohlke, 1959) and was for a long time the predominantly used system since the concurrent EI and CI still required gas phase analytes for further processing. Thus, introduction of DI techniques enabled the use of LC/MS. However, suitable ion sources for LC coupling still represented a main limiting factor, as not only conversion of molecules from the condensed to the gas phase needed to be achieved, but also the removal of the liquid solvent while maintaining an operational vacuum in the mass analyzer. Introduction of ESI for the first time addressed both of these problems and opened the door for the effective use of LC/MS today (Pitt, 2009).

Onset of the modern lipidomics research via MS can be tracked back to the 1990s, even though fundamental understandings of lipids were already achieved in the 1980s by the use of HPLC, FAB/MS and GC/MS (Chilton and Murphy, 1986). The first MS measurements of complex lipid mixtures in the 1990s were conducted by direct infusion ESI (Han and Gross, 1994; Brügger *et al.*, 1997). Such direct infusion based approaches were later on defined as shotgun lipidomics (Han and Gross, 2005) and since they preclude previous front-end chromatographic lipid separation, they require high mass accuracy and thus rely on instruments with high mass resolving power such as Q-TOF, orbitrap or FTICR (Christer S Ejsing *et al.*, 2009; Schuhmann *et al.*, 2012; Ghaste *et al.*, 2016; Wang, Wang, Han, *et al.*, 2016). Another category of lipidomic approaches was introduced with the invention of LC/MS, mainly combined with ESI, due to its benefits described above (Köfeler *et al.*, 2012). Coupling of MS and LC enables separation of lipid species based on their hydrophobicity/hydrophilicity prior to separation by mass in MS, thereby reducing mixture complexity and accordingly the accompanying matrix effects. This way, increased sensitivity of the analysis and dissection of mixture heterogeneity can be achieved. The TQMS is still the most common instrument for quantification approaches (Sommer *et al.*, 2006; Holčapek *et al.*, 2012). It has the additional advantage, due to the three in-line quadrupoles, to operate in selected reaction monitoring (SRM) scans using specific transitions for every molecule for targeted analysis, thereby enhancing specificity and sensitivity by improving the signal to noise (Fig. 2.5). For a more “semi-targeted” analysis of lipid classes, precursor ion (PIS) or neutral loss scans (NLS) can be applied (Lerner *et al.*, 2016). Meanwhile high mass resolution instruments are also more widely used for LC/MS approaches.

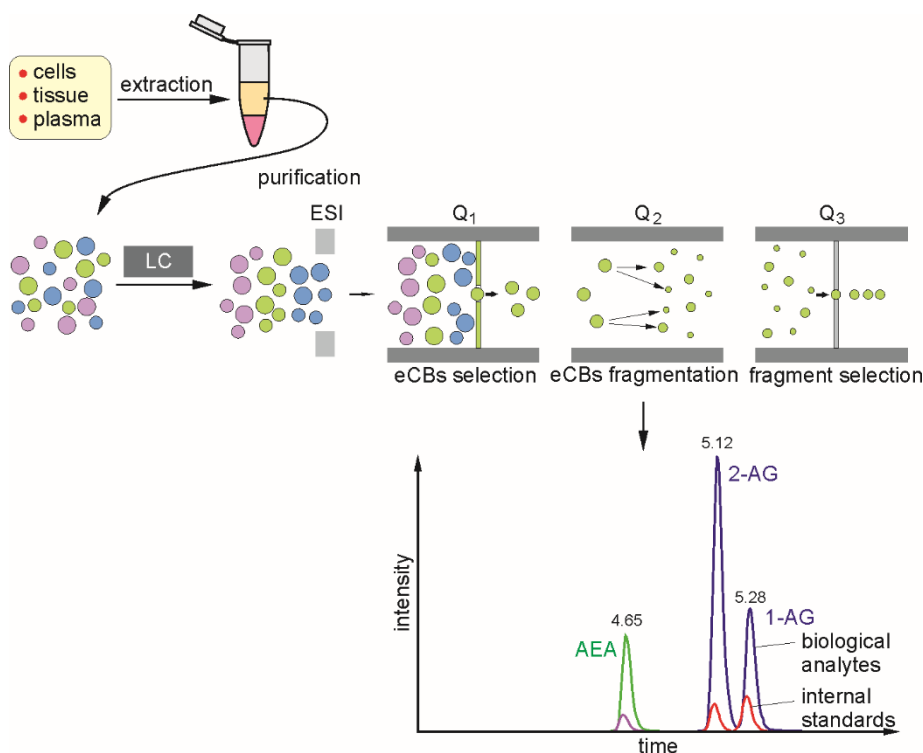


**Figure 2.5 Quantification workflow based on LC/MS:** Schematic representation of the quantification workflow of lipids (e.g. eCBs) using solvent extraction and LC/SRM quantification. Chromatographic separation as obtained on a reversed phase C18 column is illustrated, followed by  $m/z$  filtering via quadrupole MS. Each peak is assigned with the corresponding retention time and analyte identity. A representative extracted ion chromatogram in SRM mode for AEA, 2-AG and 1-AG, is depicted (from Lerner et al., 2013).

Since lipids exhibit such a large structural diversity survey scans for global lipid profiling are employed for explorative purposes and thus have so to say “untargeted” readouts. Such high mass resolution based global analyses cover a larger  $m/z$  range for identification of a broader number of lipid molecules. However, it may miss low abundant analytes, which could be identified by more tailored, targeted analyses via SRM (Cajka and Fiehn, 2016). Sample splitting and the use of multiple platforms is described to expand the types of possible applications (Tarazona et al., 2015). A more recently developed hybrid instrument, the Q Exactive for instance, combines quadrupole mass filtering with the high resolving power of the orbitrap and is thus adequate for global profiling as well as targeted analysis. Considering the ongoing technological process and regarding the large amount of possible combinations in different MS devices, their technological diversity applied in lipidomic research is not surprising. The resulting high sensitivity and specificity in lipid analysis make MS the technology of choice for lipidomic research (Wenk, 2010; Sethi and Brietzke, 2017b; Triebel et al., 2017). Relying on a citation analysis, MS exceeds meanwhile the use of NMR at a ratio of 5:2 (Cajka and Fiehn, 2016). Besides, unlike proteins, lipids rarely show specific binding and consequently reduced availability of specific antibodies for lipid analysis limits their detection via immunohistochemistry approaches such as ELISA.

However, the large structural heterogeneity of lipids still remains a challenge for MS and hinders their complete analysis in one single experiment. Moreover, the vast steady state mass of structural lipids can mask the function of individual lipid species and difficulties such as the lack of proper internal standards (ISTDs) for all distinct lipid structures are still faced by researchers. Finally, a general bottleneck represents the comprehensive data analysis. Even though a lot of progress was made in the last time regarding software development for deconvolution and processing of MS data as well as the generation of lipid databases, automated interpretation stays far behind genomics and proteomics and often requires additional time consuming manual processing and inspection (Triebel *et al.*, 2017). Nevertheless, MS is the superior tool for lipidomic research, allowing simultaneous identification and quantification of multiple lipids without the need of prior molecule identification, requires no specific antibodies and is sensitive for chemical modifications. At present, MS is the technique which renders the highest number of structural data in short analysis time, e.g. from few minutes to hour(s) and, concurrently from the lowest sample amount, e.g. in the low picogram range and at high throughput. Accordingly, it is the most suitable method for comprehensive investigations of complex lipid pathways and networks in biological systems.

### **2.2.1 Phospholipid analysis**

PL analysis in its early stages was mainly based on thin-layer chromatography (TLC) and GC/MS. Progress was pushed forward by the use of FAB/MS, which enabled the analysis of intact PL molecules and, even more, the investigation of the FA esterification site at sn-1 or sn-2 as well as the position of their double bonds via remote-site fragmentation (Gross, 1992). Invention of HPLC also strongly contributes to PL analysis because unlike TLC, exposure of PLs to atmospheric oxygen is here decreased, meaning minimization of possible autooxidation. Thus, already in 1986 HPLC - FAB/MS based analysis of human neutrophil led to the characterization of a total of 16 AA-containing PC, PE and PI species (Chilton and Murphy, 1986). Development of ESI/MS finally steered PL analysis in direction of the modern PL research predominant today (Han and Gross, 1994). Meanwhile, over 200 PLs were identified and quantified in different tissue sources such as plasma, brain or yeast, respectively using various ESI MS techniques (C. S. Ejsing *et al.*, 2009; Schuhmann *et al.*, 2012; Almeida *et al.*, 2014).

These global PL analysis are based on shotgun MS and thus typically performed by direct infusion of whole lipid extracts into the mass spectrometer. They allow fast and efficient analysis of PLs with high reproducibility. One of the preferred instruments in shotgun analysis of PLs is the hybrid LTQ orbitrap combined with ESI. The high throughput could be even increased by employment of automated chip-based nanospray technology (C. S. Ejsing *et al.*, 2009; Schuhmann *et al.*, 2011, 2012). The other main approach, applied for PL analysis, is LC/MS.

## INTRODUCTION

---

Since the majority of the PLs exhibit  $m/z$  values in a very narrow range differentiating from each other often just by their bound FAs, and/or oxidation, hydroxylation, etc. or even more represent isomeric and isobaric structures, prior separation through LC can be a very useful tool. Reversed-phase LC consisting of a very hydrophobic stationary phase separates PLs dependent on their FAs related hydrophobicity, while normal-phase LC resolves them based on their hydrophilic headgroups. This facilitates quantification of low abundant PL species. The QTRAP is the dominating instrument in this field due to its special capability as triple quadrupole to run multiple precursor ion scans and neutral loss scans in single experiment, multiplex SRM scans (MRM) and allows thereby increased sensitivity in identification and quantification of multiple, also low concentrated, PLs in a single experiment (Herrin *et al.*, 2005; Aaltonen *et al.*, 2010; Abbott *et al.*, 2013). Nowadays, Orbitrap gets more in the focus for LC/MS measurement of PLs (Taguchi and Ishikawa, 2010; Triebel *et al.*, 2014).

ESI is for both categories of approaches the preferred ion source. Generation of ions is a crucial step in PL analysis via MS and because of their structural diversity distinct PL classes own different capacities for ion formation. The neutral (or zwitterionic) PLs, PC and SM, are both better ionized in positive ion mode due to their choline-headgroup containing a quaternary nitrogen atom which dominates the behavior of the molecule and forms a cation through ESI. The neutral PE species, in contrast, produce highly abundant ions under both polarities. Even though the acidic classes of PLs PA, PG, PI and PS build both cations and anions, clearly much more abundant are the negative ions and hence the negative ion mode is the preferred mode for analysis of these PLs (Pulfer and Murphy, 2003). Accordingly, efficient PL analysis requires acquisition of both polarities. The exact  $m/z$  values from PC and SM analyzed in positive ion mode are not supposed to overlap since they own different heteroatom compositions in contrast to PC and PE for which cations with the same  $m/z$  value exist. Thus additional advantage to acquire positive and negative ion mode for PL measurement is the reduction of possible  $m/z$  overlap (Schuhmann *et al.*, 2012). In this respect, ion source is an actual tool for PL separation, based on the polarity and when combined with differential pH and polarity of the solvent for ESI admission can render a smart “in-source” PL class separation (Han *et al.*, 2006). Shortly after ESI, MALDI found its way into the laboratories as ion source for PL investigation (Harvey, 1995). However, possible interferences with ions originating from the matrix and moreover, the higher in-source decay of PLs compared to ESI and the restricted area of ionization depending on the focus of the laser beam still limit the expansion of MALDI for routine PL analysis.

Tandem MS is very beneficial for qualitative and quantitative PL analysis, not only due to available increase in sensitivity, but also by yielding several structural information about PLs, regarding their headgroups, and bound FAs. For instance, collision induced dissociation (CID) of PC and SM cations gives rise to the typical protonated choline headgroup as ion fragment at

nominal  $m/z$  184. Collisional activation of the anions originating from other PL classes yield fragment ions corresponding to their headgroups, like the PL-specific 1,2-cyclic phosphodiester of glycerol at nominal  $m/z$  153 or their FA chains. An additional feature of MS/MS is the possibility to acquire PI- and NL- scans. These scan modes allow investigations of whole lipid classes or changes in the FA content. Depending on the knowledge gained through these analyses, tailored abbreviation for PL in data assignment step are used to clearly describe the level of structural information obtained. Briefly, the headgroup is always at first notated, followed by the FAs in brackets. If the linked FAs are not known, it follows the rule: C-atoms:number of double bonds (e.g. PC (34:1)). If the linked FAs are known it is notated as: headgroup (FA\_FA) (e.g. PC (18:0\_18:1)). If also the position of the FA is proved, the FA separator is a slash: headgroup (FA at sn1/FA at sn2) (e.g. PC (16:0/18:1)) (Liebisch *et al.*, 2013).

Analysis of PLs via MS includes the capability for absolute quantification of several PL species in one experiment. Although MS is extremely advantageous in quantitative investigations, its application to PL quantification still raises different difficulties, which have to be considered to achieve reliable results. The multiple steps in quantitative assays via LC/MS, encompassing sample preparation, chromatography and MS measurement, can all lead to experimental variations of the analytes. Loss or modification of analytes during sample preparation and LC separation are common issues in molecular extraction and profiling. Furthermore, optimal ionization efficiency, a very critical factor for lipid analysis, has to be achieved for a heterogeneous lipid mixture, and is influenced by several parameters. Analytes may have different ionization efficiencies depending on the variable mobile phase composition at distinct gradient elution times. Moreover, the presence of higher abundant molecules, which compete with the analytes for ionization, may cause ion suppression. For instance highly abundant PLs such as PCs are known to induce ion suppression effects on low abundant PA species (Triebel *et al.*, 2014). Generally, even minor changes in the matrix of the lipid extract, solvent composition, co eluting molecules etc. do influence the formation of ions. Due to the strong hydrophobicity of lipids it is also likely that they may build aggregates in-source and/or in solution prior to LC/MS or MS admission, depending on their concentration and the polarity of the environment, affecting thereby ionization efficiency and their detection. Although ESI is a soft ionization process, in-source fragmentation of the PL analytes can still occur to certain extents, resulting from too high ionization temperatures or voltages. Accordingly, LPA species have been reported to be generated from LPC and LPS species through in-source fragmentation (Zhao and Xu, 2009). Since fragmentation efficiency differs between individual PL species, the CID conditions of the PL analytes in MS/MS experiments are a considerable factor for proper identification and quantification. Consequently, taken these issues into consideration, there is no rule for the direct correlation between the absolute intensity of the analytes and their initial concentration. Considering also the ongoing improvement in sensitivity obtained via MS, reaching the femtomol

## INTRODUCTION

range, even strengthen the influences of such factors. Taken together, to circumvent failures originating from the issues mentioned above in lipid analysis and allow reliable comparative studies on lipid profiling and quantification, the sample preparation and LC/MS profiling have to be thoroughly standardized and optimized. The use of ISTDs is strongly recommended, if not essential, for accurate absolute quantification, which MS enables (Wang, Wang, and Han, 2016).

In summary, all these data underlie the important role MS represents in the investigation of PLs and for the knowledge gathered so far and in consequence, for future PL analysis, MS is still without parallel.

### 2.2.2 Endocannabinoid analysis

The discovery of eCBs was achieved through the use of MS. Following this, the characterization of their functional role in various physiological and pathophysiological states was intensively investigated via MS. AEA was discovered in 1992 with the use of GC/MS. Since then various MS-based methods, either involving front-end GC or LC, were developed and implemented for the eCBs quantification; targeted quantification based on selective ion scanning, using GC/MS, LC/ESI MS and LC/APCI MS. Tandem mass spectrometry, in particular SRM, was extensively applied in combination with LC-ESI, and also with GC for eCB quantification. LC-ESI/SRM renders increased selectivity, specificity, robustness, parallelization, precision and accuracy of quantification, and has thus become the method of choice for eCB quantification (Astarita *et al.*, 2008; Lerner *et al.*, 2013, 2016).

Imperative for proper eCB quantification via LC/MS is an appropriate sample preparation and efficient extraction. The extraction of eCBs is rather challenging, especially because of their relatively low amount as compared with other lipid species and the almost invariable high lipid matrix, which can hamper quantification. Moreover, artificial changes of chemical structure of some eCBs such as isomerization of 2-AG to 1-AG through acyl migration, or oxidation readily occur due to operating temperatures, or the use of certain organic solvents (Fig 2.6).

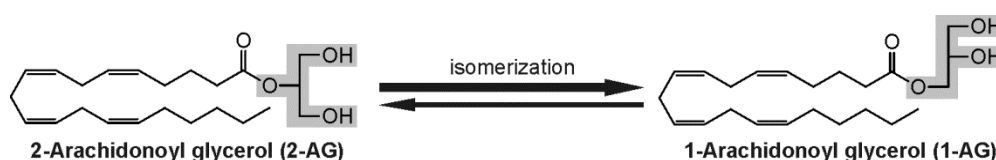


**Figure 2.6 Chemical isomerization of 2-AG to 1-AG:** Given that some eCBs are isobaric peaks and can give rise to identical fragments in MS/MS, the transitions selected for quantification are not invariably unique to a certain eCB as it is the case for 2-AG and 1-AG, which are isomeric and isobaric structures with isobaric fragment ions (from Lerner *et al.*, 2013).



Finally, adsorption of the highly lipophilic eCBs to the surface of labware used for sample preparation can lead to significant sample losses. Additionally, contamination of endogenous levels of some eCBs or ERCs, such as PEA and OEA, can occur because of their release from different tube materials in various solvents. These factors cumulate in a multistep sample processing, significantly altering the endogenous eCB concentration in any biological matrix. Artificial changes in the eCB concentration were also evidenced to occur due to ex-vivo synthesis and degradation such as the case in postmortem ischemia following decapitation or from blood cells (Vogeser *et al.*, 2006). In this context, it is worthwhile to emphasize the considerations to be taken on the sample collection, storage and transport. Thus, improvement and standardization of the methods to prevent or minimize isomerization, ex-vivo changes, contamination of eCBs, and to achieve their optimal extraction yield for different matrices is required.

Moreover, as in the case of PLs, the use of surrogate analytes as ISTDs such as deuterated eCBs is necessary to account for the artificial concentration changes of eCBs due to sample processing and allow downstream absolute quantification by LC/MS (Bindila and Lutz, 2016).

### 2.2.3 MS imaging

As described above, lipids display a huge structural and accordingly functional diversity and MS represents a powerful tool for their qualitative and quantitative characterization. However, little is known about their distribution patterns within tissue regions or even cell types. The lack of available technologies is one of the main reasons for this missing knowledge. MS imaging (MSI) with its advancing capacities may fill this gap. This technology allows the visualization of spatial lipid patterns directly from tissue surfaces without the need for previous labeling (Murphy *et al.*, 2009). MSI has its origin in the 1960s with laser microprobe MS (Liebl, 1967). Additional early development in MSI was based on static secondary ion MS (SIMS) invented in the late 1960s, combined with TOF analyzers. In SIMS, primary high energy ions are struck on a tissue surface in order to generate secondary ions, which are then released from the sample surface and enter the mass spectrometer, offering high spatial resolution (Vickerman and Briggs, 2001). However, the high energy applied through the ion beam often lead to the decomposition of the surface molecules. A paradigm shift was initiated by Caprioli and colleagues with the use of MALDI-TOF for MSI in 1997 (Caprioli *et al.*, 1997). For the soft ionization technique MALDI, a matrix is applied across the tissue surface and receives subsequently energy through a laser pulse. This energy is transferred from the matrix to the analytes by charging them and the originating ions are emitted to the mass spectrometer. This lower energy process allows the direct detection of intact molecules from complex surfaces with high sensitivity and therefore strongly facilitates the investigation of biomolecules. Nowadays also SIMS can be applied in biological studies since improvements of the technique, such as matrix-assisted SIMS, attenuate the high energy of the

## INTRODUCTION

ion beam (McDonnell and Heeren, 2007), nevertheless MALDI-MS is the predominant technique for MSI in lipidomic research (Fernández *et al.*, 2011).

Typically, in such a MALDI-MSI workflow, the tissue of interest is mounted on a conductive slide, sprayed with a matrix and scanned. Subsequent a laser beam is applied spot by spot, generating mass spectra for each single laser shot. Basically, to visualize the molecule patterns, these mass spectra, generated at each x, y coordinate, respectively, are then translated to pixels in an image, or can be used for molecule identification via MS/MS (Fig. 2.7). Pixel size and accordingly spatial resolution are mainly dependent on the size of the laser spots and matrix crystals. The lipid pattern can be visualized as distribution of single molecules with a color scale displaying their relative intensity but also as classification images resulting from statistical analysis (Fig. 2.7) (Schwamborn and Caprioli, 2010).

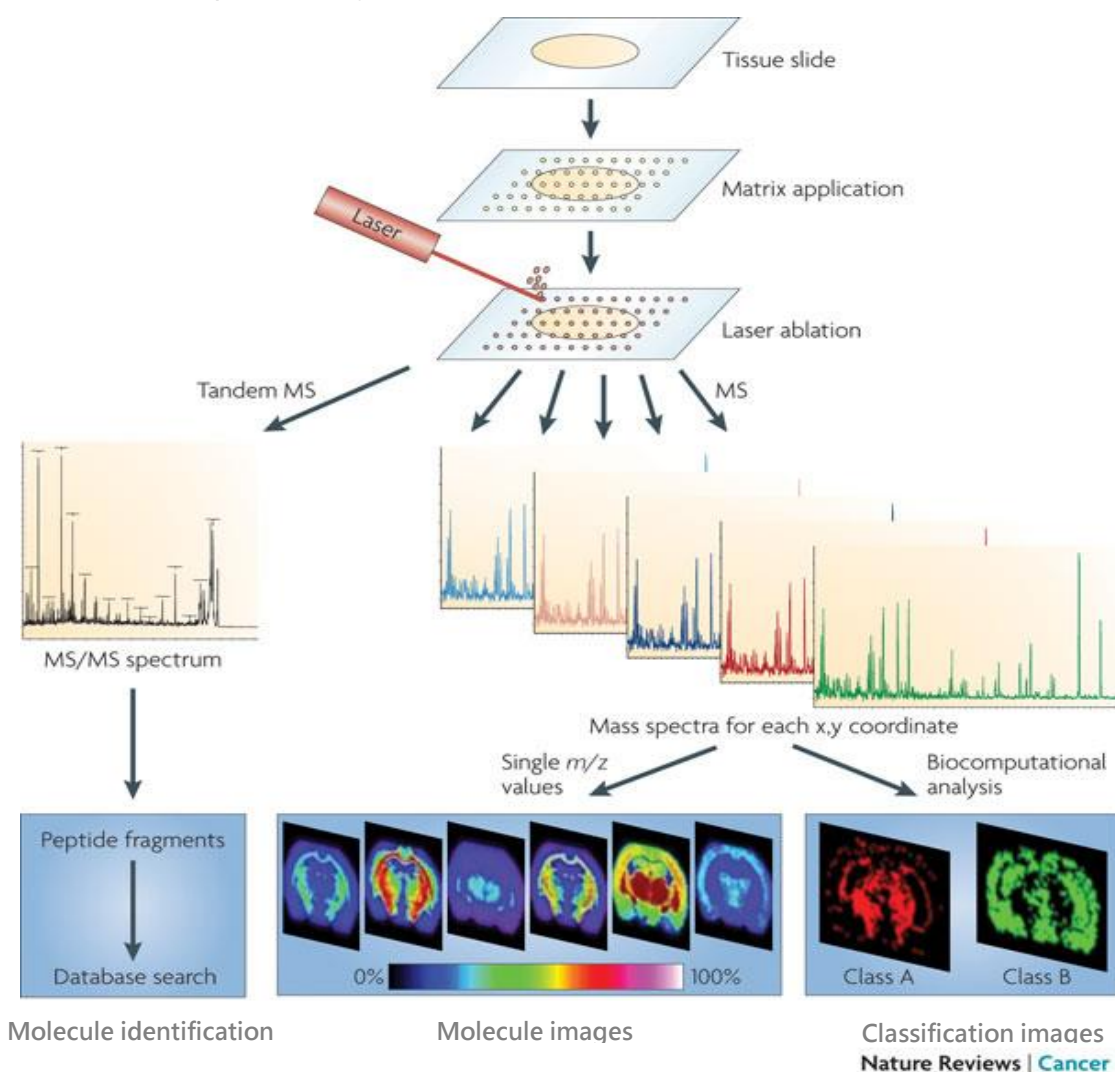


**Figure 2.7 Workflow for MALDI MSI analysis:** Exemplary overview of the schematic workflow for MSI analysis. Tissue sections, mounted on a conductive slide, are sprayed with a matrix material and ions are generated upon a laser beam. At each x, y coordinate resulting mass spectra are used for molecule identification via MS/MS and subsequent database search (left) or their spatial analysis. The latter can be visualized as distribution of single molecules (middle) or as classification images via statistical analysis (right), using color scale to display the relative intensities (modified from Schwamborn and Caprioli, 2010).

The TOF-MS serves preferentially as mass analyzer for MSI, due to its high mass resolution, the broad mass range ( $m/z \sim 1-100,000$ ) and the high mass spectrum acquisition speed. Moreover the instrumental feature, that all generated ions are collected during TOF measurement unlike scanning mass spectrometers, makes it even more attractive (Amstalden van Hove *et al.*, 2010). The QTOF is also widely been used, since it allows for additional identification via MS/MS. There is still a lot of advancement going on in order to improve mass resolving power, sensitivity, speed and spatial resolution. For instance, the invention of scanning microprobe MALDI enables lateral resolution on biological tissues as low as 8  $\mu\text{m}$  (Koestler *et al.*, 2008). Considering the crucial role of sample preparation for proper imaging studies, the diversity in matrix material and its application is not surprising. Electrospray-, airbrush- and inkjet-application have been tested, as well as a dried droplet approach or direct sublimation of an organic matrix leading to extremely small crystal size (Murphy *et al.*, 2009). Recently, a study reported the use of implanted silver nanoparticles as matrix to obtain high quality images, showing distinct lipid species alterations in a rat controlled cortical impact model with decreased SM levels near the impact site (Roux *et al.*, 2016). A future direction in MSI will be the visualization of lipids at the single cell level. High sensitivity is required for the low concentration of lipids at subcellular level and increased lateral resolution furthermore leads to reduction in available material. So far only application of SIMS-TOF due to its high spatial resolution was successful in sub cellular imaging of PL fragments for instance in the plasma membrane of *Tetrahymena pyriformis* during cell division (Lanekoff *et al.*, 2013). The disadvantage of this approach is the strong energetic impact and the relatively low sensitivity, which hinders the identification of intact PL species and thus reduced the study to the sole detection of highly abundant PL-specific fragments (Passarelli and Winograd, 2011). Ongoing developments in MALDI MSI, such as gold particle matrix deposition, may offer in the future the opportunity for detection of intact lipid species at single cell level (Passarelli and Ewing, 2013).

Taken together, although further improvements are still required, MSI is an additional feature of the MS toolbox, which can provide valuable insights in lipid localization under *in situ* conditions for further investigation of lipid interactions and biomarker discovery.

### 2.3 Aim of the study

To advance the knowledge on the mechanisms underlying neurological disorders, precise identification of the brain subareas, or cell populations involved in a disease is essential for targeted drug delivery in order to prevent unwanted side effects. Molecular profiling at increased spatial resolution can be facilitated by using techniques such as mass spectrometric analysis of brain punches, biopsies or laser microdissection, as well as by MSI. However, due to restricted amount of sample size, multimodal profiling is currently ineffective, and typically requires multiple animal batches to investigate lipids, proteins, metabolites and/or genes, with an obvious bias to the biological individual variability and tissue heterogeneity when a particular tissue is split for multiple extractions and molecular profiling.

To address these challenges and allow further progress in disease-associated lipid changes and the corresponding functional role we set two main objectives of this study:

- 1) To develop a protocol for co-extraction of PLs and eCBs that allows extraction of low and high abundant lipids with sufficient efficiency for application in brain punches or biopsies, in general, of less than 0.5 mg (Chapter 4).
- 2) To establish and implement a method for co-extraction of PLs and eCBs as well as mRNA from single brain punches or other sub microgram samples (e.g. biopsies, laser microdissection), allowing a thorough investigation of lipid signaling at lipidomic and transcriptomic level (Chapter 5).

This method should eventually help to increase the spatial resolution for quantitative neuro lipidomics and transcriptomics. Additionally, even when applied for larger tissues it would increase time-, throughput, handling and cost-effectiveness for mRNA and lipid extraction.

- 3) The third objective was to apply the above developed methods at higher spatial resolution to brain regional and subregional lipid changes associated with acute epileptic seizure state compared to controls. We therefore used a mouse model of acute epileptic seizures induced by KA injection. Combined with MS lipid imaging at higher spatial resolution across cell layers/populations, our results aim at providing new insights into the subregional and/or cellular lipid dynamics, associated with epileptic seizures (Chapter 6).

### 3 MATERIALS AND METHODS

#### 3.1 Reagents and chemicals

For multiple reaction monitoring (MRM) analysis and lipid extraction, water, n-hexane, ethylacetate, methanol, 2-propanol, acetonitrile, chloroform, formic acid and ammonium formate of LC-MS grade were invariably used (Sigma-Aldrich, St. Louis, Missouri, USA). HPLC grade methyl tert-butyl ether (MTBE), Trizma® hydrochloride solution (Tris-HCl) (pH 7.4), triethylamine (TEA) and butylhydroxytoluene (BHT) were purchased from Sigma-Aldrich (St. Louis, Missouri, USA). URB597 (KDS-4103, 3'-(aminocarbonyl) [1, 1'-biphenyl]-3-yl)-cyclohexylcarbamate) was purchased from Cayman Chemical (Ann Arbor, Michigan, USA), tetrahydrolipstatin (THL) was obtained from Santa Cruz Biotechnology, Inc. (Dallas, Texas, USA), and  $\beta$ -mercaptoethanol was obtained from Carl Roth (Karlsruhe, Germany). Kainic acid (KA) was purchased from Abcam plc. (Cambridge, UK) and isoflurane was obtained from AbbVie (North Chicago, Illinois, USA). 2',4',6'-Trihydroxyacetophenone and norharmane was purchased from Sigma Aldrich (Zwijndrecht, The Netherlands).

#### 3.2 Calibration- and internal lipid standards

**Calibration standards:** arachidonoyl ethanolamide (AEA), 2-arachidonoyl glycerol (2-AG), arachidonic acid (AA), oleoyl ethanolamide (OEA), palmitoyl ethanolamide (PEA), 1-arachidonoyl glycerol (1-AG) were obtained from BIOMOL Research Laboratories Inc. (Plymouth Meeting, PA, USA). Phosphatidylcholine 16:0/18:1 (PC 16:0/18:1), phosphatidylglycerol 16:0/18:1 (PG 16:0/18:1), phosphatidylethanolamine 16:0/18:1 (PE 16:0/18:1), phosphatidylserine 16:0/18:1 (PS 16:0/18:1), 16:0/18:1 phosphatidic acid (PA 16:0/18:1), phosphatidylinositol 16:0/18:1 (PI 16:0/18:1), lysophosphatidylcholine 18:0/0:0 (LPC 18:0), lysophosphatidic acid 16:0/0:0 (LPA 16:0), sphingomyelin d18:1/18:0 (SM d18:1/18:0) were purchased from Avanti Polar Lipids, Inc. (Alabaster, AL, USA).

**Internal standards:** arachidonoyl ethanolamide-d<sub>4</sub> (AEA-d<sub>4</sub>), arachidonoyl glycerol-d<sub>5</sub> (2-AG-d<sub>5</sub>), arachidonic acid-d<sub>8</sub> (AA-d<sub>8</sub>), oleoyl ethanolamide-d<sub>2</sub> (OEA-d<sub>2</sub>), palmitoyl ethanolamide-d<sub>4</sub> (PEA-d<sub>4</sub>), 1-arachidonoyl glycerol-d<sub>5</sub> (1-AG-d<sub>5</sub>) were obtained from BIOMOL Research Laboratories Inc. (Plymouth Meeting, PA, USA). Phosphatidylcholine 17:0/14:1 (PC 17:0/14:1), phosphatidylglycerol 17:0/14:1 (PG 17:0/14:1), phosphatidylethanolamine 17:0/14:1 (PE 17:0/14:1), phosphatidylserine 17:0/14:1 (PS 17:0/14:1), 17:0/14:1 phosphatidic acid (PA 17:0/14:1), phosphatidylinositol 17:0/14:1 (PI 17:0/14:1), lysophosphatidylcholine 17:0/0:0 (LPC 17:0), lysophosphatidic acid 17:0/0:0 (LPA 17:0), and sphingomyelin d18:1/12:0 (SM d18:1/12:0) were purchased from Avanti Polar Lipids, Inc. (Alabaster, AL, USA).

**3.3 Research equipment**

<b>devices</b>	
<b>qPCR</b>	
2100 Bioanalyzer	Agilent
ABI 7300 Real-Time PCR cycler	Applied Biosystems
NanoDrop 2000c Spectrophotometer	Thermo Scientific
T3000 Thermocycler	Biometra
<b>sample preparation</b>	
Analytical balance	Mettler Toledo
Bessmann Tissue Pulverizer	Spectrum Laboratories
Centrifuge 5417R	Eppendorf
Microtom Cryostat Cryo-Star HM 560 MV	Microm International
Precellys 24	Peqlab
Tissue Lyser	Qiagen
Vapotherm	Barkey
<b>LC/MS</b>	
1200 series LC System	Agilent
5500 QTrap triple-quadrupole linear ion trap MS	AB SCIEX
Ascentis Express 2.7 µm C18 column	Supelco
CTC HTC PAL autosampler	CTC Analytics AG
Security Guard precolumn	Phenomenex
<b>MSI</b>	
9.4T Superconducting magnet	Cryomagnetics Inc
Bruker rapifleX MALDI Tissue typer	Bruker Daltonik
SolariX XR MALDI FTICR MSI	Bruker Daltonik
SunCollect automatic pneumatic sprayer	Sunchrom
<b>kits</b>	
RNA 6000 Nano kit	Agilent
High Capacity cDNA Reverse Transcription Kit	Applied Biosystems
HybridSPE® -Phospholipid	Supelco
TaqMan Gene Expression Mastermix	Applied Biosystems
<b>software</b>	
Analyst 1.6.2	AB SCIEX
CorelDRAW X7	Corel Corporation
GraphPad Prism 4.0 software package	GraphPad Software
Lipid View software version 1.2	AB SCIEX
MultiQuant 3.0 quantitation package	AB SCIEX
SPSS 22	IBM Corp
FlexImaging	Bruker Daltonik
SCiLS lab 2016a	SCiLS

### 3.4 Mass spectrometric tools

Targeted and semi-targeted lipid profiling throughout this study was invariably carried out using a 5500 QTrap triple-quadrupole linear ion trap mass spectrometer equipped with a Turbo V Ion Source (AB SCIEX, Darmstadt, Germany), and interfaced with an Agilent 1200 series LC system (degasser, pump, and thermostated column compartment; Agilent, Waldbronn, Germany), and a CTC HTC PAL autosampler (CTC Analytics AG, Zwingen, Switzerland). Targeted lipid profiling refers strictly to LC/MRM, while semi-targeted to various scan modes: PIS, NLS.

MSI experiments were carried out using a Bruker rapifleX MALDI TissueTyper (Bruker Daltonik) and the higher spatial resolution imaging was performed with a Bruker SolariX XR MALDI FTICR MSI system coupled to 9.4T Superconducting magnet (Cryomagnetics Inc, USA).

### 3.5 Data processing and statistical analysis

Lipids were quantified by Analyst 1.6.2 software (AB SCIEX, Darmstadt, Germany) and MultiQuant 3.0 quantitation package. The obtained values were normalized to the tissue weight. The analysis of the relative gene expression (RGE) data received from the quantitative polymerase chain reaction (qPCR) was performed using the  $2^{-\Delta\Delta CT}$  method (Livak and Schmittgen 2001). Target genes were normalized to the reference gene Gusb and the normalized expression levels of the target genes then to that of the control mice. Data were analyzed with GraphPad Prism 4.0 software package (GraphPad Software, San Diego, CA, USA), presented as mean  $\pm$  SEM and considered significant at a p-value  $< 0.05$ . Statistical analyses of the difference between group means were carried out by using two-tailed unpaired Student's t-test. Prior to t-test, data were subjected to Shapiro-Wilk test and Kolmogorow-Smirnow test using SPSS 22 (IBM Corp., Armonk, NY, USA). An explorative PCA confirmed the general pattern obtained by the analysis via Student's t-test. Precursor ion scan (PIS) data were processed using Lipid View software version 1.2. One-way ANOVA was used to evaluate obtained behavioral scores. CoreIDRAW X7 was used for figure illustration. MSI data analysis and visualization was performed using FlexImaging 5.0/4.1 (Bruker Daltonik GmbH) and SCiLS lab 2016a (SCiLS GmbH, Bremen, Germany).

## 4 LIPIDOMIC PROFILING VIA MASS SPECTROMETRY

### 4.1 Introduction

This chapter describes the simultaneous quantification of PLs and eCBs from different tissue sources. As highlighted before, MS advantages the lipidomic profiling. Nevertheless, the simultaneous quantification of the lipophilic eCBs and the amphiphilic PLs represents a major challenge. Especially regarding their different endogenous concentrations, as for instance, the dynamic range of AEA compared with an abundant PL such as PC (34:1) spans over 3 orders of magnitude from pmol- to  $\mu\text{mol/g}$  tissue. Lipid extraction, LC separation and lipid profiling via MS have to be optimized in order to achieve the best compromise for efficient analysis of all distinct molecules. In this study we applied a LC/MRM approach for lipid quantification using an ESI-QTrap MS coupled to reversed phase LC. This system allows for highest sensitivity of selected compounds by substantial noise reduction due to double mass filtering in MRM mode, as well as additional separation of lipids on the LC depending on their hydrophobicity.

However, appropriate lipidomic profiling strongly requires improvement of the sample preparation and extraction procedure in order to enhance the sensitivity of lipid detection and quantification required for minute amount of samples, and facilitate high-throughput sample processing (Pati *et al.*, 2016b). The main techniques for lipid extraction represent the solid-phase extraction (SPE) and the liquid-liquid extraction (LLE). SPE, although more time consuming, provides the possibility for more discrete fractionation of lipids; for instance for additional isolation of PLs from the rest of the lipid extract, or even more separation of PLs into their individual classes (Pernet *et al.*, 2006; Fauland *et al.*, 2013). This lipid extraction approach is suitable for targeted analysis at low throughput. LLE is the more ubiquitously employed technique for lipid extraction. Basically, organic solvents such as ethyl ether, straight-chain alkanes or chloroform are used for strongly lipophilic lipids to diminish possible lipid aggregation driven by hydrophobic environments. Accordingly, more polar solvents like methanol are employed for PL extraction, since they reduce interactions among PL species as well as between PLs and membrane proteins (Berry, 2004). Traditionally, lipid extraction is carried out following the protocols of Folch (Folch *et al.*, 1957) or Bligh and Dyer (Bligh and Dyer, 1959), the latter representing a variation of the Folch protocol more tailored to biological fluids. Similar or even better lipid recoveries as compared to the traditional recipes could be achieved by a more recent extraction procedure based on MTBE, allowing faster, cleaner and higher-throughput sample handling (Matyash *et al.*, 2008; Abbott *et al.*, 2013). However, the inherent structural heterogeneity of lipid mixtures makes their analysis using a single step extraction still challenging, especially in biological studies, where often only limited sample amounts are accessible. Chen *et al.* described a lipid extraction method from mouse soleus muscle, which requires only around 2.5 mg tissue (Chen *et al.*, 2013). However, investigations of lipid metabolism in neurological diseases often require extractions from even



lower amounts such as the case of brain punches (Holter *et al.*, 2001). Supportive examples for this requirement are disorders where specific hippocampal subregions, or different cell populations are distinctly involved in (Fanselow and Dong, 2010; Small *et al.*, 2011). Therefore, we developed a method in order to achieve optimal extraction efficiency to isolate major PL classes and minor lipid species such as various lyso-PLs and eCBs from sub mg amounts of tissue e.g. brain punches.

## 4.2 Materials and methods

### 4.2.1 LC/MRM method development

In order to determine appropriate MS and LC parameters, LIPID MAPS MS calibration standards encompassing the PL classes PC, LPC, SM, PA, LPA, PE, PG, PI and PS were obtained from Avanti polar lipids. As the fatty acid species 16:0, 18:0 and 18:1 belong to the most abundant ones in mammals (Rustan and Dreven, 2005), from each lipid class a PL consisting of one or two of these fatty acids was chosen, respectively, representing endogenous PLs. In order to ensure day-to-day validation of the mass spectrometer, a quality control sample generated out of the calibration standards was produced and run with every experiment.

#### 4.2.1.1 Optimization of MS parameters for PL analysis

For compound specific optimization of MS parameters, solutions of the PL calibration standards were produced with a final concentration of 1  $\mu\text{g/mL}$  in methanol and injected with a flowrate of 7  $\mu\text{L/min}$  via direct infusion for manual tuning using the Analyst software 1.6.2. PC, LPC and SM were acquired in positive ion mode, while PA, LPA, PE, PG, PS and PI were analyzed in negative ion mode, respectively.

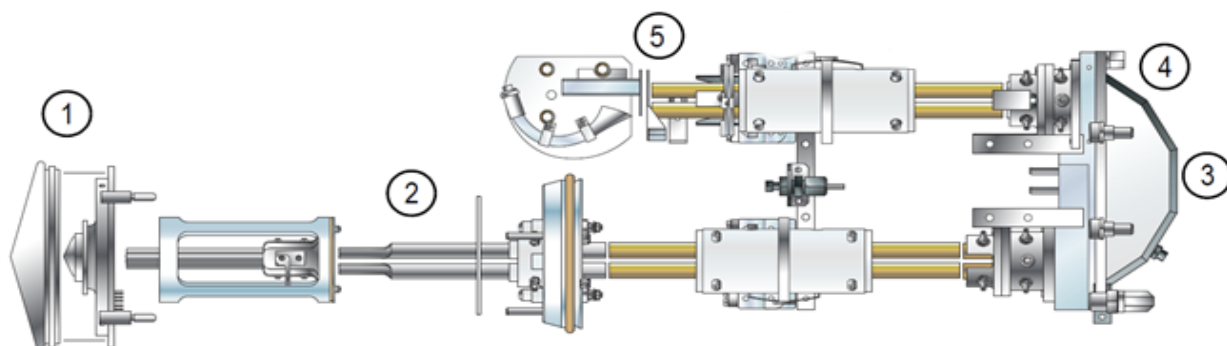


**Figure 4.1 Scheme of an AB SCIEX QTRAP® 5500 System with ion optics path and optimized parameter:** Location of the optimized parameters on the ion optics path. (1) Ion Spray Voltage/ Declustering Potential/ Curtain Gas/ TEM/ Ion Source Gas 1/ Ion Source Gas 2 (2) Entrance Potential (3) Collision Energy/ CAD Gas (4) Collision Cell Exit Potential (5) CEM.

Fig. 4.1 shows a scheme of the AB SCIEX QTRAP® 5500 System used in this study with ion optics path encompassing the location of the parameter, which were and have to be optimized. Declustering Potential (DP) and Collision Cell Exit Potential (CXP) were ramped for each compound using Q1 scans in order to achieve best peak intensities. Tandem MS ( $MS^2$ ) experiments were conducted for each compound to find the most abundant fragment ions that can be used for MRM experiments. During  $MS^2$  scans the Collision Energy (CE) was ramped for each single compound, to set optimal conditions for gaining highest fragment ion abundance while ensuring the precursor ions still detectable (Fig. 4.2).

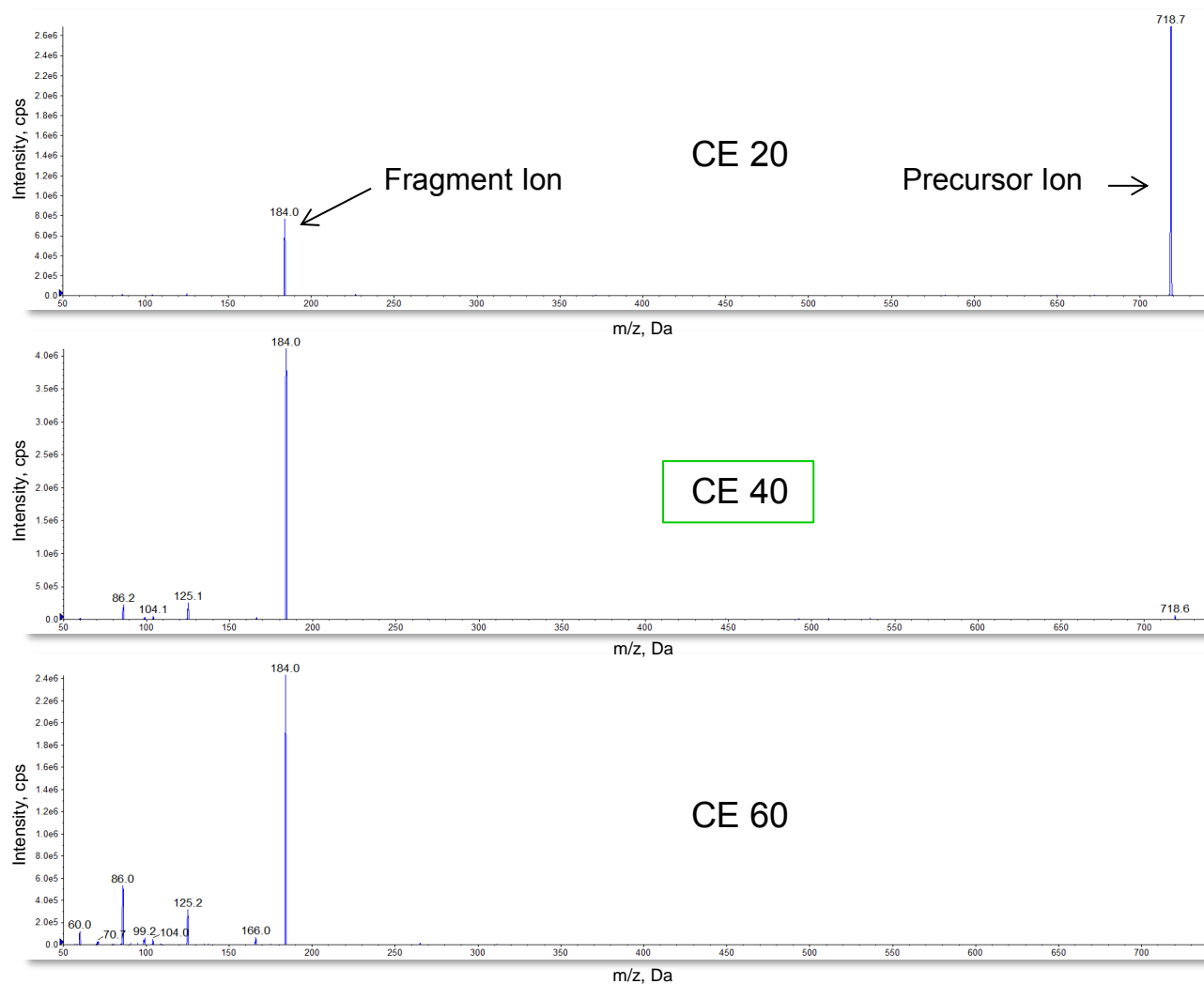


**Figure 4.2 CE Optimization:** 3 Exemplary mass spectra of PC (17:0/14:1)  $MS^2$  scans with different Collision Energies (CE) applied. Too low CE renders not enough fragment ions while too high CE leads to the loss of the precursor ion.

Further, compound-specific fragments of lower abundance were identified by  $MS^2$  scans for peak confirmation. As LPCs, PCs and SMs do not render efficient fragmentation in positive ion mode, additional experiments in negative ion mode were performed for their peak confirmation based on their FA derived fragment ions. Moreover, lithium acetate was used to improve fragmentation in positive ion mode, as lithium cationization increases the translational energy of the molecules,

thereby facilitating their fragmentation (Fig. 4.3). In order to simulate as close as possible the LC conditions, the scans were repeated with a higher flowrate of 200  $\mu\text{L}/\text{min}$  to optimize ion source parameters.

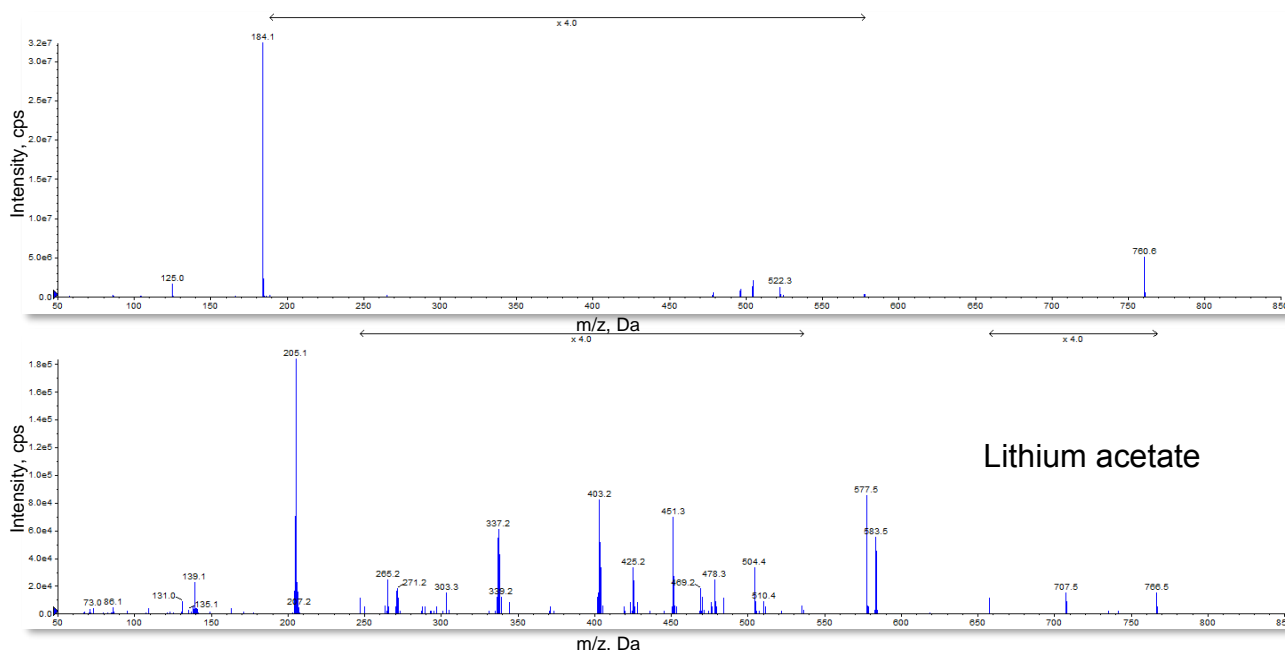


**Figure 4.3 Lithium effect:** Comparison of PC (16:0/18:1) MS2 scans with and without lithium acetate in the eluent. Addition of lithium acetate increases the fragmentation.

#### 4.2.1.2 Ascertainment of LC conditions for PL analysis

To set up LC-settings, a PL calibration standard mix of different concentrations was injected into the LC/MS via CTC HTC PAL autosampler, in order to optimize ionization, separation, peak intensity and shape of the lipid molecules. For chromatographic separation of lipids, an Ascentis Express 2.7  $\mu\text{m}$  C18 column, 100 mm x 2.1 mm (Supelco, Sigma-Aldrich, München, Germany) or a Phenomenex Luna 2.5  $\mu\text{m}$  C18(2)-HST column, 100 mm x 2 mm (Phenomenex, Aschaffenburg, Germany), combined with a Security Guard precolumn (C18, 4 mm x 2 mm; Phenomenex, Aschaffenburg, Germany), respectively, was used. Combinations of MeOH, ACN, DMSO, hexane and H<sub>2</sub>O were tested as injection solvents. Pure solution of PLs in an organic solvent diminishes interaction of the analytes with the stationary phase of the column and decreases thereby their peak intensities (Fig. 4.4).

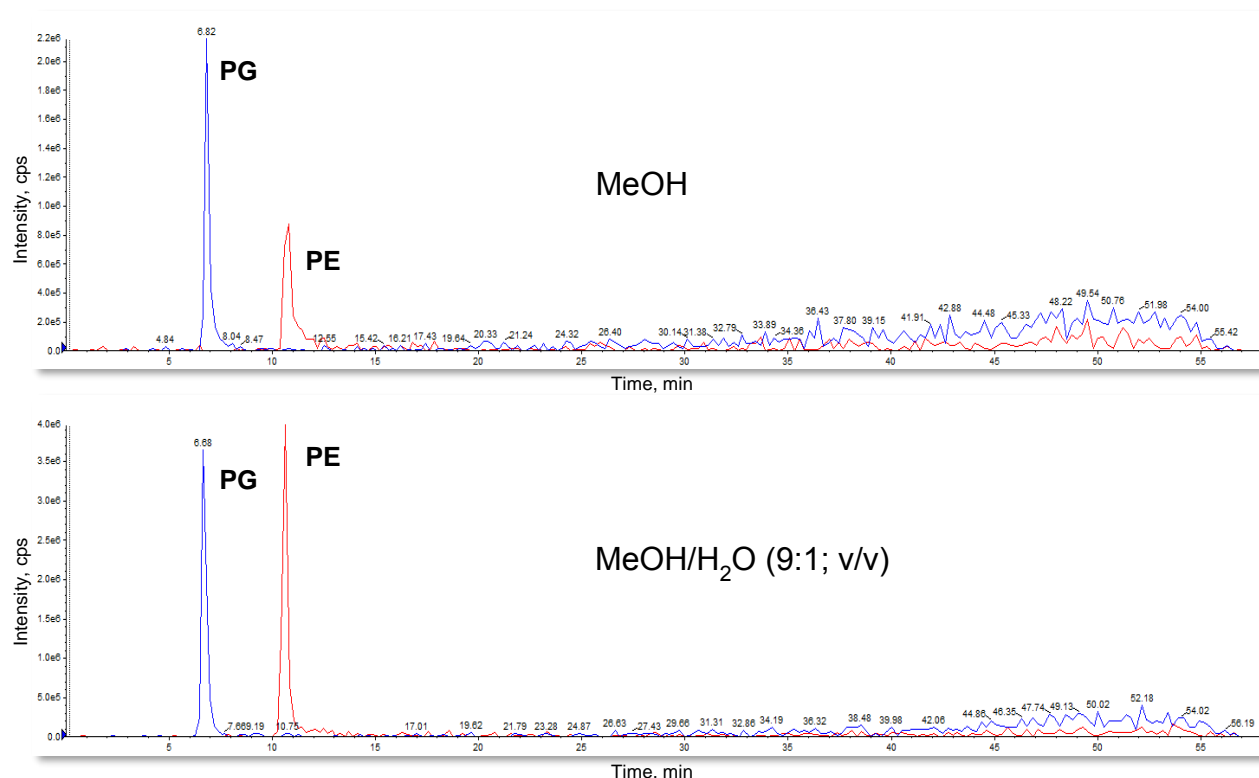


**Figure 4.4 Injection solvent optimization:** Exemplary chromatograms of PE and PG (16:0/18:1) solved in different injection solvents. Low amounts of polar water in the injection solvent increases the molecule intensities.

Conversely, too high percentage of water leads to delayed peak elution and hampers PLs ionization. As the Agilent 1200 series LC system comprises a binary pump, a gradient consisting of two different eluents was generated. Different ratios of isopropanol, MeOH and H<sub>2</sub>O were tested to find the best eluent compositions. Generally, high concentrations of nonpolar eluents (isopropanol) improve the peak separation and lead to earlier peak elution, but hinder their ionization and cause high pressures on the column. In order to improve the separation of the PLs, the percentage of eluent A and B was chosen to slow the gradient slope, and increase the separation and elution of PLs. Reagents such as the ion pairing TEA can improve the binding to the column or ionization (Fig. 4.5).

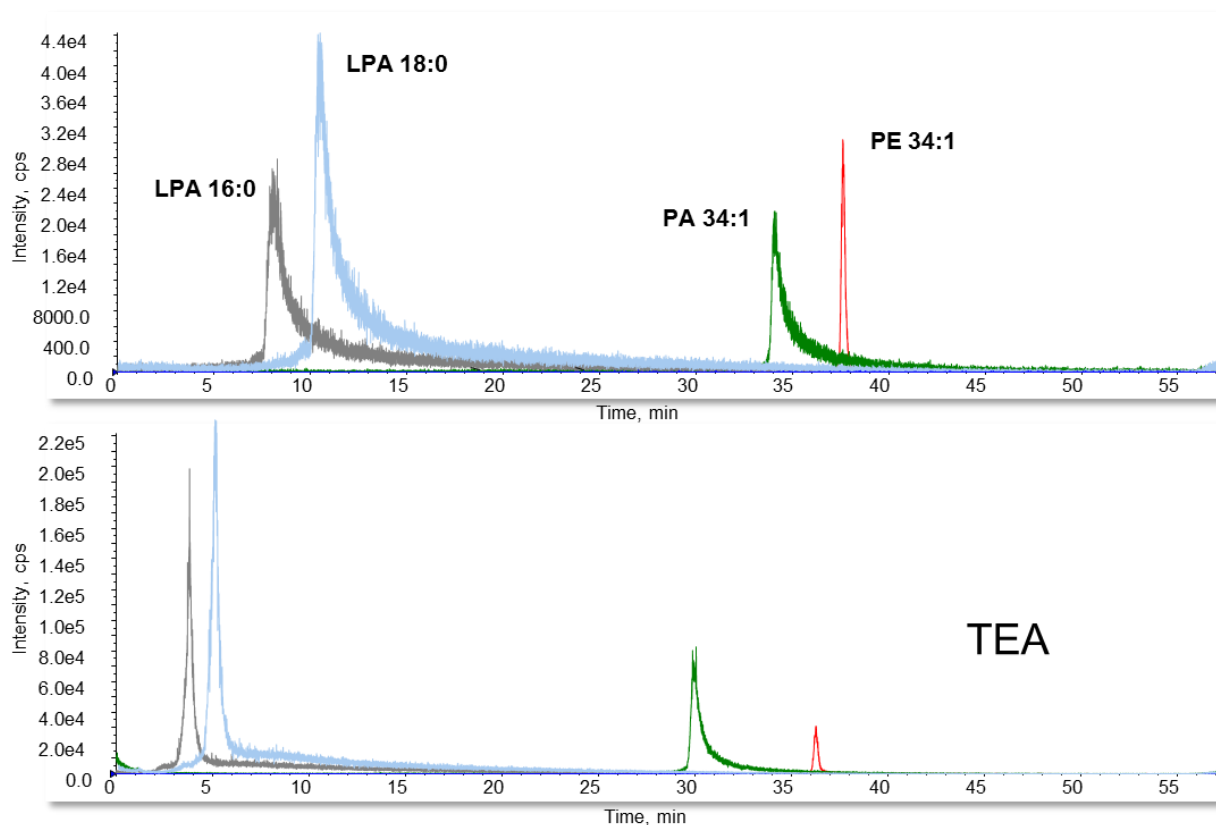


**Figure 4.5 TEA effect:** Exemplary chromatograms of four different lipid species with and without TEA in the eluent. 7.5 mM TEA improves binding efficiencies and ionization of the molecules.

For this reason, various concentrations of TEA, ammonium formate, and formic acid were tested to further optimize the eluent composition. Different flowrates were used, too, as higher flowrates lead to earlier elution of the molecules but may worsen the peak intensity and separation, and increase the pressure. Higher column oven temperatures change the binding efficiency of the analytes, as well as the viscosity of the mobile phase and decrease thereby the pressure on the column. Therefore, column oven temperature was also optimized (Fig. 4.6).

Finally, in order to verify the established LC/MRM method, a validation step following the bioanalytical guidelines was performed. For this purpose, calibration standards of specific concentrations were analyzed over a period of 18 months to determine the limit of detection (LOD), limit of quantification (LOQ), linear range, accuracy and precision of the method.

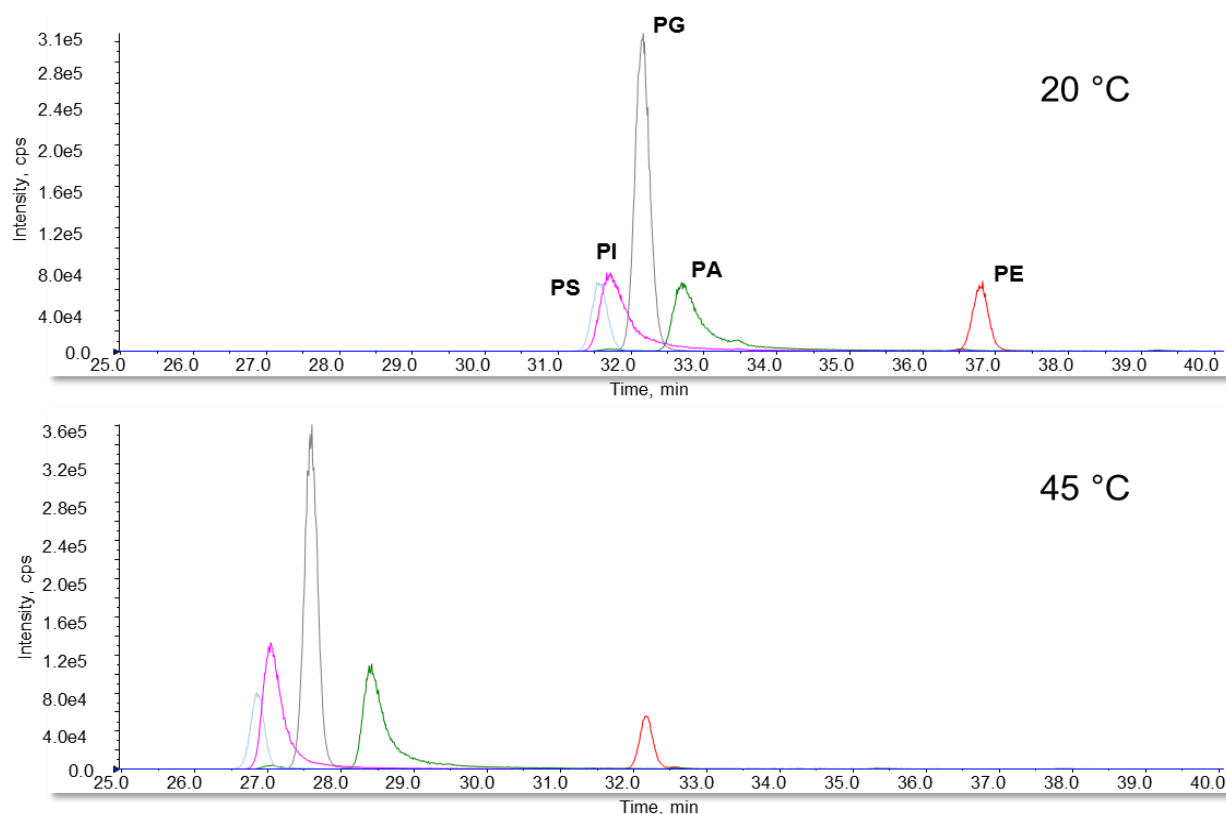


**Figure 4.6 Effect of column oven temperature:** Exemplary chromatograms of five different lipid species with two different column oven temperatures applied. A column oven temperature of 45°C improves PLs binding efficiencies.

#### 4.2.2 Development of lipid extraction protocol

To determine PL extraction efficiency and for further absolute quantification of extracted PLs, ISTDs were procured and used. ISTDs are molecules with the same structural information, owning identical chemical and physical properties, but different molecular weight as the analytes of interest, and are thus assumed to behave in the same way during the extraction procedure and measurement. Addition of a defined amount of ISTD at the earliest step possible during sample preparation is therefore used to correct for any possible analyte loss or artificial changes, e.g. chemical modification through isomerization, degradation, oxidation etc. For the eCBs and ERCs deuterated forms are commercially available. Since deuterated forms of the PLs investigated in this study are not yet provided by any company, PLs consisting of fatty acid combinations which naturally do not occur in mammals, such as containing the odd FAs 17:0 and 14:1, and in the case of SM, 18:1/12:0, respectively, were chosen as ISTDs (Fig. 4.7).

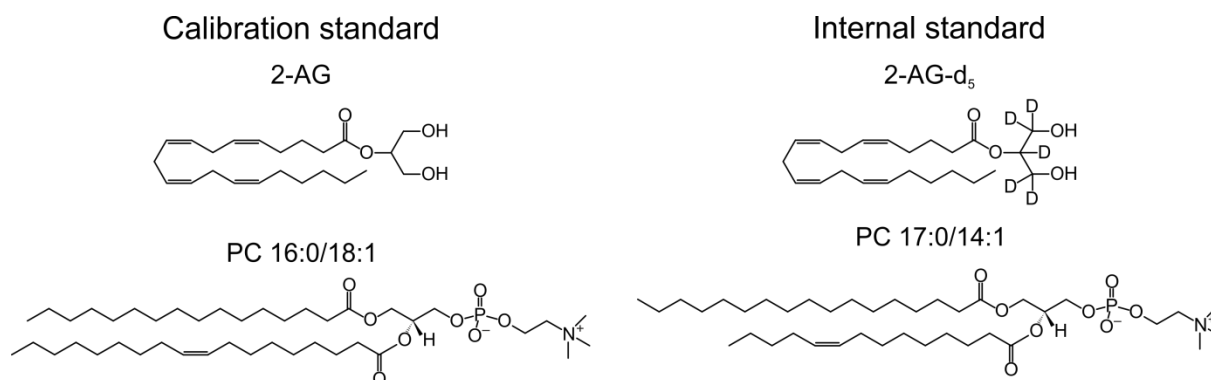


**Figure 4.7 Representative structural formulas of standards:** Two exemplary structural formulas of calibration and internal standards belonging to PLs and eCBs are depicted, respectively. For the eCB 2-AG a deuterated form was used as internal standard, while for instance the ISTD for the PL PC consists of odd fatty acid acyl chains.

#### 4.2.2.1 Animals and tissue preparation

All experiments were carried out in accordance with the European Community's Council Directive of 22 September 2010 (2010/63EU) and approved by the Ethical Committee on animal care and use of Rhineland-Palatinate, Koblenz, Germany (23 177- 07/G 13-1-021). C57BL/6N male mice (80-100 days of age) were held at a 12 h / 12 h light dark cycle with access to food and water ad libitum. Mice were shortly anesthetized with isoflurane (Forene R, AbbVie Deutschland GmbH & Co. KG, Wiesbaden, Germany) and sacrificed by decapitation. After decapitation, blood collection was performed immediately using ice-cold 500  $\mu$ L EDTA plasma extraction tubes (containing previously added chemicals: 10  $\mu$ M indomethacin; 25  $\mu$ M tetrahydrolipstatin/URB to prevent ex-vivo enzymatic activities). Plasma tubes were directly centrifuged at 2000 g for 10 min, and the resulting upper plasma phase was removed and stored at  $-80^{\circ}\text{C}$  without delay. Brains were immediately isolated and directly frozen on dry ice and stored at  $-80^{\circ}\text{C}$ . For dissection of the regions, frozen brains were thawed ( $\sim$ 2 min) in ice-cold phosphate buffer (PBS) and then transferred onto an ice-cold metal plate covered with PBS soaked tissue paper. Brain region isolation was carried out using cold forceps. Regions were invariably isolated in the following order: hypothalamus (HYP), hippocampus (HC) (right), striatum (STR) (right), cerebral cortex (cCTX) (right), HC (left), STR (left), cCTX (left), cerebellum (CER) and thalamus (THL). The whole procedure was carried out on ice and took less than 5 min per brain. Isolated tissues were immediately frozen and stored at  $-80^{\circ}\text{C}$  for further use. Based on previously performed tests in our laboratory, using this sampling/isolation procedure of tissue/plasma, post-mortem lipid level changes are similar across animal batches, allowing thus reliable comparative studies. Frozen brain regions were pulverized using the Bessmann Tissue Pulverizer from Spectrum Laboratories, Inc. (Breda, Netherlands) and then aliquoted by weighing in the cold room into 2-4 mg portions. The whole procedure was carried out on ice to avoid thawing of the tissue powder. Weighing step took about 10 sec per sample. All tissue samples were then stored at  $-80^{\circ}\text{C}$  until

further extraction. Additionally, also lower amounts of tissue powder ( $\geq 0.4$  mg) were used for extraction optimization in order to resemble extraction from brain punches.

### 4.2.2.2 eCB, ERCs and PL co-extraction from brain tissue and plasma

The co-extraction of eCBs, ERCs and PLs was based on a liquid-liquid extraction (LLE) procedure. Cerebellum is one of the biggest and most easily accessible brain regions, and therefore, aliquots of cerebellum powder were used for development of lipid extraction from tissue. In pilot experiments, the following parameters were optimized: a) homogenization and extraction solvent volumes, b) the type of homogenization and extraction tube, c) the number, size and material of homogenization balls, d) the type of homogenization device, and e) homogenization and centrifugation time. To minimize alterations of the endogenous lipid levels due to ex-vivo enzymatic activities, all extraction procedure and tissue manipulation steps were performed at 4°C, and the addition of antioxidant BHT, the lipases inhibiting enzyme THL and the fatty acid amide hydrolase inhibiting enzyme URB597 were tested. Subsequently, based on the results obtained from the pilot experiments, we tested different extraction/homogenization solvents and determined ISTD recovery, matrix effects as well as the amount of extracted endogenous analytes. We invariably used and tested tissue lysis with concurrent extraction and homogenization buffers for the PL and eCB co-extraction method development. 800  $\mu$ L of MTBE, MTBE/methanol (10:3; v/v), methanol/chloroform (1:2; v/v) or ethylacetat/n-hexane (9:1; v/v) served as the test extraction solvents. Each of this extraction solvent was added to two sub mg cerebellum powder aliquots (4.2.2.1), respectively. Then, 200  $\mu$ L of 0.1 % formic acid was added to one set of tissue aliquots containing the four extraction solvents and 50 mM Tris-HCl (pH 7.4) to the other set of tissue aliquots containing the four extraction solvents and 25  $\mu$ M THL/URB597 and 50  $\mu$ g/mL BHT were added to each approach, resulting in eight different extraction and homogenization solvent combination (Tab. 4.1). The samples were homogenized with Precellys 24 (6000 rpm; 20 sec) with cold ceramic beads and vortexed for 30 min at 4°C. After 15 min centrifugation (13000 rpm and 4°C), the upper organic phase was recovered, evaporated under a gentle stream of nitrogen at 37°C and reconstituted in 90  $\mu$ L pure methanol for storage. Out of this lipid solution, 18  $\mu$ L were diluted with 2  $\mu$ L H<sub>2</sub>O (methanol/H<sub>2</sub>O (9:1; v/v)) and used for PL analysis, and 27  $\mu$ L were evaporated again and resolubilized in 30  $\mu$ L ACN/H<sub>2</sub>O (1:1; v/v) for eCB and ERCs measurement. All different extraction experiments were performed in triplicates. All aliquots were spiked prior to extraction procedure with ISTDs to a target concentration of 150 ng/mL PC 17:0/14:1, PE 17:0/14:1, PA 17:0/14:1, 100 ng/mL PG 17:0/14:1; PS 17:0/14:1; PI 17:0/14:1; LPC 17:0; LPA 17:0; SM d18:1/12:0, 1 ng/mL AEA-d4, 60 ng/mL 2-AG-d5, 4000 ng/mL AA-d8, 2 ng/mL OEA-d2 and 3 ng/mL PEA-d4 respectively, calculated for 100  $\mu$ L final volume. In order to define the ISTD recovery and matrix effects, a second set of samples was simultaneously prepared as described above. In contrast to the first set, spiking of samples using the same ISTD mix was carried out after the extraction procedure, hence prior to injection into



LC/MS (Tab. 4.1). We tested also a solid phase extraction (HybridSPE® -Phospholipid) as an alternative for LLE, following the manufacturer's instructions. For plasma extraction a method from Schuhmann and colleagues (Schuhmann *et al.*, 2012) based on MTBE/methanol (10:3; v/v), was adapted. Therefore, different plasma volumes spanning from 5 µl to 100 µl and extraction solvent volumes e.g. 600 µl, 800 µl and 1000 µl were tested.

**Table 4.1 Scheme for extraction optimization:** In order to find the best solvents for PL, eCB and ERCs co-extraction 800 µL of MTBE, MTBE/methanol (10:3; v/v), methanol/chloroform (1:2; v/v) or ethylacetat/n-hexane (9:1; v/v) were added to tissue powder samples, respectively. Then, either 200 µL of 0.1 % formic acid or 50 mM Tris-HCl (pH 7.4), both containing 25 µM THL/URB597 and 50 µg/mL BHT were added to each approach, resulting in eight different solvent combinations. All different extraction experiments were performed in triplicates. A first set of aliquots was spiked prior to extraction procedure with the ISTD mix. In order to define the ISTD recovery and matrix effects, a second set of samples was simultaneously prepared and spiked prior to injection to MS.

3 x	3 x	3 x	3 x	3 x	3 x	3 x	3 x
MTBE	MTBE	MTBE/ methanol (10:3; v/v)	MTBE/ methanol (10:3; v/v)	methanol/ chloroform (1:2; v/v)	methanol/ chloroform (1:2; v/v)	ethylacetat/ n-hexane (9:1; v/v)	ethylacetat/ n-hexane (9:1; v/v)
0.1 % formic acid	50 mM Tris-HCl	0.1 % formic acid	50 mM Tris-HCl	0.1 % formic acid	50 mM Tris-HCl	0.1 % formic acid	50 mM Tris- HCl
25 µM THL/URB597 and 50 µg/mL BHT							
Internal standard mix added prior to extraction							

3 x	3 x	3 x	3 x	3 x	3 x	3 x	3 x
MTBE	MTBE	MTBE/ methanol (10:3; v/v)	MTBE/ methanol (10:3; v/v)	methanol/ chloroform (1:2; v/v)	methanol/ chloroform (1:2; v/v)	ethylacetat/ n-hexane (9:1; v/v)	ethylacetat/ n-hexane (9:1; v/v)
0.1 % formic acid	50 mM Tris-HCl	0.1 % formic acid	50 mM Tris-HCl	0.1 % formic acid	50 mM Tris-HCl	0.1 % formic acid	50 mM Tris- HCl
25 µM THL/URB597 and 50 µg/mL BHT							
Internal standard mix added prior to injection							

#### 4.2.3 LC/MRM qualitative and quantitative profiling

##### 4.2.3.1 Acquisition of eCBs, ERCs and PLs

Acquisition of eCBs and ERCs was performed via a method earlier developed within our group (Bindila and Lutz, 2016). For targeted investigation of PLs we applied an advanced mass spectrometry method, carried out in MRM mode using polarity switching. For initial discovery of PLs, PIS were performed in pilot experiments using mouse brain tissue and plasma. PIS were carried out in positive and negative ion mode using the specific *m/z* values of the fragment ions corresponding to fatty acids with C16:0, C18:1, C20:4 and C22:6 acyl chains, as well as to typical PL specific headgroups at *m/z* 184 (phosphocholine) and 153 (glycerophosphate), respectively.

The resulting data were assigned with Lipid View software and a preliminary list of different  $m/z$  transitions for PL quantification was generated. To validate the obtained MRM transitions and for further qualification of the PL structure, additional MRM transitions corresponding to structure-specific fragment ions but of lower abundance were acquired. Thus, for every PL several transitions to its different structure-specific fragments were used. The transitions to the most abundant fragment ions were used for the quantification of the PLs. Since PLs containing AA are of particular interest for our study, we performed additional experiments for targeted discovery using transitions of different putative PLs containing AA to the fragment ions corresponding to C20:4. Given that different transitions of the same molecule must occur at the same retention time (RT), matching of the RTs was used for molecular structure verification (Fig. 4.8 A), and prevention of lipid miss-assignment (Fig. 4.8 B). Furthermore, the proof of RTs can give an indication about the FA composition of the targeted PLs (Fig. 4.8 C). Generally, retention time matching of the endogenous analytes with calibration standards was also used as a criterion for reliable identification.

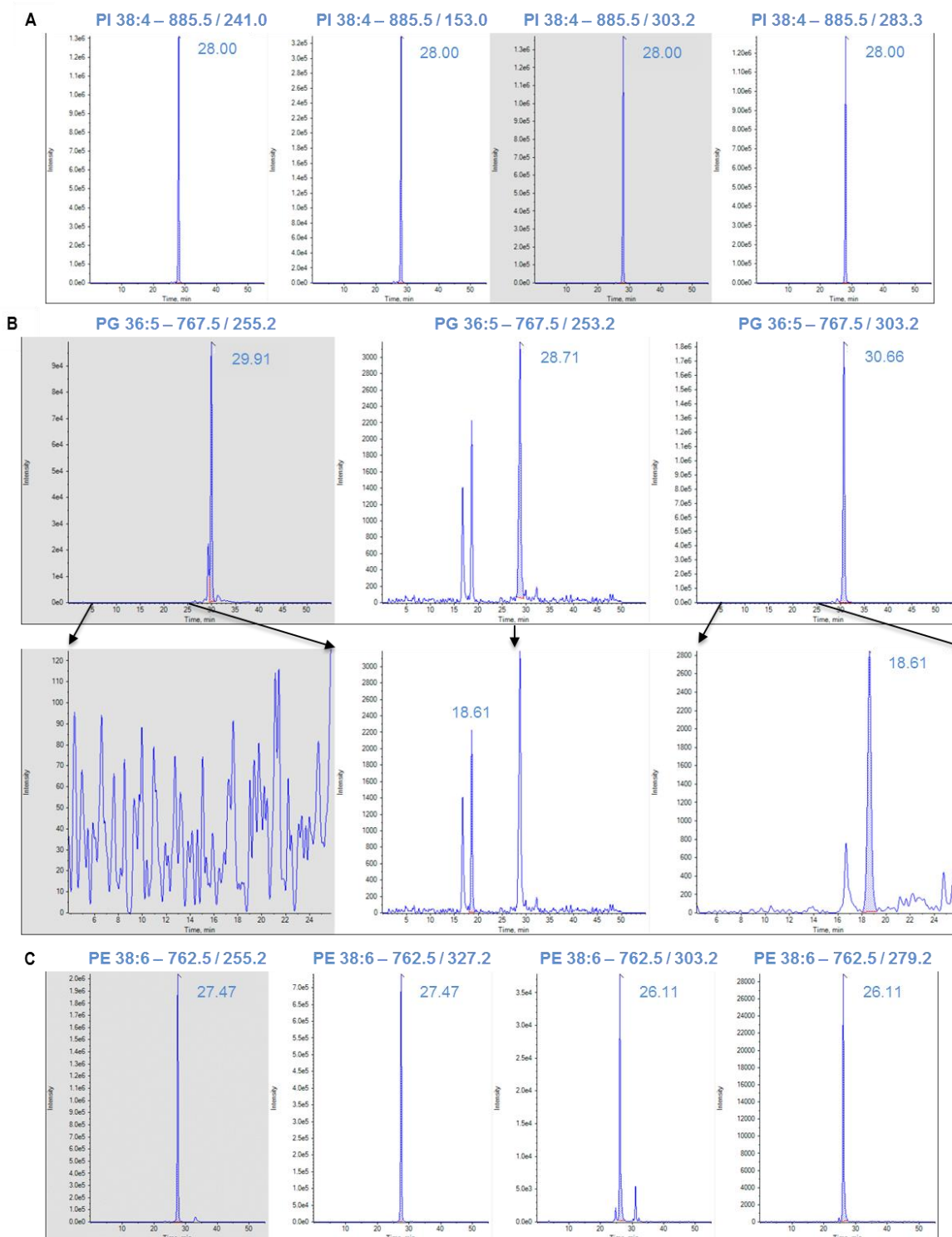


**Figure 4.8 Retention time correction:** Exemplary chromatograms obtained via MultiQuant software for RT matching. A: Chromatograms of PI 38:4 with transitions to the specific headgroup dehydrated phosphoinositol (241 Da), the headgroup glycerol 3-phosphate (153 Da), as well as to its FAs 20:4 and 18:0. All transitions have the same RT, underlining correct identification of PI 38:4. B: Chromatograms of PG 36:5 with transitions to the FAs 16:0, 16:1 and 20:4. The transition to 16:0 was obtained from the lipid view MRM list. Additional transitions to 16:1 and 20:4 were acquired for peak qualification. Every chromatogram shows a main peak around 29 min, but not at the exact same RT (upper panel). Further zoom into the chromatogram shows the correct peak at min 18.6 (lower panel), also confirmed by comparison with RTs of other PGs. Hence the originally integrated peak at min 29.91 for the unlikely molecule PG 16:0\_20:5 received from Lipid view was incorrect. C: Chromatograms of PE 38:6 with transitions to the FAs 16:0, 22:6, 20:4 and 18:2. RT matching enables the differentiation between PE 16:0\_22:6 at min 27.47 and PE 18:2\_20:4 at min 26.11.

**4.2.3.2 eCB, ERCs and PL quantification**

To facilitate future comparative studies, a map comprising basal concentrations of various lipid species in different mouse brain regions and plasma was generated to serve as reference. Quantification of eCBs and ERCs was performed via the method earlier developed by our group (Bindila and Lutz, 2016). PLs acquired as described in 4.2.3.1 were quantified using MultiQuant software. MultiQuant provides, in contrast to Analyst, the tool for quantification of multiple lipids via one calibration curve. Hence, 9 calibration curves were generated using the calibration standards described in 3.2 and 4.2.1 for each of the different PL classes investigated in this study. The calibration curves encompass 7 concentration levels, which are adapted depending on the biological source of the investigated sample (Fig. 4.9). Using these calibration curves, MultiQuant calculates the concentrations in ng/mL of the different lipids. The ng/mL values are converted to the respective amounts of lipids using the final volume of the lipid extract, and then normalized to the sample tissue weight and depicted in pmol-nmol/g. Plasma levels were normalized to the original plasma volume used for extraction.

**A: Calibration curve values for mouse plasma**

PC [ng/mL]	LPC [ng/mL]	SM [ng/mL]	PE [ng/mL]	PG [ng/mL]	PI [ng/mL]	PS [ng/mL]	PA [ng/mL]	LPA [ng/mL]
75	45	45	75	10.5	6	8.25	15	3
125	75	75	125	17.5	10	13.75	25	5
250	150	150	250	35	20	27.5	50	10
500	300	300	500	70	40	55	100	20
1000	600	600	1000	140	80	110	200	40
2000	1200	1200	2000	280	160	220	400	80
4000	2400	2400	4000	560	320	440	800	160

**B: Calibration curve values for mouse brain tissue**

PC [ng/mL]	LPC [ng/mL]	SM [ng/mL]	PE [ng/mL]	PG [ng/mL]	PI [ng/mL]	PS [ng/mL]	PA [ng/mL]	LPA [ng/mL]
150	75	120	150	60	30	45	150	12
250	125	200	250	100	50	75	250	20
500	250	400	500	200	100	150	500	40
1000	500	800	1000	400	200	300	1000	80
2000	1000	1600	2000	800	400	600	2000	160
4000	2000	3200	4000	1600	800	1200	4000	320
8000	4000	6400	8000	3200	1600	2400	8000	640

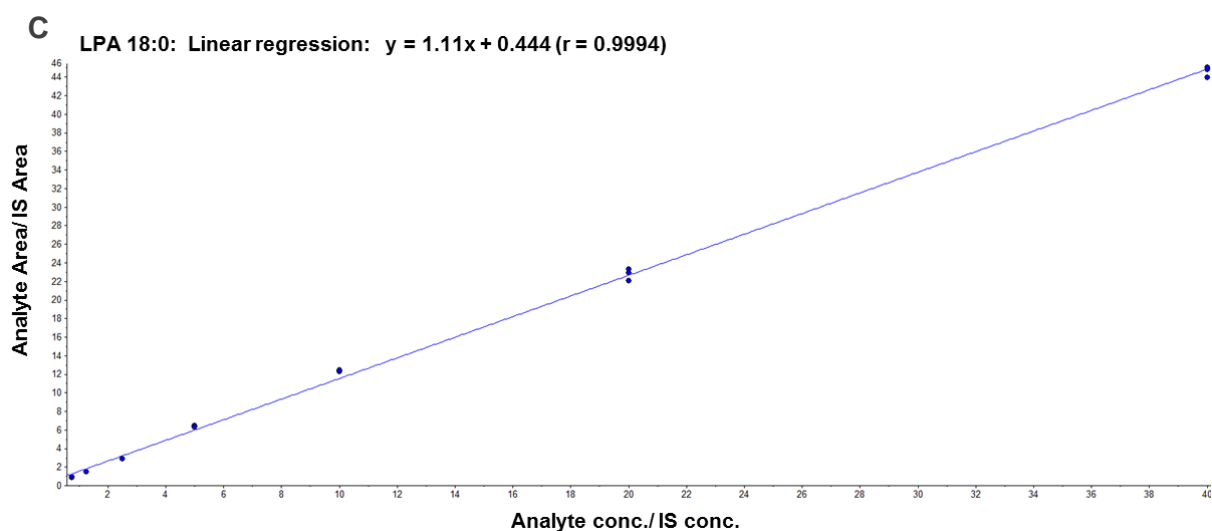


**Figure 4.9 Calibration curve:** Calibration curve values for A: mouse brain tissue and B: mouse plasma. As PL concentrations in plasma are lower compared to brain, calibrations values had to be downscaled. C: Exemplary calibration curve of LPA 18:0 generated with MultiQuant.

## 4.3 Results

### 4.3.1 LC/MRM method development

In this study, we developed a method for lipidomic profiling combined with co-extraction of eCBs, ECRs and PLs. eCBs (ECRs) and PLs were analyzed in two independent runs. MS parameters for analysis of PLs, set as described in section 4.2.2.1 through individual optimization for each calibration standard by manual tuning, are depicted in Tab. 4.2 for positive ion mode analysis and in Tab. 4.3 for negative ion mode analysis, respectively. The MS parameters for eCB and ERCs analysis are shown in Tab. 4.4. The values for compound-independent instrument settings are given in Tab. 4.5.

## LIPIDOMIC PROFILING VIA MASS SPECTROMETRY

**Table 4.2 MRM parameter for PL analysis in positive ion mode:** List of all PL molecules quantified in this study in positive ion mode. MS parameters optimized by using the PL standards are depicted. The MRM list was originally generated by Lipid View. Via targeted discovery further PLs containing AA were added. Red marks not detectable molecules. Additional transitions were acquired for qualification of all analytes.

Component	IS (V)	Precursor Ion (m/z)	Product Ion (m/z)	Dwell Time (ms)	Declustering Potential (V)	Collision Energy (V)	Collision Cell Exit Potential (V)
<b>Transitions given by Lipid View and corresponding calibration and internal standards</b>							
LPC 17:0 (ISTD)	+5200	510.355	184.073	10	+100	+40	+26
LPC 18:0 (calibration)	+5200	524.371	184.073	10	+100	+40	+26
LPC 16:1	+5200	494.350	184.073	10	+100	+40	+26
LPC 16:0	+5200	496.330	184.073	10	+100	+40	+26
LPC 18:1	+5200	522.320	184.073	10	+100	+40	+26
LPC 20:1	+5200	550.390	184.073	10	+100	+40	+26
PC 31:1 (ISTD)	+5200	718.538	184.073	10	+100	+40	+26
PC 34:1 (calibration)	+5200	760.585	184.073	10	+100	+40	+26
PC 30:1	+5200	704.570	184.073	10	+100	+40	+26
PC 30:0	+5200	706.720	184.073	10	+100	+40	+26
PC 32:2	+5200	730.570	184.073	10	+100	+40	+26
PC 32:1	+5200	732.560	184.073	10	+100	+40	+26
PC 32:0	+5200	734.610	184.073	10	+100	+40	+26
PC 34:2	+5200	758.410	184.073	10	+100	+40	+26
PC 34:0	+5200	762.680	184.073	10	+100	+40	+26
PC 36:3	+5200	784.670	184.073	10	+100	+40	+26
PC 36:2	+5200	786.680	184.073	10	+100	+40	+26
PC 36:1	+5200	788.590	184.073	10	+100	+40	+26
PC 36:0	+5200	790.660	184.073	10	+100	+40	+26
PC 38:6	+5200	806.670	184.073	10	+100	+40	+26
PC 38:4	+5200	810.660	184.073	10	+100	+40	+26
PC 38:3	+5200	812.640	184.073	10	+100	+40	+26
PC 38:2	+5200	814.550	184.073	10	+100	+40	+26
PC 38:1	+5200	816.630	184.073	10	+100	+40	+26
PC 38:0	+5200	818.600	184.073	10	+100	+40	+26
PC 40:6	+5200	834.650	184.073	10	+100	+40	+26
PC 40:5	+5200	836.630	184.073	10	+100	+40	+26
PC 40:4	+5200	838.650	184.073	10	+100	+40	+26
SM 31:1;2 (ISTD)	+5200	647.700	184.073	10	+50	+40	+26
SM 36:1;2 (calibration)	+5200	731.606	184.073	10	+50	+40	+26
SM 28:3;4	+5200	647.440	184.073	10	+50	+40	+26
SM 38:1;2	+5200	759.637	184.073	10	+50	+40	+26
SM 40:3;2	+5200	783.638	184.073	10	+50	+40	+26
SM 34:1;2	+5200	703.575	184.073	10	+50	+40	+26
<b>Additional AA containing species</b>							
LPC 20:4	+5200	544.340	184.073	10	+100	+40	+26
SM 38:4;2	+5200	753.590	184.073	10	+50	+40	+26

**Table 4.3 MRM parameter for PL analysis in negative ion mode:** List of all PL molecules quantified in this study in negative ion mode. MS parameters optimized by using the PL standards are depicted. The MRM list was originally generated by Lipid View. Via targeted discovery further PLs containing AA were added. Red marks not detectable molecules. Blue marks molecules, which were twice quantified with different FA compositions, respectively. Additional transitions were acquired for qualification of all analytes.

Component	IS (V)	Precursor Ion (m/z)	Product Ion (m/z)	Dwell Time (ms)	Declustering Potential (V)	Collision Energy (V)	Collision Cell Exit Potential (V)
<b>Transitions given by Lipid View and corresponding calibration and internal standards</b>							
LPA 17:0 (ISTD)	-4500	423.252	152.996	10.0	-100.000	-30.000	-10
LPA 16:0 (calibration)	-4500	409.236	152.996	10.0	-100.000	-30.000	-10
LPA 10:0	-4500	325.140	153.000	10.0	-100.000	-30.000	-10
LPA 12:4	-4500	345.110	153.000	10.0	-100.000	-30.000	-10
LPA 18:1	-4500	435.300	153.000	10.0	-100.000	-30.000	-10
LPA 18:0	-4500	437.330	153.000	10.0	-100.000	-30.000	-10
LPA 20:4	-4500	457.240	153.000	10.0	-100.000	-30.000	-10
LPA 20:1	-4500	462.900	153.000	10.0	-100.000	-30.000	-10
LPA 22:4	-4500	485.270	153.000	10.0	-100.000	-30.000	-10
LPG 16:0	-4500	483.270	153.000	10.0	-100.000	-30.000	-10
LPE 18:1	-4500	478.290	153.000	10.0	-100.000	-30.000	-10
LPS 18:0	-4500	524.300	153.000	10.0	-100.000	-30.000	-10
PA 31:1 (ISTD)	-4500	631.434	269.249	10.0	-50.000	-50.000	-10
PA 34:1 (calibration)	-4500	673.481	255.233	10.0	-50.000	-50.000	-10
PA 34:3	-4500	669.510	255.200	10.0	-50.000	-50.000	-10
PA 36:3	-4500	697.480	255.200	10.0	-50.000	-50.000	-10
PA 36:2	-4500	699.450	255.200	10.0	-50.000	-50.000	-10
PA 38:4	-4500	723.480	255.200	10.0	-50.000	-50.000	-10
PS 31:1 (ISTD)	-4500	718.466	269.249	10.0	-50.000	-50.000	-10
PS 34:1 (calibration)	-4500	760.513	255.233	10.0	-50.000	-50.000	-10
PS 32:5	-4500	724.420	279.000	10.0	-50.000	-50.000	-10
PS 34:2	-4500	758.500	281.240	10.0	-50.000	-50.000	-10
PS 38:0	-4500	818.590	255.230	10.0	-50.000	-50.000	-10
PI 31:1 (ISTD)	-4500	793.487	269.249	10.0	-50.000	-55.000	-10
PI 34:1 (calibration)	-4500	835.534	281.249	10.0	-50.000	-50.000	-10
PI 34:2	-4500	833.520	281.240	10.0	-50.000	-50.000	-10
PG 31:1 (ISTD)	-4500	705.471	225.186	10.0	-50.000	-50.000	-10
PG 34:1 (calibration)	-4500	747.518	281.249	10.0	-50.000	-50.000	-10
PG 34:3	-4500	743.490	255.230	10.0	-50.000	-50.000	-10
PG 36:5	-4500	767.490	255.230	10.0	-50.000	-50.000	-10
PG 36:2	-4500	773.530	281.240	10.0	-50.000	-50.000	-10
PG 36:0	-4500	777.570	255.230	10.0	-50.000	-50.000	-10
PG 38:5	-4500	795.520	281.240	10.0	-50.000	-50.000	-10
PG 38:1	-4500	803.580	255.230	10.0	-50.000	-50.000	-10
PG 38:0	-4500	805.600	255.230	10.0	-50.000	-50.000	-10

## LIPIDOMIC PROFILING VIA MASS SPECTROMETRY

PE 31:1 (ISTD)	-4500	674.477	225.186	10.0	-50.000	-50.000	-10
PE 34:1 (calibration)	-4500	716.524	281.249	10.0	-50.000	-50.000	-10
PE 36:2	-4500	742.540	255.230	10.0	-50.000	-50.000	-10
PE 36:1	-4500	744.550	281.240	10.0	-50.000	-50.000	-10
PE 38:6	-4500	762.510	255.230	10.0	-50.000	-50.000	-10
PE 38:4	-4500	766.540	255.230	10.0	-50.000	-50.000	-10
PE 38:3	-4500	768.550	255.230	10.0	-50.000	-50.000	-10
PE 38:2	-4500	770.570	281.240	10.0	-50.000	-50.000	-10
PE 38:1	-4500	772.590	281.240	10.0	-50.000	-50.000	-10
PE 40:6	-4500	790.540	255.230	10.0	-50.000	-50.000	-10
PE 40:4	-4500	794.570	281.240	10.0	-50.000	-50.000	-10
Additional AA containing species							
PI 38:4	-4500	885.550	303.233	10.0	-50.000	-50.000	-10
PI 36:4	-4500	857.518	303.233	10.0	-50.000	-50.000	-10
LPI	-4500	619.289	303.233	10.0	-100.000	-40.000	-10
PA 38:4	-4500	723.497	303.233	10.0	-50.000	-50.000	-10
PA 36:4	-4500	695.466	303.233	10.0	-50.000	-50.000	-10
PS 36:4	-4500	782.498	303.233	10.0	-50.000	-50.000	-10
PS 38:4	-4500	810.529	303.233	10.0	-50.000	-50.000	-10
PG 36:5	-4500	767.487	303.233	10.0	-50.000	-50.000	-10
PG 38:5	-4500	795.518	303.233	10.0	-50.000	-50.000	-10
PE 38:6	-4500	762.508	303.233	10.0	-50.000	-50.000	-10
PE 38:4	-4500	766.539	303.233	10.0	-50.000	-50.000	-10
PE 40:6	-4500	790.539	303.233	10.0	-50.000	-50.000	-10
PE 40:4	-4500	794.570	303.233	10.0	-50.000	-50.000	-10

**Table 4.4 MRM parameters for eCB analysis:** The table comprises all MRM parameters for analysis of eCBs and ERCs, which were previously established within our group.

Component	IS (V)	Precursor Ion (m/z)	Product Ion (m/z)	Dwell Time (ms)	Declustering Potential (V)	Collision Energy (V)	Collision Cell Exit Potential (V)
Positive ion mode							
AEA	+4800	348.3	62.1	20	+70	+22	+9
AEA-d <sub>4</sub>	+4800	352.3	66.1	20	+70	+22	+9
2-AG	+4800	379.1	287.2	20	+70	+22	+30
2-AG-d <sub>5</sub>	+4800	384.2	287.2	20	+70	+22	+30
OEA	+4800	326.2	62.1	20	+70	+21	+10
OEA-d <sub>4</sub>	+4800	328.2	66.1	20	+70	+23	+10
PEA	+4800	300.2	62.1	20	+70	+21	+10
PEA-d <sub>4</sub>	+4800	304.2	62.1	20	+70	+21	+10
Negative ion mode							
AA	-4500	303.05	259.1	50	-200	-19	-12
AA-d <sub>8</sub>	-4500	311.04	267.0	50	-200	-19	-12



**Table 4.5 Compound independent instrument settings:** Values for general MS settings used in this study independent of the different investigated analytes.

Parameter	Parameter type	
Curtain Gas (CUR)	Source and gas	40 psi
Collision Gas (CAD)	Source and gas	Medium
Temperature (TEM)	Source and gas	550 °C
Ion Source Gas 1 (GS1)	Source and gas	50 psi
Ion Source Gas 2 (GS2)	Source and gas	50 psi
Entrance Potential (EP)	Compound	10 V (pos); -10 V (neg)
CEM (CEM)	Detector	1800 V

Chromatographic separation of lipids was achieved using an Ascentis Express 2.7 µm C18 column, 100 mm x 2.1 mm (Supelco) or a Phenomenex Luna 2.5 µm C18(2)-HST column, 100 mm x 2 mm, combined with a Security Guard precolumn (C18, 4 mm x 2 mm), respectively, both showing comparative results. For PL analysis, the column was thermostated at 45°C. As injection solvents, methanol/H<sub>2</sub>O (9:1; v/v) showed the best results for PLs. The LC gradient for PL analysis shown in Tab. 4.6 was generated to allow fast polarity switching in a single run, proper ionization and detection for every lipid and tissue source, irrespective of the gradient changes.

**Table 4.6 Gradient for PL analysis:**

(A) Gradient elution began at 40 % B, held for 3 min and was then linearly increased over 42 min to 90 % B, then linearly increased to 99 % B in 1 min, held there for 7 min and decreased over 2 min to 40 % B. From minute 0-1 and 50-55 was injected into the waste. The flow rate was 200 µL/min. The gradient time of 55 minutes was chosen to enable additional analyzation of strongly hydrophobic molecules like ceramides and triacylglycerols (TGs). A shorter gradient of 42 minutes was also tested and proved sufficient for PL analysis (B).

A Total time (min)	Flow rate (µl/min)	A (%)	B (%)
0	200	60	40
3	200	60	40
45	200	10	90
46	200	1	99
53	200	1	99
55	200	60	40

B Total time (min)	Flow rate (µl/min)	A (%)	B (%)
0	200	60	40
3	200	60	40
35	200	10	90
35.5	200	1	99
41	200	1	99
42	200	60	40

The mobile phase A consisted of methanol/water (1:1; v/v) containing 7.5 mM ammonium formate and 0.1 % TEA and B methanol/isopropanol (2:8; v/v) containing 7.5 mM ammonium formate and 0.1% TEA. The flow rate was 200  $\mu$ L/min. Gradient elution began at 40 % B, held for 3 min and was then linearly increased over 42 min to 90 % B, then linearly increased to 99 % B in 1 min, held there for 7 min and decreased over 2 min to 40 % B. The LC flow-through from minute 0 to 1 and 50 to 55 was injected into the waste, to avoid unnecessary contamination of the column. The autosampler tray was kept at 4°C. Compressibility of the eluents was adapted. Additional peak confirmation using lithium acetate succeeds better when adding lithium acetate to the eluents instead of the injection solvent. All the above mentioned optimizations lead to substantial improvement of chromatographic analysis (Fig. 4.10).

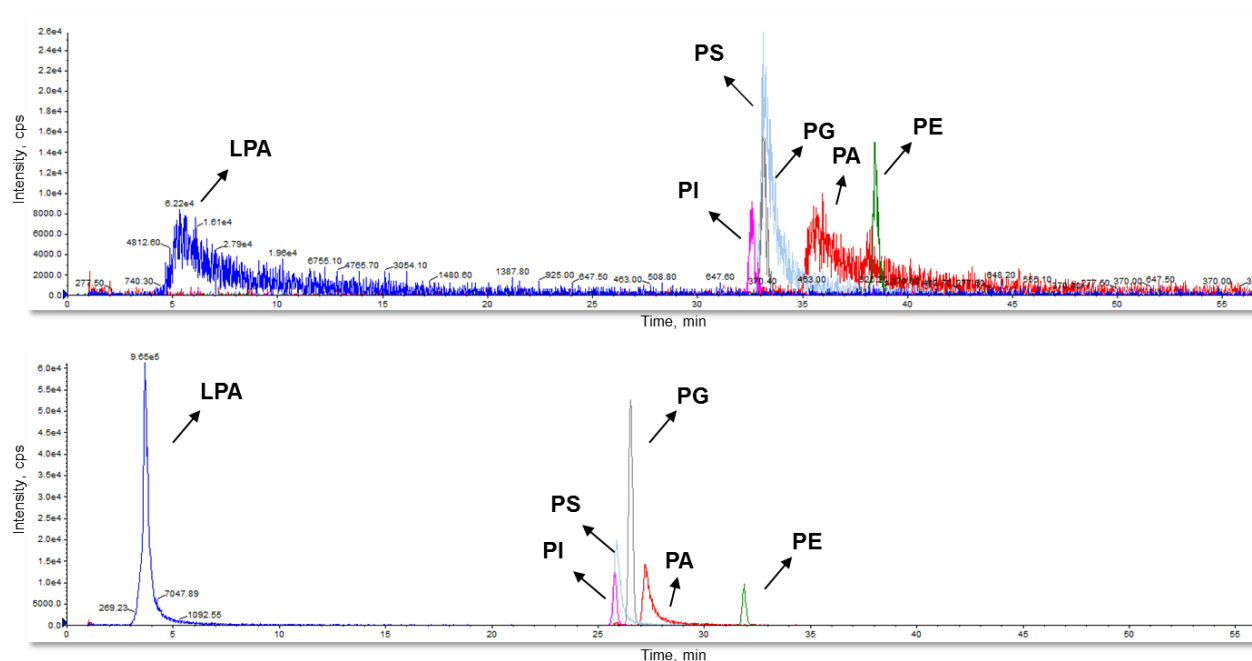


**Figure 4.10 Chromatographic optimization process:** Representative chromatograms for chromatographic optimization process showing PL peaks acquired in negative ion mode. Lower panel shows the chromatogram after the optimization of: injection solvents, eluent composition, column temperature and gradient slope. Compared to the initially obtained chromatogram depicted in the upper panel improved ionization, separation, intensity as well as peak shape of the PL molecules was achieved.

The gradient time of 55 minutes was chosen to enable additional analyses of strongly hydrophobic molecules like triacylglycerols (TGs) and cardiolipins (CLs). A shorter gradient of 42 minutes was also tested and proved sufficient for PLs analysis (Tab. 4.6 B). Altogether, LC conditions were optimized to find the best compromise in terms of separation and ionization of the different PL species and to diminish suppressive effects hindering the detection of minor abundant lipid classes, as for instance ion suppression of LPA species caused by higher abundant LPC species (Tab. 4.7).

**Table 4.7 PL retention times:** Depicted are retention times for different exemplary PL species among 8 PL classes, obtained by the acquisition method, developed in this study, using the 42 min gradient. Relative comparison of the RTs facilitates analyte qualification.

	36:5	31:1		38:6	38:5	40:6	36:4	34:1	38:4	40:4
PE		28		29		32		32	33	36
PI		22					25	26	28	
PS		22					25	27	28	
PA		23					26	28	29	
PG	21	22			24			27		
PC		29		31		33		33	34	37
	20:4	16:0	17:0	18:0						
LPC	8		13	15						
LPA	3.5	5	6.5							

Validation following international guidelines proved the established method reliable as it matches the general acceptable criteria for quantitative assays. Calibration data are presented in Tab. 4.8 indicating the limit of quantification and detection as well as correlation coefficients for all analytes between 0.995 and 0.999. The intra-day precision and accuracy data for all analytes (Tab. 4.9) are in agreement with the international acceptance criteria with %RSD of precision better than 15%.

**Table 4.8 Calibration data:** The linear range, calibration curve parameters with standard deviations (SD) and regression coefficients (R<sup>2</sup>) of all analytes. Calibration lines were generated by plotting the ratios of the areas analyte/internal standard against the nominal concentrations (ng/ml). The limit of detection (LOD) and limit of quantification (LOQ) were calculated as follows: LOD = 3.3σ/S and LOQ = 10σ/S, where σ is the standard deviation of the response (standard deviation of y-intercepts of regression lines) and S is the slope of the calibration curve.

Analyte	LOD (ng/ml)	LOQ (ng/ml)	Linear range (ng/ml)	Slope ± SD	Intercept ± SD	(R <sup>2</sup> )
2-AG	0.40	1.22	18.75 - 1000	0.726 ± 0.021	0.261 ± 0.153	0.996
AEA	0.02	0.07	0.045 - 2.4	0.709 ± 0.008	-0.015 ± 0.009	0.999
AA	0.13	0.39	375 - 20000	0.270 ± 0.008	0.036 ± 0.018	0.995
LPC 18:0	0.25	0.76	45 - 4000	0.654 ± 0.005	0.120 ± 0.086	0.999
PC 16:0/18:1	0.42	1.27	75 - 8000	0.867 ± 0.008	0.384 ± 0.191	0.999
SM d18:1/18:0	0.71	2.16	45 - 6400	0.360 ± 0.005	0.270 ± 0.135	0.999
LPA 16:0	0.09	0.26	3 - 640	1.064 ± 0.017	-0.089 ± 0.048	0.998
PA 16:0/18:1	0.23	0.70	15 - 8000	0.904 ± 0.005	-0.149 ± 0.110	0.999
PG 16:0/18:1	0.24	0.74	10.5 - 3200	0.555 ± 0.005	0.137 ± 0.071	0.999
PS 16:0/18:1	0.10	0.31	8.25 - 2400	0.466 ± 0.002	0.019 ± 0.025	0.999
PE 16:0/18:1	0.86	2.61	75 - 8000	0.137 ± 0.003	-0.053 ± 0.062	0.998
PI 16:0/18:1	0.10	0.30	6 - 1600	0.197 ± 0.002	0.019 ± 0.010	0.999

**Table 4.9 Intra-day and inter-day precisions:** Intra-day and inter-day precisions for two nominal concentrations of each compound with percent relative standard deviations (%RSD). Precisions were determined by comparison of nominal concentrations to mean calculated concentrations of spiked calibration standards. The calibration standard samples were analyzed in triplicates on one day for intra-day and 5 days (over a period of 18 months) for inter-day assay, respectively.

Analyte	Nominal conc. (ng/ml)	Precision	
		Intra-day mean %RSD (n = 3)	Inter-day mean %RSD (n = 5 days)
2-AG	62.5	0.84	2.56
	1000	0.12	7.80
AEA	0.045	2.01	8.90
	2.4	0.63	2.20
AA	1250	3.12	3.31
	20000	4.82	3.94
LPC 18:0	250	1.91	1.72
	4000	0.29	3.24
PC 16:0/18:1	500	4.59	6.46
	8000	8.35	8.74
SM d18:1/18:0	200	11.32	9.81
	6400	8.15	3.28
LPA 16:0	20	2.46	7.00
	640	1.35	4.68
PA 16:0/18:1	500	2.57	4.14
	8000	4.77	3.72
PG 16:0/18:1	60	3.03	10.23
	1600	6.94	3.85
PS 16:0/18:1	45	5.27	4.63
	1200	5.98	2.79
PE 16:0/18:1	500	11.59	1.42
	8000	0.43	0.86
PI 16:0/18:1	30	4.17	9.01
	800	14.47	2.44

#### 4.3.2 Development of lipid extraction protocol

For PL extraction only, a SPE based on zirconia was tested and proved suitable for purification of PL species. In order to find the best compromise for co-extraction of eCBs, ERCs and PLs we optimized a LLE protocol. Tissue homogenization is one of the most crucial steps. Incomplete tissue homogenization results in wrongly determined lipid concentrations, because of the inefficient, incomplete extraction of endogenous lipids. Furthermore, the use of certain consumables, such as microcentrifuge tubes, can lead to whole loss of the samples due to readily breakage and opening during the tissue lysis. 2 ml Precellys tubes combined with ceramic beads or 7 2.8 mm steel balls showed good and comparable results. Both, Tissue Lyser (30 Hz: 30 sec) as well as Precellys 24 (6000 rpm; 20 sec) are suitable for homogenization of brain tissue. Depending on the amount and tissue type, an additional homogenization step can be necessary. Different volumes of extraction/homogenization solvents were tested, with 800 µl showing the best results. 30 min vortexing at 4 °C after the homogenization was applied to

increase the lipid extraction efficiency. Subsequent centrifugation for 15 min (13000 rpm; 4°C) was sufficient to induce clear phase separation. Using these homogenization parameters different homogenization solvent mixtures were further assessed. Therefore, ISTD recovery was determined by calculating the ratio of the ISTD intensities from the samples spiked pre-extraction compared to those spiked post-extraction. Mouse cerebellum powder served as the biological matrix (4.2.2.1) and no additional re-extraction step was performed. In shotgun lipidomics, peaks corresponding to PLs with (17:0/14:1) fatty acyl chain are often detected in non-spiked samples and interfere therefore with quantification. We have tested this by injecting brain lipid extracts which were not spiked with ISTDs and did not observe any interference. This is also likely due to the low amount of tissue extract that we inject on the column and certainly the use of front-end reversed phase chromatography. The ISTD recovery varied depending on the lipid class among the different extraction methods (Fig. 4.11).

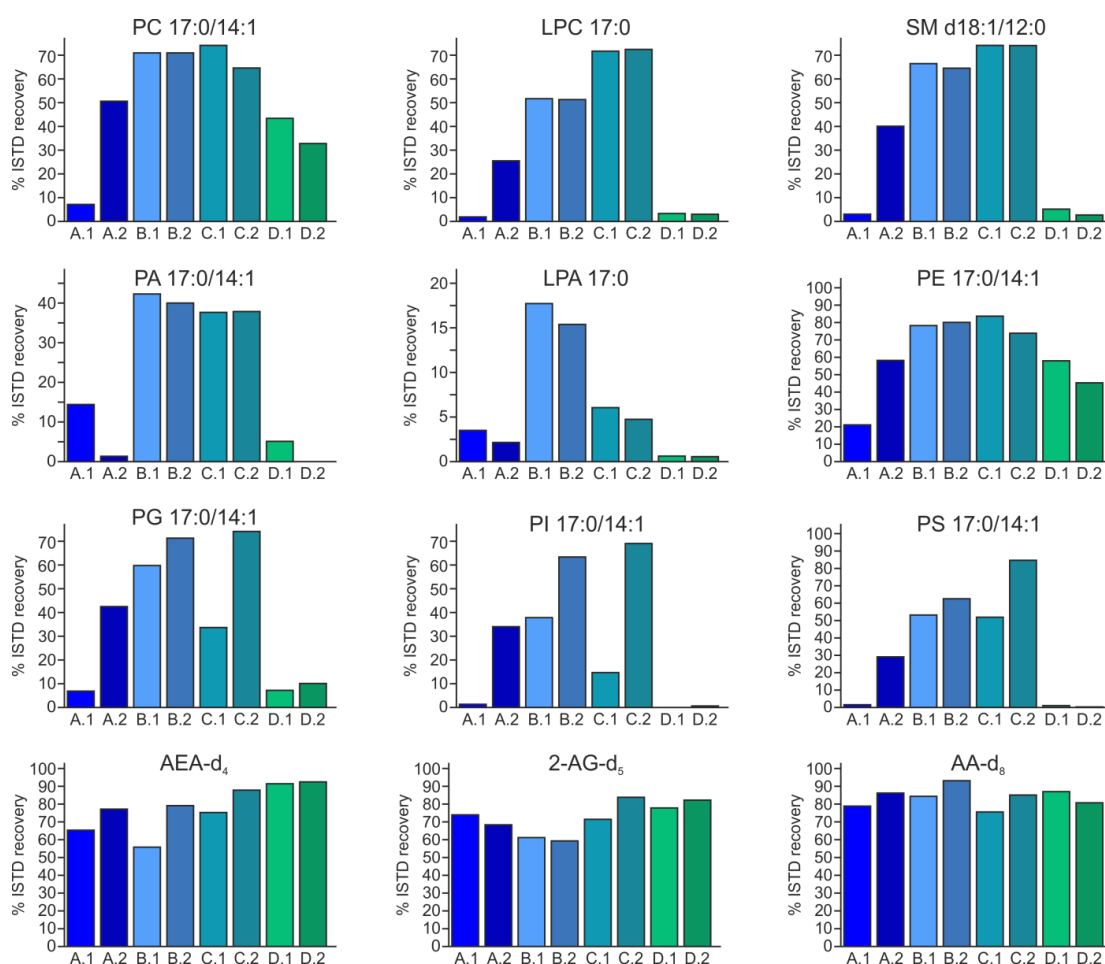


**Figure 4.11 ISTD recovery via different extraction solvents:** ISTD recovery estimated as the ratio of the ISTD intensities from the samples spiked pre-extraction as compared to those spiked after the extraction procedure (n=6) via different homogenization solvent mixtures: A.1: MTBE - 0.1 % formic acid; A.2: MTBE - 50 mM Tris-HCl; B.1: MTBE/methanol (10:3; v/v) - 0.1 % formic acid; B.2: MTBE/methanol (10:3; v/v) - 50 mM Tris-HCl; C.1: methanol/chloroform (1:2; v/v) - 0.1 % formic acid; C.2: methanol/chloroform (1:2; v/v) - 50 mM Tris-HCl; D.1: ethylacetat/n-hexane (9:1; v/v) - 0.1 % formic acid; D.2 ethylacetat/n-hexane (9:1; v/v) - 50 mM Tris-HCl.

MTBE/methanol (10:3; v/v), in agreement with Matyash et al. (Matyash *et al.*, 2008), together with 0.1 % formic acid was found to be a good compromise among the different solvent combinations regarding the recovery of all lipid ISTDs in one single step. Thereby, the achieved recovery of AEA-d<sub>4</sub>, 2-AG-d<sub>5</sub> and AA-d<sub>8</sub> ranged from 75.71 to 80.46% and for PL ISTDs from 63.58% to 86.11% except of PA 56.26%, PI 36.23% and LPA 26.23% (Fig. 4.11; Tab. 4.10).

**Table 4.10 Recovery, intra assay reproducibility and matrix effect via MTBE/MeOH FA:** For estimation of the ISTD recovery, representative brain tissue powder samples were spiked with internal standards (ISTDs) prior to extraction (n=3) and after extraction (n=3). Recovery was calculated in percent using the averages of ISTD peak areas prior to and after extraction, respectively. Intra assay reproducibility was calculated as the standard error of the mean of ISTD peak areas spiked prior to extraction. Additionally, for matrix effect evaluation, ISTD peak areas of spiked calibration mix (n=3) were compared to ISTD peak areas in samples spiked post extraction.

Analyte	Recovery %	Reproducibility SEM %	Matrix effect %
2-AG-d <sub>5</sub>	80.46	3.42	40.19
AEA-d <sub>4</sub>	75.71	6.99	32.66
AA-d <sub>8</sub>	77.41	3.97	71.67
LPC 17:0	63.58	3.33	23.73
PC 17:0/14:1	84.06	0.99	21.36
SM d18:1/12:0	76.94	1.73	10.02
LPA 17:0	26.23	14.93	10.48
PA 17:0/14:1	56.26	17.67	20.70
PG 17:0/14:1	64.74	4.30	10.46
PS 17:0/14:1	64.55	8.65	8.45
PE 17:0/14:1	86.11	8.57	25.08
PI 17:0/14:1	36.23	10.03	16.46

The low recovery of LPA 17:0 may result from its higher polarity (Triebel *et al.*, 2014). For PI analysis only, better ISTD recoveries can be obtained by addition of Tris-HCl instead of 0.1% formic acid (Fig 4.11). However, ISTD recovery achieved via extraction with MTBE/methanol (10:3; v/v) combined with 0.1 % formic acid was sufficient for the detection of all targeted endogenous molecules, even from sub mg amounts of tissue. Furthermore, intra-assay reproducibility, determined by the percentage of the standard error of the mean (SEM) of the extracted ISTDs, ranged from 10.03% for PI 17:0/14:1 to 0.99% for PC 17:0/14:1, except for LPA 17:0 (14.93 %) and PA 17:0/14:1 (17.67%) (Tab. 4.10). Concurring with Patterson *et al.* (Patterson *et al.*, 2015) best reproducibility via MTBE/methanol-formic acid extraction were obtained for PC species. Matrix effects for AEA-d<sub>4</sub>, 2-AG-d<sub>5</sub> and AA-d<sub>8</sub> were 32.66%, 40.19%, 71.67%, respectively, while all other matrix effects were less than 25.08% (Tab. 4.10). Regarding the extraction efficiency of endogenous analytes, the tested solvent combinations demonstrated considerable differences (Fig. 4.12). Herein, a crucial point affecting the yield of extracted endogenous lipids is the combination of chemical and mechanical homogenization. Tissue lysis using only homogenization buffer followed by extraction, leads only to minimal differences in

endogenous analyte extraction efficiency from tissue, irrespective of the extraction solvent used after the homogenization process (Matyash *et al.*, 2008; Abbott *et al.*, 2013) Tissue lysis using concurrent homogenization and extraction buffer leads to higher differences in extraction efficiency of the endogenous analytes among the different solvent combinations (Fig. 4.12).

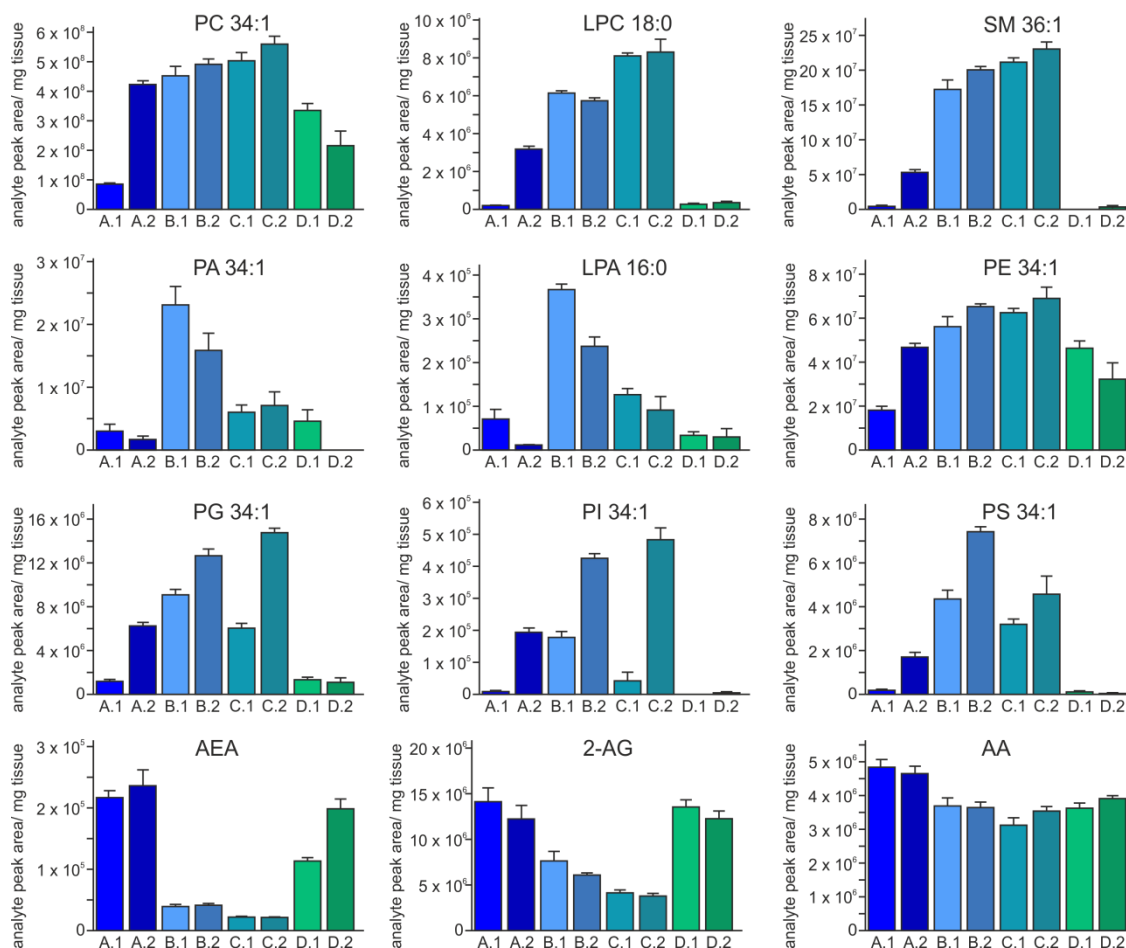


**Figure 4.12 Analyte extraction via different homogenization solvents:** Recovery (analyte peak area) of various endogenous lipid species normalized to tissue weight ( $n=6$ ), achieved by different homogenization solvent mixtures: A.1: MTBE - 0.1 % formic acid; A.2: MTBE - 50 mM Tris-HCl; B.1: MTBE/methanol (10:3; v/v) - 0.1 % formic acid; B.2: MTBE/methanol (10:3; v/v) - 50 mM Tris-HCl; C.1: methanol/chloroform (1:2; v/v) - 0.1 % formic acid; C.2: methanol/chloroform (1:2; v/v) - 50 mM Tris-HCl; D.1: ethylacetat/n-hexane (9:1; v/v) - 0.1 % formic acid; D.2: ethylacetat/n-hexane (9:1; v/v) - 50 mM Tris-HCl.

These variations likely originate from a higher release of the endogenous analytes by specific solvent combinations, due to a more effective breakdown of the lipid-lipid, lipid-protein interaction in the membranes during simultaneous chemical and mechanical homogenization. Consequently, different calculated concentrations can be obtained, here most clearly demonstrated for AEA. While the recovery of AEA- $d_4$  barely differs among the used homogenization solvents, the extraction of endogenous AEA succeeds better using MTBE only (Fig. 4.11; Fig. 4.12). This leads to a much higher final calculated concentration of AEA as compared to values obtained via other homogenization solvent combinations (Lerner *et al.*, 2016). In general, the patterns for PL ISTD

recoveries, as well as for the intensities of the corresponding endogenous analytes are mainly similar. Ethylacetate/n-hexane as well as MTBE-formic acid showed the poorest extraction efficiency for most PL species, whereas these homogenization solvents were superior in extraction of eCBs. MTBE/methanol combined with formic acid provided overall sufficient extraction efficiency across the lipid classes. Particularly for LPA and PA, MTBE/methanol-formic acid showed the best results among the tested solvent combinations (Fig. 4.12). Both lipid classes need protonation of their phosphate groups to avoid peak tailing, which can be achieved by addition of formic acid. We used 0.1 % formic acid because too high acidic conditions can render artificial formation of LPA through hydrolysis of major abundant LPC species (Aaltonen *et al.*, 2010; Triebel *et al.*, 2014). However, Triebel *et al.* (Triebel *et al.*, 2014) found, that even higher acidity caused by 0.1 M HCl did not produce relevant artifacts.

Altogether our results demonstrated that extraction with MTBE/methanol-formic acid was suitable for PL and eCB co-extraction. Furthermore, MTBE provides the advantage to form the upper lipid-containing phase, which enables faster, cleaner and high-throughput recovery, is non-toxic and non-carcinogenic, and it does not render oxidative damage of lipids during the extraction as observed with chloroform. OEA and PEA could only be relatively quantified due to the release in blank samples via this protocol. Use of THL, URB and BHT improve the stability of the method by reduction of *ex-vivo* enzymatic activities. The developed method could be also applied with small modifications according to Schuhman and colleagues for lipid extraction from human and mouse plasma. Fig. 4.13 shows the final lipid extraction protocols for both tissue and plasma.

### 4.3.3 LC/MRM qualitative and quantitative profiling

Lipid extraction as well as LC/MS conditions were optimized in order to allow reliable identification and quantification of various lipid species, irrespective of their abundance and ionization properties. Moreover, refined sample preparation enabled the measurement of lipids in different tissue types, such as mouse brain, heart, lung and human as well as mouse plasma. PC-, LPC- and SM-species were quantified in positive ion mode using the transition to their phosphocholine headgroup at  $m/z$  184, whereas transitions to their FA fragments, analyzed in negative ion mode, were used for validation. PA-, PS-, PI-, PG- and PE-species were acquired in negative ion mode, using transitions to their FA-fragments ions for qualification and quantification. For LPAs, transitions to the headgroup at  $m/z$  153 give rise to the highest signal intensity and were thus, used for quantification, while transition to their fatty acid fragment served as qualifier.



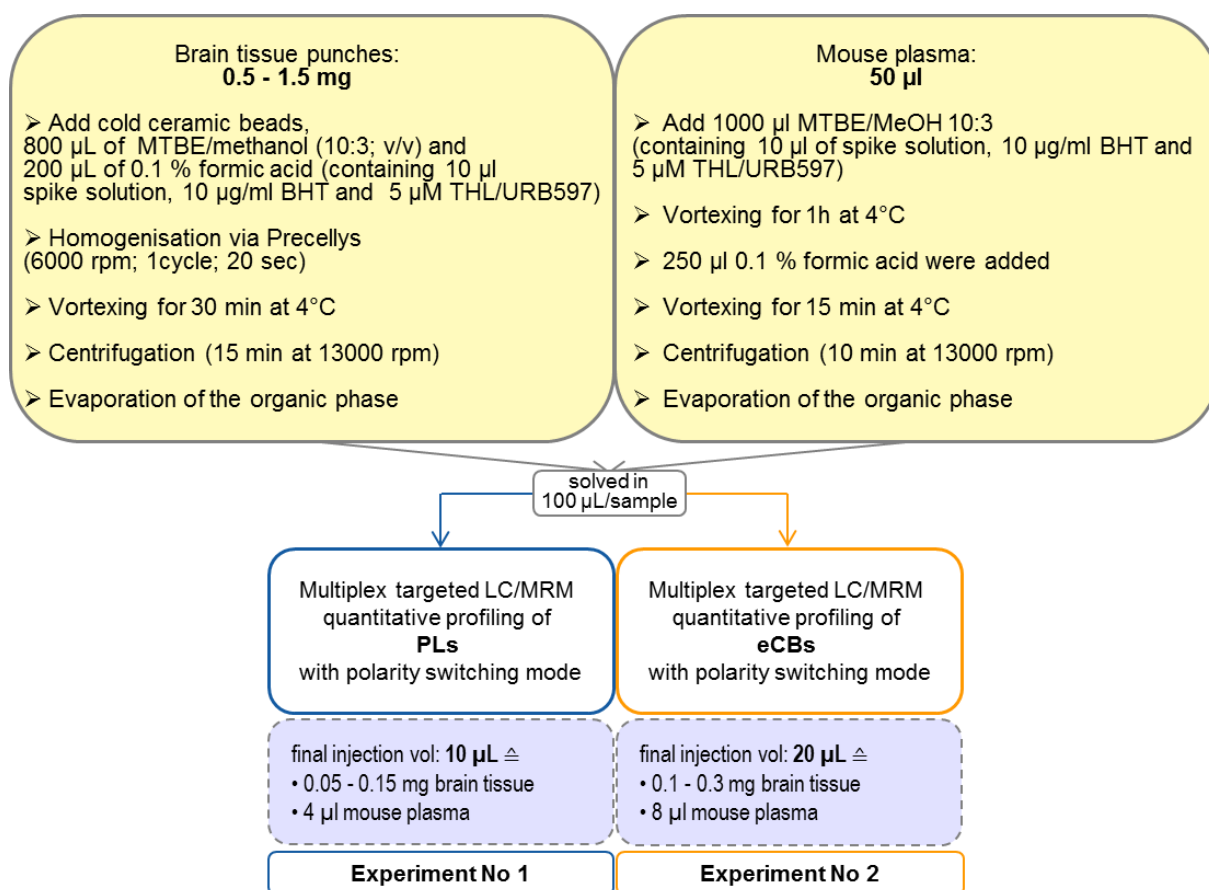


**Figure 4.13 PL and eCB co-extraction workflow:** Overview of PL and eCB co-extraction from mouse brain and plasma.

Altogether, this study comprises the quantification and statistical analysis of 74 different lipid molecules: eCBs, ERCs, and PLs corresponding to 9 different PL classes (Tab. 4.2- 4). Some of the PL molecules possess the same molecular weight, but different structural information, as they are composed of different FA combinations. Identification of these molecules was enabled due to analysis of their RTs. Furthermore, the relative comparison of retention/elution properties with structural heterogeneity of a given PL type facilitates the proper identification of different PL species. Tab. 4.7 shows RTs of certain PLs obtained by the method described here. The specific resulting RT pattern of PLs supports thereby proper molecule identification and quantification.

Exemplary results for PL concentrations obtained in the preliminary experiments for determination of mouse brain PL levels are given in Fig. 4.14. The different PL species show distinct distribution patterns among the six investigated mouse brain regions. While PC 34:1, LPC 18:0, SM 36:1 and PS 34:1 have mainly the same abundance in every analyzed brain regions, the remaining PL are unequally distributed among the six brain regions (Fig. 4.14).

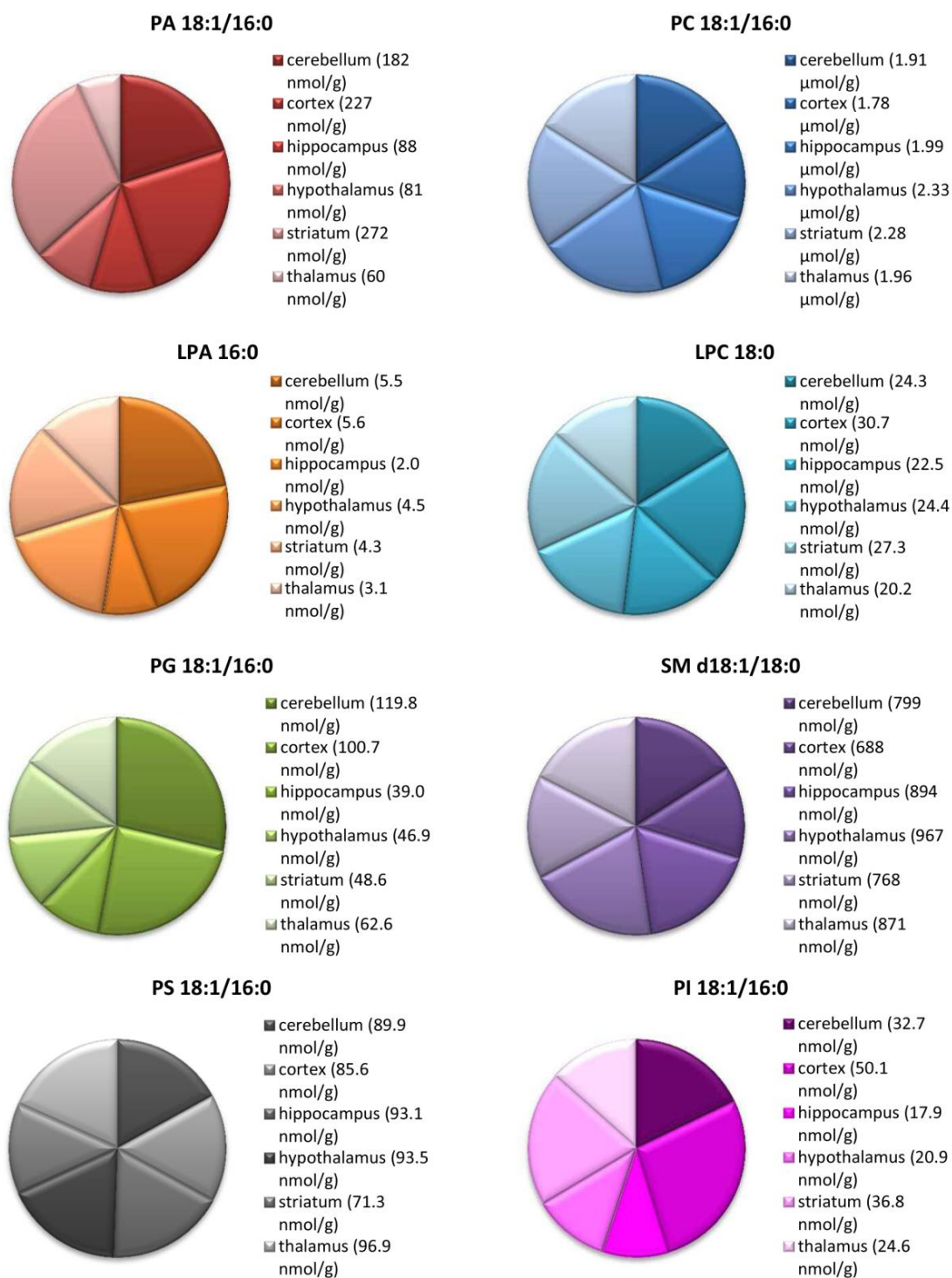


**Figure 4.14 PL concentrations among different mouse brain regions:** Absolute concentrations of 8 different PL calibration standards, obtained via the method, developed in this study for eCBs, ERCs and PL co-extraction. The different PL species show distinct distribution patterns among the six investigated mouse brain regions (from Lerner et al., 2016).

#### 4.4 Discussion

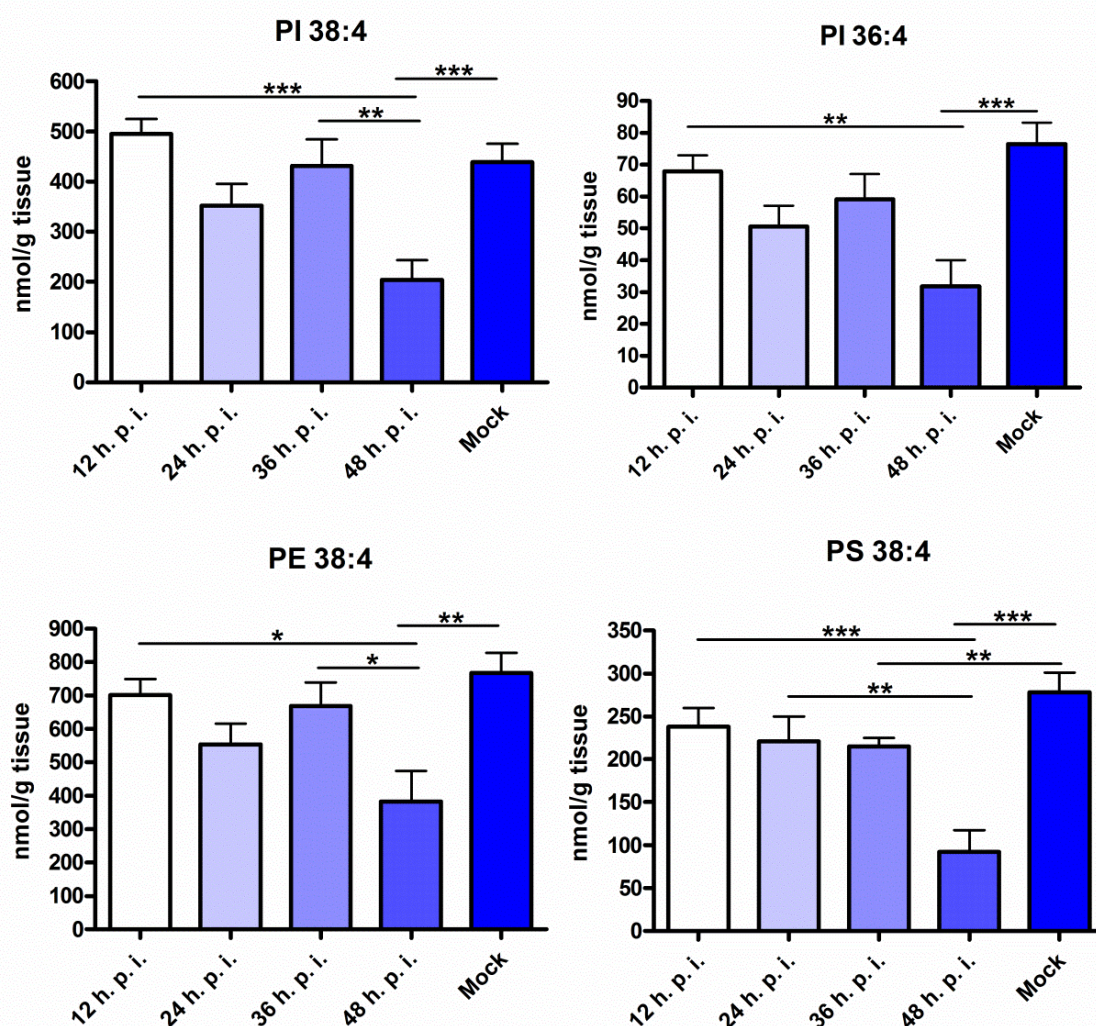
Increasing interest in the molecular metabolism of lipids and its role in diseases led to development of various approaches for lipidomic profiling using LC/MS. Even though there is a great variety of methods available for eCB or PL analysis, to our knowledge none of them is aligned to allow simultaneous extraction of eCBs and PLs in one step from the same tissue. Here we report the development of a reliable method suitable for eCB, ERCs and PL co-extraction even from sub mg amounts of tissue. An interesting outcome of the method development highlighted the importance of the homogenization process. The use of different homogenization solvents during mechanical homogenization led to different calculated concentrations of some of the measured analytes, since the ratio between ISTD- and endogenous analyte recovery differed among the tested homogenization solvent combinations. Therefore exact comparison of molecule concentrations especially between different studies requires comparable sample preparation. Furthermore, adjusted usage of homogenization solvents may improve lipid extraction from specific structures, for instance membrane or cell lumen. Despite variations due to different extraction protocols or the kind of tissue investigated, we found analyte concentrations within a range consistent with previous reports, thus further validating our method (Abbott *et al.*, 2013; Triebel *et al.*, 2014).

Fig. 4.14 shows absolute values of PLs among six different brain regions. Noteworthy, the distribution patterns vary among such PLs. The typical membrane constituent PC 34:1 is almost equally distributed among the six brain regions, whereas PLs directly involved in lipid signaling such as LPA 16:0 show alternating lipid levels. In the latter case, the lowest abundance was found in the HC. This distribution differences may underlie a homology between functional role of lipids and their basal concentration pattern across brain regions. Such variations underline also the importance of spatially specified analysis. Using whole brain homogenates for the investigation of pathogenic events occurring in the HC can lead to dilution of potential alterations in the lipid levels due to the higher concentrations in the other brain regions.

In this study we identified and quantified 74 molecules, including 69 different PL species. However, these PL species represent only a part of the lipids that can be detected and quantified via this method. Depending on the PLs of interest, the acquisition method can be extended with the relevant transitions. Via previous targeted discovery those transitions can be approved. Furthermore enables additional analysis of PIS relative comparison of the FA content. Finally allows the expanded gradient time of 55 min also the additional analysis of stronger lipophilic components such as TGs and CLs.

To our knowledge, this is the first study rendering the quantification of such a large panel of lipids across multiple brain regions and periphery, thereby allowing the comparison of lipid

concentrations throughout different tissue types. Since such data can be already obtained from only 10 µl out of 100 µl final lipid extract, the developed method offers the additional opportunity for multiple further analyses via e.g. PIS and NLS. Moreover, as an additional perspective, we adapted the established method in order to extract PLs from bio banked blood drops, which gave us already first promising results for its further implementation for lipid analysis in our lab. Finally, a translational study profiling lipids after bacterial infection, proved our method as applicable in other labs. Using our protocol to quantify PLs in a lethal murine model for *Francisella tularensis* (subcutaneous injection of *Fn*), they identified depletion of several AA-containing PLs in the splenic white pulp of mice 48 h post injection, thereby potentially serving as an AA pool for splenic eiCs production (Fig. 4.15) (Scott *et al.*, 2017).



**Figure 4.15 Arachidonic acid (AA)-containing PLs of the splenic white pulp are depleted during *Francisella novicida* (Fn) infection:** Quantitative LC/MS of parent PL containing arachidonyl group normalized to total input splenic tissue (grams) evaluated every 12 hours post-infection (h.p.i.), lethal dose Fn, SQ. Lipid levels were analyzed using one-way ANOVA for injection time points and considered significant at a p-value < 0.05 (n=10). Error bars denote SEM.

### 5 DUAL EXTRACTION METHOD FOR LIPIDOMIC AND TRANSCRIPTOMIC PROFILING

#### 5.1 Introduction

Lipidomics seeks to characterize the lipid profile within a biological system. Yet, also the role of proteins and genes involved in the regulation of lipids is important to be determined in order to comprehensively understand and unravel the lipid function. Accordingly, early protein and gene studies in yeast species already had a valuable contribution to our present understanding of PL metabolism and function (Buré *et al.*, 2013). Studies of disease related genes reveal also the involvement of proteins important for lipid function, such as lipid binding proteins, lipid transporters or enzymes involved in lipid metabolism (van Meer, Dennis R Voelker, *et al.*, 2008). Such data highlight the requirement to advance our insight into the complete molecular plasticity associated with neurological disorders, in order to attain an interrelated picture of the role of biomolecules that underlie an altered cellular function with disease, hence to set basis for further biomarker identification, development of therapeutic targets and monitoring of treatment efficacy. Typically, such comprehensive studies are performed using multiple animal batches, hence suffering from the variability originating from different individuals. Splitting of tissue is also a common way to profile multiple molecule species, even though tissue heterogeneity may negatively influence the output conclusion. A more recent study circumvents this bias by previous pulverization of the tissue, albeit requiring a large amount of material (Reiser *et al.*, 2011). Thus, to provide a mean for successful treatment of disease, in this chapter we present the implementation of a method for simultaneous extraction of PLs, eCBs and RNA from the same, small tissue sample for combined lipidomic and transcriptomic profiling.

#### 5.2 Materials and methods

##### 5.2.1 RNA and lipid co-extraction

In order to isolate both RNA and lipids from the same tissue sample and particularly from discrete amounts resembling a brain punch, we established an improved LLE method, combined with RNA extraction via RNeasy® Mini Kit. Brain cerebellum powder as described in 4.2.2.1 was used to optimize the extraction process. Therefore, aliquots of the cerebellum powder smaller than 1 mg were weighed into RNase-free precellys tubes, containing cold ceramic beads. Subsequently, 600 µL of RLT buffer (supplied with the RNeasy® Mini Kit) containing 5 µM THL/URB597, 10 µg/mL BHT and 1 % β-mercaptoethanol in final volume were added together with 200 µL chloroform to the aliquots. All samples were spiked with 10 µL ISTD mixture, corresponding to concentrations used for eCB, ERCs and PL co-extraction (see 4.2.2.2) and homogenized using

Precellys 24 (PepLab, Erlangen, Germany) (6000 rpm; 20 sec). The lysate was then transferred into a new microcentrifuge tube and centrifuged for 5 min at full speed and 4°C, hence building two phases. The originating upper phase was used for further RNA extraction using the RNeasy® Mini Kit according to the manufacturer's instructions, including the on-column DNA digestion step (RNase-Free DNase Set, Qiagen, Hilden, Germany). The RNA was eluted in a total volume of 50 µL RNase free water and stored at -80° C. The lower chloroform-containing phase was used for lipid extraction according to 4.2.2.2. Briefly, 800 µL of MTBE/methanol (10:3; v/v), were added to each chloroform-containing phase, respectively together with 200 µL of 0.1 % formic acid and vortexed for 45 min at 4°C. After subsequent centrifugation (15 min, 13000 rpm and 4°C) the upper organic phase was recovered, evaporated and reconstituted in 90 µL methanol for storage at -20°C. Out of this lipid solution 18 µL diluted with 2 µL H<sub>2</sub>O (methanol/H<sub>2</sub>O (9:1; v/v)) were used for PL analysis and 27 µL were evaporated again and resolubilized in 30 µL ACN/H<sub>2</sub>O (1:1; v/v) for eCB and ERCs measurement, respectively. All extraction procedure steps, except the RNA extraction steps (see RNeasy® Mini Kit protocol), were carried out at 4°C. In previous pilot experiments, the chronological order of lipid and RNA extraction, the RNA extraction method, e.g. Trizol® Reagent (Invitrogen, Darmstadt, Germany) versus RNeasy® Mini Kit, as well as the tissue homogenization process including the choice of MTBE or chloroform as homogenization solvent were tested (data not shown). In order to evaluate the lipid extraction efficiency of the established method the ISTD recovery and matrix effects were determined in triplicates, analogue to eCB, ERCs and PL co-extraction (see 4.2.2.2) and analyte intensities as well as RNA content were measured. A workflow overview of the established method (which is further referred to as dual protocol) is depicted in Fig. 5.1.

### 5.2.2 Lipidomic profiling

The LC conditions for eCBs and PLs as well as their targeted qualitative and quantitative profiling were set as previously described 4.3.1. Calibrations standards and ISTDs were acquired for method optimization and mouse cerebellum powder served as test tissue for method development according to 4.2.2.1.

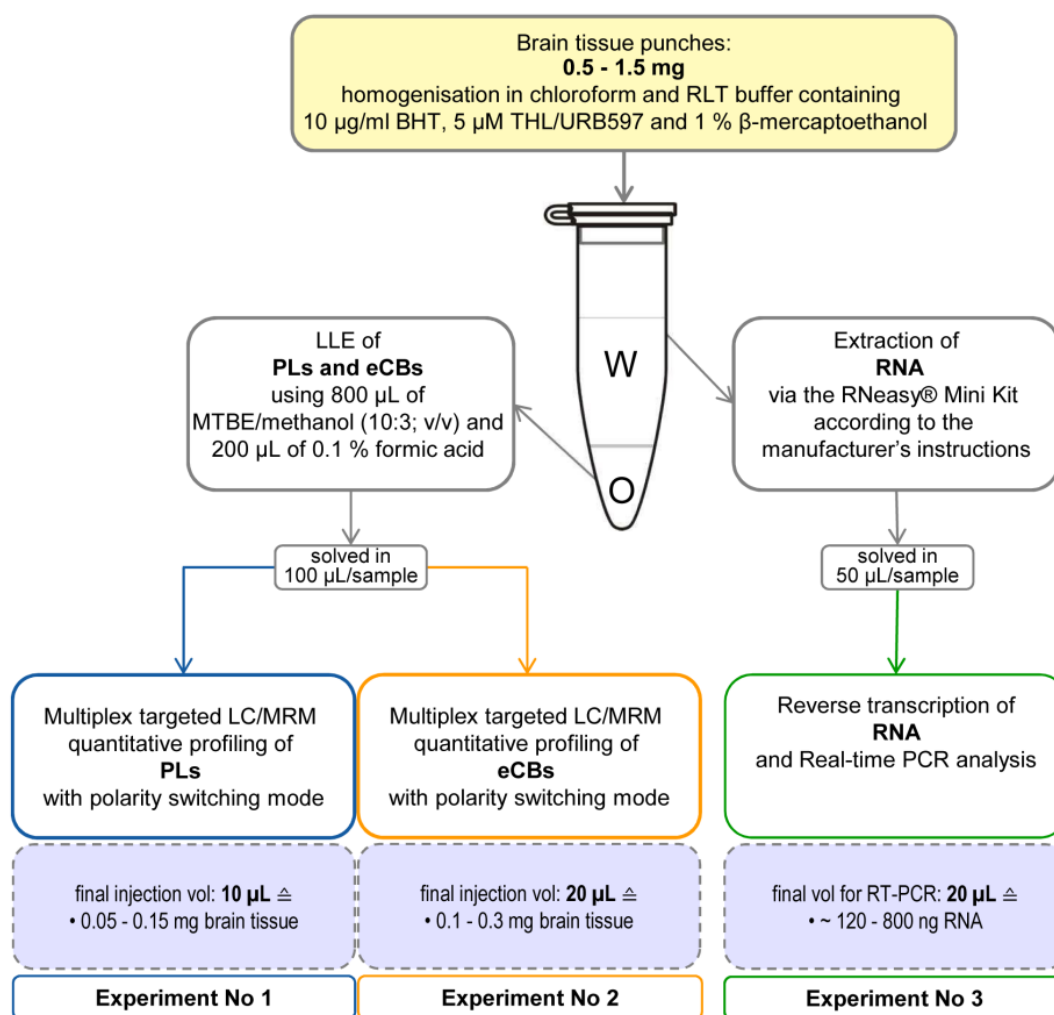


**Figure 5.1 Overview of the dual extraction workflow:** Overview of the dual extraction protocol performed in this study. Brain tissue punches spanning from 0.5 to 1.5 mg were used to co-extract PLs and eCBs, as well as RNA, respectively. The PL and eCB extracts were subjected to multiplex targeted LC/MRM quantitative profiling, while the RNA extracts were subjected to Real-time PCR analysis.

## 5.2.3 Transcriptomic profiling

### 5.2.3.1 RNA quantification and integrity assessment

For comparison of RNA extraction efficiency among the different RNA and lipid co-extraction strategies, RNA quantity and quality was assessed. Therefore, isolated RNA was quantified via the NanoDrop 2000c spectrometer (Thermo Scientific, St. Leon-Rot, Germany), and RNA integrity was determined using the 2100 Bioanalyzer and the RNA 6000 Nano kit protocol, both from Agilent (Waldbronn, Germany) to obtain the RNA integrity numbers (RIN = 1; lowest RNA quality to RIN = 10; highest RNA quality).

**5.2.3.2 Reverse transcription and real-time PCR analysis**

Approximately 120 – 800 ng isolated RNA per brain punch was reverse-transcribed in order to generate complementary DNA (cDNA) using the High Capacity cDNA Reverse Transcription Kit with random primer hexamers (Applied Biosystems/ Life Technologies, Darmstadt, Germany). The cDNA was diluted 1:5 in H<sub>2</sub>O and amplified in the qPCR using commercial FAM dye-labeled TaqMan assays (Applied Biosystems/ Life Technologies, Darmstadt, Germany) detecting mRNA encoding fatty acid amide hydrolase (FAAH), N-acyl phosphatidylethanolamine phospholipase D (NAPE-PLD), cytosolic phospholipase A2 (Pla2g4a), cannabinoid type-1 receptor (Cnr1), c-fos, brain-derived neurotrophic factor (BDNF), and as reference gene Gusb (Tab. 5.1). The qPCR reactions were performed in duplicates via TaqMan Gene Expression Mastermix (Applied Biosystems/ Life Technologies, Darmstadt, Germany) and analyzed with an ABI 7300 Real-Time PCR cyler (Applied Biosystems/ Life Technologies, Darmstadt, Germany).

**Table 5.1 List of TaqMan assays obtained for qPCR:** For each gene, the pair of primers with the best coverage was selected according to the manufacturer suggestion.

Gene symbol	Gene name	Assay code
Mgll	monoglyceride lipase	Mm00449274_m1
Dagla	diacylglycerol lipase, alpha	Mm00813830_m1
Daglb	diacylglycerol lipase, beta	Mm00523381_m1
Faah	fatty acid amide hydrolase	Mm00515684_m1
Cnr1	cannabinoid receptor 1	Mm00432621_s1
Gusb	glucuronidase, beta	Mm01197698_m1
Gapdh	glyceraldehyde-3-phosphate dehydrogenase	Mm99999915_g1
Napepld	N-acyl phosphatidylethanolamine phospholipase D	Mm00724596_m1
Pla2g4a	cytosolic phospholipase A2, group IVA	Mm00447040_m1
Bdnf	brain derived neurotrophic factor	Mm04230607_s1
Fos	FBJ osteosarcoma oncogene	Mm00487425_m1

**5.3 Results**

Lipidomic and transcriptomic profiling is typically carried out in distinct experiments (animals/tissue areas), due to a general lack of extraction protocols suitable to isolate both RNA and lipids from the same discrete tissue sample. In order to circumvent these limitations, we went one step further to try if the method established for eCB and PL co-extraction can also be suitable for simultaneous RNA extraction. In the first phase of the method development, the practicable chronological order of RNA and lipid extraction was determined. When lipid extraction was carried out prior to RNA extraction, irrespective of the homogenization solvent used or the addition of RNases denaturing substances like GTC, a high or total loss of the RNA content was observed. Therefore, RNA followed by lipid extraction was further assessed. Two common standard RNA extraction protocols (Trizol® Reagent vs Qiagen RNeasy® Mini Kit) were



compared, especially regarding their suitability for subsequent lipid extraction. Although Trizol® Reagent provided higher extraction efficiency concerning the RNA yield compared to standard Qiagen RNeasy® Mini Kit (Grabmüller *et al.*, 2015), it is not applicable to RNA and lipid co-extraction, because its ingredient phenol is not evaporable and hinders subsequently the LC/MS analysis via column contamination, peak tailing, carry-over etc. Unfortunately, extraction of lipids using the method described above from the pellet obtained after RNA extraction following the Qiagen RNeasy® Mini Kit protocol instructions resulted in poor endogenous analyte yield and ISTD recoveries. As previous experiments revealed the importance of simultaneous chemical and mechanical homogenization, we improved the Qiagen RNeasy® Mini Kit protocol by addition of 200 µl chloroform to RLT buffer before the homogenization step via Precellys 24. Several advantages were attained due to this optimization. First of all, by addition of chloroform, two clearly separated phases were created, facilitating the isolation of RNA and lipids. Furthermore, a substantial enhancement in endogenous lipid extraction, as well as ISTD recovery could be observed with this protocol. The peak areas of endogenous analytes were increased up to one potency among the different lipid species by addition of chloroform, indicating an improved homogenization and extraction efficiency using the dual protocol (Fig. 5.2).

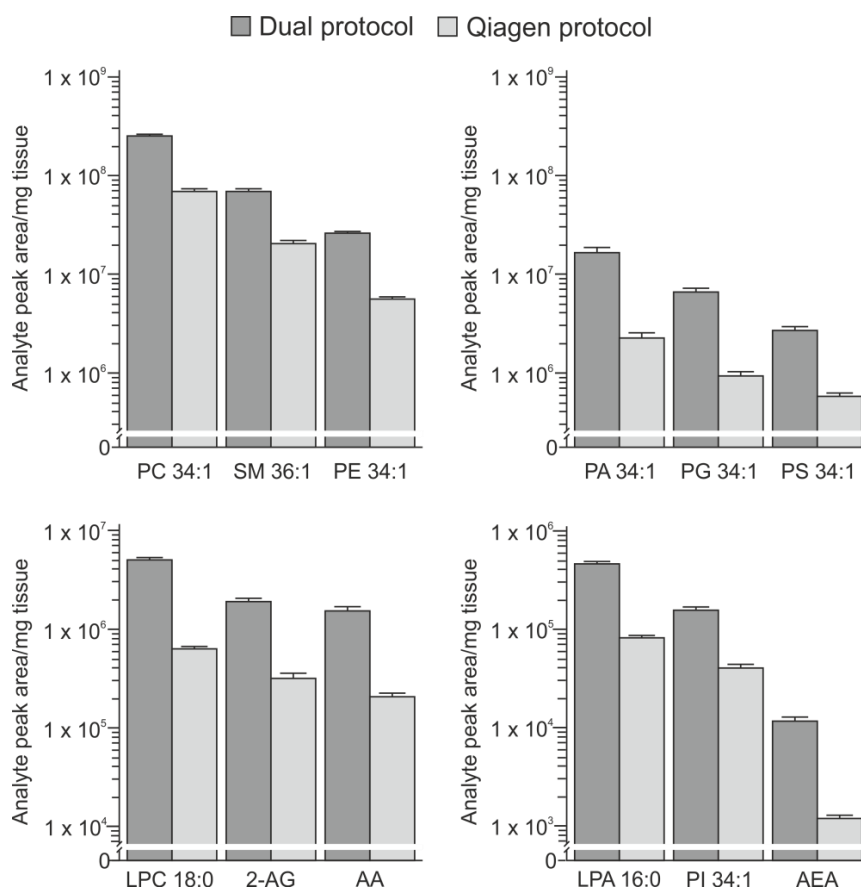


**Figure 5.2 Analyte extraction via dual- vs. standard Qiagen protocol:** Recovery (analyte peak area) of various endogenous lipid species normalized to tissue weight (n=6), achieved by two different extraction protocols (light grey: standard Qiagen protocol; dark grey: dual protocol).

Moreover, the ISTD recoveries achieved via application of the dual protocol are up to 10 times higher for each of the investigated lipids (Tab. 5.2).

**Table 5.2 Percentage of ISTD recovery via dual- or Qiagen extraction protocol:** For estimation of the recovery, cerebellum tissue powder samples were spiked with internal standards (ISTDs) prior to extraction (n=3) and post-extraction (n=3). Recovery was calculated in percentage by comparing averages of ISTD peak areas obtained prior to and post-extraction, respectively.

Analyte	Recoveries [%]	
	Dual protocol	Qiagen protocol
2-AG-d <sub>5</sub>	64.8	7.7
AEA-d <sub>4</sub>	41.0	4.3
AA-d <sub>8</sub>	61.6	6.8
LPC 17:0	74.9	8.2
PC 17:0/14:1	50.4	5.9
SM d18:1/12:0	67.9	7.2
LPA 17:0	67.2	6.8
PA 17:0/14:1	53.6	5.7
PG 17:0/14:1	69.5	6.1
PS 17:0/14:1	70.7	5.0
PE 17:0/14:1	63.5	5.5
PI 17:0/14:1	77.7	7.3

This may result from the initial organic environment due to chloroform, which enables a better solubility of the ISTD analytes through the entire procedure and thereby, may further prevent the formation of micelles or lipid protein binding. Different homogenization solvents other than chloroform were also tested. However, chloroform, which is also used in standard TRIzol-chloroform extraction protocols, was superior to other organic solvents like MTBE in terms of the obtained total RNA concentrations and furthermore, facilitates the extraction and handling first of the RNA, due to its characteristic to form the lower lipid containing phase. The total RNA quantity was even higher using the dual protocol (664.4 ± 36.73 ng/mg tissue) as compared to the standard Qiagen protocol (210.4 ± 15.03 ng/mg tissue) (Fig. 5.3).

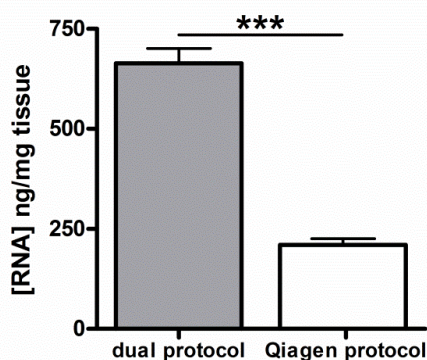


**Figure 5.3 Extracted whole RNA content via dual- vs standard Qiagen protocol:** Total RNA yield normalized to tissue weight, obtained by standard Qiagen protocol (light grey) vs. dual protocol (dark grey). Statistical analyses of the difference between group means were carried out by using two-tailed unpaired Student’s t-test and considered significant at a p-value < 0.05 (n=6).

Generally we could observe, that homogenization following the dual protocol obtained better results via Precellys 24 (PecqLab, Erlangen, Germany) (6000 rpm; 20 sec) as compared to TissueLyser II (Qiagen, Hilden, Germany) (30 Hz; 30 sec) regarding the RNA. Moreover, the dual protocol exhibited even higher RNA quality as represented by the RIN number as compared to the standard Qiagen protocol (Tab. 5.3).

**Table 5.3 RNA quality achieved via dual- or Qiagen protocol:** RNA integrity was determined using the 2100 Bioanalyzer and the RNA 6000 Nano kit protocol, to obtain the RNA integrity numbers (RIN = 1; lowest RNA quality to RIN = 10; highest RNA quality).

RIN number	
<u>Dual protocol:</u>	
sample 1	10
sample 2	10
sample 3	10
<u>Qiagen protocol:</u>	
sample 4	8.6
sample 5	8.9
sample 6	8.8

In addition, values obtained for reproducibility and matrix effects proved the dual method as reliable (Tab. 5.4). Finally, using cerebellum punches from wildtype mice we were able to detect via the dual protocol all targeted molecules even from sub mg amounts of tissue. We then applied the method to punches, obtained from a mouse model of KA-induced seizures (see Chapter 6). Altogether, these results highlight the developed dual protocol as an excellent tool for combined lipidomic and transcriptomic profiling.

**Table 5.4 Intra assay reproducibility and matrix effect via dual extraction:** Intra assay reproducibility was calculated as the standard error of the mean of ISTD peak areas spiked prior to extraction. Additionally, for matrix effect evaluation, ISTD peak areas of spiked calibration mix (n=3) were compared to ISTD peak areas in samples spiked post extraction.

Analyte	Reproducibility SEM %	Matrix effect %
2-AG-d <sub>5</sub>	1.95	42.16
AEA-d <sub>4</sub>	0.87	50.69
AA-d <sub>8</sub>	3.37	43.11
LPC 17:0	5.45	4.05
PC 17:0/14:1	7.98	6.68
SM d18:1/12:0	8.02	3.91
LPA 17:0	10.13	11.63
PA 17:0/14:1	6.11	11.51
PG 17:0/14:1	10.34	9.12
PS 17:0/14:1	7.02	8.57
PE 17:0/14:1	9.04	40.05
PI 17:0/14:1	12.57	12.71

### 5.4 Discussion

Increasing interest in the molecular metabolism of lipids and its role in diseases led to development of various approaches for lipidomic profiling using LC/MS. However, to comprehensively elucidate a lipid-related signaling pathway in a disease, the corresponding transcriptome and proteome needs to be concurrently investigated. Yet, this typically requires three distinct samples, e.g. either from multiple cohorts or splitting of tissues in pieces, to allow for the different extractions of: proteins, mRNAs and lipids, respectively (Reiser *et al.*, 2011).

Many neurological diseases may require extractions from very low tissue amounts such as brain punches (Holter *et al.*, 2001), as for instance in disorders where specific brain subregions or different cell populations are distinctly involved in (Fanselow and Dong, 2010; Brody *et al.*, 2014) and additionally, so far, multiomic studies are mostly restricted to RNA and protein research (HU *et al.*, 2015; Schouten *et al.*, 2016).

Here we report an advanced extraction method for simultaneous lipidomic and transcriptomic profiling from the same discrete tissue sample. Therefore, we developed an extraction protocol for eCB and PL and concurrently RNA isolation (5.2.1). To date, lipidomic and transcriptomic profiling is typically carried out in distinct experiments (animals/tissue regions). By combining the isolation of lipids and RNA in one experiment it is possible to not only reduce the number of animal models, but also the time and costs necessary to carry out lipidomic and transcriptomic profiling. Moreover, analysis of signaling pathways is more reliable by obtaining the molecular components from the same tissue rather than from two distinct samples, circumventing thereby the pitfalls originating from tissue heterogeneity. This is all the more true for discrete amounts of tissues, such as often affordable when needed to localize specific physiological or pathophysiological events. Thus, the here described method, enables efficient co-extraction of lipids and RNA from the same tissue punch, thereby providing the possibility for reliable lipidomic and transcriptomic profiling under pathogenic conditions. Since RNA sequencing or lipid discovery via MS are available methods for profiling, a large molecular spectrum can be targeted this way.

Limitations: At present, the proteins cannot be investigated by proteomic tools from the extract generated using this method. Although the aqueous phase containing proteins is available, it seems that some of the chemicals used in the RNA kit interfere with a proper protein analysis. Prospective studies will be directed to inquire whether clean-up strategies of the protein phase can be applied to enable proteome analysis.

## 6 APPLICATION TO ACUTE EPILEPTIC SEIZURE MODEL

### 6.1 Introduction

The methods developed within the scope of this study provide the potential for comprehensive quantitative molecular profiling in biological systems at enhanced spatial resolution under pathological conditions. Applied in comparative studies, changes in lipid related molecular pathways induced by disorders can be identified. For early diagnosis, predictability of the in vivo response and thus effectiveness of a treatment, it is important to gain a complete understanding of interacting lipid signaling pathways in the progression of a disease. In this context, we employed the established methods to a mouse model of acute epileptic seizures induced by KA. Using this mouse model, it was previously shown within our group that the ECS controls key epileptogenic circuits in the HC (Monory *et al.*, 2006). KA is a ligand for a specific group of ionotropic glutamate receptors. Binding to the receptors leads to strong neuronal activation causing excitotoxicity predominantly in the limbic system, hence mimicking mainly seizures observed in TLE (Sperk, 1994; Ben-Ari and Cossart, 2000). Continuous postsynaptic excitation results in eCB production, which attenuate the excitotoxicity by decreasing transmitter releases at the presynapse via CB1, also supported by a more recent study within our group (Guggenhuber *et al.*, 2010). Another study of KA-induced neuronal injury from Guan and colleagues reported decreased levels of major PLs mainly consisting of PUFAs in the HC, as well as increment in acylated forms of PE, a precursor of AEA (Guan *et al.*, 2006). Although distinct alterations of PLs, eCBs, as well as eiCs have been previously evidenced in distinct epileptic seizure models, these studies were typically confined to specific brain areas, such as HC, cCTX or whole brain homogenates, thereby often requiring large tissue amounts.

The first aim of our study was to extend our knowledge of the lipid plasticity associated with acute epilepsy through investigation of various brain regions, as well as peripheral organs and plasma to unravel the changes affecting the whole body.

The second aim was to increase the spatial resolution for quantitative neurolipidomics in acute epilepsy model in order to accurately pinpointing the brain subregions involved in epileptic seizures and the corresponding lipid fingerprints. Moreover, lipidomic and consequently combined transcriptomic profiling at this enhanced spatial resolution was applied in order to get a deeper understanding of the mRNAs and lipid players in the epilepsy-affected pathways.

Finally, the application of MSI to brain sections derived from this mouse model, e.g. at higher spatial resolution than brain punches, should lead to new insights into the lipid distribution under such pathological conditions

### 6.2 Material and methods

#### 6.2.1 Induction of acute excitotoxic seizures

In order to induce acute epileptic seizures in mice, KA was used as described above (Sperk, 1994; Ben-Ari and Cossart, 2000; Monory *et al.*, 2006). All experiments were carried out in accordance with the European Community's Council Directive of 22 September 2010 (2010/63EU) and approved by the Ethical Committee on animal care and use of Rhineland-Palatinate, Koblenz, Germany (23 177- 07/G 13-1-021). C57BL/6N male mice (80-100 days of age) were held at a 12 h / 12 h light dark cycle with access to food and water ad libitum. Experimenters (n=2) were blind to injection. Mice were injected intraperitoneally with either KA at a dose of 30 mg/kg body weight (Sigma-Aldrich, St. Louis, USA) or vehicle (0.9% saline). Subsequently, animals were monitored for the duration of 1 h and scored at 15 min intervals. Animals were scored according to the following scale: 0 – no response; 1 – immobility and staring; 2 – forelimb and/or tail extension, rigid posture; 3 – repetitive movements, head bobbing; 4 – rearing and falling; 5 – continuous rearing and falling; 6 – severe clonic-tonic seizures; 7 – death (Monory *et al.*, 2006). 1 h after injection mice were shortly anesthetized with isoflurane (Forene R, AbbVie Deutschland GmbH & Co. KG, Wiesbaden, Germany) and sacrificed by decapitation. Seizure induced mice and control mice were sacrificed in alternate order. Blood, peripheral organs and brains were isolated in parallel by 2 experimenters. Brain and peripheral organs were directly frozen on dry ice and blood was collected in ice-cold 500 µL EDTA plasma extraction tubes (containing previously added chemicals: 10 µM indomethacin; 25 µM tetrahydrolipstatin/URB to prevent ex-vivo enzymatic activities). This collection procedure took 30 s per mouse. All tissue samples were then stored at -80°C till further processing. Plasma tubes were directly centrifuged at 4°, 2000 g for 10 min, and the resulting upper plasma phase was removed and stored at -80°C without delay. This whole procedure was invariably applied for every project, to keep the possibility of measuring additional sources even if only a specific selection of tissue was of interest.

#### 6.2.2 Preparation of six brain regions and periphery from KA-induced / control mice and extraction for lipidomic profiling

Investigation of lipid changes in various brain regions and periphery was performed as part of a collaborative work within our group. In this context additional analysis of eiCs and ERCs was possible. Fig. 6.1 shows an overview of the workflow for PL, eCB, ERCs and eiC analysis. In total, 18 mice were injected intraperitoneally with either KA (9 animals) or vehicle (0.9% saline, 9 control animals). Isolation of the brain regions and detailed weighing procedure are described in 4.2.2.1. Frozen brain regions, as well as frozen peripheral organs were pulverized and then aliquoted by weighing in the cold room into 2-4 mg portions. From each tissue sample, two

aliquots were generated: one for PLs and one for eCB, ERCs and eiC co-extraction. All tissue samples were then stored at  $-80^{\circ}\text{C}$  until further extraction. For the detailed description of eCB, ERCs and eiC extraction procedure and measurement see Lerner et al. 2016 (Lerner *et al.*, 2016). PLs were analyzed according to 4.3.1. PLs having the same composition as the calibration standards and additionally, specific AA-containing PLs were targeted (Tab. 4.2-4). Measurement of eCBs was conducted as part of the ERCs and eiC analysis (Fig. 6.1).

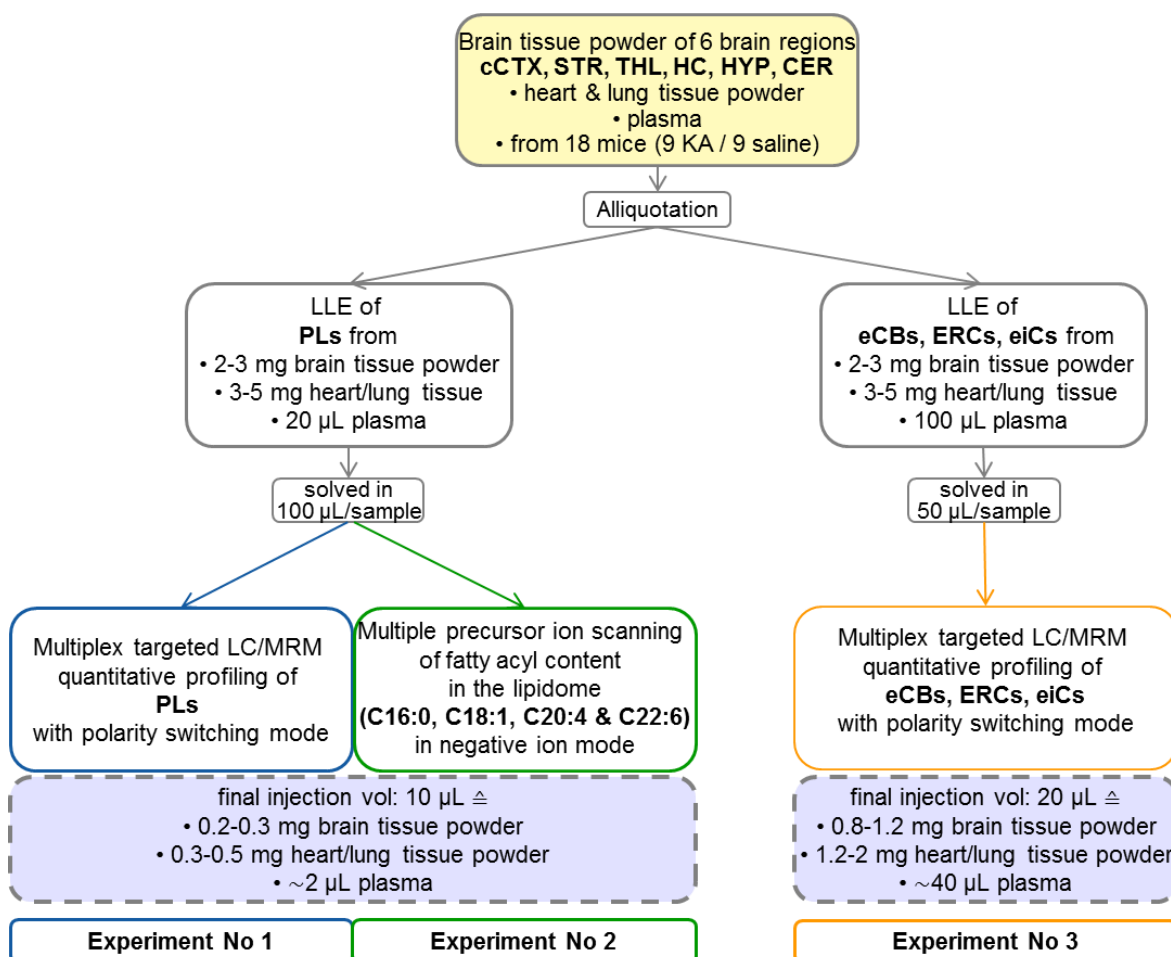


**Figure 6.1 Overview of the workflow for PL, eCB, ERCs and eiC analysis.** Overview of the three experiments combined in this study. Two aliquots of tissue and plasma samples were used to extract PLs and co-extract eCBs, ERCs and eiCs, respectively. The PLs extract was subjected to multiplex targeted LC/MRM quantitative profiling of PLs (Experiment No 1), and multiple precursor ion scanning of fatty acyl content in the lipidome (Experiment No 2). The second extract, containing eCBs, ERCs and eiCs was subjected to multiplex targeted LC/MRM quantitative profiling of eCBs, ERCs, eiCs (Experiment No 3) (modified from Lerner et al., 2016).

### 6.2.3 Punching of brain regions from KA-induced / control mice and simultaneous lipidomic and transcriptomic profiling

For simultaneous lipidomic and transcriptomic profiling, in total 20 mice were injected intraperitoneally with either KA (10 animals) or vehicle (0.9% saline, 10 control animals).

Punching of the brains was performed using the cryostat Leica CM3050 S (Leica Biosystems, Nussloch, Germany). Whole brains were mounted via Tissue Tek (Polysciences, Warrington, PA, USA) and tissue punches with a 0.8 - 1.0 mm diameter were taken with sample corers (Fine Science Tools, Heidelberg, Germany) from HYP, basolateral amygdala (BLA), dorsal hippocampus (dHC) and ventral hippocampus (vHC). Punches from both hemispheres were pooled. Subsequently, frozen punches were weighed in the cold room, with weights ranging from 0.4 to 1.9 mg and transferred in 2 ml pre-cooled Precellys tubes, containing ice cold ceramic beads. The procedure was carried out on ice to avoid thawing. Further Lipid and RNA extraction was performed via the method described in Chapter 5 (Fig. 5.1). Analysis of PLs and eCBs was carried out according to 4.3.1. All PLs depicted in Tab. 4.2,3 were targeted, except the additional AA-containing PLs.

### 6.2.4 Brain sectioning from KA-induced / control mice and MS imaging

Cryosectioning of the brains was performed using the cryostat Leica CM3050 S (Leica Biosystems, Nussloch, Germany). Whole brains were mounted via freezing water and 12  $\mu\text{m}$  tissue sections were cut, respectively. For MSI sections from bregma -1.06 mm to bregma -3.4 mm, spanning the HC, were used. MALDI-MSI was performed using a Bruker rapifleX MALDI TissueTyper (Bruker Daltonik GmbH, Bremen, Germany) (Ogrinc Potočnik *et al.*, 2015). Data analysis and visualization was performed using FlexImaging 5.0/4.1 (Bruker Daltonik GmbH) and SCiLS lab 2016a (SCiLS GmbH, Bremen, Germany). Brain sections were imaged at 50x50  $\mu\text{m}^2$  spatial resolution using 40x40  $\mu\text{m}^2$  laser scan with 200 laser shots acquired from each position. Mass calibration was performed using red phosphorous clusters. Adjacent sections were used for positive and negative ion mode acquisition. For positive and negative ion mode 2',4',6'-Trihydroxyacetophenone (20 mg/mL) and norharmane matrix (7 mg/mL) was used, respectively and purchased from Sigma Aldrich (Zwijndrecht, The Netherlands). Matrix was dissolved in methanol/chloroform (1:2; v/v) and applied to tissue using a SunCollect automatic pneumatic sprayer (Sunchrom GmbH, Friedrichsdorf, Germany). For lipid assignments and higher spatial resolution imaging of several tissues a Bruker SolariX XR MALDI FTICR MSI system coupled to 9.4T Superconducting magnet (Cryomagnetics Inc, USA) was used. Data was acquired using a 25  $\mu\text{m}$  raster size from m/z 100-2000 using a 2Mword/~0.7s transient providing a mass resolution in the lipid range of 80000-90000. 300 laser shots were summed at each position. External calibration was performed using well known brain lipids prior to starting the image. Positive mode data was acquired from the left HC from a control and KA-induced control mice while negative mode data was acquired from the right HC of each. Norharmane matrix was used for both polarities and prepared as described above.



### 6.3 Results

Pertaining the rigorous criteria of the standard operating procedure concerning cold tissue handling, transport, extraction and storage conditions already developed in the lab for eCBs, in order to strictly control and reduce the artificial alterations of their endogenous levels among the controls and KA-induced epileptic seizure models (Lerner *et al.*, 2013; Wenzel *et al.*, 2013; Lomazzo *et al.*, 2014; Bindila and Lutz, 2016) assured the validity of this comparative study.

Nevertheless, ischemic effects induced by generic decapitation methods and their implementations on fatty acid metabolism i.e. the post-mortem accumulation of AA and AA-derived eiCs occur. Microwave irradiation was described to enable analysis of brain lipids at their endogenous levels (Bazan *et al.*, 1982; Farias *et al.*, 2008; Nomura *et al.*, 2011; Puppolo *et al.*, 2014) but would not have been applicable to the collection of peripheral organs as well as blood sampling as performed in our study. Additionally, different lipid species require different irradiation conditions, hence, the comprehensive lipid profiling within our study is not compatible with microwave irradiation procedure. Despite, levels of AA and eiCs seem to be affected in the same manner comparing control and non-control groups in mice sacrificed by head-focused microwave irradiation or decapitation (Nomura *et al.*, 2011), thus, supporting the reliability of comparative studies using decapitation to determine bioactive lipid changes under pathological conditions.

#### 6.3.1 Lipid signal profiling in six brain regions and periphery from KA-induced epileptic seizure mice

Significant effects were observed in the behavior of KA-seizure induced mice (n=9) compared to controls (n=9) over one hour (Fig. 6.2). Targeted quantification via LC/MRM with on-line polarity switching (Fig. 6.3) enabled concurrent eCB, ERCs and eiC quantification while offering sufficient tissue amount from the same sample source for additional PL extraction. Moreover, using this approach, sufficient lipid extracts could be achieved to perform multiple discovery experiments e.g. PIS of various FAs to obtain information on the FA composition changes associated with acute epilepsy (Fig. 6.1). To investigate interrelations between brain and peripheral lipidome plasticity with acute epilepsy, the analytical strategy was also used for plasma as well as heart and lung tissue analysis. Notably, to circumvent bias originating from tissue heterogeneity, mechanically tissue homogenization and aliquotation of the produced tissue powder was performed prior to extraction procedure (Fig. 6.1).

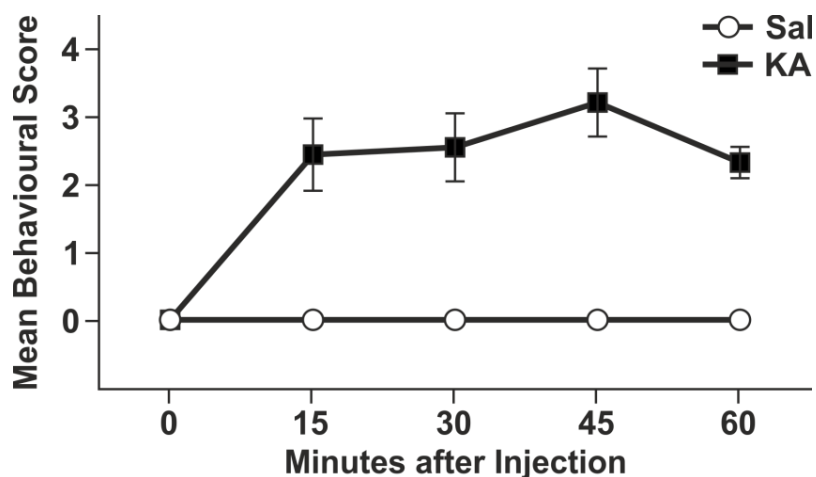


**Figure 6.2 Behavioral scores:** Mean behavioral scores of kainic acid (KA) and saline injected mice. Error bars denote SEM. ANOVA repeated measurement yielded significant interactions between time points of measurements and test groups, indicating significant effects of KA treatment on behavioral scores (from Lerner et al., 2016).

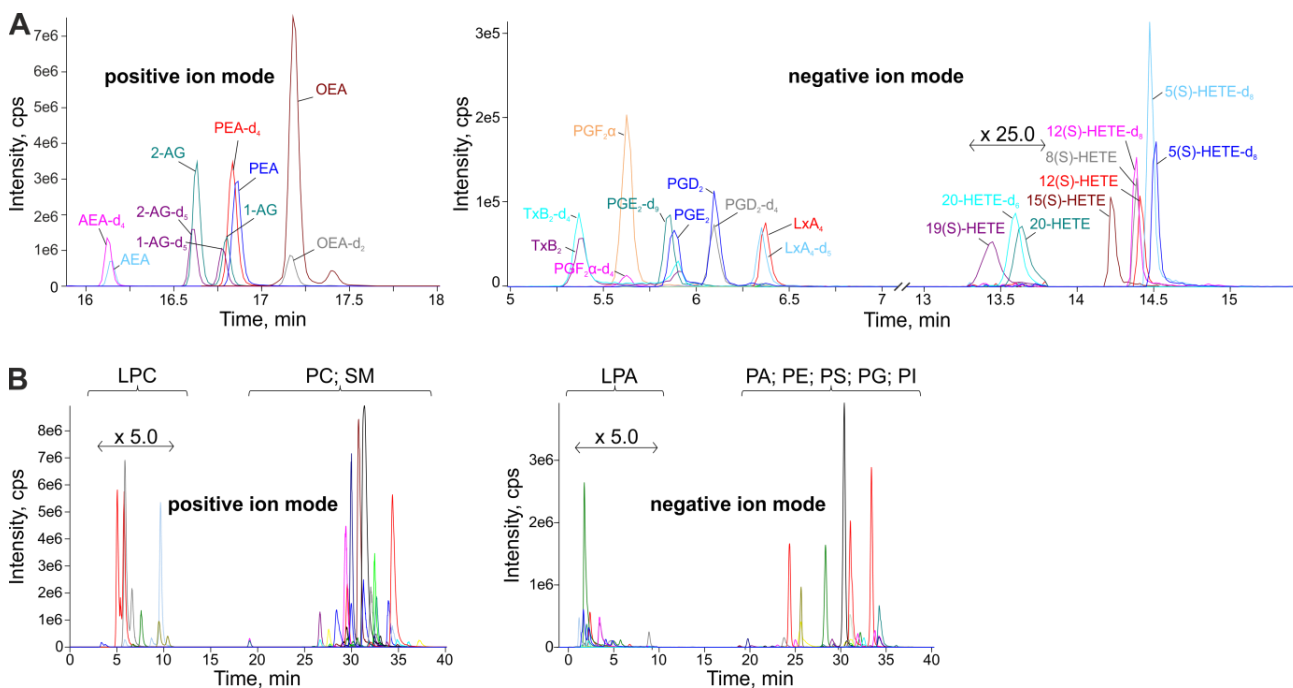


**Figure 6.3 Extracted ion current chromatograms:** Representative LC/MRM extracted ion current chromatograms using polarity switching of A) a calibration standard for eCBs and ERCs detected in positive ion mode (left panel) and eICs detected in negative ion mode (right panel) and B) PLs detected in positive ion mode (left panel) and negative ion mode (right panel) obtained from cerebellum extract (from Lerner et al., 2016).

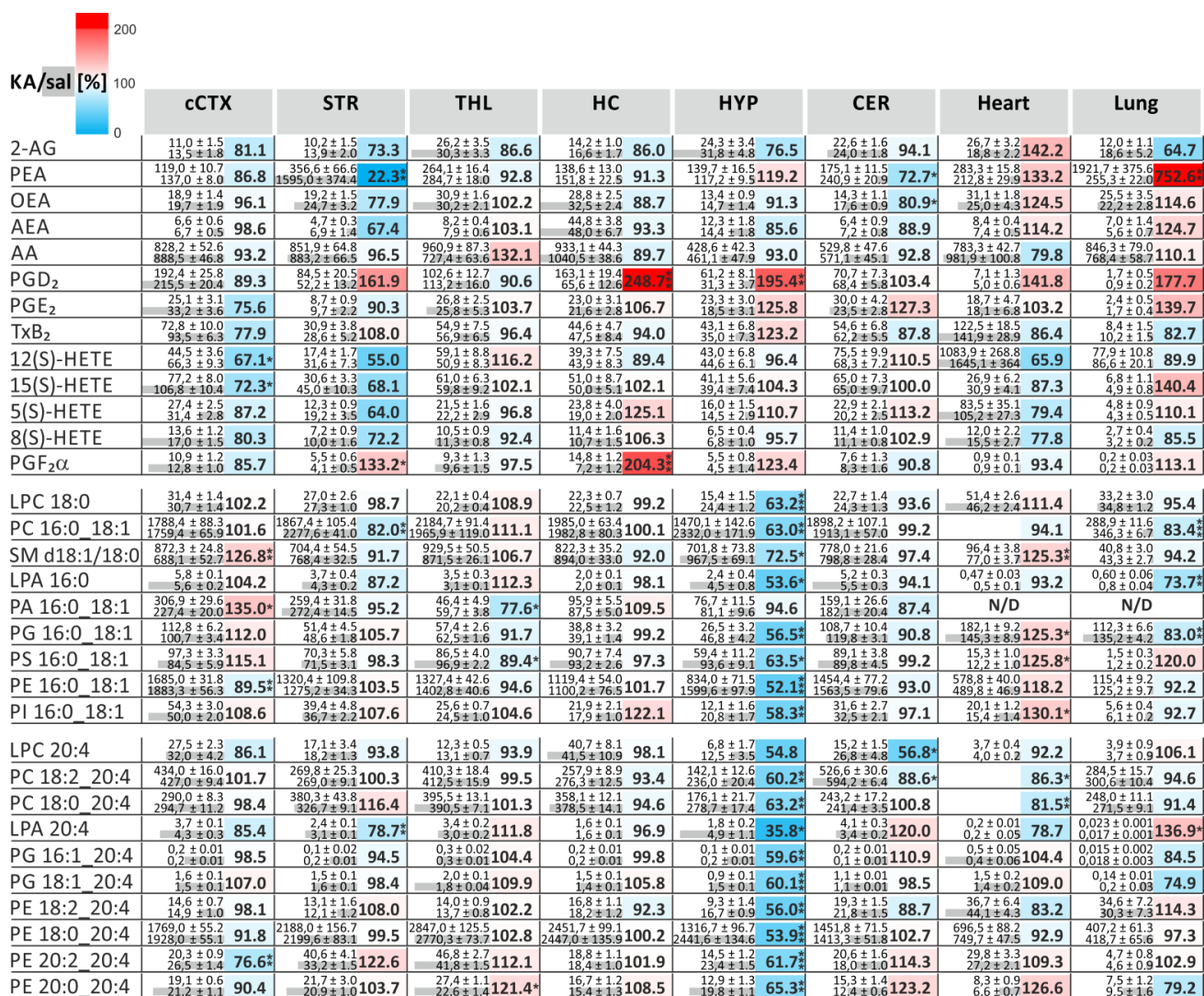


**Figure 6.4 Brain and peripheral tissue lipid levels in epileptic seizures:** Distribution of PL, NAE, eCB and eiC concentrations obtained across the six brain regions: cerebral cortex (cCTX), striatum (STR), thalamus (THL), hippocampus (HC), hypothalamus (HYP), cerebellum (CER), as well as heart and lung tissue in KA-induced epileptic mice (upper value) and controls (lower value), presented as mean value ± SEM. The lipid concentrations presented for both, KA-induced epileptic mice and control mice are strictly valid under the conditions of animal sacrificing, tissue sampling, handling and extraction procedures used in this study. The ratio of control lipid levels across tissues are depicted in grey, whereby the highest level was set to 100%. The values of PLs, 2-AG and AA are given in nmol/g and for PEA/OEA, eiCs and AEA in pmol/g, respectively, all normalized to the tissue weight. To highlight KA-specific molecular changes, lipid levels of the KA-treated mice are represented as percentage of the saline-injected mice (KA/sal) in a heat map displaying decreased values compared to control in light blue and increased levels compared to control in red, respectively. Lipid level alterations are considered significant at a p-value < 0.05 (n=9). Statistical analyses of the difference between group means were carried out by using two-tailed unpaired Student's t-test. PCA analysis additionally confirmed the statistical changes. (from Lerner et al., 2016).

**Cerebral cortex**

In the region of cerebral cCTX significantly elevated levels of PA 16:0\_18:1 (\*) and SM d18:1/18:0 (\*\*), as well as significant decreases of PE 16:0\_18:1 (\*\*) and PE 20:2\_20:4 (\*\*) were detected. A further slightly elevated level was found for PS 16:0\_18:1 (115.1 %). Levels of eCBs, ERCs and eiCs only underwent reduction to different extents or rather remained unchanged (Fig. 6.4)

Significant decreases were found for 12(S)-HETE (\*) and 15(S)-HETE (\*), while non-significantly reduced levels were observed for 2-AG (81.1 %), PGE2 (75.6 %) and TxB2 (77.9 %).

### Cerebellum.

The exhibited significantly decreased levels of LPC 20:4 (\*) and PC 18:2\_20:4 (\*). PE 20:0\_20:4 (123.2 %) and LPA 20:4 (120.0 %) exhibited non-significant increment. Significant alterations regarding eCBs, ERCs and eiCs were confined to OEA (\*) and PEA (\*), which significantly decreased. Non-significant increases were observed for PGE2 (127.3 %).

### Thalamic region.

Regarding the levels of PLs, significant elevation was exclusively found for PE 20:0\_20:4 (\*). In addition, the total content of C16:0 (\*\*) in the lipidome of this region was significantly increased (Fig. 6.5). In contrast, the levels of PA 16:0\_18:1 (\*) and PS 16:0\_18:1 (\*) underwent significant reduction. Virtually, no changes were observed for the other PLs. None of the eCBs, ERCs or eiCs were significantly altered in the thalamic region, however non-significantly increased levels were found for AA (132.1 %) and 12(S)-HETE (116.2 %).

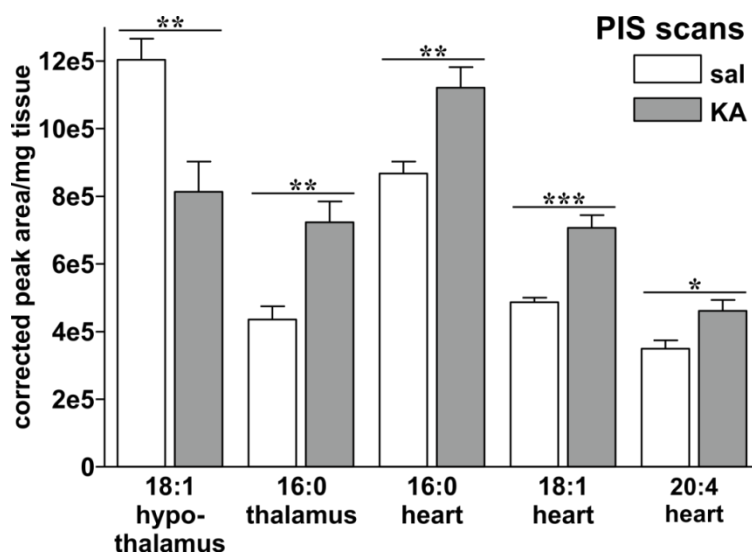


**Figure 6.5 Precursor ion scan:** Significant changes of the C16:0, C18:1, C20:4 lipid content in different brain regions, heart and lungs, as obtained by PIS analysis in negative ion mode. Statistical analyses of the difference between group means were carried out by using two-tailed unpaired Student's t-test and were considered significant at a p-value < 0.05 (n=9) (from Lerner et al., 2016).

### Hypothalamus

The region of the HYP exhibited significantly reduced levels of PE 16:0\_18:1 (\*\*\*), PG 18:1\_20:4 (\*\*\*), PE 18:0\_20:4 (\*\*\*), PE 20:2\_20:4 (\*\*\*), LPC 18:0 (\*\*\*), PC 16:0\_18:1 (\*\*), PG 16:0\_18:1 (\*\*), PI 16:0\_18:1 (\*\*), PC 18:2\_20:4 (\*\*), PC 18:0\_20:4 (\*\*), PG 16:1\_20:4 (\*\*), PE 18:2\_20:4 (\*\*), PE 20:0\_20:4 (\*\*), PS 16:0\_18:1 (\*), SM d18:1/18:0 (\*), LPA 16:0 (\*), LPA 20:4 (\*) and a non-

significant reduction was observed for LPC 20:4 (54.8%). In contrast, only PA 16:0\_18:1 remained unchanged. The changes were paralleled by a significant decrease of the C18:1 (\*\*) content of the hypothalamic lipidome (Fig. 6.5). Among eiCs, ERCs and eCBs, significant increase was exclusively found for PGD2 (\*\*). Additionally non-significantly enhanced levels were exhibited by TxB2 (123.2 %), PGF2 $\alpha$  (123.4 %), PGE2 (125.8 %) and PEA (119.2 %). 2-AG (76.5 %) underwent non-significant decrease.

### *Hippocampus*

1-h after systemic KA administration no significant changes were observed between groups for any of the targeted PLs in the HC, only for PI 16:0\_18:1 (122.1 %) non-significantly enhanced levels could be detected. In contrast, eiCs levels were significantly enhanced in the case of PGD2 (\*\*\*) and PGF2 $\alpha$  (\*\*\*). In addition a non-significant increment was found for 5(S)-HETE (125.1 %).

### *Striatum*

Among the investigated PLs significantly decreased levels were exhibited by PC 16:0\_18:1 (\*\*) and LPA 20:4 (\*\*). Slight increment could be detected in case of PE 20:2\_20:4 (122.6 %) and PC 18:0\_20:4 (116.4 %). Regarding eCBs, ERCs and eiCs, significant enhancement was found for PGF2 $\alpha$  (\*), as well as non-significantly elevated levels of PGD2 (161.9 %). In contrast, significantly reduced levels of PEA (\*\*) were detected. Further, levels of all HETEs investigated underwent non-significant decreases: 12(S)-HETE (55.0 %), 5(S)-HETE (64.0 %), 15(S)-HETE (68.1 %) and 8(S)-HETE (72.2 %) as well as those of AEA (67.4 %), 2-AG (73.3 %), and OEA (77.9 %), while only AA, TxB2 and PGE2 remained almost unaltered.

### *Heart & lung*

Regarding the PLs levels investigated in heart tissue 1h after KA injection, significant enhancements were observed for SM d18:1/18:0 (\*\*), PG 16:0\_18:1 (\*), PS 16:0\_18:1 (\*) and PI 16:0\_18:1 (\*) paralleled by non-significantly increased levels of PE 20:0\_20:4 (126.6%) and PE 16:0\_18:1 (118.2 %). Moreover, the heart lipidome exhibited significant elevation of the C18:1 (\*\*\*), C16:0 (\*\*) and the C20:4 (\*) content (Fig. 6.5). In contrast, significantly decreased levels were found in case of PC 18:0\_20:4 (\*\*) and PC 18.2\_20:4 (\*). LPA 20:4 and PE 18:2\_20:4 were reduced to 78.7 % and 83.2 %, respectively. None of the ERCs, eCBs or eiCs investigated exhibited significant changes. But non-significantly enhanced levels were observed for 2-AG (142.2 %), PEA (133.2 %) and PGD2 (141.8 %), while non-significantly reduced levels were found for 12(S)-HETE (65.9 %), AA (79.8 %), 8(S)-HETE (77.8 %) and 5(S)-HETE (79.4 %). In the lung tissue significantly reduced levels were observed for PC 16:0\_18:1 (\*\*\*), LPA 16:0 (\*\*) and PG 16:0\_18:1 (\*\*), while non-significant decreases were found for PG 16:1\_20:4 (84.5 %), PG 18:1\_20:4 (74.9 %) and PE 20:0\_20:4 (79.2 %). On the other hand, significantly enhanced levels were detected in case of LPA 20:4 (\*) and further non-significantly enhanced levels were

found for PS 16:0\_18:1 (120.0 %). Alterations among the eCBs, ERCs and eiCs were restricted to significant increase of PEA (\*\*). Further non-significantly enhanced levels were observed for PGD2 (177.7 %), 15(S)-HETE (140.4 %), PGE2 (139.7 %) and AEA (124.7 %). On the other side, non-significant reduction was exhibited by 2-AG (64.7 %).

*Plasma*

Plasma analysis unraveled significantly reduced levels for AEA (\*\*\*), OEA (\*\*\*), PEA (\*\*) and AA (\*\*) and in contrast significant increments in case of 2-AG (\*\*\*) and PGD2 (\*) 1 h after KA-induced seizure (Fig. 6.6). Regarding PLs, significantly reduced levels were observed for PG 16:0\_18:1 (\*\*), PS 16:0\_18:1 (\*\*), SM d18:1/18:0 (\*), PE 16:0\_18:1 (\*) and PG 18:1\_20:4 (\*) (Fig. 6.6). Non-significant changes (data not shown) were observed for 12(S)-HETE (56.8 %), 15(S)-HETE (56.8 %), 19(S)-HETE (81.5 %) and PE 20:4\_20:0 (83.0 %), PE 20:4\_18:2 (81.1 %) and PE 20:4\_18:0 (75 %).

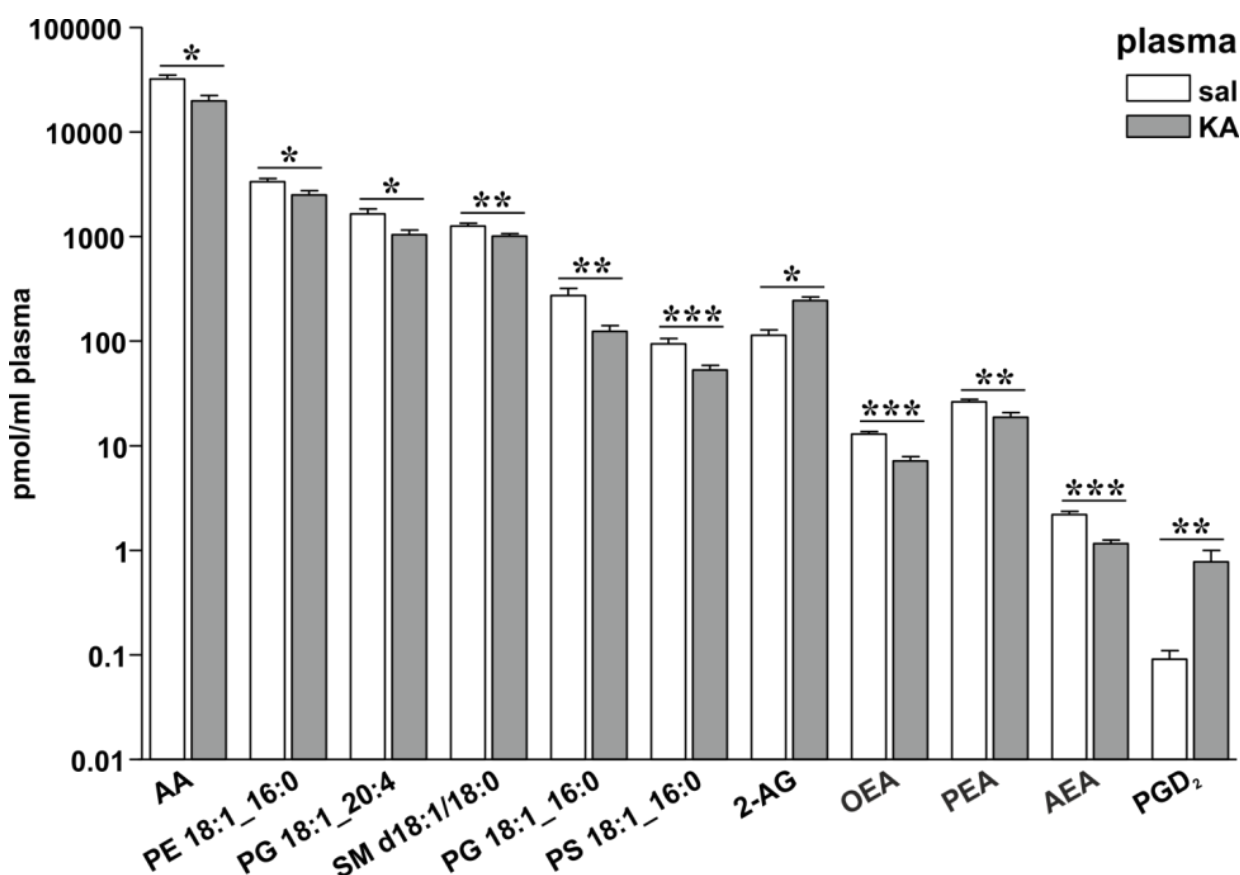


**Figure 6.6 Plasma lipids:** Significant lipid level alterations obtained in plasma after KA-induced seizure as compared to controls. The values for the PLs, OEA and PEA are given in pmol/mL plasma, for AA in nmol/mL plasma and for AEA and PGD2 in fmol/mL plasma, respectively. Statistical analyses of the difference between group means were carried out by using two-tailed unpaired Student's t-test and were considered significant at a p-value < 0.05 (n=9) (from Lerner et al., 2016).

### 6.3.2 Lipidomic and transcriptomic profiling in brain punches from KA-induced epileptic seizure mice

To exemplify the analytical workflow for RNA and lipid co-extraction (Chapter 5), we applied the developed method to mouse models of KA-induced epileptic seizure (KA 10 animals; saline 10 animals). The significant effects in the behavior of KA-seizure induced mice (n=10) compared to controls (n=10) over one hour are shown in Fig. 6.7. The approach rendered a panel of lipid signatures for acute epileptic seizures encompassing PLs and eCBs, as well as mRNAs involved in synthesis and degradation of lipid signals and neuronal activity. The obtained values of lipid levels from four different brain regions, as well as their percentual changes 1 h after systemic KA administration, are depicted in Fig. 6.8. The corresponding changes in mRNA levels are shown in Fig. 6.9. Changes in the levels of representative mRNAs involved in the: i) eCB signaling; FAAH, NAPE-PLD and CB1R ii) breakdown of membrane lipids and synthesis of other signaling lipids; cPLA<sub>2</sub>, and iii) in neuronal activity; BDNF and c-fos were investigated. For this purpose, total RNA was extracted and levels of the specific mRNAs were assessed by qPCR (see Chapter 5.2.3.2).

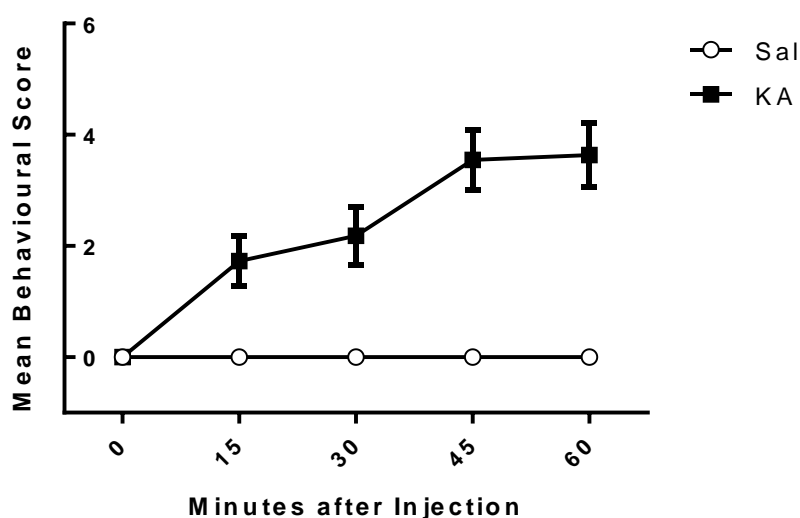


**Figure 6.7 Behavioral scores:** Mean behavioral scores of kainic acid (KA) and saline injected mice. Error bars denote SEM. ANOVA repeated measurement yielded significant interactions between time points of measurements and test groups, indicating significant effects of KA treatment on behavioral scores (n=10).

# APPLICATION TO ACUTE EPILEPTIC SEIZURE MODEL

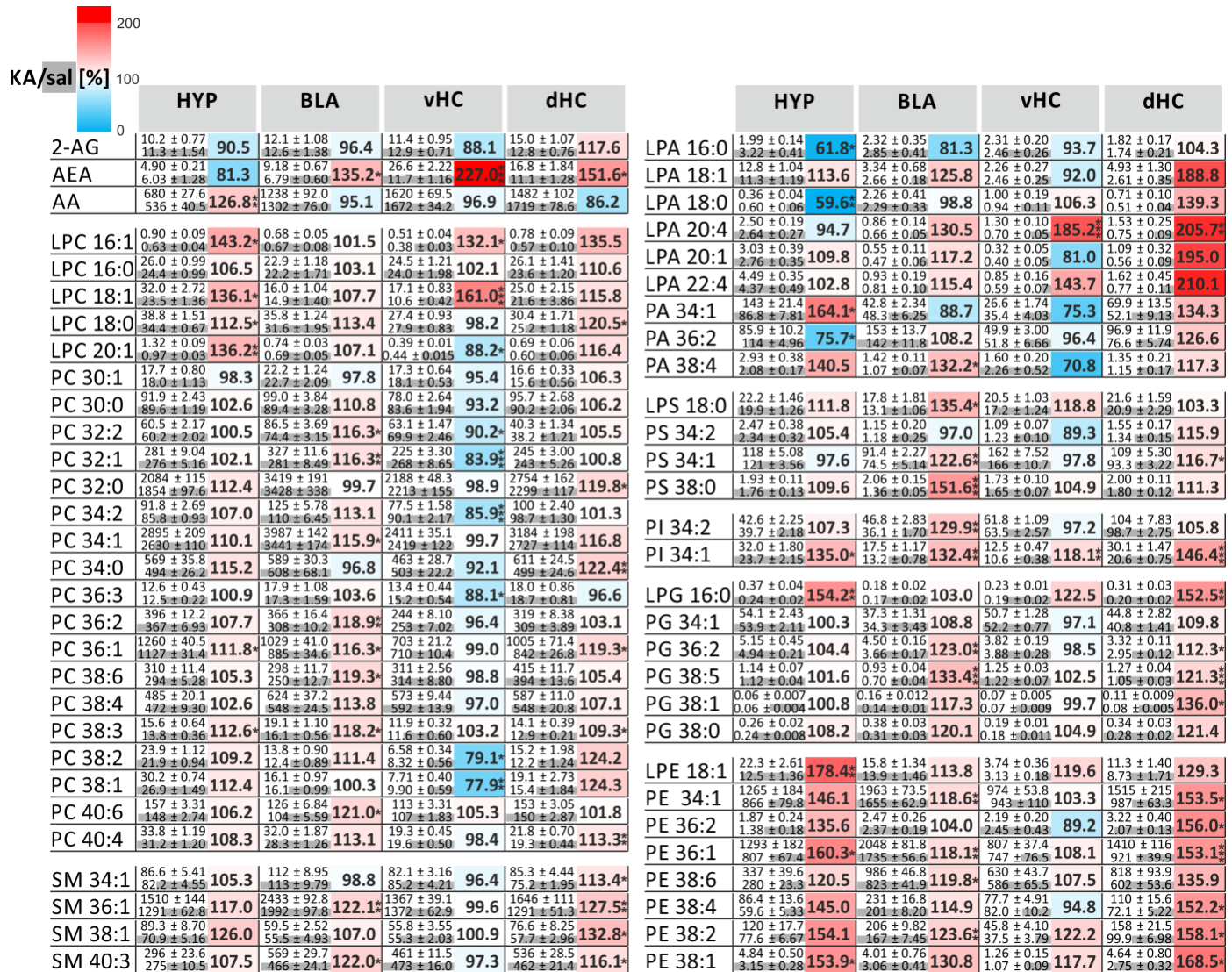


**Figure 8.8 Tissue lipid levels of brain subregions in epileptic seizures:** Quantitative distribution of selected PLs and eCBs across the brain regions hypothalamus (HYP), basolateral amygdala (BLA) and the brain subregions ventral- (vHC) and dorsal- (dHC) hippocampus, from KA-induced epileptic seizure mice (upper value) versus controls (lower value) in nmol/g (only for AEA = pmol/g) normalized to the tissue weight (punches  $\pm$  0.5 - 1.5 mg), presented as mean value  $\pm$  SEM. The ratio of control lipid levels across brain regions are depicted in grey, whereby the highest level was set to 100%. To highlight the KA-specific molecular changes, the lipid levels of the KA-treated mice are represented as percentage of the saline-injected mice (KA/sal) in a heat map displaying decreased values compared to control in light blue and increased levels compared to control in red, respectively and they are considered significant at a p-value  $<$  0.05 (n=10). Statistical analyses of the difference between group means were carried out by using two-tailed unpaired Student's t-test. PCA analysis additionally confirmed the statistical changes.



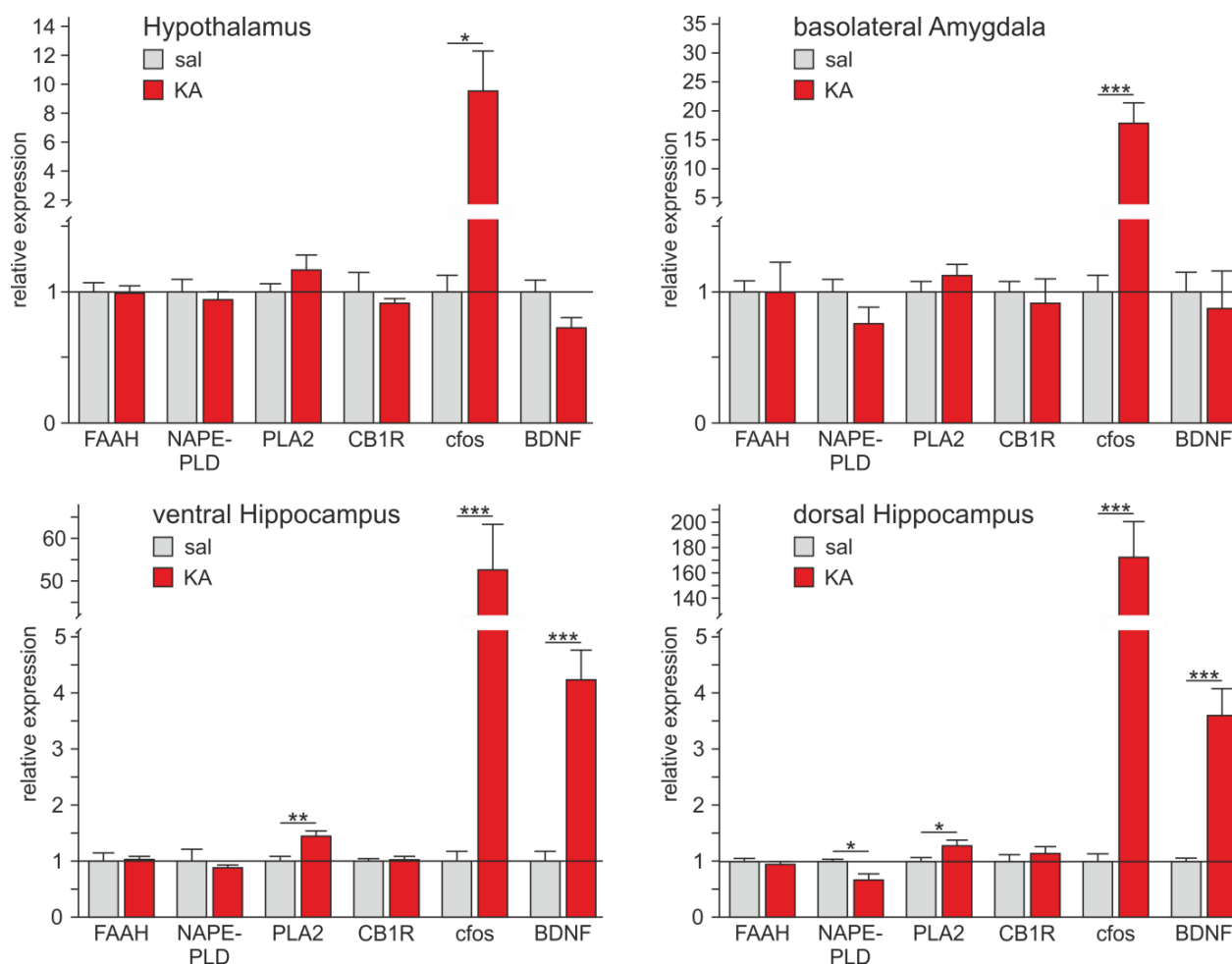


**Figure 6.9 Relative mRNA expression levels in epileptic seizures:** Relative expression levels of endogenous enzymes and receptors involved in lipid signaling, as well as markers for brain activity, investigated at mRNA level in different brain regions/subregions from mice subjected to kainic acid (KA)-induced epileptic seizure (red) and control (light grey). Statistical analyses of the difference between group means were carried out by using two-tailed unpaired Student's t-test and considered significant at a p-value < 0.05 (n=10)

### *Hypothalamus*

In the hypothalamic region, interestingly, a high number of signaling PLs underwent significant changes. Hence, most prominent changes were found in particular for lyso-species 1 h after systemic KA-administration. The levels of all LPCs analyzed, except of LPC 16:0, were significantly increased, as well as LPG 16:0 (\*\*) and LPE 18:1 (\*\*), whereas LPA 16:0 (\*) and LPA 18:0 (\*\*) were significantly decreased. Only PA 36:2 (\*) underwent significant reduction as well. The other detected significant changes were increments as it is the case for AA (\*\*), which significantly altered levels were restricted to this area, as well as for PC 36:1; PC 38:3; PA 34:1; PI 34:1; PE 36:1 and PE 38:1 (\*), whereby for all analyzed PE species enhanced levels spanning from 120 % to 160 % could be observed. In the hypothalamic region only mRNAs encoding the immediate early gene *cfos* (\*), which served as a marker for neuronal activity, were significantly enhanced 1 h after systemic KA-administration.

### *Basolateral Amygdala*

Almost half of the PC species were found to be significantly increased, as well as two out of four targeted SM species. LPS 18:0 (\*) was the only lyso- species that was significantly enhanced. The strongest increase was observed for PS 38:0 (\*\*\*), which together with LPS 18:0 was exclusively changed in the BLA. Both analyzed PI (\*\*) species were significantly elevated along with the two polyunsaturated PG species (36:2 \*\*, 38:5 \*\*\*), four PE species (34:1; 36:1; 38:2 \*\*, 38:6 \*), PA 38:4 (\*), and the AEA (\*), respectively. Regarding the transcriptomic profiling, the BLA exhibited also significantly increased levels of *cfos* (\*\*\*) mRNA as it was detected in HYP, but even to a higher extent.

### *Hippocampus*

The HC exhibited the most significant and strongest changes one hour after KA injection, with obvious differences between the dorsal and ventral area. As in the case of BLA, all significant changes in the dHC were increments of lipid levels, in contrast, the vHC exhibit mostly decreased lipid levels. This effect became especially apparent regarding PC species, from which six underwent a significant reduction in the vHC, whereas five were significantly elevated in the dHC. Furthermore all targeted SM species showed significantly enhanced levels in the dHC, while they remained unchanged in the vHC. The analyzed LPC species showed the same trend of increment in the dHC with LPC 18:0 (\*) being significant, while they had varying levels in the vHC; LPC 18:1 (\*\*\*) and 16:1 (\*) exhibited a strong increase and LPC 20:1 (\*) was found to be significantly decreased. An overall strong enhancement of LPA levels was observed in the dHC except for LPA 16:0 although not significant. Only the enhancement of LPA 20:4 was significant (\*\*), accompanied by a highly significant increase of LPA 20:4 (\*\*\*) in the vHC. Another PL, which was significantly elevated in both, ventral (\*\*) and dorsal HC (\*\*\*) was PI 34:1, thereby being the only targeted lipid, which underwent significant increment in every analyzed brain region. Further changes were observed in the dHC, where every targeted PS, PG and PE species was found to be enhanced, almost all of them in a significant way. This overall trend of enhanced lipid levels in the dHC was also exhibited by AEA only among the eCBs and ERCs, which was slight significantly increased in the dHC (\*) and in the vHC (\*\*\*). The prominent alterations in lipid levels could be also observed at mRNA level. A huge increase in *cfos* expression was found for both vHC (\*\*\*) and dHC (\*\*\*), of even higher magnitude for dHC. Moreover, mRNAs encoding the neurotrophic factor BDNF (vHC \*\*\*, dHC \*\*\*), and the enzyme cPLA<sub>2</sub> (vHC \*\*, dHC \*) underwent increment in vHC and dHC. Differences in terms of mRNA yield between hippocampal subregions could also be observed for the enzyme NAPE-PLD, whose expression was only significantly reduced in the dHC (\*).

### 6.3.3 MS imaging on brain sections from KA-induced epileptic seizure mice

Not only that the vHC and dHC are distinctly affected at the lipid level with epilepsy, but higher spatial resolution as obtained by MSI (Fig. 6.10) revealed that certain lipid changes shift between sal and KA injected animal throughout the dHC, such as the case for SM 36:1 and PC 32:0 (Fig. 6.10). Both lipids exhibit a significant increase with epilepsy in the entire dHC as determined by LC/MRM (Fig. 6.8). An increase of these lipids was also observed by MSI in the 3rd slice of the dHC, whereas in the 4th slice they seem to show an inverse trend: in the control (sal) slice these lipids are increased compared to epilepsy (KA). For SM 36:1, this inverse trend is also observable in the 2nd slice (Fig. 6.10).

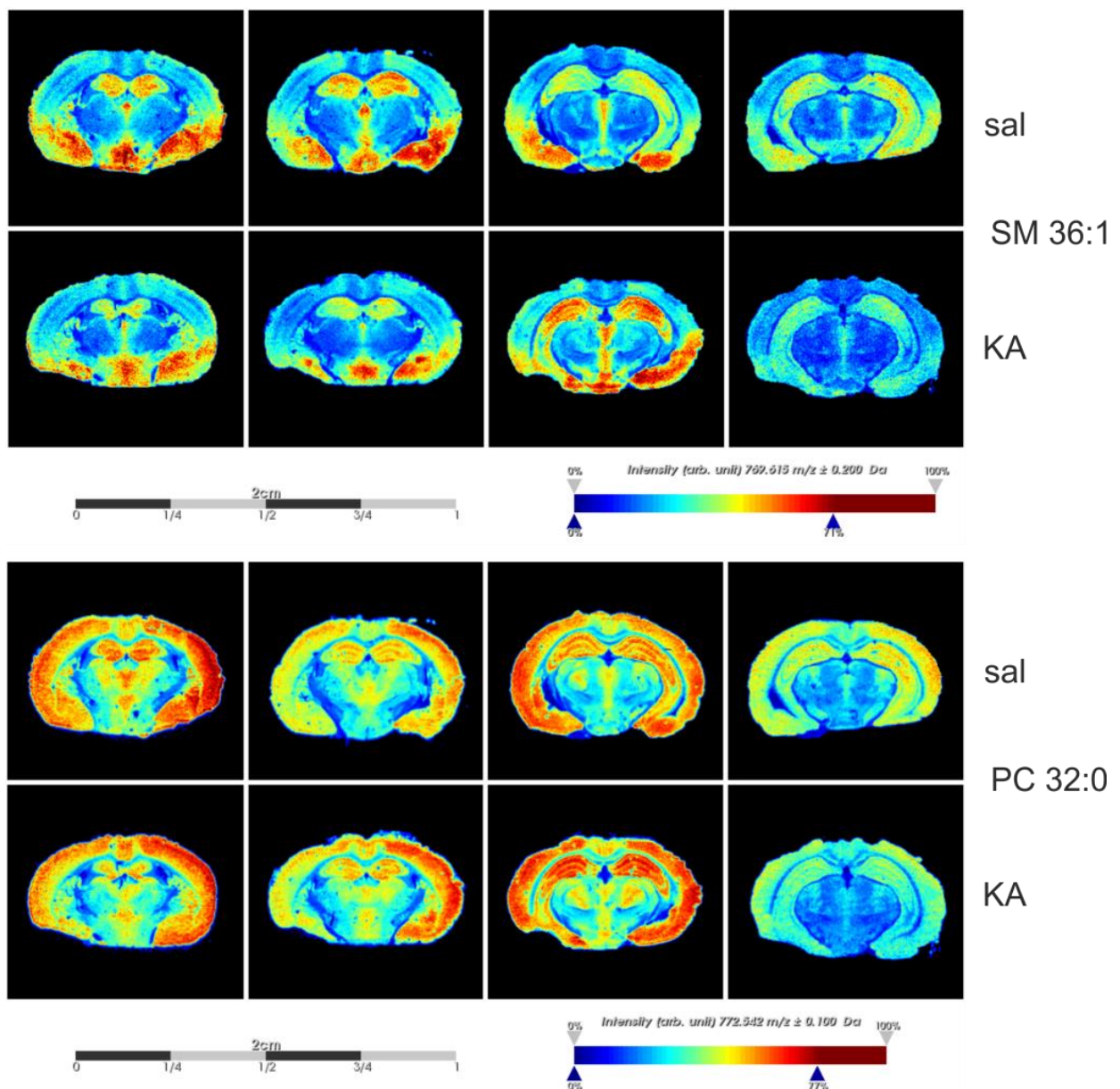


**Figure 6.10 MSI of PLs at acute epileptic seizure phases:** Brain sections were imaged at 50×50 μm<sup>2</sup> spatial resolution. Adjacent sections were used for positive and negative ion mode acquisition. MSI of SM 36:1 and PC 32:0 across the hippocampal area of epileptic (KA) vs control (sal) mice are depicted, showing spatially distinct dynamics of PLs associated with acute epilepsy.

Additionally, higher spatial resolution MSI experiments (25  $\mu\text{m}$  raster size) revealed that in the dHC the PC 32:0 and PI 38:4 are almost complementary distributed. PI 38:4 seems to be restricted to the pyramidal cell layer and the granular cell layer of the dentate gyrus, which consists mainly of cell bodies, whereas PC 32:0 is predominantly found in their corresponding axons e.g. Mossy fibers and Schaffer collaterals (Fig. 6.11).

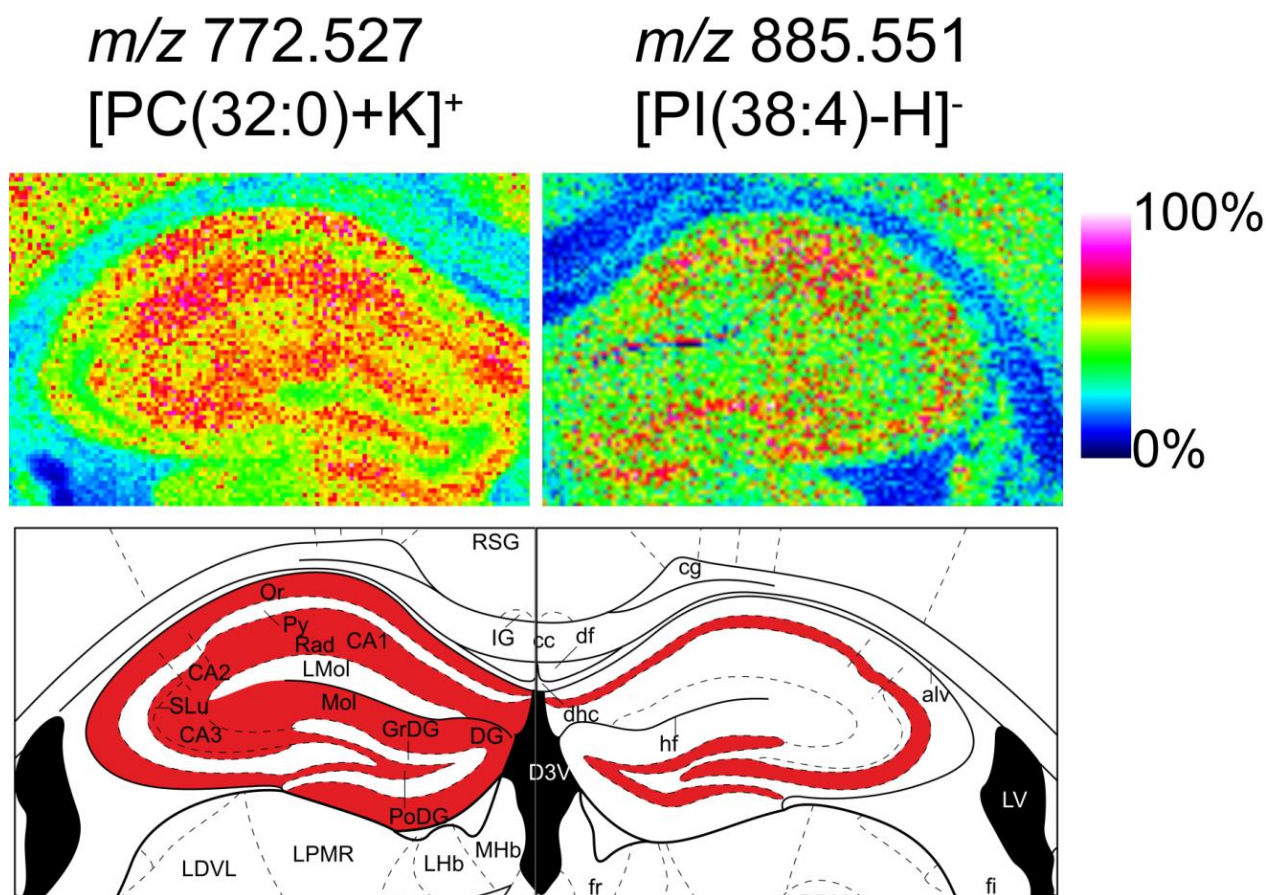


**Figure 6.11 MSI of PLs in hippocampus with high spatial resolution:** Data was acquired using a 25  $\mu\text{m}$  raster size from  $m/z$  100-2000 using a 2Mword/ $\sim$ 0.7s transient providing a mass resolution in the lipid range of 80000-90000 for lipid assignments and higher spatial resolution images. Positive mode data was acquired from the left hippocampus from a control mouse while negative mode data was acquired from the right hippocampus. Depicted are images for PC 32:0 (left) and PI 38:4 (right). A cell layer specific distribution within the hippocampus is proposed for both molecules.

Finally, MSI of different ion adducts within epileptic seizures indicate contrary alterations among the distinct adducts. Fig. 6.12 displays PC 32:0 and PC 34:1 as  $\text{H}^+$  ion or potassium ( $\text{K}^+$ ) adduct, respectively. Both protonated ions are increased in the KA injected animals compared to controls, whereas the levels of the  $\text{K}^+$  adducts are decreased, respectively.

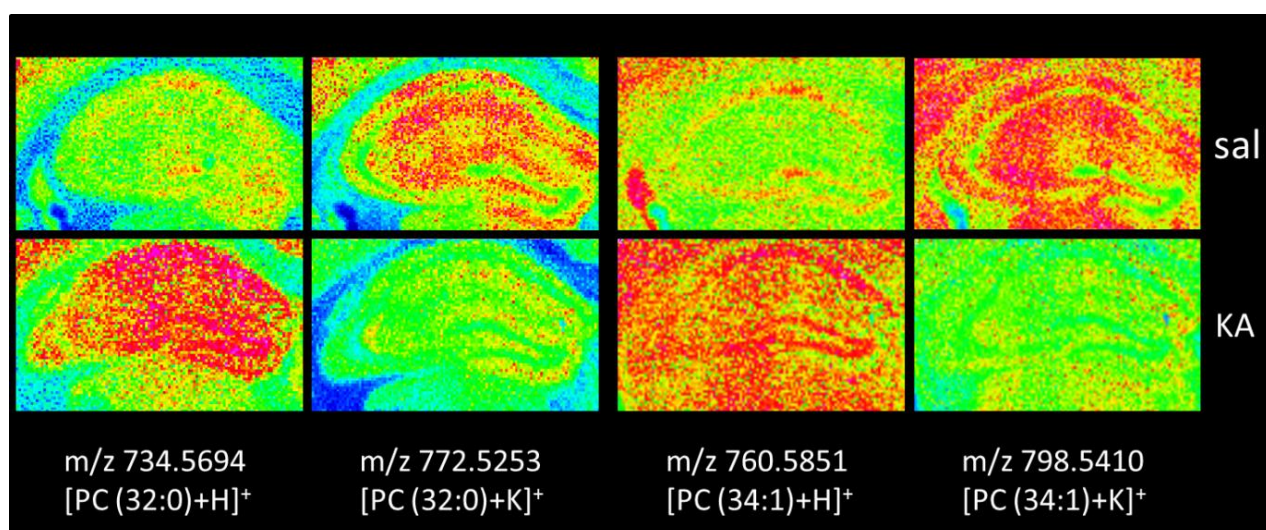


**Figure 6.12 MSI of different ion adducts within epileptic seizures:** Data was acquired using a 25  $\mu\text{m}$  raster size from  $m/z$  100-2000 using a 2Mword/ $\sim 0.7\text{s}$  transient providing a mass resolution in the lipid range of 80000-90000 for lipid assignments and higher spatial resolution images. Depicted are PC 32:0 and PC 34:1 as H<sup>+</sup> ion or potassium (K<sup>+</sup>) adduct in the dorsal hippocampal region, respectively. Both H<sup>+</sup> ions are increased in the KA injected animals compared to controls, whereas the levels of the K<sup>+</sup> adducts are decreased.

## 6.4 Discussion

### 6.4.1 Lipid signal profiling in six brain regions and periphery from KA-induced epileptic seizure mice

This study unveiled a broad lipid plasticity occurring with acute seizure reflected by changes of the selected lipids, as well as of fatty acyl content of the lipidome at 1 h after the KA-induced seizure in all mouse brain regions investigated (Fig. 6.4; Fig. 6.5). Noteworthy, the statistically significant lipid changes are region-specific, indicating distinct, specific involvement of these lipids in the acute epileptic phase. These findings concur with former research showing that different neuronal circuits are involved in initiation and spread of epileptic seizures across various brain regions (Bertram, 2013).

All of the investigated PLs underwent statistically significant decreases in the HYP, suggesting a massive membrane lipid remodeling (Fig. 6.4) Due to our knowledge, this is the first time that such an effect was reported in in HYP of a KA model of seizure and that lipid molecular correlates with acute epileptic seizure phase could be detected. The biological relevance of these drastic PL changes is not yet clear. But in view of the fact that the control of the hypothalamic pituitary-adrenal (HPA) axis by the limbic circuitry is dysregulated in epileptic seizures (Hanstein *et al.*, 2008) and that the HPA axis mediates the physiological response to stress, including that caused by seizures, these massive membrane changes might correlate with these impairments of HPA

axis function. The disturbed membrane PL metabolism and elevation of lipid peroxide levels occurs with neurodegenerative events in several pathological conditions, including epileptic disorder. The underlying mechanism typically involves the stimulation of cPLA<sub>2</sub>, which is supported here by the decreased levels of PLs in the HYP. This has direct consequences on the membrane permeability, fluidity and ion homeostasis. Additionally or alternatively the stimulation of cPLA<sub>2</sub> is engaged in AA release prompting enhanced formation of inflammatory eiCs and reactive oxygen species (ROS) production during PL degradation followed by oxidative stress. These molecular events correlate with apoptotic and necrotic cell damage (Hansen *et al.*, 2002; Farooqui *et al.*, 2004). The AA is not significantly changed at 1 h after seizure induction in the HYP but the PGD<sub>2</sub> is significantly increased demonstrating a fast conversion of AA to PGD<sub>2</sub>, hence COX pathway activation that is inflammatory signaling.

LPA signaling is involved in the regulation of synaptic activity and neuronal survival/apoptosis. LPA signaling can serve both a neuroprotective and neurotoxic function (JJW Choi and Chun, 2013). The role of LPA signaling in the hypothalamus during acute seizures is supported by a significant decrease of LPA 20:4 and LPA 16:0, while in the STR only LPA 20:4 is decreased, indicating a distinct signaling activity in the two brain regions.

HC is involved in the genesis and progression of epileptic disorders, and was accordingly the most investigated brain region in epilepsy models. Stimulation of hippocampal KA receptors leads to extensive neuronal stimulation, increased ROS levels and finally selective excitotoxic cell damage in the CA1 and CA3 subfields and dentate gyrus, but not in CA2 pyramidal neurons and dentate granule cells. Differential effects of oxidative stress within and between brain subregions are due to selective neuronal vulnerability to oxidative stress (Wang, 2010; Méndez-Armenta *et al.*, 2014). These features require a prospective, functional investigation of molecular fingerprints with acute epileptic phase in brain subregions, as highlighted in the next section. eCB tone was not altered in the HC at 1 h after KA injection, since neither AEA nor 2-AG were changed. Based on research by our laboratory and others, evidence has accumulated on the endogenous neuroprotective and anticonvulsive functions of the eCB system in various epileptic seizure models (Abdullah *et al.*, 2014; Fezza *et al.*, 2014). AEA was previously shown to exert an important role in alleviating neurotoxicity (Wallace *et al.*, 2002), whereby hippocampal levels showed rapid increment (at 20 min) and were set back to basal 1 h post KA injection (Marsicano, Goodenough, *et al.*, 2003; Guggenhuber *et al.*, 2016). This concurs well with our data on hippocampal AEA level, where the AEA level 1 h post KA injection was similar to controls (Figure 6.4 Brain and peripheral tissue lipid levels). Noteworthy though, a significant decrease of AEA after seizures was found in plasma (see below).

Previous studies investigating hippocampal tissue, demonstrated lipid peroxidation and neurotoxicity caused by oxidative stress in KA- and pilocarpine-induced epileptic seizure models (Freitas *et al.*, 2004; Júnior *et al.*, 2009; Shin *et al.*, 2011). Although in rat models of epilepsy, hippocampal levels of PE, PS and PI were decreased 1 hour after seizure induction (Yegin *et al.*, 2002) in our mouse model the selected PLs remained unchanged at 1 h post KA injection. Regarding eiC levels, the most significant alterations were found in the HC, where significant increases of PGD<sub>2</sub> and PGF<sub>2α</sub> were observed 1 h after KA injection (Yoshikawa *et al.*, 2006). These findings concur and support previous studies implicating COX-2 activation in HC as the cause of neuro-inflammation rendered by epileptic seizures and in turn their re-occurrence (Takemiya *et al.*, 2006, 2007, 2011; Shimada *et al.*, 2014).

The thalamus is involved in the initiation and spread of the epileptic seizures. Levels of PS (16:0\_18:1) are exclusively altered in the brain regions of THL and HYP. PS species are largely departed in the inner leaflet of membrane bilayers and undergo extracellular exposure if required, under certain conditions such as apoptotic processes as described in the introduction. The reduced levels of PS (16:0\_18:1) might correlate with such extracellular events, possibly due to irreversible cell damage previously caused by seizure induction. While all investigated PE species containing C20:4 fatty acyls are significantly decreased in HYP, in cCTX only the PE 20:2\_20:4 is significantly decreased. On the other side, in the thalamic region only the PE 20:0\_20:4 shows a significant alteration, e.g. increase (Fig. 6.4). This indicates once more distinct brain region responses to seizure activity. Furthermore, the C16:0 content of the thalamic lipidome undergoes a significant increase due to epileptic seizures (Fig. 6.4) (Bertram, 2013), demonstrating a more exhaustive alteration of the thalamic membrane.

The STR and CER are the only brain regions that exhibited significant changes of PEA, e.g. significant reduction. PEA is synthesized from N-palmitoylethanolamine-PLs and degraded by FAAH or N-acylethanolamine-hydrolyzing acid amidase (Mattace Raso *et al.*, 2014). PEA was shown to exert neuroprotective effects and to modulate inflammatory processes (Lo Verme *et al.*, 2005). In our epilepsy model however, the precursors for PEA are not changed. The only notable aspect is that in STR PEA decreases whereas PGF<sub>2α</sub> is strongly increased. Whether a functional role connecting these opposite changes exist, remains to be clarified.

The significant increase of PGF<sub>2α</sub> levels in the striatal region concurs with previous data showing increased striatal PGF<sub>2α</sub> in gerbils with spontaneous seizures (Simmet *et al.*, 1988). PGF<sub>2α</sub> serves as inflammation marker in various pathological conditions (Ricciotti and Fitzgerald, 2011), being involved in the onset of neuro-inflammation, cytokine secretion, amplifying and maintaining inflammatory responses. LOX signaling pathways, which are implicated in neuronal cell death and vascular injury, are exclusively altered in the cCTX, where significantly reduced levels of

12(S)-HETE and 15(S)-HETE were detected. Previous findings suggested that cortical regions are strongly affected by nitric oxide (NO) during KA-induced excitotoxicity, possibly because of the greater blood flow in the cCTX. 12/15-LOX can oxidize PLs containing PUFAs and can directly target and modify membranes leading to cell damage (Kwon *et al.*, 2005; Leyen, 2013). On the other hand, 12(S)-HETE and 15(S)-HETE were shown to exert neuroprotective effects in cortical neuron cultures with excitotoxicity (Hampson and Grimaldi, 2002).

### *Periphery*

In acute and chronic seizure state patients often experience serious cardiorespiratory problems, e.g. increased bradycardia and changes in respiratory pattern, which can also lead to sudden death (Kennedy and Seyal, 2015). Recurrent generalized tonic-clonic epileptic seizures cause enhanced capillary pressure, followed by structural damage of the alveolar-capillary barrier subsequently leading to pulmonary hemorrhage and hemoptysis (Ueno *et al.*, 2005; Azuma *et al.*, 2012). On another level, a link between peripheral and brain inflammation mediated by immune processes was recently proposed as a key mechanism in pathogenesis of epileptic disorders (Bertram, 2013; Vezzani *et al.*, 2013; Xu *et al.*, 2013). Glutamate receptors for KA are also found in peripheral tissues, including heart, so that the general toxic effects of KA when injected intraperitoneally are likely potentiated through the peripheral to brain inflammation cycle (Skerry and Genever, 2001).

In this context, we aimed at exploring if acute seizure render alteration of the lipid signaling in heart and lungs and therefore we quantitatively assessed the same lipids as in brain. Interestingly, 1 h post KA injection distinct and specific mechanisms of PL alteration in heart and lung are supported by our data in the acute phase of seizure (Fig. 6.4). Except for PEA in the lung, the changes were confined to PLs. Notably, in heart, a significant increase of C16:0, C18:1 and C20:4-containing lipids, respectively, was detected, but not in lungs. Several reasons may contribute to these changes, such as degradation by phospholipases, degradation of surface proteins, damage by ROS or disruption of the air-water interface caused by alveolar edema (Da Cunha *et al.*, 2014).

Plasma is the ubiquitously used biological matrix for diagnosis, follow-up and predictive monitoring of diseases due to the non-invasive manner for collection. In case of neurodegenerative diseases in humans, where various brain tissue sampling is restricted or impossible, the detection of molecular signatures in plasma for a particular disease is of utmost importance to advance the disease management. Our study revealed for the first time lipid signatures of acute epileptic seizure in mouse plasma with KA-induced epileptic seizures, hence demonstrating the potential of lipidomics profiling for provision of epilepsy markers. These plasma lipid fingerprints rather comprehensively reflect the dysregulation of a) the eCB system through



the AEA and 2-AG changes, b) the inflammatory processes through AA and PGD<sub>2</sub> changes, and c) the specific membrane lipid metabolism through PL changes (Fig. 6.4) occurring with epileptic seizures 1 h post KA injection. Interestingly, the dysregulation of the ECS, a major factor in the pathogenesis of epilepsy, has been reflected at the lipid level (see AEA and 2-AG) exclusively in plasma. The opposite change of 2-AG and AEA (Fig. 6.4) is specific for certain conditions, e.g., acute stress (Popoli *et al.*, 2012; Lutz *et al.*, 2015).

#### **6.4.2 Lipidomic and transcriptomic profiling in brain punches from KA-induced epileptic seizure mice and PLs in MS imaging**

Lipid plasticity occurring with acute seizures as discussed in Chapter 6.4.1 was also found in the mouse brain punches 1 h after KA-induced seizure (Fig. 6.8). The very strong breakdown of PLs in the whole HYP could not be observed in the brain punches out of this region. HYP is a brain region known to be composed of multiple nuclei, all exerting different functions (Canteras *et al.*, 1994; Simerly, 2015). The HYP punch is enriched in specific nuclei types compared to the whole region. A new aspect revealed by our study is that the HYP punch exhibited specifically strong variation of lyso-species and PAs, e.g. decrease with epileptic seizures, which belong to the signaling PLs and therefore indicate a high level of signaling events within this region. This is likely correlated with the enriched nuclei types and their apparent signaling events within this subregion. LPA species were significantly decreased in the whole HYP as described in Chapter 6.4.1, and in the HYP punch. LPA is known to increase excitability in CA1 pyramidal neurons in a LPA<sub>2</sub> receptor dependent manner (Trimbuch *et al.*, 2009), generally rather pointing toward increment of LPA levels with acute seizures. However, this effect was receptor specific and LPA is known to act through several receptors among them at least 6 GPCRs, named LPA<sub>(1-6)</sub> as well as PPARs, all exerting various roles despite synaptic transmission (McIntyre *et al.*, 2003; J Choi and Chun, 2013). Moreover the effect was HC dependent and contrary functions of LPA species are already described for different cell types (J Choi and Chun, 2013). Nonetheless, a possible protective mechanism related with the reduced LPA levels can't be ruled out. Furthermore, it would be also possible that the decreased LPA levels may be a direct metabolic consequence of reduced LPC turnover (the precursor of LPA), given the significantly elevated level of almost all LPC species in the HYP. Like LPAs, LPCs are described to function in the regulation of the immune system and elevated signaling of these lipids is implied in several chronic inflammatory diseases (Sevastou *et al.*, 2013). Despite their action as signaling molecules, decrease of LPA levels and increase of the fusiogenic LPC species may directly influence synaptic vesicle exocytosis and therefore synaptic transmission, further bolstered by the increase of several fusiogenic PE species. AA was only found to be significantly increased in the HYP punch. Generally, fluctuations in AA levels are difficult to target, since AA is a precursor and product in plenty of metabolic pathways thus underlying a high turnover rate (Rapoport, 2008) and

moreover, AA is much higher abundant compared to others lipids in particular to signaling lipids (Lerner *et al.*, 2016). The detectable increase of AA in the investigated part of the HYP could be eventually related to the specifically altered levels of inflammatory signaling lipids in this region, without the concurrent strong increase of other lipid molecules, as observed in BLA and dHC. Even though expression of kainite receptor RNA was found in the HYP (Van Den Pol *et al.*, 1994), this brain region was not considered to be a main brain region which plays a central role in seizures (Sperk, 1994; Ben-Ari, 2010). The lipid pattern obtained from the investigated HYP area may rather indicate increased activity in this subregion than general damage. Since most part of the HYP punch belongs to the dorsomedial hypothalamic nucleus and ventromedial nucleus, which have a central neuroendocrine function and play a role in the elevation of heart rate and blood pressure as cardiovascular responses to stress (Stotz-Potter *et al.*, 1996), increased activity could be also associated with the PL alterations found in the heart (Fig. 6.4).

The BLA in contrast displays almost no changes in lipid signaling molecules but instead exhibits a more overall significant increment of PL species for every targeted PL class. Notable is the significant increase of the PS species, which is to this extent only found in this area. As described above PS is known to be a receptor mediated apoptotic signal, hence increased levels could be a sign for irreversible cell damage caused by the KA-induced seizures. Another function of the elevated PS levels could be also enhanced synaptic transmission efficiency through binding of PS species to proteins of the exocytosis machinery as described above.

Most changes in lipid levels 1 h after KA-induced seizure were found in the vHC and dHC. A previous study by Guan and colleagues also using KA injection to model epileptiform seizures in rats already investigated changes in hippocampal PL levels (Guan *et al.*, 2006). The study revealed 10 min after KA treatment reductions in the major PLs containing predominantly polyunsaturated fatty acyl chains, as well as elevations in acylated forms of PEs (the precursor for AEA) and ceramides in the rat HC. They attributed the alterations to calcium-influx initiated increase of PLA activity which induces unequal PL degradation and subsequent formation of second messengers. To elucidate the mechanism underlying PL degradation, they point to the necessity for additional characterization of enzyme expressions, as well as the analysis of lipid molecules such as AEA, which was so far beyond the scope of their study. The here developed method for lipidomic and transcriptomic profiling makes it possible to address these points. Moreover, the efficiency of our extraction method, enabling the analysis of sub mg tissue amounts, revealed mainly contrary lipid changes in the hippocampal subregions. Accordingly, a PL breakdown as reported by Guan et al was in our study restricted to the vHC 1 h after KA-induced seizures, whereas strong increase of all investigated PE species (except for two PEs all were significantly increased), was found in the dHC of mice. This PE increment in the dHC was accompanied by additional strong elevations among every investigated PL class.

The measured levels of *cfos* mRNA basically correlate with these obtained lipid patterns. The immediate early gene *c-fos* is widely used as a marker for neural activity and its activities assumed to be involved in neuroprotection (Chung, 2015). Former studies demonstrated already expression induction of this gene in KA-seizure model (Popovici *et al.*, 1990; Marsicano, Goodenough, *et al.*, 2003). In this study a significant upregulation of *cfos* expression was found in all brain regions, with the most affected brain regions BLA and HC exhibiting higher levels than HYP. The dHC, where also the most lipid changes occurred, exhibited the highest *cfos* mRNA level, indicating highest KA-induced neuronal activity in this hippocampal subregion. The mRNAs encoding the neurotrophic factor BDNF were exclusively found to significantly increase with epilepsy in the both hippocampal subregions. Levels of both BDNF mRNA and BDNF protein are known to be up-regulated in epilepsy (Gall *et al.*, 1991). BDNF modulates excitatory and inhibitory synaptic transmission by inhibiting GABA-receptor-mediated post-synaptic currents (Tanaka *et al.*, 1997), further underlying the strong impact of KA treatment on the HC.

The detected increase in expression of in neurodegeneration implicated *cPLA<sub>2</sub>* is also in agreement with previous findings, demonstrating increased *cPLA<sub>2</sub>* mRNA and protein levels and thus enhanced *cPLA<sub>2</sub>* activity in neurons and astrocytes accompanied by alterations in neural membrane PL composition after systemic KA-administration in rats (Sandhya *et al.*, 1998). The fact, that the significant increase in *cPLA<sub>2</sub>* expression in our study was restricted to the hippocampal subareas, to a slightly higher extent in the vHC, further supports a region specific seizure response. The *PLA<sub>2</sub>* superfamily comprises *cPLA<sub>2</sub>*, *iPLA<sub>2</sub>*, *PlsEtn-PLA<sub>2</sub>* and the secretory *PLA<sub>2</sub>* (*sPLA<sub>2</sub>*). The upregulation of the *cPLA<sub>2</sub>* family members is described to be involved in breakdown of neuronal membrane PLs, as seen in the vHC (Ong *et al.*, 2010). However, even though in both hippocampal subregions *cPLA<sub>2</sub>* expression is significantly increased, only the vHC exhibited the expected PL decrease, while the dHC displayed strong increase in PL levels, indicating the elevated activity of the targeted *cPLA<sub>2</sub>* as unlikely to be solely the reason of the strong PL breakdown in the vHC. Accordingly, one cannot always directly conclude from varying enzyme amounts to lipid level changes and vice versa. Moreover, *iPLA<sub>2</sub>s* are shown to act as essential “housekeeping” enzymes under normal conditions to prevent neuropsychiatric disease (Ong *et al.*, 2010). These data all the more support the necessity to increase the knowledge about the functions of the different *PLA<sub>2</sub>* isomers for drug treatment to ensure precise targeting of specific pathways in specific regions.

Similarly unexpected results were found for AEA levels and the expression of its primary synthesizing enzyme NAPE-PLD. AEA which was previously shown to exert neuroprotective effects in KA-induced epileptic seizure model peaking in the HC 20 min after injection (Marsicano, Goodenough, *et al.*, 2003), underwent significant enhancement in the BLA, dHC and vHC, the latter showing the strongest increment. Interestingly, levels of NAPE-PLD were exclusively

altered only in the dHC, showing as opposed to AEA, reduced levels. Thus, epileptic seizure induced increase of the neuroprotective AEA seems not to be mediated by NAPE-PLD, but via a distinct biosynthetic pathway as described above (Leung *et al.*, 2006). That levels of NAPE-PLD are decreased in the dHC may point toward a compensatory mechanism to counteract the high amounts of AEA, possibly resulting in the lower levels of AEA in the dHC compared to vHC. Interestingly, AA levels are not altered in the two hippocampal subregions, so that a correlation between AA pool and AEA levels cannot be concluded. Generally, a direct correlation through the consumption of AA to produce AEA is ambiguous, given the much higher levels of AA compared to AEA and the multiple pathway origin of the AA pool (Fig. 2.3). Thus, for a better understanding, targeting more enzymes involved in the metabolic pathways is required.

Even though enhanced levels of AEA, observed in this study, may be upregulated in order to exert neuroprotection, the levels of CB1R mRNA remained unaffected. Generally, the activity of CB1R in acute state is more ligand-dependent and less from its amount, while CB1R up- or down-regulation more likely displays long term compensatory mechanisms. Accordingly, a study by Wallace and colleagues described enhanced CB1R expression 1 year after status epilepticus throughout the CA regions of epileptic rat hippocampi (Wallace *et al.*, 2003). Nevertheless, neuroprotective effects by AEA could also possibly be mediated via other receptors, such as vanilloid receptors or PPAR1 which remains to be further investigated. Moreover, it was recently suggested that also the membrane bilayer can serve as a modulator of hCB1/GPCR signal transduction in that changes in the structural composition and heterogeneity of membrane lipids leads to differential mechanochemical environment that shape accordingly the signal transduction events (Tiburru *et al.*, 2011).

If comparing the here described application studies, the higher calculated AEA concentrations, as obtained in the first study from HYP and HC (Fig. 6.4), become conspicuous. This outcome can be explained by the better extraction efficiency of MTBE for AEA (Fig. 4.12) used in the first application study for eCB analysis (Lerner *et al.*, 2016) and supports the result of the lipidomic profiling optimization to use concurrent homogenization and extraction buffer for optimal tissue lysis and molecule extraction. Noteworthy, when investigating the HC region as a whole tissue, no significant differences were observed at the PL level 1 h after KA injection, as well as for AEA (Lerner *et al.*, 2016). Hence, the significant changes of the dHC and vHC determined here are likely masked when an entire HC is investigated which strongly underlines the demand for higher spatial resolution to clarify locally restricted mechanism and unravel the specific molecular plasticity, e.g. lipids under pathological conditions. The differences between lipidomic and genomic alterations in the dHC compared to vHC shown in this study could be related to their distinct functions; while dHC performs primarily cognitive tasks, the vHC relates to stress, emotion and affect (Fanselow and Dong, 2010; Small *et al.*, 2011; Strange *et al.*, 2014;

Cembrowski *et al.*, 2016). Thus, the vHC exhibits only increase in signaling molecules such as LPCs, the two polyunsaturated LPAs and AEA, while PC species are mainly decreased, in contrast to the overall increase of lipids found in the dHC. Breakdown of PC species and enhanced LPA signaling as seen in the vHC was also associated with other disease such as SCZ and proposed to be involved in demyelination as described above (Schmitt *et al.*, 2004; Velasco *et al.*, 2017). The general PL increase in the dHC comprises also complete enhancement of all targeted SM species, which was to a lower extent also found in the BLA. As mentioned above, SM is an important regulator of protein binding and synaptic transmission. Increase of SM levels, as seen in synaptosomes of aged mice to exert the function as regulator of synaptic transmission by reducing membrane curvature, seems to be unlikely in this seizure model. The high neuronal activity in the excitotoxic state and the related high transmitter release, as well as the concurrent increase in fusiogenic PLs, contradict this hypothesis. More likely, the enhancement of SM species occurs in order to conduct their role as lipid rafts regulator by binding of survival receptors to prevent apoptosis (Paratcha and Ibáñez, 2002).

Notably, the increment in SM species with aging was shown to be brain region-specific and, indeed, various age-related brain disorders such as AD and PD, display regional susceptibility (Ledesma *et al.*, 2012), what again underlines the requirement of functional lipidomic studies pointing to specifically regions of interest. Moreover, subregion-specific cell responses exist which are even more difficult to target. For instance in epilepsy, accumulation of ROS plays a major role in the onset and progression likewise in other neurodegenerative diseases, such as AD or PD. Of note is, that selective vulnerability of neurons occurs in relative sensitivity to stress and diseases, e.g. the dopaminergic neurons of the substantia nigra are more vulnerable to oxidative stress in PD, whereas in epileptic disorder CA1 neurons of the hippocampus exhibit much more vulnerability than CA3 neurons (Wang, 2010; Kim *et al.*, 2015). The increased vulnerability of the CA1 region may related to its relatively lower levels of mitochondrial oxidative enzyme (Davolio and Greenamyre, 1995).

In order to allow targeting of lipids across cell layers/populations to generate pictures of lipid alterations and thus, defining lipid patterns under pathological conditions with higher spatial resolution, MSI experiments were performed. A basic outcome of these experiments was the cell layer specific localization of different PL species (Fig. 6.11) PC 32:0 and PI 38:4 are almost complementary distributed. While PI 38:4 seems to be restricted to the pyramidal cell layer and the granular cell layer of the dentate gyrus, PC 32:0 is predominantly found in their corresponding axons e.g. Mossy fibers and Schaffer collaterals. This differential distribution can possibly be related to their predominant function. PC represents the main membrane component in cells and the donor of choline to SM, a main component of myelin membranes. Axons in turn consist to a relatively high extent of membranes in particular due to the surrounding myelin sheath which

comprises approximately 70 % a relatively high lipid content (Jackman *et al.*, 2009). Thus, the high abundance of PC in the axons and its detected alterations associated with epileptic seizures underlines the hypothesis of its involvement in demyelination processes. PI vice versa, was mainly found in cell layers corresponding to cell bodies, supporting its role as direct signaling molecule or main precursor of PI phosphates, which are known to play important roles in cell signaling (Ledesma *et al.*, 2012). Interestingly, PI 34:1 is the only targeted molecule, which was upregulated in all investigated brain regions, possibly serving as potential biomarker.

Additional MSI experiments using the mouse model of epileptic seizure revealed that certain lipid changes shift between sal and KA injected animal throughout the dHC, such as the case for SM 36:1 and PC 32:0 (Fig. 6.10). Both lipids exhibit a significant increase with epilepsy in the entire dHC as determined by LC/MRM (Fig. 6.8). Such an increase of these lipids was also observed by MSI in the 3rd slice of the dHC, whereas in the 4th slice they seem to show an inverse trend, hence reduction with epilepsy. For SM 36:1, this inverse trend is also observable in the 2nd slice (Fig. 6.10). Thus, the data obtained via MSI apparently show an alternating response in the lipid levels throughout the dHC associated with epilepsy, emphasizing the complexity of epileptic manifestations. The origin of these shifts is not known and requires future detailed investigation. However, these data underline once more how likely it is to mask molecule alterations when analyzing whole brain regions and highlight the advantage and requirement of combined quantitative analysis at high spatial resolution in brain and MSI throughout various brain cell layers in order to prevent misinterpretation of pathological status.

Finally, MSI experiments for the analysis of PL adducts revealed distinct alterations in their levels 1 h after KA injection, as shown for PC 32:0 and PC 34:1 in the dHC, depicted as their protonated ( $H^+$ ) forms or potassium ( $K^+$ ) adducts (Fig. 6.12). Changes in potassium adduct formation of PC species have been previously shown in livers from hepatitis B infected mice, with higher potassium adduct intensities relative to  $H^+$  in vector infected and less potassium adducts relative to  $H^+$  ions in hepatitis B infected mice (Park *et al.*, 2014). In our study we found similar results as both  $H^+$  ions show elevated levels in the KA injected animals compared to controls, while in contrast the levels of the corresponding  $K^+$  adducts are decreased with epileptic seizures. Such data might suggest direct conversion of  $K^+$  containing PLs into their protonated ion forms via metabolism or spontaneous exchange in order to release potassium. Under the pathological high activity of neurons within epileptic seizures, it might well be that the  $Na^+/K^+$ -ATPase, which maintains the resting potential, fails to completely restore the intracellular potassium levels. A previous study already reported ROS and calcium-influx dependent downregulation of  $Na^+/K^+$ -ATPase within hypoxia (Gusarova *et al.*, 2011). Interestingly, pilocarpine-induced status epilepticus in rats was shown to decrease  $Na^+/K^+$ -ATPase activity in the HC 1.5 h after seizure induction but not later, leading to neuronal death 24 h after seizure induction (De Oliveira *et al.*,

2011). Accordingly, a potentially resulting gap in the intracellular  $K^+$  pool may be refilled from PL precursors. Since different adduct cationization alters the translational energy and shape of the affected PLs, such an event might disturb the membrane integrity and therefore support the neuronal death as seen in the CA1 subfield (De Oliveira *et al.*, 2011). Thus,  $Na^+/K^+$ -ATPase activity might be a possible target to circumvent such pathological effects. However, these results are still preliminary and additional quantitative LC/MRM experiments have to be performed for MSI data confirmation and further investigation of this hypothesis

### 7 CONCLUSIONS AND PERSPECTIVES

In conclusion, new methods were established and demonstrated as valuable aids to the lipidomic and transcriptomic profiling toolbox in preclinical research. Their application in KA-induced epileptic seizure models offered new insights into the lipid plasticity associated with epilepsy. Essentially, i) brain regional and peripheral lipid fingerprints, ii) lipid and mRNA fingerprints in functional brain subregions, and iii) plasma lipid markers of acute epileptic seizures were determined. The preliminary investigation of the acute epilepsy phase using these strategies, rendered already a yet, unparalleled level of molecular information in terms of the distinct involvement of various molecules and their subregional specificity in KA-mouse model of epilepsy. Future data have to be gathered to draw unequivocal conclusions on the functional role of these molecules to support proper design of new patient treatment. Since levels of enzyme mRNAs involved in the lipid biosynthesis and metabolism and of the corresponding lipids do not invariably, directly correlate, on one hand, and the reductionist interrogation of metabolic/signaling pathways is not compliant with the huge complexity of biological systems, on the other hand, it is necessary to expand the knowledge of affected pathways by unbiased molecular profiling. In our particular model of epilepsy, prospective application of the dual extraction method combined with RNA sequencing and shot-gun lipidomics will increase the plethora of investigated molecules and help generate an interrelated profile in order to attain a complete picture of molecule function. Accordingly, future studies will hence prioritize the targeted molecules associated with pathologies for a better understanding of the underlying complex mechanisms to enable new opportunities for focused disease treatment. Finally, the developed methods are adaptable for any tissue type and size, allow high spatial resolution due to their high extraction efficiency, and thus are suitable to perform lipidomic and transcriptomic profiling for every pathological state.

Referring to our lipid imaging MSI experiments, additional quantitative data via LC/MRM are required to verify and contextualize the results regarding the differential ion exchange of PL with epilepsy. In this context, analysis of the major PL species and their most abundant adduct ions should be performed, in order to obtain new insights into the intracellular ionic homeostasis associated with epileptic seizures. Furthermore, targeting enzymes involved in this molecular mechanism such as the Na<sup>+</sup>/K<sup>+</sup>-ATPase may give additional insights into the molecular events underlining epilepsy. In general, this outcome raises the question, whether when investigating PLs in pathology, analysis of all possible cations and anions and/or their ratio is required, in order to prevent misinterpretation of altered PL levels which are indeed only caused by ion adduct conversion and/or determine if ion exchange is pathology specific.

Another very interesting point for designing new therapeutic approaches is to elucidate the mechanism, which mediates epileptic seizure-induced increase of the endogenous neuro-



protectant AEA in HC and BLA subregions. Since NAPE-PLD seems unlikely to be involved, a first analysis would address the other enzymes which are known to mediate AEA synthesis, such as lyso-PLD, ABHD4 or PLC. Of course, also the other molecules, involved in eCB signaling and metabolism such as degrading enzymes and receptors should be investigated. For instance MAGL represents an important candidate, as it is also described to produce the major AA precursor pool for neuroinflammatory prostaglandins via 2-AG hydrolysis (Nomura *et al.*, 2011). In this context, other members of the ABHD family are interesting candidates too, since blockade of ABHD6 was reported to mediate antiepileptic effects in pilocarpine-induced seizures and spontaneous seizures in R6/2 mice, a genetic model for juvenile Huntington's disease (Naydenov *et al.*, 2014). Furthermore, in order to better understand the changes occurring in PL level, it would be necessary to analyze a broader repertoire of the synthesizing and hydrolyzing enzymes. Hence, as mentioned above, the different phospholipases are important targets, in particular the PLA2 family. Moreover, as SM exerts several important roles in cognitive functions and aging, investigating sphingomyelinase, which was found to increase with aging (Sackett *et al.*, 2009), as well as SM synthase, might give further information especially about potential demyelination processes in progression of epilepsy. As indicated in the introduction, PUFAs are also involved in several crucial processes and thus, extending the amount of examined PUFAs by analyzing also DHA and the corresponding desaturase, might be helpful to elucidate associated pathways as found with aging. Other important lipids such as the signaling lipids PI phosphates, or cholesterol, which is also a main component of the myelin sheath and lipid rafts, should be included in future experiments.

Certainly, the lipidome, hence lipid signaling, is spatially and temporally dynamic and thus, perspective time course analysis of the specific lipid changes and functional lipidomic and transcriptomic analysis are necessary to clarify the mechanism of action. Establishing of new animal models for functional lipidomic and transcriptomic studies will be necessary. Ideally, this would be also accompanied by a proteomic and functional protein analysis. This multi-omic approach, though demanding, it is necessary at least in diseases with such a broad spectrum of causalities and manifestations as the case of epilepsy, in order to increase the specificity of mechanisms elucidation and the discrimination efficiency of biomarkers for diagnosis and disease progression monitoring. Additionally, comparison of different epileptic seizure models would be necessary to derive the commonalities and distinctive features of lipidome and transcriptome changes with epileptic disorder. Moreover, drug treatment experiments, using anti-inflammatory substances such as COX-2 and FAAH inhibitors, PEA, and combinations thereof might be promising (Keppel Hesselink *et al.*, 2014). Given that our study revealed epilepsy-specific lipid fingerprints in plasma, lipids are highlighted as promising biomarker candidates in translational studies with human patients suffering from epilepsy to monitor therapeutic responses and disease progression.

In conclusion, the developed analytical techniques represent valuable tools to advance our understanding of the physiological function of lipids under high spatial resolution, to optimize the effectiveness of diagnosis and treatment of neurological diseases in particular and, more broadly, in diseases associated with lipid dysregulation.

## 8 REFERENCES

- Aaltonen N, Laitinen JT, and Lehtonen M (2010) Quantification of lysophosphatidic acids in rat brain tissue by liquid chromatography-electrospray tandem mass spectrometry. *J Chromatogr B Anal Technol Biomed Life Sci* **878**:1145–1152, Elsevier B.V.
- Abbott SK, Jenner AM, Mitchell TW, Brown SHJ, Halliday GM, and Garner B (2013) An improved high-throughput lipid extraction method for the analysis of human brain lipids. *Lipids* **48**:307–318.
- Abbott SK, Jenner AM, Spiro AS, Batterham M, Halliday GM, and Garner B (2015) Fatty acid composition of the anterior cingulate cortex indicates a high susceptibility to lipid peroxidation in Parkinson's disease. *J Parkinsons Dis* **5**:175–185.
- Abdullah L, Evans JE, Ferguson S, Mouzon B, Montague H, Reed J, Crynen G, Emmerich T, Crocker M, Pelot R, Mullan M, and Crawford F (2014) Lipidomic analyses identify injury-specific phospholipid changes 3 mo after traumatic brain injury. *FASEB J* **28**:5311–5321.
- Alhouayek M, and Muccioli GG (2014) COX-2-derived endocannabinoid metabolites as novel inflammatory mediators. *Trends Pharmacol Sci* **35**:284–292, Elsevier Ltd.
- Allen J a, Halverson-Tamboli R a, and Rasenick MM (2007) Lipid raft microdomains and neurotransmitter signalling. *Nat Rev Neurosci* **8**:128–140.
- Almeida R, Pauling JK, Sokol E, Hannibal-Bach HK, and Ejsing CS (2014) Comprehensive lipidome analysis by shotgun lipidomics on a hybrid quadrupole-orbitrap-linear ion trap mass spectrometer. *J Am Soc Mass Spectrom* **26**:133–148.
- Amini E, Rezaei M, Mohamed Ibrahim N, Golpich M, Ghasemi R, Mohamed Z, Raymond AA, Dargahi L, and Ahmadiani A (2015) A Molecular Approach to Epilepsy Management: from Current Therapeutic Methods to Preconditioning Efforts. *Mol Neurobiol* **52**:492–513.
- Amstalden van Hove ER, Smith DF, and Heeren RMA (2010) A concise review of mass spectrometry imaging. *J Chromatogr A* **1217**:3946–3954, Elsevier B.V.
- Antony B, Vanni S, Shindou H, and Ferreira T (2015) From zero to six double bonds: phospholipid unsaturation and organelle function. *Trends Cell Biol* **25**:427–436.
- Astarita G, Ahmed F, and Piomelli D (2008) Identification of biosynthetic precursors for the endocannabinoid anandamide in the rat brain. *J Lipid Res* **49**:48–57.
- Aston FW (1919) A positive-ray spectrograph. *Philos Mag* **38**:707–715.
- Azuma M, Ito I, Matsumoto R, Hirai T, and Mishima M (2012) Pulmonary hemorrhage induced by epileptic seizure. *Hear Lung J Acute Crit Care* **41**:290–293, Elsevier Inc.
- Barber M, Bordoli RS, Sedgwick RD, and Tyler AN (1981) Fast atom bombardment of solids (F.A.B.): a new ion source for mass spectrometry. *J Chem Soc Chem Commun* **325**.
- Bard L, and Groc L (2011) Glutamate receptor dynamics and protein interaction: Lessons from the NMDA receptor. *Mol Cell Neurosci* **48**:298–307.
- Bazán NG (1970) Effects of ischemia and electroconvulsive shock on free fatty acid pool in the brain. *Biochim Biophys Acta (BBA)/Lipids Lipid Metab* **218**:1–10.

## REFERENCES

---

- Bazan NG, Morelli de Liberti S a, and Rodriguez de Turco EB (1982) Arachidonic acid and arachidonoyl-diglycerols increase in rat cerebrum during bicuculline-induced status epilepticus. *Neurochem Res* **7**:839–43.
- Beckey HD (1969) Determination of the structures of organic molecules and quantitative analyses with the field ionization mass spectrometer. *Angew Chem, Int Ed Engl* **8**:623–639.
- Ben-Ari Y (2010) Kainate and temporal lobe epilepsies: Three decades of progress. *Epilepsia* **51**:40.
- Ben-Ari Y, and Cossart R (2000) Kainate, a double agent that generates seizures: Two decades of progress. *Trends Neurosci* **23**:580–587.
- Berry S (2004) Lipid Analysis: Isolation, Separation, Identification and Structural Analysis of Lipids. *Nutr Bull* **29**:72–73.
- Bertram EH (2013) Neuronal circuits in epilepsy: Do they matter? *Exp Neurol* **244**:67–74, Elsevier B.V.
- Bilkei-Gorzo A (2012) The endocannabinoid system in normal and pathological brain ageing. *Philos Trans R Soc L B Biol Sci* **367**:3326–3341.
- Bindila L, and Lutz B (2016) Endocannabinoid Signaling. **1412**:9–18.
- Bisogno T, Howell F, Williams G, Minassi A, Cascio MG, Ligresti A, Matias I, Schiano-Moriello A, Paul P, Williams EJ, Gangadbaran U, Hobbs C, Di Marzo V, and Doherty P (2003) Cloning of the first sn1-DAG lipases points to the spatial and temporal regulation of endocannabinoid signaling in the brain. *J Cell Biol* **163**:463–468.
- Blankman JL, and Cravatt BF (2013) Chemical probes of endocannabinoid metabolism. *Pharmacol Rev* **65**:849–71.
- Blankman JL, Simon GM, and Cravatt BF (2007) A Comprehensive Profile of Brain Enzymes that Hydrolyze the Endocannabinoid 2-Arachidonoylglycerol. *Chem Biol* **14**:1347–1356.
- Bligh EG, and Dyer WJ (1959) A rapid method of total lipid extraction and purification. *Can J Biochem Physiol* **37**:911–917.
- Boden G, She P, Mozzoli M, Cheung P, Gumireddy K, Reddy P, Xiang X, Luo Z, and Ruderman N (2005) Free fatty acids produce insulin resistance and activate the proinflammatory nuclear factor-kappaB pathway in rat liver. *Diabetes* **54**:3458–65.
- Bojnik E, Turunç E, Armağan G, Kanit L, Benyhe S, Yalçın A, and Borsodi A (2012) Changes in the cannabinoid (CB1) receptor expression level and G-protein activation in kainic acid induced seizures. *Epilepsy Res* **99**:64–68.
- Brody H, May M, Grayson M, Miller K, Gray S, Pope I, Piper W, Smith Y, and Hurst S (2014) Introduction. *Nat OUTLOOK Vol* **511**:S1.
- Brown HA, and Marnett LJ (2011) Introduction to lipid biochemistry, metabolism, and signaling. *Chem Rev* **111**:5817–5820.
- Brügger B, Erben G, Sandhoff R, Wieland FT, and Lehmann WD (1997) Quantitative analysis of biological membrane lipids at the low picomole level by nano-electrospray ionization tandem

- mass spectrometry. *Proc Natl Acad Sci U S A* **94**:2339–2344.
- Buré C, Ayciriex S, Testet E, and Schmitter JM (2013) A single run LC-MS/MS method for phospholipidomics. *Anal Bioanal Chem* **405**:203–213.
- Caccin P, Scorzeto M, Damiano N, Marin O, Megighian A, and Montecucco C (2015) The synaptotagmin juxtamembrane domain is involved in neuroexocytosis. *FEBS Open Bio* **5**:388–396.
- Cajka T, and Fiehn O (2016) Toward Merging Untargeted and Targeted Methods in Mass Spectrometry-Based Metabolomics and Lipidomics. *Anal Chem* **88**:524–545.
- Cameron AE, and Eggers DF (1948) An ion “velocitron.” *Rev Sci Instrum* **19**:605–607.
- Cannon CP (2005) The endocannabinoid system: A new approach to control cardiovascular disease. *Clin Cornerstone* **7**:17–26.
- Canteras NS, Simerly RB, and Swanson LW (1994) Organization of projections from the ventromedial nucleus of the hypothalamus: A Phaseolus vulgaris- Leucoagglutinin study in the rat. *J Comp Neurol* **348**:41–79.
- Caprioli RM, Farmer TB, and Gile J (1997) Molecular imaging of biological samples: localization of peptides and proteins using MALDI-TOF MS. *Anal Chem* **69**:4751–4760.
- Castillo PE, Younts TJ, Chávez AE, and Hashimoto Y (2012) Endocannabinoid Signaling and Synaptic Function. *Neuron* **76**:70–81.
- Cembrowski MS, Bachman JL, Wang L, Sugino K, Shields BC, Cembrowski MS, Bachman JL, Wang L, Sugino K, Shields BC, and Spruston N (2016) Spatial Gene-Expression Gradients Underlie Prominent Heterogeneity of CA1 Pyramidal Neurons Article Spatial Gene-Expression Gradients Underlie Prominent Heterogeneity of CA1 Pyramidal Neurons. *Neuron* **89**:351–368, Elsevier Inc.
- Chang C-Y, Ke D-S, and Chen J-Y (2009) Essential fatty acids and human brain. *Acta Neurol Taiwan* **18**:231–241.
- Chávez AE, Chiu CQ, and Castillo PE (2010) TRPV1 activation by endogenous anandamide triggers postsynaptic long-term depression in dentate gyrus. *Nat Neurosci* **13**:1511–8.
- Chen S, Hoene M, Li J, Li Y, Zhao X, Häring HU, Schleicher ED, Weigert C, Xu G, and Lehmann R (2013) Simultaneous extraction of metabolome and lipidome with methyl tert-butyl ether from a single small tissue sample for ultra-high performance liquid chromatography/mass spectrometry. *J Chromatogr A* **1298**:9–16, Elsevier B.V.
- Cheng HT, and London E (2011) Preparation and properties of asymmetric large unilamellar vesicles: Interleaflet coupling in asymmetric vesicles is dependent on temperature but not curvature. *Biophys J* **100**:2671–2678.
- Chevalyere V, Takahashi KA, and Castillo PE (2006) Endocannabinoid-mediated synaptic plasticity in the CNS. *Annu Rev Neurosci* **29**:37–76.
- Chiarlone A, Bellocchio L, Blazquez C, Resel E, Soria-Gomez E, Cannich A, Ferrero JJ, Sagredo O, Benito C, Romero J, Sanchez-Prieto J, Lutz B, Fernandez-Ruiz J, Galve-Roperh I, and

## REFERENCES

---

- Guzman M (2014) A restricted population of CB1 cannabinoid receptors with neuroprotective activity. *Proc Natl Acad Sci* **111**:8257–8262.
- Chilton FH, and Murphy RC (1986) Characterization of the arachidonate-containing molecular species of phosphoglycerides in the human neutrophil. *Prostaglandins, Leukot Med* **23**:141–148.
- Choi J, and Chun J (2013) Lysophospholipids and their receptors in the central nervous system. *Biochim Biophys Acta* **1831**:20–32.
- Choi JJW, and Chun J (2013) Lysophospholipids and Their Receptors in the Central Nervous System. *Biochim Biophys Acta* **1831**:20–32, Elsevier B.V.
- Choquet D, and Triller A (2003) The role of receptor diffusion in the organization of the postsynaptic membrane. *Nat Rev Neurosci* **4**:251–265.
- Chung L (2015) A Brief Introduction to the Transduction of Neural Activity into Fos Signal. *Dev Reprod* **19**:61–7.
- Comisarow MB, and Marshall AG (1974) Fourier transform ion cyclotron resonance spectroscopy. *Chem Phys Lett* **25**:282–283.
- Contreras F-X, Ernst AM, Haberkant P, Björkholm P, Lindahl E, Gönen B, Tischer C, Elofsson A, von Heijne G, Thiele C, Pepperkok R, Wieland F, and Brügger B (2012) Molecular recognition of a single sphingolipid species by a protein's transmembrane domain. *Nature* **481**:525–529.
- Craven K (2013) Delivering Accurate Collision Cross Section Measurements with SYNAPT High Definition Mass Spectrometry (HDMS). *Waters Tech Note* 1–2.
- Cully M (2014) Illuminated targets. *Nat OUTLOOK* **511**:S12 S13.
- Da Cunha MJ, Da Cunha AA, Scherer EBS, Machado FR, Loureiro SO, Jaenisch RB, Guma F, Lago PD, and Wyse ATS (2014) Experimental lung injury promotes alterations in energy metabolism and respiratory mechanics in the lungs of rats: Prevention by exercise. *Mol Cell Biochem* **389**:229–238.
- Dahl PF (1997) Flash of the Cathode Rays: A History of J J Thomson's Electron. *Eur J Phys* **6**:122–185.
- Davolio C, and Greenamyre JT (1995) Selective vulnerability of the CA1 region of hippocampus to the indirect excitotoxic effects of malonic acid. *Neurosci Lett* **192**:29–32.
- de Freitas RM, do Nascimento KG, Ferreira PMP, and Jordán J (2010) Neurochemical changes on oxidative stress in rat hippocampus during acute phase of pilocarpine-induced seizures. *Pharmacol Biochem Behav* **94**:341–345, Elsevier Inc.
- De Oliveira DL, Bavaresco C, Mussulini BH, Fischer A, Souza DO, Wyse ATS, and Wofchuk S (2011) Early life LiCl-pilocarpine-induced status epilepticus reduces acutely hippocampal glutamate uptake and Na<sup>+</sup>/K<sup>+</sup> ATPase activity. *Brain Res* **1369**:167–172.
- Dempster AJ (1918) A new Method of Positive Ray Analysis. *Phys Rev* **11**:316–325.
- Denisov E, Damoc E, Lange O, and Makarov A (2012) Orbitrap mass spectrometry with resolving

- powers above 1,000,000. *Int J Mass Spectrom* **325–327**:80–85.
- Deutsch DG, Ueda N, and Yamamoto S (2002) The fatty acid amide hydrolase (FAAH). *Prostaglandins Leukot Essent Fat Acids* **66**:201–210.
- Devane WA, Hanus L, Breuer A, Pertwee RG, Stevenson LA, Griffin G, Gibson D, Mandelbaum A, Etinger A, and Mechoulam R (1992) Isolation and structure of a brain constituent that binds to the cannabinoid receptor. *Science* **258**:1946–9.
- Diana MA, and Marty A (2004) Endocannabinoid-mediated short-term synaptic plasticity: depolarization-induced suppression of inhibition (DSI) and depolarization-induced suppression of excitation (DSE). *Br J Pharmacol* **142**:9–19.
- Di Paolo G, and De Camilli P (2006) Phosphoinositides in cell regulation and membrane dynamics. *Nature* **443**:651–657.
- Downward J (2001) The ins and outs of signalling. *Nature* **411**:759–62.
- Eisenstein M (2014) Unrestrained excitement. *Nat OUTLOOK* **511**:S4 S5.
- Ejsing CS, Sampaio JL, Surendranath V, Duchoslav E, Ekroos K, Klemm RW, Simons K, and Shevchenko A (2009) Global analysis of the yeast lipidome by quantitative shotgun mass spectrometry. *Proc Natl Acad Sci U S A* **106**:2136–2141.
- Ejsing CS, Sampaio JL, Surendranath V, Duchoslav E, Ekroos K, Klemm RW, Simons K, and Shevchenko A (2009) Global analysis of the yeast lipidome by quantitative shotgun mass spectrometry. *Proc Natl Acad Sci* **106**:2136–2141.
- Ettre LS, and Sakodynskii KI (1993) M. S. Tswett and the discovery of chromatography I: Early work (1899–1903). *Chromatographia* **35**:223–231.
- Fahy E, Cotter D, Sud M, and Subramaniam S (2011) Lipid classification, structures and tools. *Biochim Biophys Acta - Mol Cell Biol Lipids* **1811**:637–647.
- Fahy E, Subramaniam S, Brown HA, Glass CK, Merrill AH, Murphy RC, Raetz CRH, Russell DW, Seyama Y, Shaw W, Shimizu T, Spener F, Meer G Van, Vannieuwenhze MS, White SH, Witztum JL, and Dennis EA (2005) A comprehensive classification system for lipids 1. **46**.
- Fahy E, Subramaniam S, Murphy RC, Nishijima M, Raetz CRH, Shimizu T, Spener F, van Meer G, Wakelam MJO, and Dennis EA (2009) Update of the LIPID MAPS comprehensive classification system for lipids. *J Lipid Res* **50**:S9–S14.
- Fanselow MS, and Dong HW (2010) Are the Dorsal and Ventral Hippocampus Functionally Distinct Structures? *Neuron* **65**:7–19, Elsevier Inc.
- Farias SE, Basselin M, Chang L, Heidenreich KA, Rapoport SI, and Murphy RC (2008) Formation of eicosanoids, E2/D2 isoprostanes, and docosanoids following decapitation-induced ischemia, measured in high-energy-microwaved rat brain. *J Lipid Res* **49**:1990–2000.
- Farooqui AA, Ong WY, and Horrocks LA (2004) Biochemical aspects of neurodegeneration in human brain: Involvement of neural membrane phospholipids and phospholipases A 2. *Neurochem Res* **29**:1961–1977.
- Farooqui AA, Ong WY, Horrocks LA, and Farooqui T (2000) Brain cytosolic phospholipase A(2):

## REFERENCES

---

- Localization, role, and involvement in neurological diseases. *Neuroscientist* **6**:169–180.
- Fauland A, Trötz Müller M, Eberl A, Afuni-Zadeh S, Köfeler H, Guo X, and Lankmayr E (2013) An improved SPE method for fractionation and identification of phospholipids. *J Sep Sci* **36**:744–751.
- Favrelère S, Stadelmann-Ingrand S, Huguet F, De Javel D, Piriou a, Tallineau C, and Durand G (2000) Age-related changes in ethanolamine glycerophospholipid fatty acid levels in rat frontal cortex and hippocampus. *Neurobiol Aging* **21**:653–60.
- Fernández JA, Ochoa B, Fresnedo O, Giralt MT, and Rodríguez-Puertas R (2011) Matrix-assisted laser desorption ionization imaging mass spectrometry in lipidomics. *Anal Bioanal Chem* **401**:29–51.
- Fezza F, Marrone MC, Avvisati R, Di Tommaso M, Lanuti M, Rapino C, Mercuri NB, Maccarrone M, and Marinelli S (2014) Distinct modulation of the endocannabinoid system upon kainic acid-induced in vivo seizures and in vitro epileptiform bursting. *Mol Cell Neurosci* **62**:1–9, Elsevier Inc.
- Flemming A (2014) Epilepsy: Endocannabinoid metabolism offers handle to dampen down excitability. *Nat Rev Drug Discov* **13**:1, Nature Publishing Group.
- Folch J, Lees M, and Stanley GHS (1957) A simple method for the isolation and purification of total lipids from animal tissues. *J Biol Chem* **226**: 497-509.
- Freitas RM, Sousa FCF, Vasconcelos SMM, Viana GSB, and Fonteles MMF (2004) Pilocarpine-induced status epilepticus in rats: Lipid peroxidation level, nitrite formation, GABAergic and glutamatergic receptor alterations in the hippocampus, striatum and frontal cortex. *Pharmacol Biochem Behav* **78**:327–332.
- Gall C, Lauterborn J, Bundman M, Murray K, and Isackson P (1991) Seizures and the regulation of neurotrophic factor and neuropeptide gene expression in brain. *Epilepsy Res Suppl* **4**:225–45.
- Gallagher RT, Balogh MP, Davey P, Jackson MR, Sinclair I, and Southern LJ (2003) Combined electrospray ionization-atmospheric pressure chemical ionization source for use in high-throughput LC-MS applications. *Anal Chem* **75**:973–977.
- Gaoni Y, and Mechoulam R (1964) Isolation, Structure, and Partial Synthesis of an Active Constituent of Hashish. *J Am Chem Soc* **86**:1646–1647.
- Ghaste M, Mistrik R, and Shulaev V (2016) Applications of Fourier Transform Ion Cyclotron Resonance (FT-ICR) and Orbitrap Based High Resolution Mass Spectrometry in Metabolomics and Lipidomics. *Int J Mol Sci* **17**:816.
- Giusto NM, Roque ME, and Ilincheta de Boscherio MG (1992) Effects of aging on the content, composition and synthesis of sphingomyelin in the central nervous system. *Lipids* **27**:835–839.
- Gluchowski NL, Becuwe M, Walther TC, and Farese R V. (2017) Lipid droplets and liver disease: from basic biology to clinical implications. *Nat Rev Gastroenterol Hepatol* **3**–5.



- Gohlke RS (1959) Time-of-Flight Mass Spectrometry and Gas-Liquid Partition Chromatography. *Anal Chem* **31**:535–541.
- Goldstein E (1898) Ueber eine noch nicht untersuchte Strahlungsform an der Kathode inducirter Entladungen. *Ann Phys* **300**:38–48.
- Gonsiorek W, Lunn C, Fan X, Narula S, Lundell D, and Hipkin RW (2000) Endocannabinoid 2-arachidonyl glycerol is a full agonist through human type 2 cannabinoid receptor: antagonism by anandamide. *Mol Pharmacol* **57**:1045–1050.
- Grabmüller M, Madea B, and Courts C (2015) Comparative evaluation of different extraction and quantification methods for forensic RNA analysis. *Forensic Sci Int Genet* **16**:195–202, Elsevier Ireland Ltd.
- Gross ML (1992) Charge-remote fragmentations: method, mechanism and applications. *Int J Mass Spectrom Ion Process* **118–119**:137–165.
- Guan XL, He X, Ong W-Y, Yeo WK, Shui G, and Wenk MR (2006) Non-targeted profiling of lipids during kainate-induced neuronal injury. *FASEB J* **20**:1152–1161.
- Guggenhuber S, Monory K, Lutz B, and Klugmann M (2010) AAV vector-mediated overexpression of CB1 cannabinoid receptor in pyramidal neurons of the hippocampus protects against seizure-induced excitotoxicity. *PLoS One* **5**:1–8.
- Guggenhuber S, Romo-Parra H, Bindila L, Leschik J, Lomazzo E, Remmers F, Zimmermann T, Lerner R, Klugmann M, Pape H-C, and Lutz B (2016) Impaired 2-AG Signaling in Hippocampal Glutamatergic Neurons: Aggravation of Anxiety-Like Behavior and Unaltered Seizure Susceptibility. *Int J Neuropsychopharmacol* **19**:pyv091.
- Gusarova G a, Trejo HE, Dada L a, Briva A, Welch LC, Hamanaka RB, Mutlu GM, Chandel NS, Prakriya M, and Sznajder JI (2011) Hypoxia Leads to Na,K-ATPase Downregulation via Ca<sup>2+</sup> Release-Activated Ca<sup>2+</sup> Channels and AMPK Activation. *Mol Cell Biol* **31**:3546–3556.
- Hager JW, and Yves Le Blanc JC (2003) Product ion scanning using a Q-q-Q linear ion trap (Q TRAP) mass spectrometer. *Rapid Commun Mass Spectrom* **17**:1056–64.
- Hampson AJ, and Grimaldi M (2002) 12-hydroxyeicosatetraenoate (12-HETE) attenuates AMPA receptor-mediated neurotoxicity: evidence for a G-protein-coupled HETE receptor. *J Neurosci* **22**:257–264.
- Han X (2003) Global analyses of cellular lipidomes directly from crude extracts of biological samples by ESI mass spectrometry: a bridge to lipidomics. *J Lipid Res* **44**:1071–1079.
- Han X, and Gross RW (1994) Electrospray ionization mass spectroscopic analysis of human erythrocyte plasma membrane phospholipids. *Proc Natl Acad Sci* **91**:10635–10639.
- Han X, and Gross RW (2005) Shotgun lipidomics: Electrospray ionization mass spectrometric analysis and quantitation of cellular lipidomes directly from crude extracts of biological samples. *Mass Spectrom Rev* **24**:367–412.
- Han X, Yang K, Yang J, Fikes KN, Cheng H, and Gross RW (2006) Factors influencing the electrospray intrasource separation and selective ionization of glycerophospholipids. *J Am*

## REFERENCES

---

- Soc Mass Spectrom* **17**:264–274.
- Hansen HS, Moesgaard B, Petersen G, and Hansen HH (2002) Putative neuroprotective actions of N-acyl-ethanolamines. *Pharmacol Ther* **95**:119–126.
- Hanstein R, Lu A, Wurst W, Holsboer F, Deussing JM, Clement AB, and Behl C (2008) Transgenic overexpression of corticotropin releasing hormone provides partial protection against neurodegeneration in an in vivo model of acute excitotoxic stress. *Neuroscience* **156**:712–721.
- Haque E, McIntosh TJ, and Lentz BR (2001) Influence of lipid composition on physical properties and PEG-mediated fusion of curved and uncurved model membrane vesicles: “Nature’s own” fusogenic lipid bilayer. *Biochemistry* **40**:4340–4348.
- Harizi H, Corcuff JB, and Gualde N (2008) Arachidonic-acid-derived eicosanoids: roles in biology and immunopathology. *Trends Mol Med* **14**:461–469.
- Harkany T, Keimpema E, Barabás K, and Mulder J (2008) Endocannabinoid functions controlling neuronal specification during brain development. *Mol Cell Endocrinol* **286**:S84–S90.
- Harvey DJ (1995) Matrix-assisted laser desorption/ionization mass spectrometry of phospholipids. *J Mass Spectrom* **30**:1333–1346.
- Hazel JR, and Eugene Williams E (1990) The role of alterations in membrane lipid composition in enabling physiological adaptation of organisms to their physical environment. *Prog Lipid Res* **29**:167–227.
- Heine M, Groc L, Frischknecht R, Béïque J-C, Lounis B, Rumbaugh G, Huganir RL, Cognet L, and Choquet D (2008) Surface mobility of postsynaptic AMPARs tunes synaptic transmission. *Science* **320**:201–205.
- Hering H, Lin C, and Sheng M (2003) Lipid rafts in the maintenance of synapses, dendritic spines, and surface AMPA receptor stability. *J Neurosci* **23**:3262–3271.
- Herrin GL, McCurdy HH, and Wall WH (2005) Investigation of an LC-MS-MS (QTrap) method for the rapid screening and identification of drugs in postmortem toxicology whole blood samples. *J Anal Toxicol* **29**:599–606.
- Hoffmann E de (1996) Tandem mass spectrometry: a primer. *J mass Spectrom* **31**:129–137.
- Holčápek M, Jirásko R, and Lída M (2012) Recent developments in liquid chromatography–mass spectrometry and related techniques. *J Chromatogr A* **1259**:3–15.
- Holemans T, Sørensen DM, van Veen S, Martin S, Hermans D, Kemmer GC, Van den Haute C, Baekelandt V, Günther Pomorski T, Agostinis P, Wuytack F, Palmgren M, Eggermont J, and Vangheluwe P (2015) A lipid switch unlocks Parkinson’s disease-associated ATP13A2. *Proc Natl Acad Sci* **112**:9040–9045.
- Holter JL, Humphries A, Crunelli V, and Carter DA (2001) Optimisation of methods for selecting candidate genes from cDNA array screens: Application to rat brain punches and pineal. *J Neurosci Methods* **112**:173–184.
- Horning EC, Horning MG, Carroll DI, Dzidic I, and Stillwell RN (1973) New picogram detection

- system based on a mass spectrometer with an external ionization source at atmospheric pressure. *Anal Chem* **45**:936–943.
- Houstis N, Rosen ED, and Lander ES (2006) Reactive oxygen species have a causal role in multiple forms of insulin resistance. *Nature* **440**:944–948.
- HU X, FU X, JIANG A, YANG X, FANG X, GONG G, and WEI C (2015) Multiomic analysis of mice epilepsy models suggest that miR-21a expression modulates mRNA and protein levels related to seizure deterioration. *Genet Res (Camb)* **97**:e22.
- Huang YH, Schäfer-Elinder L, Wu R, Claesson HE, and Frostegård J (1999) Lysophosphatidylcholine (LPC) induces proinflammatory cytokines by a platelet-activating factor (PAF) receptor-dependent mechanism. *Clin Exp Immunol* **116**:326–331.
- Iannotti FA, Di Marzo V, and Petrosino S (2016) Endocannabinoids and Endocannabinoid-Related Mediators: Targets, Metabolism and Role In Neurological Disorders. *Prog Lipid Res* **62**:107–128, Elsevier Ltd.
- Jackman N, Ishii A, and Bansal R (2009) Oligodendrocyte development and myelin biogenesis: parsing out the roles of glycosphingolipids. *Physiology (Bethesda)* **24**:290–7.
- Júnior HVN, de França Fonteles MM, and Mendes de Freitas R (2009) Acute seizure activity promotes lipid peroxidation, increased nitrite levels and adaptive pathways against oxidative stress in the frontal cortex and striatum. *Oxid Med Cell Longev* **2**:130–7.
- Kano M, Ohno-Shosaku T, Hashimoto-dani Y, Uchigashima M, and Watanabe M (2009) Endocannabinoid-mediated control of synaptic transmission. *Physiol Rev* **89**:309–380.
- Karas M, Karas M, Hillenkamp F, Hillenkamp F, Bachmann D, and Bachmann D (1985) Influence of the Wavelength in High-Irradiance Ultraviolet Laser Desorption Mass Spectrometry of Organic Molecules. *AnalChem* **57**:2935–2939.
- Karkheiran S, Shahidi GA, and Walker RH (2015) PLA2G6-associated Dystonia-Parkinsonism : Case Report and Literature Review. *Tremor Other Hyperkinetic Movements* **5**:317.
- Karl T, Cheng D, Garner B, and Arnold JC (2012) The therapeutic potential of the endocannabinoid system for Alzheimer’s disease. *Expert Opin Ther Targets* **16**:407–420.
- Katona I, and Freund TF (2012) Multiple functions of endocannabinoid signaling in the brain. *Annu Rev Neurosci* **35**:529–558.
- Kegel-Gleason KB (2013) Huntingtin interactions with membrane phospholipids: strategic targets for therapeutic intervention? *J Huntingtons Dis* **2**:239–50.
- Kennedy JD, and Seyal M (2015) Respiratory pathophysiology with seizures and implications for sudden unexpected death in epilepsy. *J Clin Neurophysiol* **32**:10–13.
- Keppel Hesselink JM, Kopsky DJ, and Witkamp RF (2014) Palmitoylethanolamide (PEA)—“Promiscuous” anti-inflammatory and analgesic molecule at the interface between nutrition and pharma. *PharmaNutrition* **2**:19–25.
- Kim GH, Kim JE, Rhie SJ, and Yoon S (2015) The Role of Oxidative Stress in Neurodegenerative Diseases. *Exp Neurobiol* **24**:325–40.

## REFERENCES

---

- Koestler M, Kirsch D, Hester A, Leisner A, Guenther S, and Spengler B (2008) A high-resolution scanning microprobe matrix-assisted laser desorption/ionization ion source for imaging analysis on an ion trap/Fourier transform ion cyclotron resonance mass spectrometer. *Rapid Commun Mass Spectrom* **22**:3275–3285.
- Köfeler HC, Fauland A, Rechberger GN, and Trötz Müller M (2012) Mass Spectrometry Based Lipidomics: An Overview of Technological Platforms. *Metabolites* **2**:19–38.
- Kosicek M, and Hecimovic S (2013) Phospholipids and Alzheimer's disease: Alterations, mechanisms and potential biomarkers. *Int J Mol Sci* **14**:1310–1322.
- Kosicek M, Kirsch S, Bene R, Trkanjec Z, Titlic M, Bindila L, Peter-Katalinic J, and Hecimovic S (2010) Nano-HPLC-MS analysis of phospholipids in cerebrospinal fluid of Alzheimer's disease patients—a pilot study. *Anal Bioanal Chem* **398**:2929–2937.
- Kreitzer a C, and Malenka RC (2007) Endocannabinoid-mediated rescue of striatal LTD and motor deficits in Parkinson's disease models. *Nature* **445**:643–647.
- Kwon KJ, Jung Y-S, Lee SH, Moon C-H, and Baik EJ (2005) Arachidonic acid induces neuronal death through lipoxygenase and cytochrome P450 rather than cyclooxygenase. *J Neurosci Res* **81**:73–84.
- Lamari F, Mochel F, Sedel F, and Saudubray JM (2013) Disorders of phospholipids, sphingolipids and fatty acids biosynthesis: Toward a new category of inherited metabolic diseases. *J Inherit Metab Dis* **36**:411–425.
- Lambert DM, and Di Marzo V (1999) The palmitoylethanolamide and oleamide enigmas: are these two fatty acid amides cannabimimetic? *Curr Med Chem* **6**:757–773.
- Lanekoff I, Phan NT, Van Bell CT, Winograd N, Sjövall P, and Ewing AG (2013) Mass spectrometry imaging of freeze-dried membrane phospholipids of dividing *Tetrahymena pyriformis*. *Surf Interface Anal* **45**:211–214.
- Lauwers E, Goodchild R, and Verstreken P (2016) Membrane Lipids in Presynaptic Function and Disease. *Neuron* **90**:11–25.
- Leary O, Labeling S, Fadok VA, Bratton DL, Rose DM, Pearson A, Ezekewitz RAB, and Henson PM (2000) A receptor for phosphatidylserine- specific clearance of apoptotic cells. *Nature* **260**:85–90.
- Ledesma MD, Martin MG, and Dotti CG (2012) Lipid changes in the aged brain: Effect on synaptic function and neuronal survival. *Prog Lipid Res* **51**:23–35.
- Lee JY, Sohn KH, Rhee SH, and Hwang D (2001) Saturated fatty acids, but not unsaturated fatty acids, induce the expression of cyclooxygenase-2 mediated through Toll-like receptor 4. *J Biol Chem* **276**:16683–16689.
- Lerner R, Lutz B, and Bindila L (2013) Tricks and Tracks in the Identification and Quantification of Endocannabinoids, in *eLS p*, John Wiley & Sons, Ltd, Chichester, UK.
- Lerner R, Post J, Loch S, Lutz B, and Bindila L (2016) Targeting brain and peripheral plasticity of the lipidome in acute kainic acid-induced epileptic seizures in mice via quantitative mass

- spectrometry. *Biochim Biophys Acta - Mol Cell Biol Lipids* **1862**:255–267, Elsevier B.V.
- Leung D, Saghatelian A, Simon GM, and Cravatt BF (2006) Inactivation of N-Acyl phosphatidylethanolamine phospholipase D reveals multiple mechanisms for the biosynthesis of endocannabinoids. *Biochemistry* **45**:4720–4726.
- Lev S (2010) Non-vesicular lipid transport by lipid-transfer proteins and beyond. *Nat Rev Mol Cell Biol* **11**:739–750.
- Levinson R (2001) 5. Chromatography. *Mod Chem Tech* 116–159.
- Leyen K van (2013) Lipoxygenase: An Emerging Target for Stroke Therapy. *CNS Neurol Disord Drug Targets* **12**:191–199.
- Li G, Kim J, Huang Z, St. Clair JR, Brown DA, and London E (2016) Efficient replacement of plasma membrane outer leaflet phospholipids and sphingolipids in cells with exogenous lipids. *Proc Natl Acad Sci* **113**:14025–14030.
- Li Q, Bozek K, Xu C, Guo Y, Sun J, Paabo S, Sherwood CC, Hot PR, Ely JJ, Li Y, Willmitzer L, Giavalisco P, and Khaitovich P (2017) Changes in lipidome composition during brain development in humans, chimpanzees, and macaque monkeys. *Discoveries* **34**:1155–1166.
- Liebisch G, Vizcaíno JA, Köfeler H, Trötz Müller M, Griffiths WJ, Schmitz G, Spener F, and Wakelam MJO (2013) Shorthand notation for lipid structures derived from mass spectrometry. *J Lipid Res* **54**:1523–30.
- Liebl H (1967) Ion microprobe mass analyzer. *J Appl Phys* **38**:5277–5283.
- Liu X, Zheng P, Zhao X, Zhang Y, Hu C, Li J, Zhao J, Zhou J, Xie P, and Xu G (2015) Discovery and validation of plasma biomarkers for major depressive disorder classification based on liquid chromatography-mass spectrometry. *J Proteome Res* **14**:2322–2330.
- Lo Verme J, Fu J, Astarita G, La Rana G, Russo R, Calignano A, and Piomelli D (2005) The nuclear receptor peroxisome proliferator-activated receptor- $\alpha$  mediates the anti-inflammatory actions of palmitoylethanolamide. *Mol Pharmacol* **67**:15–9.
- Lomazzo E, Bindila L, Remmers F, Lerner R, Schwitter C, Hoheisel U, and Lutz B (2014) Therapeutic Potential of Inhibitors of Endocannabinoid Degradation for the Treatment of Stress-Related Hyperalgesia in an Animal Model of Chronic Pain. *Neuropsychopharmacology* **40**:1–46.
- Londry FA, and Hager JW (2003) Mass selective axial ion ejection from a linear quadrupole ion trap. *J Am Soc Mass Spectrom* **14**:1130–1147.
- Lu XR, Ong WY, Halliwell B, Horrocks LA, and Farooqui AA (2001) Differential effects of calcium-dependent and calcium-independent phospholipase A2 inhibitors on kainate-induced neuronal injury in rat hippocampal slices. *Free Radic Biol Med* **30**:1263–1273.
- Lutz B (2009) Endocannabinoid signals in the control of emotion. *Curr Opin Pharmacol* **9**:46–52.
- Lutz B (2004) On-demand activation of the endocannabinoid system in the control of neuronal excitability and epileptiform seizures. *Biochem Pharmacol* **68**:1691–1698.
- Lutz B, Marsicano G, Maldonado R, and Hillard CJ (2015) The endocannabinoid system in

## REFERENCES

---

- guarding against fear, anxiety and stress. *Nat Rev Neurosci* **16**:705–718.
- Makarov A (2000) Electrostatic axially harmonic orbital trapping: A high-performance technique of mass analysis. *Anal Chem* **72**:1156–1162.
- Malfitano AM, Basu S, Maresz K, Bifulco M, and Dittel BN (2014) What we know and do not know about the cannabinoid receptor 2 (CB2). *Semin Immunol* **26**:369–379.
- Mamyrin BA (1994) Laser assisted reflectron time-of-flight mass spectrometry. *Int J Mass Spectrom Ion Process* **131**:1–19.
- Mamyrin BA (2001) Time-of-flight mass spectrometry (concepts, achievements, and prospects). *Int J Mass Spectrom* **206**:251–266.
- March RE (1997) An Introduction to Quadrupole Ion Trap Mass Spectrometry. *J MASS Spectrom J Mass Spectrom* **32**:351–369.
- Marsicano G, Goodenough S, Monory K, Hermann H, Eder M, Cannich A, Azad SC, Cascio MG, Gutiérrez SO, van der Stelt M, López-Rodríguez ML, Casanova E, Schütz G, Zieglgänsberger W, Di Marzo V, Behl C, and Lutz B (2003) CB1 cannabinoid receptors and on-demand defense against excitotoxicity. *Science* **302**:84–88.
- Marsicano G, and Lafenêtre P (2009) Roles of the Endocannabinoid System in Learning and Memory, in *Current Topics in Behavioral Neurosciences* pp 201–230.
- Marsicano G, and Lutz B (1999) Expression of the cannabinoid receptor CB1 in distinct neuronal subpopulations in the adult mouse forebrain. *Eur J Neurosci* **11**:4213–4225.
- Marsicano G, Stelt M Van Der, and Lo ML (2003) CB1 Cannabinoid Receptors and On-Demand Defense. *Science (80- )* **84**:84–88.
- Massa F, Mancini G, Schmidt H, Steindel F, Mackie K, Angioni C, Oliet SHR, Geisslinger G, and Lutz B (2010) Alterations in the hippocampal endocannabinoid system in diet-induced obese mice. *J Neurosci* **30**:6273–81.
- Matsuda L a, Lolait SJ, Brownstein MJ, Young a C, and Bonner TI (1990) Structure of a cannabinoid receptor and functional expression of the cloned cDNA. *Nature* **346**:561–564.
- Mattace Raso G, Russo R, Calignano A, and Meli R (2014) Palmitoylethanolamide in CNS health and disease. *Pharmacol Res* **86**:32–41, Elsevier Ltd.
- Matyash V, Liebisch G, Kurzchalia T V, Shevchenko A, and Schwudke D (2008) Lipid extraction by methyl-tert-butyl ether for high-throughput lipidomics. *J Lipid Res* **49**:1137–46.
- McDonnell LA, and Heeren RMA (2007) Imaging mass spectrometry. *Mass Spectrom Rev* **26**:606–643.
- McEvoy J, Baillie RA, Zhu H, Buckley P, Keshavan MS, Nasrallah HA, Dougherty GG, Yao JK, and Kaddurah-Daouk R (2013) Lipidomics Reveals Early Metabolic Changes in Subjects with Schizophrenia: Effects of Atypical Antipsychotics. *PLoS One* **8**:1–12.
- McGahon B, Murray CA, Clements MP, and Lynch MA (1998) Analysis of the effect of membrane arachidonic acid concentration on modulation of glutamate release by interleukin-1: An age-related study. *Exp Gerontol* **33**:343–354.

- McGahon BM, Martin DS, Horrobin DF, and Lynch MA (1999) Age-related changes in synaptic function: analysis of the effect of dietary supplementation with omega-3 fatty acids. *Neuroscience* **94**:305–314.
- McIntyre TM, Pontsler A V, Silva AR, St Hilaire A, Xu Y, Hinshaw JC, Zimmerman GA, Hama K, Aoki J, Arai H, and Prestwich GD (2003) Identification of an intracellular receptor for lysophosphatidic acid (LPA): LPA is a transcellular PPARgamma agonist. *Proc Natl Acad Sci U S A* **100**:131–6.
- McNamara JR, Warnick GR, and Cooper GR (2006) A brief history of lipid and lipoprotein measurements and their contribution to clinical chemistry. *Clin Chim Acta* **369**:158–167.
- Mechoulam R, Ben-Shabat S, Hanus L, Ligumsky M, Kaminski NE, Schatz AR, Gopher A, Almog S, Martin BR, Compton DR, Pertwee RG, Griffin G, Bayewitch M, Barg J, and Vogel Z (1995) Identification of an endogenous 2-monoglyceride, present in canine gut, that binds to cannabinoid receptors. *Biochem Pharmacol* **50**:83–90.
- Mechoulam R, and Lichtman a H (2003) Neuroscience. Stout guards of the central nervous system. *Science* **302**:65–7.
- Mehrotra A, Sood A, and Sandhir R (2015) Mitochondrial modulators improve lipid composition and attenuate memory deficits in experimental model of Huntington's disease. *Mol Cell Biochem* **410**:281–292, Springer US.
- Méndez-Armenta M, Nava-Ruiz C, Juárez-Rebollar D, Rodríguez-Martínez E, and Yescas Gómez P (2014) Oxidative Stress Associated with Neuronal Apoptosis in Experimental Models of Epilepsy. *Oxid Med Cell Longev* **2014**:1–12.
- Miller PE, and Denton MB (1986) The quadrupole mass filter: Basic operating concepts. *J Chem Educ* **63**:617.
- Mirendil H, Thomas E, De Loera C, Okada K, Inomata Y, and Chun J (2015) LPA signaling initiates schizophrenia-like brain and behavioral changes in a mouse model of prenatal brain hemorrhage. *Transl Psychiatry* **5**:e541-10, Nature Publishing Group.
- Monory K, Massa F, Egertová M, Eder M, Blaudzun H, Westenbroek R, Kelsch W, Jacob W, Marsch R, Ekker M, Long J, Rubenstein JL, Goebbels S, Nave KA, During M, Klugmann M, Wölfel B, Dodt HU, Zieglgänsberger W, Wotjak CT, Mackie K, Elphick MR, Marsicano G, and Lutz B (2006) The Endocannabinoid System Controls Key Epileptogenic Circuits in the Hippocampus. *Neuron* **51**:455–466.
- Moreira FA, and Crippa JAS (2009) The psychiatric side-effects of rimonabant. *Rev Bras Psiquiatr* **31**:145–153.
- Morrison JD (1991) Personal reminiscences of forty years of mass spectrometry in Australia. *Org Mass Spectrom* **26**:183–194.
- Munson MSB, and Field FH (1966) Chemical Ionization Mass Spectrometry. I. General Introduction. *J Am Chem Soc* **88**:2621–2630.
- Murphy RC, Hankin J a, and Barkley RM (2009) Imaging of lipid species by MALDI mass

## REFERENCES

---

- spectrometry. *J Lipid Res* **50**:S317–S322.
- Narain C (2014) Complex expressions. *Nat OUTLOOK* **511**:S8 S9.
- Naydenov A V., Horne EA, Cheah CS, Swinney K, Hsu KL, Cao JK, Marrs WR, Blankman JL, Tu S, Cherry AE, Fung S, Wen A, Li W, Saporito MS, Selley DE, Cravatt BF, Oakley JC, and Stella N (2014) ABHD6 blockade exerts antiepileptic activity in PTZ-induced seizures and in spontaneous seizures in R6/2 Mice. *Neuron* **83**:361–371, Elsevier Inc.
- Neef AB, and Schultz C (2009) Selective fluorescence labeling of lipids in living cells. *Angew Chemie - Int Ed* **48**:1498–1500.
- Nomura DK, Hudak CSS, Ward AM, Burston JJ, Issa RS, Fisher KJ, Abood ME, Wiley JL, Lichtman AH, and Casida JE (2008) Monoacylglycerol lipase regulates 2-arachidonoylglycerol action and arachidonic acid levels. *Bioorganic Med Chem Lett* **18**:5875–5878.
- Nomura DK, Morrison BE, Blankman JL, Long JZ, Kinsey SG, Marcondes MCG, Ward AM, Hahn YK, Lichtman AH, Conti B, and Cravatt BF (2011) Endocannabinoid Hydrolysis Generates Brain Prostaglandins That Promote Neuroinflammation. *Science (80- )* **334**:809–813.
- Norn S, Permin H, Kruse PR, and Kruse E (2009) From Willow Bark to Acetylsalicylic Acid. *Dan Medicinhist Arbog* **37**:79–98.
- Ogrinc Potočnik N, Porta T, Becker M, Heeren RMA, and Ellis SR (2015) Use of advantageous, volatile matrices enabled by next-generation high-speed matrix-assisted laser desorption/ionization time-of-flight imaging employing a scanning laser beam. *Rapid Commun Mass Spectrom* **29**:2195–2203.
- Ogura Y, Parsons WH, Kamat SS, and Cravatt BF (2016) A calcium-dependent acyltransferase that produces N-acyl phosphatidylethanolamines. *Nat Chem Biol* **12**:669–671.
- Ong W-Y, Farooqui T, Kokotos G, and Farooqui AA (2015) Synthetic and natural inhibitors of phospholipases A2: their importance for understanding and treatment of neurological disorders. *ACS Chem Neurosci* **6**:814–831.
- Ong W, Farooqui T, and Farooqui AA (2010) Involvement of Cytosolic Phospholipase A 2 , Calcium Independent Phos- pholipase A 2 and Plasmalogen Selective Phospholipase A 2 in Neurodegen- erative and Neuropsychiatric Conditions. **2**:2746–2763.
- Ong WY, Lu XR, Horrocks LA, Farooqui AA, and Garey LJ (2003) Induction of astrocytic cytoplasmic phospholipase A2 and neuronal death after intracerebroventricular carrageenan injection, and neuroprotective effects of quinacrine. *Exp Neurol* **183**:449–457.
- Pacher P, Batkai S, and Kunos G (2006) The endocannabinoid system as an emerging target of pharmacotherapy. *Pharmacol Rev* **58**:389–462.
- Palczewski K, Kumasaka T, Hori T, Behnke CA, Motoshima H, Fox BA, Le Trong I, Teller DC, Okada T, Stenkamp RE, Yamamoto M, and Miyano M (2000) Crystal Structure of Rhodopsin: A G Protein-Coupled Receptor. *Sci (New York, NY)* **289**:739–745.
- Paratcha G, and Ibáñez CF (2002) Lipid rafts and the control of neurotrophic factor signaling in



- the nervous system: variations on a theme. *Curr Opin Neurobiol* **12**:542–549.
- Park E-S, Lee JH, Hong JH, Park YK, Lee JW, Lee W-J, Lee JW, Kim KP, and Kim K-H (2014) Phosphatidylcholine Alteration Identified Using MALDI Imaging MS in HBV-Infected Mouse Livers and Virus-Mediated Regeneration Defects. *PLoS One* **9**:e103955.
- Passarelli MK, and Ewing AG (2013) Single-cell imaging mass spectrometry. *Curr Opin Chem Biol* **17**:854–859.
- Passarelli MK, and Winograd N (2011) Lipid imaging with time-of-flight secondary ion mass spectrometry (ToF-SIMS). *Biochim Biophys Acta* **1811**:976-990
- Pati S, Nie B, Arnold RD, and Cummings BS (2016a) Extraction, chromatographic and mass spectrometric methods for lipid analysis. *Biomed Chromatogr* **30**:695–709.
- Pati S, Nie B, Arnold RD, and Cummings BS (2016b) Extraction, chromatographic and mass spectrometric methods for lipid analysis. *Biomed Chromatogr* **30**:695–709.
- Patterson RE, Ducrocq AJ, McDougall DJ, Garrett TJ, and Yost RA (2015) Comparison of blood plasma sample preparation methods for combined LC-MS lipidomics and metabolomics. *J Chromatogr B Anal Technol Biomed Life Sci* **1002**:260–266, Elsevier B.V.
- Paul W, and Steinwedel H (1953) Notizen: Ein neues Massenspektrometer ohne Magnetfeld. *Zeitschrift für Naturforsch A* **8**:448–450.
- Pernet F, Pelletier CJ, and Milley J (2006) Comparison of three solid-phase extraction methods for fatty acid analysis of lipid fractions in tissues of marine bivalves. *J Chromatogr A* **1137**:127–137.
- Pettegrew JW, Klunk WE, Kanal E, Panchalingam K, and McClure RJ (1995) Changes in brain membrane phospholipid and high-energy phosphate metabolism precede dementia. *Neurobiol Aging* **16**:973–975.
- Piomelli D (2003) The molecular logic of endocannabinoid signalling. *Nat Rev Neurosci* **4**:873–884.
- Pitt JJ (2009) Principles and applications of liquid chromatography-mass spectrometry in clinical biochemistry. *Clin Biochem Rev* **30**:19–34.
- Pomorski T, and Menon AK (2006) Lipid flippases and their biological functions. *Cell Mol Life Sci* **63**:2908–2921.
- Popoli M, Yan Z, McEwen BS, and Sanacora G (2012) The stressed synapse: the impact of stress and glucocorticoids on glutamate transmission. *Nat Rev Neurosci* **13**:22–37.
- Popovici T, Represa A, Crepel V, Barbin G, Beaudoin M, and Ben-ari Y (1990) Effects of kainic acid-induced seizures and ischemia on proteins in rat brain c-fos-like. *Brain Res* **536**:183–194.
- Porter AC, Sauer J-M, Knierman MD, Becker GW, Berna MJ, Bao J, Nomikos GG, Carter P, Bymaster FP, Leese AB, and Felder CC (2002) Characterization of a novel endocannabinoid, virodhamine, with antagonist activity at the CB1 receptor. *J Pharmacol Exp Ther* **301**:1020–1024.

## REFERENCES

---

- Prasad MR, Lovell MA, Yatin M, Dhillon H, and Markesbery WR (1998) Regional membrane phospholipid alterations in Alzheimer's disease. *Neurochem Res* **23**:81–88.
- Pulfer M, and Murphy RC (2003) Electrospray mass spectrometry of phospholipids. *Mass Spectrom Rev* **22**:332–364.
- Puppolo M, Varma D, and Jansen SA (2014) A review of analytical methods for eicosanoids in brain tissue. *J Chromatogr B Anal Technol Biomed Life Sci* **964**:50–64, Elsevier B.V.
- Rapoport SI (2008) Arachidonic acid and the brain. *J Nutr* **138**:2515–20.
- Rapoport SI, Basselin M, Kim H-W, and Rao JS (2009) Bipolar disorder and mechanisms of action of mood stabilizers. *Brain Res Rev* **61**:185–209.
- Redmond WJ, Cawston EE, Grimsey NL, Stuart J, Edington AR, Glass M, and Connor M (2016) Identification of N-arachidonoyl dopamine as a highly biased ligand at cannabinoid CB1 receptors. *Br J Pharmacol* **173**:115–127.
- Reiser V, Smith RC, Xue J, Kurtz MM, Liu R, LeGrand C, He X, Yu X, Wong P, Hinchcliffe JS, Tanen MR, Lazar G, Zieba R, Ichetovkin M, Chen Z, O'Neill EA, Tanaka WK, Marton MJ, Liao J, Morris M, Hailman E, Tokiwa GY, and Plump AS (2011) High-throughput simultaneous analysis of RNA, protein, and lipid biomarkers in heterogeneous tissue samples. *Clin Chem* **57**:1545–1555.
- Ricciotti E, and Fitzgerald GA (2011) Prostaglandins and inflammation. *Arterioscler Thromb Vasc Biol* **31**:986–1000.
- Rosenthal SL, and Kamboh MI (2014) Late-Onset Alzheimer's Disease Genes and the Potentially Implicated Pathways. *Curr Genet Med Rep* **2**:85–101.
- Roux A, Muller L, Jackson SN, Post J, Baldwin K, Hoffer B, Balaban CD, Barbacci D, Schultz JA, Gouty S, Cox BM, and Woods AS (2016) Mass spectrometry imaging of rat brain lipid profile changes over time following traumatic brain injury. *J Neurosci Methods* **272**:19–32, Elsevier B.V.
- Rouzer CA, and Marnett LJ (2011) Endocannabinoid Oxygenation by Cyclooxygenases, Lipoxygenases, and Cytochromes P450: Cross-Talk between the Eicosanoid and Endocannabinoid Signaling Pathways. *Chem Rev* **111**:5899–5921.
- Rustan AC, and Drevon CA (2005) Fatty Acids: Structures and Properties, in *Encyclopedia of Life Sciences* pp 1–7, John Wiley & Sons, Ltd, Chichester.
- Sackett SJ, Chung H-Y, Okajima F, and Im D-S (2009) Increase in sphingolipid catabolic enzyme activity during aging. *Acta Pharmacol Sin* **30**:1454–61.
- Saito A, Ballinger MDL, Pletnikov M V., Wong DF, and Kamiya A (2013) Endocannabinoid system: Potential novel targets for treatment of schizophrenia. *Neurobiol Dis* **53**:10–17.
- Sandhya TL, Ong WY, Horrocks LA, and Farooqui AA (1998) A light and electron microscopic study of cytoplasmic phospholipase A2 and cyclooxygenase-2 in the hippocampus after kainate lesions. *Brain Res* **788**:223–231.
- Savage N (2014) The Complexities of Epilepsy. *Nat OUTLOOK* **511**:S2.

- Savinainen JR, Saario SM, and Laitinen JT (2012) The serine hydrolases MAGL, ABHD6 and ABHD12 as guardians of 2-arachidonoylglycerol signalling through cannabinoid receptors. *Acta Physiol* **204**:267–276.
- Schmitt A, Wilczek K, Blennow K, Maras A, Jatzko A, Petroianu G, Braus DF, and Gattaz WF (2004) Altered thalamic membrane phospholipids in schizophrenia: A postmortem study. *Biol Psychiatry* **56**:41–45.
- Schouten M, Bielefeld P, Fratantoni SA, Hubens CJ, Piersma SR, Pham T V, Voskuyl RA, Lucassen PJ, Jimenez CR, and Fitzsimons CP (2016) Multi-omics profile of the mouse dentate gyrus after kainic acid-induced status epilepticus. *Sci data* **3**:160068.
- Schuhmann K, Almeida R, Baumert M, Herzog R, Bornstein SR, and Shevchenko A (2012) Shotgun lipidomics on a LTQ Orbitrap mass spectrometer by successive switching between acquisition polarity modes. *J Mass Spectrom* **47**:96–104.
- Schuhmann K, Herzog R, Schwudke D, Metelmann-Strupat W, Bornstein SR, and Shevchenko A (2011) Bottom-up shotgun lipidomics by higher energy collisional dissociation on LTQ orbitrap mass spectrometers. *Anal Chem* **83**:5480–5487.
- Schwamborn K, and Caprioli RM (2010) Molecular imaging by mass spectrometry — looking beyond classical histology. *Nat Rev Cancer* **10**:639–646, Nature Publishing Group.
- Schwarz E, Prabakaran S, Whitfield P, Major H, Leweke FM, Koethe D, McKenna P, and Bahn S (2008) High throughput lipidomic profiling of schizophrenia and bipolar disorder brain tissue reveals alterations of free fatty acids, phosphatidylcholines, and ceramides. *J Proteome Res* **7**:4266–4277.
- Scott A, Post JM, Lerner R, Ellis S, Lieberman J, Shirey KA, Heeren R, Bindila L and Ernst R (2017) 3D Host-Pathogen Interface Mapping Defines a Lethal Role for Inflammatory Lipids. *Proc. Natl. Acad. Sci.* [Epub ahead of print]
- Sengupta P, Baird B, and Holowka D (2007) Lipid rafts, fluid/fluid phase separation, and their relevance to plasma membrane structure and function. *Semin Cell Dev Biol* **18**:583–90.
- Serrano GE, Lelutiu N, Rojas a., Cochi S, Shaw R, Makinson CD, Wang D, FitzGerald G a., and Dingledine R (2011) Ablation of Cyclooxygenase-2 in Forebrain Neurons is Neuroprotective and Dampens Brain Inflammation after Status Epilepticus. *J Neurosci* **31**:14850–14860.
- Sethi S, and Brietzke E (2017a) Recent advances in lipidomics: Analytical and clinical perspectives. *Prostaglandins Other Lipid Mediat* **128–129**:8–16.
- Sethi S, and Brietzke E (2017b) Recent advances in lipidomics: Analytical and clinical perspectives. *Prostaglandins Other Lipid Mediat* **128–129**:8–16, Elsevier Inc.
- Sethi S, Hayashi M, Sussulini A, Tasic L, and Brietzke E (2015) Analytical Approaches for Lipidomics and Its Potential Applications in Neuropsychiatric Disorders. *World J Biol Psychiatry* **2975**:1–49.
- Sevastou I, Kaffe E, Mouratis MA, and Aidinis V (2013) Lysoglycerophospholipids in chronic inflammatory disorders: The PLA 2/LPC and ATX/LPA axes. *Biochim Biophys Acta - Mol*

## REFERENCES

---

- Cell Biol Lipids* **1831**:42–60.
- Sezgin E, Levental I, Mayor S, and Eggeling C (2017) The mystery of membrane organization: composition, regulation and roles of lipid rafts. *Nat Rev Mol Cell Biol* **18**:361–374, Nature Publishing Group.
- Shimada T, Takemiya T, Sugiura H, and Yamagata K (2014) Role of Inflammatory Mediators in the Pathogenesis of Epilepsy. *Mediators Inflamm* **2014**:1–8, Hindawi Publishing Corporation.
- Shin E-J, Jeong JH, Chung YH, Kim W-K, Ko K-H, Bach J-H, Hong J-S, Yoneda Y, and Kim H-C (2011) Role of oxidative stress in epileptic seizures. *Neurochem Int* **59**:122–37, Elsevier B.V.
- Simerly RB (2015) Organization of the Hypothalamus, in *The Rat Nervous System* pp 267–294, Elsevier.
- Simmet T, Seregi A, and Hertting G (1988) Characterization of Seizure-Induced Cysteinyl-Leukotriene Formation in Brain Tissue of Convulsion-Prone Gerbils. *J Neurochem* **50**:1738–1742.
- Simons K, and Ikonen E (1997) Functional rafts in cell membranes. *Nature* **387**:569–72.
- Simons K, and Toomre D (2000) Lipid rafts and signal transduction. *Nat Rev Mol Cell Biol* **1**:31–39.
- Singer SJ, and Nicolson GL (1972) The Fluid Mosaic Model of the structure of cell membranes. *Science (80- )* **175**:720–731.
- Skerry TM, and Genever PG (2001) Glutamate signalling in non-neuronal tissues. *Trends Pharmacol Sci* **22**:174–181.
- Skosnik PD, and Yao JK (2003) From membrane phospholipid defects to altered neurotransmission: is arachidonic acid a nexus in the pathophysiology of schizophrenia? *Prostaglandins, Leukot Essent Fat Acids* **69**:367–384.
- Slotte JP, and Ramstedt B (2007) The functional role of sphingomyelin in cell membranes. *Eur J Lipid Sci Technol* **109**:977–981.
- Small SA, Schobel SA, Buxton RB, Witter MP, and Barnes CA (2011) A pathophysiological framework of hippocampal dysfunction in ageing and disease. *Nat Rev Neurosci* **12**:585–601, Nature Publishing Group.
- Smith WL (1989) The eicosanoids and their biochemical mechanisms of action. *Biochem J* **259**:315–24.
- Söderberg M, Edlund C, Kristensson K, and Dallner G (1990) Lipid compositions of different regions of the human brain during aging. *J Neurochem* **54**:415–23.
- Soltész I, Alger BE, Kano M, Lee S-H, Lovinger DM, Ohno-Shosaku T, and Watanabe M (2015) Weeding out bad waves: towards selective cannabinoid circuit control in epilepsy. *Nat Rev Neurosci* **16**:264–277.
- Solymosi K, and Kofalvi A (2017) Cannabis: A Treasure Trove or Pandora's Box? *Mini-Reviews Med Chem* **17**:000–000.
- Sommer U, Herscovitz H, Welty FK, and Costello CE (2006) LC-MS-based method for the

- qualitative and quantitative analysis of complex lipid mixtures. *J Lipid Res* **47**:804–814.
- Sperk G (1994) Kainic acid seizures in the rat. *Prog Neurobiol* **42**:1–32.
- Stephenson DT, Lemere C a, Selkoe DJ, and Clemens J a (1996) Cytosolic phospholipase A2 (cPLA2) immunoreactivity is elevated in Alzheimer's disease brain. *Neurobiol Dis* **3**:51–63.
- Stotz-Potter EH, Willis LR, and DiMicco J a (1996) Muscimol acts in dorsomedial but not paraventricular hypothalamic nucleus to suppress cardiovascular effects of stress. *J Neurosci* **16**:1173–9.
- Strange BA, Witter MP, Lein ES, and Moser EI (2014) Functional organization of the hippocampal longitudinal axis. *Nat Publ Gr* **15**:655–669, Nature Publishing Group.
- Südhof TC (2012) The Presynaptic Active Zone. *Neuron* **75**:11–25.
- Südhof TC, and Malenka RC (2008) Understanding Synapses: Past, Present, and Future. *Neuron* **60**:469–476.
- Taguchi R, and Ishikawa M (2010) Precise and global identification of phospholipid molecular species by an Orbitrap mass spectrometer and automated search engine Lipid Search. *J Chromatogr A* **1217**:4229–4239.
- Takemiya T, Maehara M, Matsumura K, Yasuda S, Sugiura H, and Yamagata K (2006) Prostaglandin E2 produced by late induced COX-2 stimulates hippocampal neuron loss after seizure in the CA3 region. *Neurosci Res* **56**:103–110.
- Takemiya T, Matsumura K, Sugiura H, Yasuda S, Uematsu S, Akira S, and Yamagata K (2011) Endothelial microsomal prostaglandin e synthase-1 facilitates neurotoxicity by elevating astrocytic Ca<sup>2+</sup> levels. *Neurochem Int* **58**:489–496, Elsevier Ltd.
- Takemiya T, Matsumura K, and Yamagata K (2007) Roles of prostaglandin synthesis in excitotoxic brain diseases. *Neurochem Int* **51**:112–120.
- Tanaka T, Saito H, and Matsuki N (1997) Inhibition of GABA<sub>A</sub> synaptic responses by brain-derived neurotrophic factor (BDNF) in rat hippocampus. *J Neurosci* **17**:2959–2966.
- Tarazona P, Feussner K, and Feussner I (2015) An enhanced plant lipidomics method based on multiplexed liquid chromatography-mass spectrometry reveals additional insights into cold- and drought-induced membrane remodeling. *Plant J* **84**:621–633.
- Tassoni D, Kaur G, Weisinger RS, and Sinclair AJ (2008) The role of eicosanoids in the brain. *Asia Pac J Clin Nutr* **17**:220–228.
- Tiburu EK, Tyukhtenko S, Zhou H, Janero DR, Struppe J, and Makriyannis A (2011) Human cannabinoid 1 GPCR C-terminal domain interacts with bilayer phospholipids to modulate the structure of its membrane environment. *AAPS J* **13**:92–8.
- Triebel A, Hartler J, Trötz Müller M, and C. Köfeler H (2017) Lipidomics: Prospects from a technological perspective. *Biochim Biophys Acta - Mol Cell Biol Lipids* **1862**:740–746.
- Triebel A, Trötz Müller M, Eberl A, Hanel P, Hartler J, and Köfeler HC (2014) Quantitation of phosphatidic acid and lysophosphatidic acid molecular species using hydrophilic interaction liquid chromatography coupled to electrospray ionization high resolution mass spectrometry.

## REFERENCES

---

- J Chromatogr A* **1347**:104–110, Elsevier B.V.
- Trimbuch T, Beed P, Vogt J, Schuchmann S, Maier N, Kintscher M, Breustedt J, Schuelke M, Streu N, Kieselmann O, Brunk I, Laube G, Strauss U, Bettefeld A, Wende H, Birchmeier C, Wiese S, Sendtner M, Kawabe H, Kishimoto-Suga M, Brose N, Baumgart J, Geist B, Aoki J, Savaskan NE, Bräuer AU, Chun J, Ninnemann O, Schmitz D, and Nitsch R (2009) Synaptic PRG-1 Modulates Excitatory Transmission via Lipid Phosphate-Mediated Signaling. *Cell* **138**:1222–1235.
- Trovo L, Van Veldhoven PP, Martin MG, and Dotti CG (2011) Sphingomyelin upregulation in mature neurons contributes to TrkB activity by Rac1 endocytosis. *J Cell Sci* **124**:1308–1315.
- Ueno Y, Takagi A, Kawana M, and Kasanuki H (2005) Pulmonary hypertension during epileptic seizure with evidence of increased angiotensin II in pulmonary artery. *Heart Vessels* **20**:37–38.
- Van Den Pol AN, Hermans-Borgmeyer I, Hofer M, Ghosh P, and Heinemann S (1994) Ionotropic glutamate-receptor gene expression in hypothalamus: Localization of AMPA, kainate, and NMDA receptor RNA with in situ hybridization. *J Comp Neurol* **343**:428–444.
- van der Veen JN, Kennelly JP, Wan S, Vance JE, Vance DE, and Jacobs RL (2017) The critical role of phosphatidylcholine and phosphatidylethanolamine metabolism in health and disease. *Biochim Biophys Acta - Biomembr* **1859**:1558–1572, Elsevier B.V.
- van Meer G, Voelker DR, and Feigenson GW (2008) Membrane lipids: where they are and how they behave. *Nat Rev Mol Cell Biol* **9**:112–124.
- Velasco M, O'Sullivan C, and Sheridan GK (2017) Lysophosphatidic acid receptors (LPARs): Potential targets for the treatment of neuropathic pain. *Neuropharmacology* **113**:608–617, Elsevier Ltd.
- Vemuri VK, Janero DR, and Makriyannis A (2008) Pharmacotherapeutic targeting of the endocannabinoid signaling system: Drugs for obesity and the metabolic syndrome. *Physiol Behav* **93**:671–686.
- Vercueil L (2006) Epilepsy and neurodegenerative diseases in adults: a clinical review. *Epileptic Disord* **8**:S44–S54.
- Verkleij AJ, Zwaal RFA, Roelofsen B, Comfurius P, Kastelijn D, and van Deenen LLM (1973) The asymmetric distribution of phospholipids in the human red cell membrane. A combined study using phospholipases and freeze-etch electron microscopy. *BBA - Biomembr* **323**:178–193.
- Vezzani A, Aronica E, Mazarati A, and Pittman QJ (2013) Epilepsy and brain inflammation. *Exp Neurol* **244**:11–21.
- Viani P, Zini I, C G, Biagini G, A LF, and C B (1995) Effect of Endothelin-1 Induced Ischemia on Peroxidative Damage and Membrane Properties in Rat Striatum Synaptosomes. **20**:689–695.
- Vickerman JC, and Briggs D (2001) *ToF-SIMS: Surface analysis by mass spectrometry*.
- Vila A, Rosengarth A, Piomelli D, Cravatt B, and Marnett LJ (2007) Hydrolysis of prostaglandin

- glycerol esters by the endocannabinoid- hydrolyzing enzymes, monoacylglycerol lipase and fatty acid amide hydrolase. *Biochemistry* **46**:9578–9585.
- Vodicka P, Mo S, Tousley A, Green KM, Sapp E, Iuliano M, Sadri-Vakili G, Shaffer SA, Aronin N, DiFiglia M, and Kegel-Gleason KB (2015) Mass Spectrometry Analysis of Wild-Type and Knock-in Q140/Q140 Huntington's Disease Mouse Brains Reveals Changes in Glycerophospholipids Including Alterations in Phosphatidic Acid and Lyso-Phosphatidic Acid. *J Huntingtons Dis* **4**:187–201.
- Vogeser M, Hauer D, Azad SC, Huber E, Storr M, and Schelling G (2006) Release of anandamide from blood cells. *Clin Chem Lab Med* **44**:488–491.
- Wallace MJ, Blair RE, Falenski KW, Martin BR, and Delorenzo RJ (2003) The Endogenous Cannabinoid System Regulates Seizure Frequency and Duration in a Model of Temporal Lobe Epilepsy. *Pharmacol Exp Ther* **307**:129–137.
- Wallace MJ, Martin BR, and DeLorenzo RJ (2002) Evidence for a physiological role of endocannabinoids in the modulation of seizure threshold and severity. *Eur J Pharmacol* **452**:295–301.
- Wang (2010) Selective neuronal vulnerability to oxidative stress in the brain. *Front Aging Neurosci* **2**.
- Wang M, Wang C, Han RH, and Han X (2016) Novel advances in shotgun lipidomics for biology and medicine. *Prog Lipid Res* **61**:83–108, Elsevier B.V.
- Wang M, Wang C, and Han X (2016) Selection of Internal Standards for Accurate Quantification of Complex Lipid Species in Biological Extracts by Electrospray Ionization Mass Spectrometry—What, How and Why? *Mass Spectrom Rev* **9999**:1–22.
- Wang S, Zhang S, Liou L-C, Ren Q, Zhang Z, Caldwell G a, Caldwell K a, and Witt SN (2014) Phosphatidylethanolamine deficiency disrupts  $\alpha$ -synuclein homeostasis in yeast and worm models of Parkinson disease. *Proc Natl Acad Sci U S A* **111**:E3976-85.
- Watson JT, and Sparkman OD (2007) *Introduction to Mass Spectrometry*, John Wiley & Sons, Ltd, Chichester, UK.
- Wei Y, Wang D, Topczewski F, and Pagliassotti MJ (2006) Saturated fatty acids induce endoplasmic reticulum stress and apoptosis independently of ceramide in liver cells. *Am J Physiol Endocrinol Metab* **291**:E275-81.
- Weisbrod CR, Kaiser NK, Skulason GE, and Bruce JE (2008) Trapping ring electrode cell: A FTICR mass spectrometer cell for improved signal-to-noise and resolving power. *Anal Chem* **80**:6545–6553.
- Welte MA (2015) Expanding Roles for Lipid Droplets. *Curr Biol* **25**:R470–R481.
- Wenk MR (2010) Lipidomics: New tools and applications. *Cell* **143**:888–895, Elsevier Inc.
- Wenzel D, Matthey M, Bindila L, Lerner R, Lutz B, Zimmer A, and Fleischmann BK (2013) Endocannabinoid anandamide mediates hypoxic pulmonary vasoconstriction. *Proc Natl Acad Sci* **110**:18710–18715.

## REFERENCES

---

- Wheeler TG, Benolken RM, and Anderson RE (1975) Visual membranes: specificity of fatty acid precursors for the electrical response to illumination. *Science* **188**:1312–4.
- Wien WC, (1898) Die elektrostatische und magnetische Ablenkung der Kanalstrahlen. *Berlin Physikalische Gesellschaft Verhandlungen* **17**: 10-12.
- Wierzbicki AS (2006) Rimonabant: endocannabinoid inhibition for the metabolic syndrome. *Int J Clin Pract* **60**:1697–1706.
- Williams D, Vicogne J, Zaitseva I, McLaughlin S, and Pessin JE (2009) Evidence that Electrostatic Interactions between Vesicle-associated Membrane Protein 2 and Acidic Phospholipids May Modulate the Fusion of Transport Vesicles with the Plasma Membrane. *Mol Biol Cell* **20**:4910–4919.
- Winkler E, Kamp F, Scheuring J, Ebke A, Fukumori A, and Steiner H (2012) Generation of Alzheimer Disease-associated Amyloid  $\beta$  42/43 Peptide by  $\gamma$ -Secretase Can Be Inhibited Directly by Modulation of Membrane Thickness. *J Biol Chem* **287**:21326–21334.
- Wymann MP, and Schneider R (2008) Lipid signalling in disease. *Nat Rev Mol Cell Biol* **9**:162–76.
- Xiang SY, Dusaban SS, and Brown JH (2013) Lysophospholipid receptor activation of RhoA and lipid signaling pathways. *Biochim Biophys Acta - Mol Cell Biol Lipids* **1831**:213–222, Elsevier B.V.
- Xu D, Miller SD, and Koh S (2013) Immune mechanisms in epileptogenesis. *Front Cell Neurosci* **7**:195.
- Yamaji A, Sekizawa Y, Emoto K, Sakuraba H, Inoue K, Kobayashi H, and Umeda M (1998) Lysenin, a novel sphingomyelin-specific binding protein. *J Biol Chem* **273**:5300–5306.
- Yamamoto N, Matsubara T, Sato T, and Yanagisawa K (2008) Age-dependent high-density clustering of GM1 ganglioside at presynaptic neuritic terminals promotes amyloid  $\beta$ -protein fibrillogenesis. *Biochim Biophys Acta - Biomembr* **1778**:2717–2726.
- Yamashita M, and Fenn JB (1984) Electrospray ion source. Another variation on the free-jet theme. *J Phys Chem* **88**:4451–4459.
- Yang K, and Han X (2016) Lipidomics: Techniques, Applications, and Outcomes Related to Biomedical Sciences. *Trends Biochem Sci* **41**:954–969.
- Yegin A, Akbas SH, Ozben T, and Korgun DK (2002) Secretory phospholipase A(2) and phospholipids in neural membranes in an experimental epilepsy model. *Acta Neurol Scand* **106**:258–262.
- Yetukuri L, Ekroos K, Vidal-Puig A, and Oresic M (2008) Informatics and computational strategies for the study of lipids 38. *MolBiosyst* **4**:121–127.
- Yoshikawa K, Kita Y, Kishimoto K, and Shimizu T (2006) Profiling of eicosanoid production in the rat hippocampus during kainic acid-induced seizure: Dual phase regulation and differential involvement of COX-1 AND COX-2. *J Biol Chem* **281**:14663–14669.
- Yost RA, and Enke CG (1978) Selected ion fragmentation with a tandem quadrupole mass spectrometer. *J Am Chem Soc* **100**:2274–2275.



- Yu Y, Ramachandran P V., and Wang MC (2014) Shedding new light on lipid functions with CARS and SRS microscopy. *Biochim Biophys Acta - Mol Cell Biol Lipids* **1841**:1120–1129.
- Zhao Y-Y, Cheng X, and Lin R-C (2014) Lipidomics Applications for Discovering Biomarkers of Diseases in Clinical Chemistry, in *International Review of Cell and Molecular Biology* pp 1–26.
- Zhao Z, and Xu Y (2009) Measurement of endogenous lysophosphatidic acid by ESI-MS/MS in plasma samples requires pre-separation of lysophosphatidylcholine. *J Chromatogr B Anal Technol Biomed Life Sci* **877**:3739–3742.
- Zhu L, Zhong M, Elder GA, Sano M, Holtzman DM, Gandy S, Cardozo C, Haroutunian V, Robakis NK, and Cai D (2015) Phospholipid dysregulation contributes to ApoE4-associated cognitive deficits in Alzheimer's disease pathogenesis. *Proc Natl Acad Sci U S A* **112**:11965–70.

## 9 APPENDIX

## 9.1 Abbreviations

---

2-AG	2-arachidonyl glycerol
5(S)-HETE	5S-hydroxyeicosatetraenoic acid
8(S)-HETE	8(S)-hydroxyeicosatetraenoic acid
12(S)-HETE	12(S)-hydroxyeicosatetraenoic acid
15(S)-HETE	15(S)-hydroxyeicosatetraenoic acid
19(S)-HETE	19S-hydroxyeicosatetraenoic acid
20(S)-HETE	20-hydroxyeicosatetraenoic acid
AA	arachidonic acid
ABHD	$\alpha$ - $\beta$ hydrolase
ACN	acetonitrile
AD	Alzheimer disease
AEA	arachidonoyl ethanolamide
APCI	atmospheric pressure chemical ionization
BBB	blood brain barrier
BD	bipolar disorder
BDNF	brain-derived neurotrophic factor
BHT	butylhydroxytoluene
BLA	basolateral amygdala
CB1R	cannabinoid receptor type 1
CB2R	cannabinoid receptor type 2
cCTX	cerebral cortex
cDNA	complementary DNA
CER	cerebellum
CE	collision energy
CI	chemical ionization
CID	collision induced decomposition
CL	cardiolipin
COX	cyclooxygenase
cPLA2	cytosolic PLA2
CXP	collision cell exit
DAG	1,2-diacylglycerol
DAGL	diacylglycerol lipases
DBS	dried blood spots
DHA	docosahexaenoic acid
dHC	dorsal hippocampus
DI	desorption/ionization
DP	declustering potential
DSE	depolarization-induced suppression of excitation
DSI	depolarization induced suppression of inhibition
eCB	endocannabinoid
ECS	endocannabinoid system
EI	electron ionization
eiCs	eicosanoids
ER	endoplasmic reticulum

---

ERCs	eCBs related compounds
ESI	electrospray ionization
FA	fatty acid
FAAH	fatty acid amide hydrolase
FAB	fast atom bombardment
FAAH	fatty acid amide hydrolase
<i>Fn</i>	<i>Francisella tularensis</i>
FTICR	fourier transform ion cyclotron resonance
FWHM	full width at half maximum
GABA	$\gamma$ -aminobutyric acid
GC	gas chromatography
GPCR	G-protein coupled receptor
GPI	glycosylphosphatidylinositol
HC	hippocampus
HPA axis	hypothalamus pituitary-adrenal axis
HPLC	high performance liquid chromatography
HYP	hypothalamus
iPLA2	independent PLA2
ISTD	internal standard
KA	kainic acid
LC	liquid chromatography
LC/MS	liquid chromatography/ mass spectrometry
LIT	linear ion trap
LLE	liquid-liquid extraction
LMSD	LIPID MAPS Nature Lipidomic Gateway
LOD	limit of detection
LOQ	limit of quantification
LOX	lipoxygenases
LPA	lysophosphatidic acid
LPC	lysophosphatidylcholine
LxA <sub>4</sub>	5(S),6(R)-lipoxin A <sub>4</sub>
<i>m/z</i>	mass to charge
MAGL	monoacylglycerol lipase
MALDI	matrix-assisted laser desorption/ionization
MDD	major depressive disorder
MRM	multiple reaction monitoring
MS	mass spectrometry
MS/MS or MS <sup>2</sup>	tandem mass spectrometry
MSI	mass spectrometry imaging
MTBE	methyl <i>tert</i> -butyl ether
NADA	N-arachidonoyl dopamine
NAPE-PLD	n-acyl phosphatidylethanolamine phospholipase D
NArPE	N-arachidonoyl phosphatidylethanolamine
NLS	neutral loss scanning
NMR	nuclear magnetic resonance
noladin ether	2-arachidonoyl glyceryl ether
NSAID	non-steroidal anti-inflammatory drugs
OEA	oleoyl ethanolamide

## APPENDIX

---

PA	phosphatidic acid
PC	phosphatidylcholine
PE	phosphatidylethanolamine
PEA	palmitoyl ethanolamide
PG	phosphatidylglycerol
PGD <sub>2</sub>	prostaglandin D <sub>2</sub>
PGE <sub>2</sub>	prostaglandin E <sub>2</sub>
PGF <sub>2</sub> α	prostaglandin F <sub>2</sub> α
PI	phosphatidylinositol
PIS	precursor ion scanning
PL	phospholipid
PLA <sub>2</sub>	phospholipase A <sub>2</sub>
PLC	phospholipase C
PPAR	peroxisome proliferator-activated receptor
PS	phosphatidylserine
PtdInsP	phosphatidylinositol phosphates
PUFA	poly unsaturated fatty acid
Q-TOF	quadrupole-TOF
QIT	quadrupole ion trap
qPCR	quantitative polymerase chain reaction
RGE	relative gene expression
ROS	reactive oxygen species
RT	retention time
SCZ	schizophrenia
SIMS	secondary ion mass spectrometry
SM	sphingomyelin
SPE	solid-phase extraction
SRM	selected reaction monitoring
STR	striatum
TEA	triethylamine
TG	triacylglycerol
THC	Δ <sup>9</sup> -tetrahydrocannabinol
THL	thalamus
TLC	thin-layer chromatography
TLE	temporal lobe epilepsy
TOF	time-of-flight
TQMS	triple quadrupole mass spectrometer
TRPV1	transient receptor potential vanilloid 1
TxB <sub>2</sub>	thromboxane B <sub>2</sub>
URB597	3-(3-Carbamoylphenyl)phenyl] N-cyclohexylcarbamate
vHC	ventral hippocampus
virodhamine	O-arachidonoyl ethanolamine

---

Further abbreviations were used according to the international system of units (SI).

## 9.2 List of figures

Figure 2.1 Exemplary structures of lipid categories:.....	8
Figure 2.2 Exemplary structures of targeted lipids: .....	11
Figure 2.3 Interplay of lipid signaling: .....	18
Figure 2.4 Conceptual illustration of a mass spectrometer:.....	25
Figure 2.5 Quantification workflow based on LC/MS:.....	30
Figure 2.6 Chemical isomerization of 2-AG to 1-AG: .....	34
Figure 2.7 Workflow for MALDI MSI analysis:.....	36
Figure 4.1 Scheme of an AB SCIEX QTRAP® 5500 System with ion optics path and optimized parameter:.....	43
Figure 4.2 CE Optimization:.....	44
Figure 4.3 Lithium effect: .....	45
Figure 4.4 Injection solvent optimization: .....	46
Figure 4.5 TEA effect:.....	47
Figure 4.6 Effect of column oven temperature: .....	48
Figure 4.7 Representative structural formulas of standards: .....	49
Figure 4.8 Retention time correction: .....	53
Figure 4.9 Calibration curve:.....	55
Figure 4.10 Chromatographic optimization process: .....	60
Figure 4.11 ISTD recovery via different extraction solvents: .....	63
Figure 4.12 Analyte extraction via different homogenization solvents: .....	65
Figure 4.13 PL and eCB co-extraction workflow: .....	67
Figure 4.14 PL concentrations among different mouse brain regions: .....	68
Figure 4.15 Arachidonic acid (AA)-containing PLs of the splenic white pulp are depleted during <i>Francisella novicida</i> (Fn) infection: .....	70
Figure 5.1 Overview of the dual extraction workflow: .....	73
Figure 5.2 Analyte extraction via dual- vs. standard Qiagen protocol:.....	75
Figure 5.3 Extracted whole RNA content via dual- vs standard Qiagen protocol:.....	76
Figure 6.1 Overview of the workflow for PL, eCB, ERCs and eiC analysis:.....	81
Figure 6.2 Behavioral scores: .....	84
Figure 6.3 Extracted ion current chromatograms: .....	84
Figure 6.4 Brain and peripheral tissue lipid levels in epileptic seizures: .....	85
Figure 6.5 Precursor ion scan:.....	86
Figure 6.6 Plasma lipids: .....	88
Figure 6.7 Behavioral scores: .....	89
Figure 6.8 Tissue lipid levels of brain subregions in epileptic seizures:.....	90
Figure 6.9 Relative mRNA expression levels in epileptic seizures: .....	91
Figure 6.10 MSI of PLs at acute epileptic seizure phases:.....	93

Figure 6.11 MSI of PLs in hippocampus with high spatial resolution:.....	94
Figure 6.12 MSI of different ion adducts within epileptic seizures: .....	95

### **9.3 List of tables**

Table 2.1 LIPID MAPS Classification system: .....	7
Table 2.2 LIPID MAPS Classification system - PLs: .....	12
Table 2.3 LIPID MAPS classification system – eCBs and ERCs: .....	16
Table 4.1 Scheme for extraction optimization: .....	51
Table 4.2 MRM parameter for PL analysis in positive ion mode: .....	56
Table 4.3 MRM parameter for PL analysis in negative ion mode: .....	57
Table 4.4 MRM parameters for eCB analysis: .....	58
Table 4.5 Compound independent instrument settings:.....	59
Table 4.6 Gradient for PL analysis: A: .....	59
Table 4.7 PL retention times:.....	61
Table 4.8 Calibration data: .....	61
Table 4.9 Intra-day and inter-day precisions:.....	62
Table 4.10 Recovery, intra assay reproducibility and matrix effect via MTBE/MeOH FA: .....	64
Table 5.1 List of TaqMan assays obtained for qPCR:.....	74
Table 5.2 Percentage of ISTD recovery via dual- or Qiagen extraction protocol: .....	76
Table 5.3 RNA quality achieved via dual- or Qiagen protocol: .....	77
Table 5.4 Intra assay reproducibility and matrix effect via dual extraction:.....	77

---

## 9.4 Curriculum vitae

**Name:** Raissa Lerner  
Date of birth: 24<sup>th</sup> September 1985  
Place of birth: Bad Schwalbach  
Marital status: Single  
Nationality: German  
E-Mail: lernerr@uni-mainz.de

### Education:

08/1996 - 06/2005 Diltheyschule, altsprachliches Gymnasium Wiesbaden, Grade: Allgemeine Hochschulreife (Note: 2,1)

10/2005 - 11/2010 Degree in Biology (Dipl.): Thesis at the Institute for Physiological Chemistry, University Medical Center of the Johannes Gutenberg University Mainz  
Topic: „*Differentielle Signalkopplung von Cannabinoid-Rezeptor Typ1 in glutamatergen und GABAergen Neuronen*“  
Grade: **Sehr gut**

04/2011 - present Promotion at the Institute for Physiological Chemistry, University Medical Center of the Johannes Gutenberg University Mainz  
Topic: „*Development of quantitative lipidomic strategies in neurological diseases for discovery and monitoring of tissue and blood markers - Application to kainic acid mouse model of epilepsy*“

### Stays abroad:

02/2015 Maastricht MultiModal Molecular Imaging Institute, Maastricht University  
**Collaboration:** MSI of PLs in epileptic seizures

**Professional activities:****Publications**

- [1] A. Wojtalla, F. Herweck, M. Granzow, S. Klein, J. Trebicka, S. Huss, **R. Lerner**, B. Lutz, F.A. Schildberg, P.A. Knolle, T. Sauerbruch, M.V. Singer, A. Zimmer, S.V. Siegmund, R. Lerner, B. Lutz, S. Fa, K. Pa, T. Sauerbruch, The endocannabinoid N -arachidonoyl dopamine (NADA) selectively induces oxidative stress-mediated cell death in hepatic stellate cells but not in hepatocytes, (2012) 873–887.
- [2] M. Bauer, A. Chicca, M. Tamborrini, D. Eisen, **R. Lerner**, B. Lutz, O. Poetz, G. Pluschke, Identification and Quantification of a New Family of Peptide Endocannabinoids (Pepcans) Showing Negative Allosteric Modulation at CB1 Receptors, 287 (2012) 36944–36967.
- [3] F.A. Pamplona, J. Ferreira, O. Menezes de Lima, F.S. Duarte, A.F. Bento, S. Forner, J.G. Villarinho, L. Bellocchio, C.T. Wotjak, **R. Lerner**, K. Monory, B. Lutz, C. Canetti, I. Matias, J.B. Calixto, G. Marsicano, M.Z.P. Guimaraes, R.N. Takahashi, Anti-inflammatory lipoxin A4 is an endogenous allosteric enhancer of CB1 cannabinoid receptor, Proc. Natl. Acad. Sci. 109 (2012) 21134–21139.
- [4] F. Steindel, **R. Lerner**, M. Häring, S. Ruehle, G. Marsicano, B. Lutz, K. Monory, Neuron-type specific cannabinoid-mediated G protein signalling in mouse hippocampus, J. Neurochem. 124 (2013) 795–807.
- [5] G.D. Duerr, J.C. Heinemann, S. Dunkel, A. Zimmer, B. Lutz, **R. Lerner**, W. Roell, F. Mellert, C. Probst, B. Esmailzadeh, A. Welz, O. Dewald, Myocardial hypertrophy is associated with inflammation and activation of endocannabinoid system in patients with aortic valve stenosis, Life Sci. 92 (2013) 976–983.
- [6] **R. Lerner**, B. Lutz, L. Bindila, Tricks and Tracks in the Identification and Quantification of Endocannabinoids, eLS. (2013).
- [7] D. Wenzel, M. Matthey, L. Bindila, **R. Lerner**, B. Lutz, A. Zimmer, B.K. Fleischmann, Endocannabinoid anandamide mediates hypoxic pulmonary vasoconstriction, Proc. Natl. Acad. Sci. 110 (2013) 18710–18715.
- [8] F.F. Hoyer, M. Khoury, H. Slomka, M. Keschull, **R. Lerner**, B. Lutz, H. Schott, D. Lütjohann, A. Wojtalla, A. Becker, A. Zimmer, G. Nickenig, Inhibition of endocannabinoid-degrading enzyme fatty acid amide hydrolase increases atherosclerotic plaque vulnerability in mice, J. Mol. Cell. Cardiol. 66 (2014) 126–132.
- [9] E. Lomazzo, L. Bindila, F. Remmers, **R. Lerner**, C. Schwitter, U. Hoheisel, B. Lutz, Therapeutic Potential of Inhibitors of Endocannabinoid Degradation for the Treatment of Stress-Related Hyperalgesia in an Animal Model of Chronic Pain., Neuropsychopharmacology. 40 (2014) 1–46.
- [10] Guggenhuber, H. Romo-Parra, L. Bindila, J. Leschik, E. Lomazzo, F. Remmers, T. Zimmermann, **R. Lerner**, M. Klugmann, H.-C. Pape, B. Lutz, Impaired 2-AG Signaling in Hippocampal Glutamatergic Neurons: Aggravation of Anxiety-Like Behavior and Unaltered Seizure Susceptibility., Int J Neuropsychopharmacol. (2015) 1–13.
- [11] A. Piyanova, E. Lomazzo, L. Bindila, **R. Lerner**, O. Albayram, T. Ruhl, B. Lutz, A. Zimmer, A. Bilkei-gorzo, Age-related changes in the endocannabinoid system in the mouse hippocampus, Mech. Ageing Dev. 150 (2015) 55–64.
- [12] **R. Lerner**, J. Post, S. Loch, B. Lutz, L. Bindila, Targeting brain and peripheral plasticity of the lipidome in acute kainic acid-induced epileptic seizures in mice via quantitative mass spectrometry, Biochim. Biophys. Acta - Mol. Cell Biol. Lipids. 1862 (2016) 255–267.
- [13] A. Scott, J.M. Post, **R. Lerner**, S. Ellis, J. Lieberman, K.A. Shirey, R. Heeren, L. Bindila, R. Ernst, 3D Host-Pathogen Interface Mapping Defines a Lethal Role for Inflammatory Lipids, Proc. Natl. Acad. Sci. (2017) [Epub ahead of print]



Under review

- [14] **R. Lerner**, J.M. Post, S.R. Ellis, R.M.A. Heeren, B. Lutz, L. Bindila, Simultaneous lipidomic and transcriptomic profiling in brain punches applied to acute epileptic seizure model. Submitted to Journal of Lipid Research
- [15] A. Thomazeau, D. Neuhofer, M. Eisenhardt, S. Leixner, O. Lassalle, M.J. Canduela, A. Ramos-Uriarte, N. Puente, **R. Lerner**, C. Schwitter, P. Grandes, B. Lutz, O. Manzoni, R. Spanagel, A. Bilbao, Endocannabinoid LTD in accumbal D1 neurons mediates reward-seeking behavior. Submitted to Cell Reports.
- [16] J.M. Post, S. Loch, **R. Lerner**, F. Remmers, E. Lomazzo, B. Lutz, L. Bindila, The neuroprotective effect of PEA in a mouse model of epileptic seizure: Temporal changes of the endocannabinoids and eicosanoids correlate with reduced seizure intensity upon acute and subchronic systemic PEA administration. Under Review: Frontiers in Molecular Neuroscience.

**Poster presentations**First Author 2012-2016

1. **Lerner R**, Schwitter C, Lomazzo E, Guggenhuber S, Lutz B. Dynamics of endocannabinoid concentrations. Poster presented at: 6<sup>th</sup> Summer Course for Mass Spectrometry in Biotechnology and Medicine; 2012 July 8-14; Dubrovnik, Croatia.
2. **Lerner R**, Gerhardt A, Eich W, Bindila L, Lutz B. A targeted LC-MS based quantification of bioactive lipids, in particular endocannabinoids, in plasma from patients with chronic musculoskeletal pain. Poster presented at: Gordon research conference; 2013 August 2-10; New Hampshire, USA.
3. **Lerner R**, Lutz B, Bindila L. Dual extraction protocol of bioactive lipids and RNA for lipidomic and transcriptomic profiling in the same tissue. Poster presented at: 47. Jahrestagung der Deutschen Gesellschaft für Massenspektrometrie (DGMS); 2014 March 2-5; Frankfurt, Germany.
4. **Lerner R**, Post J, Ellis S, Lutz B, Bindila L. Simultaneous extraction of bioactive lipids and RNA for lipidomic and transcriptomic profiling in mouse brain punches. Poster presented at: 49. Jahrestagung der Deutschen Gesellschaft für Massenspektrometrie (DGMS); 2016 February 28 - March 2; Hamburg, Germany.

Co-author 2011-2016

1. Steindel F, Häring M, **Lerner R**, Marsicano G, Monory K, Lutz B. Differential coupling of G-proteins to CB1 receptors in hippocampal glutamatergic and GABAergic neurons. Poster presented at: Cannabinoid Conference; 2011 September 8-10; Bonn, Germany.
2. Lomazzo E, **Lerner R**, Schwitter C, Lutz B. The endocannabinoid system and stress-mediated enhancement of pain susceptibility in mice. Poster presented at: The 22nd Annual International Cannabinoid Research Society Symposium on the Cannabinoids (ICRS); 2012 July 22-27; Freiburg, Germany.
3. Legler A, **Lerner R**, Bilkei-Gorzo A, Lutz B, Monory K. Circuit specific functions of cannabinoid CB1 receptor in aging. Poster presented at: Society for neuroscience (SfN); 2012 October 11-18; New Orleans, USA.
4. Lomazzo E, Bindila L, **Lerner R**, Schwitter C, Hoheisel U, Lutz B. The endocannabinoid system modulates long-lasting hyperalgesia associated to chronic stress. Poster presented at: Society for neuroscience (SfN); 2013 November 9-13; San Diego, USA.
5. Monory K, Steindel F, **Lerner R**, Häring M, Rühle S, Marsicano G, Lutz B. Neuron-type specific cannabinoid CB1 receptor signaling in mouse hippocampus. Poster presented at: 9<sup>th</sup> FENS; 2014 July 5-9; Milan, Italy.

6. Post J, **Lerner R**, Lutz B, Bindila L. Novel approach for simultaneous profiling of eicosanoids and endocannabinoids, as well as phospholipids in acute epileptic seizures. Poster presented at: 8<sup>th</sup> Summer Course for Mass Spectrometry in Biotechnology and Medicine; 2014 July 6-12; Dubrovnik, Croatia.
7. Post J, **Lerner R**, Lutz B, Bindila L. Investigation of lipid mediators as potential antiepileptic drugs and drug targets in epileptic seizure models. Poster presented at: 9<sup>th</sup> Summer Course for Mass Spectrometry in Biotechnology and Medicine; 2015 July 5-11; Dubrovnik, Croatia.
8. Post J, **Lerner R**, Loch S, Shane E, Lutz B, Bindila L. Investigation of lipid mediators as potential antiepileptic drugs and drug targets in epileptic seizure model. Poster presented at: Focus of Translational Neuroscience Advisory Meeting; 2016 March 3-5; Mainz, Germany.
9. Post J, **Lerner R**, Loch S, Shane E, Lutz B, Bindila L. Investigation of lipid mediators as potential antiepileptic drugs and drug targets in epileptic seizure model. Poster presented at: 53. Jahrestagung der deutschen Gesellschaft für Epileptologie e.V.; 2016 March 2-5; Jena, Germany.

### Posteraward

JEOL LC/MS Poster Award

presented at: 49. Jahrestagung der deutschen Gesellschaft für Massenspektrometrie (DGMS), Hamburg March 2016

### Conferences

- |         |  |
|---------|--|
| 09/2011 | 6 <sup>th</sup> Conference on Cannabinoids of the Internationale Arbeitsgemeinschaft Cannabis als Medizin (IACM), Bonn |
| 06/2012 | 2 <sup>rd</sup> rmn <sup>2</sup> - Rhine-Main Neuroscience Network biennial meeting, Oberwesel                         |
| 07/2012 | 6 <sup>th</sup> Annual Summer School for Mass Spectrometry in Biotechnology & Medicine (MSBM), Dubrovnik               |
| 11/2012 | 42 <sup>nd</sup> Annual meeting of the Society for Neuroscience (SfN), New Orleans                                     |
| 08/2013 | Gordon Research Conference on "Cannabinoid function in the CNS", New Hampshire   |
| 06/2014 | 3 <sup>rd</sup> rmn <sup>2</sup> - Rhine-Main Neuroscience Network biennial meeting, Oberwesel                         |
| 07/2014 | 8 <sup>th</sup> Annual Summer School for Mass Spectrometry in Biotechnology & Medicine (MSBM), Dubrovnik               |
| 03/2016 | 49. Jahrestagung der deutschen Gesellschaft für Massenspektrometrie (DGMS), Hamburg                                    |
| 06/2016 | 4 <sup>th</sup> rmn <sup>2</sup> - Rhine-Main Neuroscience Network biennial meeting, Oberwesel                         |

**Workshops and certificates**

10/2011	Basic Training AB Sciex QTRAP 5500 LC/MS/MS
05/2012	Advanced Training AB Sciex QTRAP 5500 LC/MS/MS
09/2013	Phenomenex-Seminar: HPLC – Troubleshooting
09/2013	Workshop für Biochromatographie
10/2013	Seminar: “from Technology to Solutions“
07/2014	Workshop “Lipidomics for Biomarker and Clinical Analysis

**Skills:****Languages**

German	native
English	fluent oral and written
Italian	basic

**Computer literacy**

Microsoft Office, Corel Draw, Adobe Photoshop, Analyst, Multiquant, Lipid View, GraphPad, SPSS

**Activities:**

Since 09/2006	Member of the “Wing Tjuen club” (HTWTA) (since 2015 George Ford academy) 10th degree
Since 01/2015	Member of the oriental dance group “Gutes Bauchgefühl“